

**SIMULATION AND MANAGEMENT OF  
ON-DEMAND IRRIGATION SYSTEMS:**

**A combined agrohydrological and remote sensing approach**

Promotor: Prof. Dr.Ir. R.A. Feddes  
Hoogleraar in de bodemnatuurkunde, agrohydrologie en  
grondwaterbeheer

Co-promotor: Prof. Dr. M. Menenti  
Visiting professor, Université Louis Pasteur,  
Strasbourg, France

Samenstelling promotiecommissie:  
Prof. Dr. Ir. C.B. Vreugdenhil (Universiteit Twente)  
Prof. Dr. W.G.M. Bastiaanssen (ITC Enschede)  
Prof. Dr. P. A. Troch (Wageningen Universiteit)  
Dr. Ing. W. Verhoef (NLR Emmeloord)

Simulation and management of  
on-demand irrigation systems:

A combined agrohydrological and remote sensing approach

Guido D'Urso

**Proefschrift**

ter verkrijging van de graad van doctor  
op gezag van de rector magnificus  
van Wageningen Universiteit,  
Prof. Dr. Ir. L. Speelman,  
in het openbaar te verdedigen  
op vrijdag 6 April 2001  
des namiddags om vier uur in de Aula.

W108701, 2961

*There are more things in heaven and earth, Horatio,  
than are dreamt of in your philosophy*

(Shakespeare, "The tragedy of Hamlet, Prince of Denmark", Act I, Scene V)

## Propositions (Stellingen)

1. Whenever you can measure what you are speaking about and express it in numbers, you know something about it (*Lord Kelvin, 1824-1907*)
2. Rational use of water resources in agriculture requires a combination of deeper knowledge of the physical processes involved in the management of irrigation and suitable monitoring techniques (*this dissertation*)
3. A perfect simulation cannot substitute reliable measurements of comparable costs and quickness (*this dissertation*)
4. Measurements of reflection coefficient may give useful estimates of leaf growth without destructive sampling (*J.L. Monteith, 1957, Annual Report of Rothamsted Experimental Station*)
5. Remote sensing is a valuable source of information in the application of distributed agrohydrological simulation models (*this dissertation*)
6. Mapping actual evapotranspiration at regional scale is of limited support in the estimation of water demand for irrigation (*this dissertation*)
7. Farmers' behaviour introduces an erratic component in the simulation of irrigation systems operation (*this dissertation*)
8. Irrigation water is not yet fully considered as an economic good subject to the rules of economic market, even in areas with serious water scarcity (*this dissertation*)
9. As the complexity of a system increases, our ability to make precise and yet significant statements about its behaviour diminishes until a threshold is reached beyond which precision and significance become

almost mutually exclusive characteristics (*L.A. Zadeh, 1973; Memorandum ERL-M 411, Berkeley*)

10. Difficult professors, boring textbooks, voluminous prior work scattered in numerous references, dissertation committees and lack of funding are fog-shrouded barriers to scientific progress (*D. Hillel, 1998; Environmental Soil Physics, Academic Press*)
11. Dutch people do not merely meet; they confront each other (*C.Nooteboom, 1984; In the Dutch mountains*)
12. You can certainly find more ideas during a sailing cruise than navigating the Internet
13. Sometimes a good simulation is better than a bad action
14. Children need models rather than critics

Propositions (Stellingen) attached to the thesis:

**Simulation and Management of On-Demand Irrigation Systems:**  
A combined agrohydrological and remote sensing approach

Guido D'Urso

Wageningen, 6<sup>th</sup> april 2001

*A Luciana*

D'Urso G., 2001. *Simulation and Management of On-Demand Irrigation Systems: A combined agrohydrological and remote sensing approach*. PhD thesis, Wageningen University, Wageningen, The Netherlands, 174 p., English, Dutch and Italian summary

Rational use of water resources in agriculture requires improvements in the efficiency of irrigation. Many irrigation systems, particularly in Mediterranean regions, have been enhanced by replacing open channel conveyance systems with pressurised pipelines. This allows to provide water on-demand. Increased demand of water for civil and industrial uses and a progressive reduction of available water resources compel a more efficient use of irrigation water. To achieve this goal irrigation managers need to understand and to monitor the processes which determine the operation of an irrigation system.

In this thesis a procedure integrating the agrohydrological aspects of irrigation with hydraulic and management aspects has been developed. The procedure named SIMODIS (SIMulation and Management of On-Demand Irrigation Systems) is based on the integration of different tools such as agrohydrological and hydraulic simulation models, remote sensing and GIS techniques.

An irrigation system is described as a set of elementary units (e.g. individual fields) connected by the pressurised conveyance system. The spatial distribution of soil water deficit in each unit is computed daily by combining the soil water model SWAP with occasional satellite-based estimates of crop water requirements. A methodology has been developed to obtain spatially distributed input data for the soil water model SWAP i.e. the soil hydraulic properties and the upper and lower boundary conditions.

Multispectral satellite images are used to map the crop coefficients needed for the definition of the SWAP upper boundary condition in each elementary unit of the irrigation district. Two different approaches have been proposed. The first is based on classification techniques, where clustering algorithms are applied to derive the spectral classes corresponding to different crop coefficient values. In the second approach, the crop coefficient is analytically related to the canopy variables determining the potential evapotranspiration i.e. leaf area index, surface albedo and crop height. At-surface directional spectral reflectance are used to estimate these canopy variables from which the value of crop coefficient is calculated.

The spatial distribution of farmers' water demand is derived on a daily basis from the soil water deficit according to predefined irrigation scheduling criteria. Before applying this farmers' water demand distribution for the given day, the SIMODIS procedure assess whether water demand is consistent with the available amount of water resources and with the structural and operational constraints imposed by the conveyance and distribution system. For this purpose a steady-state simulation model of pipeline hydraulics is used in SIMODIS. The final distribution of farmers' water demand is then resulting from a three-tiered adaptation of irrigation schedule considering: i) the limitation of flow rate at delivery outlets, ii) the limitation of available water resources, iii) the required minimum hydraulic head at the delivery outlets.

The procedure SIMODIS has been applied in the Gromola irrigation district of approximately 3000 ha in southern Italy. Measurements of irrigation volumes were used to identify the parameters driving irrigation scheduling. Irrigation efficiency indicators were calculated from the spatial distribution of actual transpiration rates and of the corresponding irrigation volumes applied. To illustrate the use of SIMODIS in support of irrigation decision making, alternative scenarios of water management were simulated and compared.



## Preface

Many times, during the years spent on this book, I have been thinking of the moment when I would have been ready to write this preface. The completion of this type of work marks a clear delineation in the career of a researcher, and sometimes it is also the opportunity to take stock of the experiences during the past years.

In some cases, including mine, the personal experience of the "promovendus" is tightly connected to many, long steps leading to this final one. Along this tortuous path the "promovendus" has unique opportunities to meet many people that not only enrich his scientific knowledge but also his human experience.

This is definitely what happened to me.

It wouldn't have been possible to carry out this thesis without the continuous support of my promoters, Prof. Dr. Ir. Reinder Feddes and Prof. Dr. Massimo Menti. The chance to meet these outstanding scientists has been an invaluable experience. Every meeting with them has always been an intense moment of enthusiastic discussions, with new ideas and great improvements to the manuscript. I would like to express to both of them all my gratefulness for their patient guidance during these years.

Once back in Italy, to continue this work, I have always found in Prof. Alessandro Santini, the passionate encouragement, made of fruitful suggestions and precious scientific comments. Without his advice, either during the field activities and during the writing of the text, it would have been much more difficult to bring to completion this work.

There are many persons that helped me in many ways while in Wageningen. With all of them the professional contacts have turned into a sincere friendship.

I would like to remember my friend Ir. Peter Brussel, who first introduced me among the people of several research Institutions in Wageningen and made possible the first contacts with my future promoters.

Drs. Cecilia Stanghellini has not only tried to ensure always a pleasant stay in Wageningen for me and my family members but she has often contributed to the scientific discussion, during perfectly organised Italian dinners.

I would like to thank Dott.ssa Susanna Azzali who introduced me in the study of image processing techniques and helped me in the early organisation of the work.

Special thanks are addressed to Dr.Ir. Erik Querner, for his valuable support in the application of regional groundwater flow models, to Dr. Wout Verhoef for the help given in the atmospheric correction of Landsat TM images and to Dr. Jos van Dam for his suggestions on the use of SWAP.

During my work in Italy, great support in the elaboration of soil hydrological data was given by Dott. Angelo Basile of CNR-Irrigation Institute (Ercolano, Italy). I wish also to thank Mrs. Paola Di Fiore of the Department of Agricultural Engineering and Agronomy at the University of Naples "Federico II" for her assistance in the soil hydraulic characterisation and Dott. Ugo Lazzaro for the continuous collaboration in the field work.

The technical staff, the Director and the President of the "Consorzio di Bonifica di Paestum" offered their patient collaboration in the organisation of field campaigns.

The fruitful collaboration of Dott. Maurizio Buonanno in setting up the GIS techniques for the case study and the competent dedication of Ing. Massimo Nicolazzo and Pasquale Eduardo in the development of the software are gratefully acknowledged.

Finally, I have been pleased that Ir. Claire Jacobs and Ir. Martijn Boss accepted the role of "paranimfen" and I warmly thank them for their friendly assistance in the last steps of this experience.

## List of Symbols

Some of the symbols used in few consecutive equations falling outside the mean argumentation, are defined in the text only

Symbol	Interpretation	Unit
$A$	irrigated area	ha
$A^*$	normalised thresholding index	-
$B$	pipeline loss factor	$s^2 m^{-1}$
$c_p$	specific heat of air	$J kg^{-1} K^{-1}$
$C_G$	ratio $G/Q^*$	-
$CP$	global performance indicator for classification	-
$d$	day	d
$d^0$	sun-Earth distance	a.u.
$D$	pipeline diameter	m
$D_x$	Mahalanobis distance	-
$DN$	quantum radiance	-
$e_a$	air vapour pressure	kPa
$e_s$	saturated vapour pressure	kPa
$E$	actual evapotranspiration rate	$cm d^{-1}$
$E_{ref}$	reference evapotranspiration rate	$cm d^{-1}$
$E_{ref}^*$	mean annual reference evapotranspiration	cm
$E_p$	potential evapotranspiration rate	$cm d^{-1}$
$E_s$	soil evaporation rate	$cm d^{-1}$
$E_{s,p}$	potential soil evaporation rate	$cm d^{-1}$
$E_{\lambda}^0$	extraterrestrial solar irradiance	$W m^{-2}$
$f$	irrigation flag for tertiary units	-
$G$	heat flux density into the soil	$W m^{-2}$
$h$	soil water pressure head	cm
$h_c$	crop height	m
$h_{crit}$	threshold soil pressure head for irrigation starting	cm
$H$	hydraulic head (network)	m
$H_{min}$	minimum hydraulic head at outlet of irrigation network	m
$i$	subscript for the primary unit level	-
$i_j$	subscript for the secondary unit level	-
$i_{j,k}$	subscript for the tertiary unit level	-
$i_r$	soil water deficit irrigation fraction	-
$I$	irrigation water volume	$m^3$
$I_n$	irrigation flow rate per unit soil surface, net of interception	$cm d^{-1}$
$JM$	Jeffries-Matusita distance	-
$JM^*$	normalised separability index	-
$k$	soil hydraulic conductivity	$cm d^{-1}$
$k_s$	soil hydraulic conductivity at saturation	$cm d^{-1}$

$K^{\downarrow}$	global incoming short-wave radiation flux density	$\text{W m}^{-2}$
$K^{\uparrow}$	reflected solar radiation flux density	$\text{W m}^{-2}$
$K_c$	crop coefficient	-
$L$	pipeline length	m
$L^*$	net incoming long-wave radiation flux density	$\text{W m}^{-2}$
$LAI$	leaf area index	$\text{m}^2 \text{m}^{-2}$
$M$	solid mass fraction of soil	-
$n_{VG}$	van Genuchten parameter for soil water retention curve	-
$p$	probability	-
$p_a$	atmospheric pressure	kPa
$P$	precipitation rate	$\text{cm d}^{-1}$
$\bar{P}$	mean annual precipitation	cm
$P_n$	net precipitation rate	$\text{cm d}^{-1}$
$q$	pipeline flow rate	$\text{m}^3 \text{s}^{-1}$
$Q$	discharge of outlet in the irrigation network	$\text{m}^3 \text{s}^{-1}$
$Q^*$	net radiation flux density	$\text{W m}^{-2}$
$r$	surface albedo	-
$r_p$	planetary albedo	-
$r_{\lambda}$	planetary reflectance at wavelength $\lambda$	-
$r_{a,H}$	aerodynamic resistance	$\text{s m}^{-1}$
$r_c$	canopy resistance	$\text{s m}^{-1}$
$r_{c,\min}$	minimum canopy resistance	$\text{s m}^{-1}$
$r_{\text{leaf},\min}$	minimum stomatal resistance for unit leaf area	$\text{s m}^{-1}$
$R$	particle radius	cm
$Re$	Reynolds' number	-
$RH$	percentage of air humidity respect to saturated conditions	-
$s$	slope of vapour pressure-temperature relationship	$\text{kPa } ^\circ\text{C}^{-1}$
$s_c$	fractional vegetation cover	-
$S$	sink term for root water extraction	$\text{d}^{-1}$
$Se$	soil water saturation degree	-
$S_f$	stress factor	-
$t$	duration of irrigation application ref. to hydr. network	s
$T$	actual transpiration rate	$\text{cm d}^{-1}$
$T^*$	actual transpiration rate without applying irrigation	$\text{cm d}^{-1}$
$T_0$	surface temperature	$^\circ\text{C}$
$T_a$	air temperature	$^\circ\text{C}$
$T_p$	potential transpiration	$\text{cm d}^{-1}$
$U_z$	wind speed, measured at height $z$	$\text{m s}^{-1}$
$v$	water flux density through the lower boundary of soil profile	$\text{cm d}^{-1}$
$v^*$	water flux density through the upper boundary of soil profile	$\text{cm d}^{-1}$
$V$	variance-covariance matrix of reflectance of a spectral class	-
$VI$	vegetation index	-
$VI_s$	vegetation index for bare soil	-

$VI_{\infty}$	vegetation index for fully covering canopy	-
$V_{RES}$	daily available volume of water resources	$m^3$
$V_{TOT}$	cumulative seasonal irrigation water consumption	$m^3$
$w_{\lambda}$	weighting factors for solar extraterrestrial irradiance	-
$W$	specific soil water storage	cm
$W_0$	specific soil water storage at beginning or irrigation season	cm
$WDVI$	weighted difference vegetation index	-
$WDVI_{\infty}$	weighted diff. vegetation index for fully covering canopies	-
$x$	vector of reflectance values for a single pixel	-
$z$	elevation	cm
$z_R$	thickness of rooting zone	cm
$\alpha$	root extraction function	-
$\alpha^*$	extinction coefficient for $LAI$ estimation	-
$\alpha_{VG}$	van Genuchten parameters for soil water retention curve	-
$\beta$	extinction coefficient for solar radiation through canopy	-
$\gamma$	psychrometric constant	$kPa K^{-1}$
$\Gamma$	soil refraction index	-
$\delta$	soil water deficit	cm
$\Delta W$	soil water storage variation	cm
$\varepsilon$	irrigation efficiency indicator	-
$\varepsilon_a$	apparent soil permittivity	-
$\eta$	farm irrigation efficiency	-
$\vartheta$	observation zenith angle	rad
$\vartheta^0$	sun zenith angle	rad
$\theta$	soil water content	$m^3 m^{-3}$
$\lambda$	latent heat of vaporisation of water	$J kg^{-1}$
$\lambda$	wavelength	nm
$\lambda E$	latent heat flux density	$W m^{-2}$
$\Lambda$	pipeline friction coefficient	-
$\mu$	mean reflectance vector of a spectral class	-
$\rho$	soil bulk density	$kg m^{-3}$
$\rho_a$	air density	$kg m^{-3}$
$\rho_i$	canopy reflectance in the infrared band	-
$\rho_p$	soil particle density	$kg m^{-3}$
$\rho_r$	canopy reflectance in the red band	-
$\rho_{s,i}$	soil reflectance in the infrared band	-
$\rho_{s,r}$	soil reflectance in the red band	-
$\rho_{\lambda}$	surface reflectance at wavelength $\lambda$	-
$\varphi$	pore radius	cm
$\phi$	groundwater table depth	cm

---

$\Phi$	observation azimuth angle	rad
$\psi$	empirical factor for retention curve	-
$\omega$	pipeline internal wall roughness	m

---

# Contents

<b>1</b>	<b>Introduction.....</b>	<b>1</b>
1.1	Needs for improved management of on-demand irrigation systems.....	1
1.2	Towards an integrated approach for the simulation of on-demand irrigation management.....	3
1.3	Overview of the thesis.....	7
<b>2</b>	<b>The model SIMODIS (Simulation and Management of On Demand Irrigation Systems).....</b>	<b>11</b>
2.1	Schematisation of the irrigation network.....	11
2.2	Simulation of on-demand irrigation systems.....	12
2.3	Evaluation of the efficiency of irrigation with SIMODIS.....	15
<b>3</b>	<b>Spatial distribution of farmers' water demand.....</b>	<b>17</b>
3.1	Outline of calculation steps.....	17
3.2	Estimation of evapotranspiration.....	17
3.3	The soil water balance model.....	21
3.4	Calculation of farmers' water demand.....	23
3.5	Definition of boundary conditions.....	24
3.6	Regional application of SWAP to irrigation districts.....	26
3.6.1	Spatial distribution of the upper boundary condition.....	27
3.6.2	Spatial distribution of the lower boundary condition.....	28
3.6.3	Spatial distribution of the soil hydraulic characteristics.....	28
3.7	Conclusions.....	34
<b>4</b>	<b>Satellite remote sensing approach to determine crop coefficients.....</b>	<b>37</b>
4.1	Current uses of remote sensing in support of irrigation management.....	37
4.2	New methodology to estimate crop coefficients from satellite images.....	39
4.3	Classification approach.....	40
4.3.1	Class formation and evaluation.....	41
4.3.2	Pixel class membership and reliability of the classification.....	42
4.4	Analytical approach.....	44
4.4.1	Estimation of spectrally integrated hemispherical reflectance (albedo).....	46
4.4.2	Estimation of Leaf Area Index.....	47
4.4.3	Estimation of canopy aerodynamic properties.....	51
4.5	Conclusions.....	52
<b>5</b>	<b>Case-study in the Sele Plain, Italy: the Gromola irrigation district.....</b>	<b>53</b>
5.1	Irrigation in the Sele plain.....	53
5.2	Description of the study-area in the Gromola irrigation district.....	55
5.3	Data acquisition.....	58
5.3.1	Topographic data.....	58
5.3.2	Characteristics of water conveyance and distribution system.....	58
5.3.3	Agrometeorological data acquisition.....	60

5.3.4	Acquisition of Landsat TM images and geometrical rectification.....	61
5.3.5	Land use and cropping pattern .....	62
5.3.6	Soil hydrological data .....	67
5.3.7	Monitoring of groundwater table depth.....	72
5.3.8	Map of lower boundary condition .....	74
5.4	Validation of the SWAP model.....	77
5.5	Conclusions .....	80
<b>6</b>	<b>Mapping crop coefficients in the Gromola irrigation district from Landsat TM images.....</b>	<b>81</b>
6.1	Estimation of at-surface directional spectral reflectance. ....	81
6.1.1	Methodological approach.....	81
6.1.2	Application to the case-study area .....	83
6.2	Application of the classification approach for mapping crop coefficients. ....	85
6.2.1	Signature extraction and spectral classes.....	85
6.2.2	Performance assessment of classifier .....	88
6.3	Application of the analytical approach for mapping crop coefficients .....	90
6.3.1	Sensitivity of crop coefficient values to meteorological variables and canopy properties.....	90
6.3.2	Estimation of hemispherical surface reflectance and <i>LAI</i> from directional surface reflectance.....	95
6.3.3	Derivation of the crop coefficient map.....	99
6.4	Conclusions .....	101
<b>7</b>	<b>Application of SIMODIS in the Gromola irrigation district.....</b>	<b>103</b>
7.1	Data organisation. ....	103
7.2	Estimation of potential evapotranspiration in the Gromola irrigation district. ....	104
7.3	Spatial distribution of soil water deficit.....	106
7.4	Spatial distribution of farmers' water demand and first adaptation of schedule. ....	107
7.5	Adaptation of irrigation schedule for excessive total water demand. ....	109
7.6	Adaptation of schedule for insufficient hydraulic head at delivery outlet .....	111
7.6.1	Distribution of flow rates.....	111
7.6.2	Hydraulic simulation model of the conveyance system .....	112
7.6.3	Irrigation schedule adaptation for insufficient hydraulic head at outlet.....	114
7.7	Irrigation scheduling parameters in the Gromola district. ....	116
7.8	Evaluation of irrigation efficiency. ....	120
7.9	Influence of the uncertainty of <i>LAI</i> and $K_c$ values on SIMODIS. ....	122
7.10	Conclusions .....	125
<b>8</b>	<b>Supporting decisions in water management of the Gromola irrigation district with SIMODIS. ....</b>	<b>127</b>
8.1	Reference Scenario .....	127
8.2	Unlimited on-demand irrigation schedule: Scenario 2 .....	128



8.3	Higher hydraulic head at the outlet: Scenario 3 .....	129
8.4	Reduction of irrigation water application: Scenario 4 .....	130
8.5	Reduction of water resources daily available: Scenarios 5 and 6 .....	131
8.6	Conclusions.....	134
<b>9</b>	<b>Outlook to the future.....</b>	<b>139</b>
	<b>Summary and conclusions .....</b>	<b>141</b>
	<b>Samenvatting en conclusies .....</b>	<b>147</b>
	<b>Riassunto e conclusioni .....</b>	<b>153</b>
	<b>References .....</b>	<b>161</b>
	<b>Appendix I <i>Correction coefficients and background reflectance</i></b>	
	<b><i>for the Landsat images .....</i></b>	<b>173</b>
	<b>Colour Plates .....</b>	<b>175</b>

# 1 Introduction

---

## 1.1 Needs for improved management of on-demand irrigation systems.

World-wide 70 % of the water resources depletion is due to agricultural water use; irrigation systems however operate with an average overall efficiency of 37% (Postel, 1992). Unrealistic designs, rigid water delivery schedules and operational problems are among the principal reasons for the poor performance of irrigation systems (Plusquellec et al., 1994). Rangeley (1986) estimated that 150 million hectares, corresponding to 50% of the total irrigated area in the world, need some form of modernisation. For this reason, the modernisation and rehabilitation of irrigation systems is one of the most important challenges to address water scarcity in agriculture. In the future, it is possible that public investments in irrigation will be more and more devoted to the improvement of conveyance and distribution systems rather than to the expansion of irrigated areas.

In Italy and other Mediterranean regions, the rehabilitation of irrigation systems has been carried out by transforming the open-channel schemes into pressurised pipeline networks. Almost the total irrigated area in Israel, Cyprus and Jordan is now served by pressurised networks (Tuijl van, 1993) and pilot projects have been undertaken in Egypt (Mankarious, 1991). This modernisation may greatly enhance the overall efficiency of the irrigation systems, with tangible benefits for crop production and water conservation (Merriam et al. 1986; Battikhi et al., 1994).

In the southern regions of Italy pipeline pressurised networks convey irrigation water to 378 412 hectares, corresponding to 66.8% of irrigated area (Fig. 1.1). The modernisation of irrigation networks in southern Italy occurred particularly during the 1970-80's (Indelicato et al., 1981) and has produced a radical transformation of the traditional rural economy into a highly specialised, profit-making agriculture. In most cases, the "on-demand" method for water distribution has been adopted in substitution of the old rotational schedule.

On-demand schedule is the most flexible system for delivering irrigation water, because in principle there is no restriction on water use by farmers. According to the definition of Reploge and Merriam (1980), the on-demand schedule does not limit the frequency, rate and duration of irrigation water applications. This degree of flexibility would require large capabilities of the irrigation system in terms of water storage and pipeline diameter to meet theoretical peak demand.

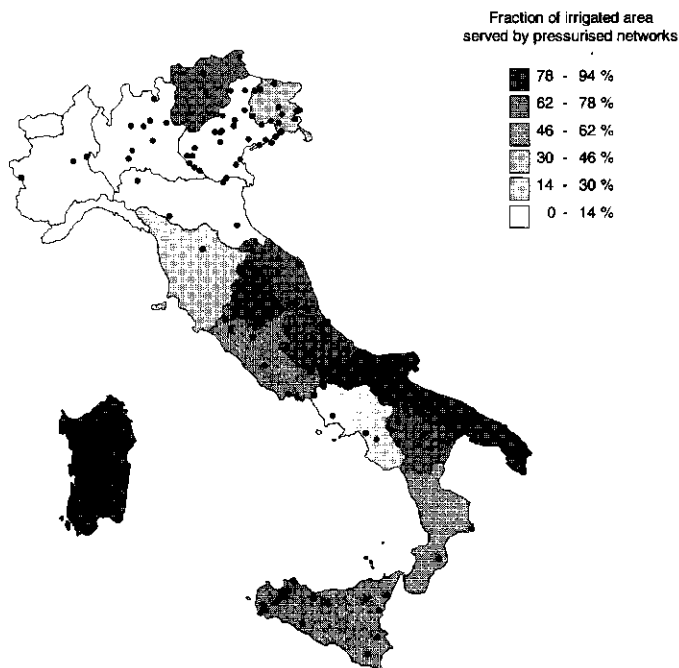


Fig. 1.1 Importance of pressurised irrigation networks in Italy. Each dot corresponds to 2000 hectares served by pipeline distribution networks.

By limiting the maximum flow rate diverted to each outlet, the construction costs may be reduced and an excessive depletion of water resources be avoided. The resulting distribution system is called “*limited rate on-demand*” schedule (Merriam, 1987).

More recently, many modernised irrigation areas have experienced an increase in the demand of water for civil and industrial use and a contemporary reduction of water availability for agriculture. Therefore, irrigation agencies and farmers’ associations have been asked to further improve the efficiency of their irrigation networks and delivery systems by means of a more rational use of limited water resources.

Actual management of water resources for irrigation is thus a compromise between the strategies of irrigation agencies and regional policy. Environmental concerns and different water uses are the main aspects on one hand, and the actual farmer water needs, related to crop production, on the other.

In an on-demand irrigation system, these two management levels are strictly connected. Hydrological and agronomic conditions at farm level determine the spatial and temporal patterns of farmers’ water demand. At the same time, water demand has to be adapted to match the structural capabilities of the conveyance and distribution network. Thus, the ‘irrigation system’ becomes very

complex where water management has economical and technical constraints both at farm and scheme level. If water shortage conditions occur frequently, the flexibility of on-demand irrigation systems may collapse. Without timely and expert management, the expected revenues of capitals invested for the rehabilitation of irrigation systems may be substantially reduced (Schul, 1982). Therefore, irrigation managers are urged to foresee the failures of (part of) the system and to formulate ways and means to overcome such failures. To achieve this task, irrigation managers should be able to evaluate the water demand in relation to the actual availability of water resources and the capability of the conveyance system. This evaluation should be carried out in accordance with some criteria of water use efficiency (Burt et al., 1997).

The spatial distribution of farmers' water demand depends on crop water use, which results from physical processes, related to soil and climate, and from the behaviour of farmers, which can not be exactly defined a priori. Farmers' irrigation criteria do not necessarily meet the same rationale of irrigation managers. As long as farmers' demand is compatible with efficient usage of water, irrigation managers should be able to fulfil this demand in time and space, taking into account the available water resources and delivery structures. In the contrary case, any usage which is not beneficial for crop production should be avoided.

In this context, the use of '*decision support tools*' may significantly enhance the management of on-demand irrigation systems. In general terms, a '*Decision Support System*' consists of hardware and software instruments for monitoring a set of variables which determine the behaviour of a complex system (*diagnosis*) and for evaluating the system response following interventions (*prognosis*).

The general requirements of a Decision Support System for water management purposes can be found in Rey et al. (1994). In most cases, the core of such a system is an automated procedure for simulating the relevant processes governing the system. Advanced technical tools are nowadays available for monitoring and simulating the different physical processes involved in an irrigation system. These tools can be used in an integrated way for simulating the operation of on-demand irrigation networks.

## **1.2 Towards an integrated approach for the simulation of on-demand irrigation management.**

Different types of procedures for supporting the decision making process in irrigation management are proposed in literature. In the analysis of water resources systems, many procedures are based on *multicriteria optimisation* techniques (Bogardi et al., 1994). These methods have shown their potentiality in the definition of optimal allocation of irrigation water in basins with conflicting water uses or limited resources (Ilich, 1993; Thiessen et al., 1994; Hongyuan et

al., 1994; Burton, 1994; Hannan et al., 1995). Several applications for irrigation water management at scheme level have also been described (Menenti et al., 1992a, 1992b; Morales et al., 1992; Teoh, 1997). Many different variables concerning social and economical indicators can be included in the optimisation, and alternative strategies for water allocation can be ranked accordingly to pre-defined criteria. Because of their computational complexity, these models are however mainly suitable for *macro*-analyses of large water resource schemes (Kularathna, 1992) and a detailed description of water demand at the farm scale, as required for simulating the operation of on-demand irrigation networks, cannot be achieved easily. This latter issue is therefore a strong limiting factor for the application of these models for on-demand irrigation management.

Traditionally, in the design of on-demand irrigation systems, the distribution of water flow rates is considered as a stochastic variable. The probabilistic model proposed by Clement (1966) is still widely used to estimate the peak flow rate in an irrigation pipeline connecting several delivery nodes having the same flow rate. The irrigation requirement per unit area and a 'coefficient of usage' are fixed design parameters. Under these assumptions the probability of operation of a single delivery node is proportional to the corresponding irrigated area. Crop and farm characteristics are not considered in the stochastic model. The number of delivery nodes simultaneously operating is modelled by means of a normal distribution while the design flow rate can be related to a probability level. It has been shown that the value of the coefficient of usage is a critical parameter to assess the degree of flexibility of the network and its value should be carefully evaluated for a reliable design (Lamaddalena et al., 2000).

On the same approach, a different methodology has been proposed by Abdellaoui (1986) and Ait Kadi (1990). Instead of the number of nodes, the physical characteristics of each farm served, i.e. crop and soil type, farm extension and irrigation efficiency, are considered as stochastic variables. The number of fields to be irrigated and the corresponding water amount are determined from soil water budget calculations. Queuing theory is then applied to reproduce the temporal variability of irrigation water flow rate in each node of the conveyance network within each day. This approach introduces the water balance among the factors influencing the operation of the network, but the spatial distribution of water demand is still estimated in a stochastic way. The model may become computationally heavy and so far has never been applied to real situations.

With the availability of new technologies and a better understanding of the physical processes involved in the different components of an on-demand irrigation system, we can describe the operation of such system in an integrated, deterministic way. *The approach proposed in this study aims to the definition of a*

*decision support tool for the operation of on-demand irrigation systems* which describes the following aspects of irrigation:

- *spatial and temporal variability of soil water deficit*
- *spatial and temporal variability of farmers' water demand*
- *water resources availability*
- *structural capability of the conveyance and distribution irrigation network.*

The spatial distribution of *soil water deficit* is the result of the actual evapotranspiration and it is calculated from the vertical distribution of water content. As such it depends on a combination of agrohydrological factors. Several techniques are available to estimate soil water content and actual evapotranspiration at local and regional scale (Engman et al., 1995; Itier and Brunet, 1996), but they cannot be used on a routinely basis in irrigation management. In practice, the crop water demand can be obtained from estimation of *potential evapotranspiration* and from *soil water balance* calculations. Often in the estimation of *potential evapotranspiration* limited information on crop development, such as crop type and planting date, is considered (F.A.O., 1998). This information is used to estimate the actual canopy development from generalised crop growth curves. A substantial improvement can however be achieved by using *remote sensing* techniques. Land use patterns, crop related variables and identification of irrigated areas can be monitored in space and time by processing multispectral satellite images at different dates during the growing season. Recent studies have shown how to use remotely sensed data to produce maps of potential evapotranspiration and crop water requirements (Menenti et al., 1990; 1995). So doing, these techniques can be applied to improve the quality of *input data to numerical models for the simulation of soil water flow*. From these models it is possible to estimate all the terms of the soil water balance, including crop water use, as determined by the local hydrological conditions such as soil properties, groundwater flow and the like.

Simulation models of water flow in the soil root zone have been widely used to improve irrigation scheduling at scheme level (FAO, 1994). In these algorithms, the soil water balance can be described by means of simple steady state relationships (Smith, 1992; Teixeira et al., 1993a, 1993b; Singh et al., 1995) or by solving the differential equations describing the transient water flow in the soil-crop system (Feddes et al., 1978, 1988; Belmans et al., 1983; Murty et al., 1992; Santini, 1992; Sharda et al., 1993; Garcia et al., 1995; Joshi et al., 1995). Menu-driven procedures that enable an easy adaptation of the available soil, crop and meteorological data sets to one of the above mentioned type of models, have been proposed by Jacucci et al. (1994). Geographical Information Systems (GIS) are often used for the spatial extrapolation and analysis of simulation results (Younos et al., 1993; San-Payo et al., 1996). Usually, one-dimensional

calculations are performed for the different crop and soil type combinations that can be found in the area under study.

Different criteria are used in soil water flow models to establish the start of irrigation and the optimal supply of water. In a simplified way these criteria take into account the behaviour of crops to water stress following soil water deficit. The irrigation criteria mentioned above contribute to establish an objective, yet theoretical, amount of water needed for irrigation on a given day. But not only the soil hydrological processes influence the *spatial and temporal variability of farmers' water demand*, other technical and management issues are also concerned. They may relate to soil hydraulic properties, crop type and farm irrigation facilities, i.e. to methods and labour availability. Management issues relate to the irrigation habits of individual farmers and to their perception of soil water deficit. Farmers' habits and perception determine to a large extent the starting time of irrigation and the gross amount of irrigation water, thus influencing the final *on-farm efficiency*. Farmers' behaviour in irrigation practice, and by analogy the value of farm efficiency, can be related to certain farm characteristics, i.e. the size of farm, the crop and the soil type, the availability of machinery and man-power, as shown by Baars and Logchem (1993). Under this assumption, *the spatial and temporal variability of crop and soil properties determines the distribution of irrigation volumes* required each day.

The fulfilment of the total irrigation demand determined before depends on *water resources availability* and on storage capacities of the irrigation system. For example, restrictions could exist on the maximum flow rate that can be diverted from the resource or compensation volumes may not be sufficient.

Besides the aforementioned limitations, the capability of the system in meeting the water demand distribution is bound by the hydraulic *capacity of the conveyance and distribution network*. The spatial distribution of irrigation volumes previously determined can be translated in many possible *flow rate configurations*. The hydraulic verification of the conveyance network can be performed starting from the heaviest condition, i.e. simultaneous operation of all the outlets demanding water. In case of malfunctioning, alternative flow rate configurations may be identified which are compatible with the hydraulic capacity of the network.

Therefore, with the availability of different tools, such as numerical simulation models and remote sensing techniques, it is possible to create an effective link between agrohydrological and engineering aspects for simulating the operation of an on-demand irrigation system. The flow of information and the cross-checking of data between different modules can be assured by means of Data Base Management Systems and Geographical Information Systems (GIS) (Fig.1.2).

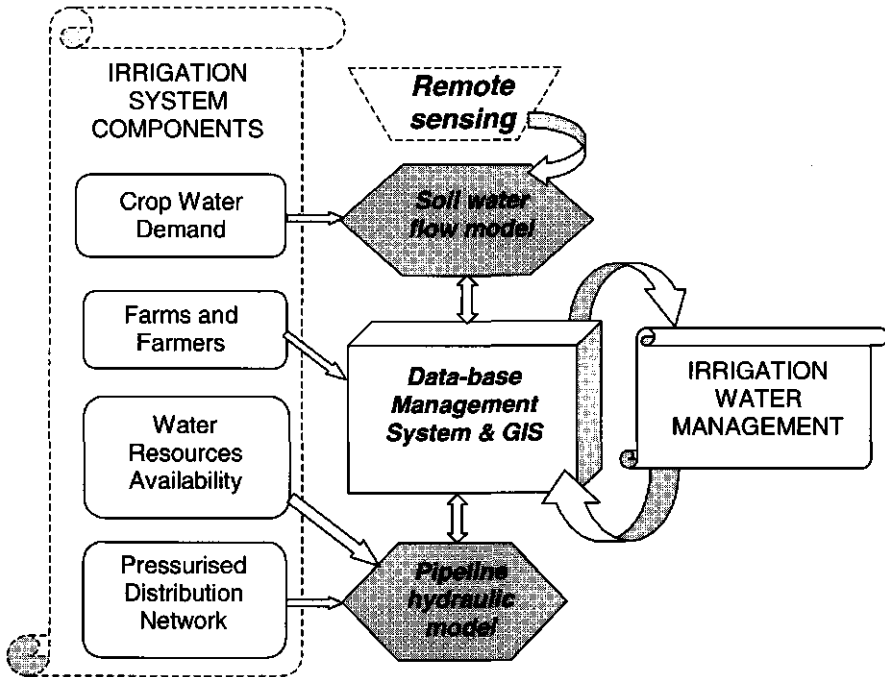


Fig. 1.2 Conceptual diagram of the Decision Support System described in this study.

These techniques may also provide the visualisation of input and output data as maps of easy interpretation for the final user, i.e. the irrigation management board. The result of the integration of hydrological and hydraulic simulation models and remote sensing techniques is a procedure that can be used either during the operation of an irrigation system or in the planning stage.

### 1.3 Overview of the thesis

*The aim of this research is to simulate the behaviour of an on-demand irrigation system by means of a combined use of remote sensing satellite data with a numerical water flow model of the soil-crop system and a hydraulic model of the pressurised conveyance.*

The methodology described in this study involves theoretical aspects in the fields of remote sensing, hydrological and hydraulic modelling. The conceptual schematisation of the operation of an on-demand irrigation district are described in Chapter 2. This schematisation has been applied for the procedure SIMODIS



(Simulation of On-Demand Irrigation Systems) described here. The output of SIMODIS is used to evaluate the irrigation efficiency using indicators defined in this chapter.

In Chapter 3 the estimation of farmers' water requirements from the calculation of the soil water balance with the model of Dam et al., (1997) SWAP (Soil Water Atmosphere Plant) is described. The criteria for the definition of the boundary conditions in the model are outlined, with special concern to the techniques for the regionalisation of SWAP. These include the knowledge of spatially distributed parameters concerning vegetation status and groundwater interaction, needed to define the boundary conditions in SWAP, and the soil hydraulic behaviour. A procedure based on the use of Pedo-Transfer-Functions is proposed for the definition of the soil hydraulic properties.

In Chapter 4, the contribution of remote sensing techniques in the estimation of crop water requirements is discussed. Two different approaches for mapping potential evapotranspiration are analysed. Firstly, the technique for the definition of spectral classes corresponding to different crop coefficient values is described (*classification* approach). Secondly, the possibility of using analytical relationships between the surface reflectance and the geometrical characteristic of the canopy, needed for the calculation of the potential evapotranspiration, is investigated (*analytical* approach).

In Chapter 5, the case study developed for the irrigation district of Gromola in southern Italy is presented. Main aspects of current irrigation management in this area are analysed. Successively, the experimental activities and data acquisition performed to implement SIMODIS are described. In particular, the results of the methodologies described in Chapter 3 for the definition of the lower boundary condition and of soil hydraulic properties in the Gromola irrigation district are reported.

Chapter 6 reports on the application of the crop coefficient mapping algorithms developed in Chapter 3 for the study area. A detailed description of the different steps in the image processing is given. In particular, the methodology applied to estimate the directional spectral reflectance at surface is described. The results of the classification and analytical approaches for mapping crop coefficients in the study area are evaluate.

In Chapter 7, the set-up of SIMODIS for the study area is described. The criteria implemented in SIMODIS to estimate the spatial distribution of farmers' water demand are described. In particular, the algorithm used to simulate the operation and the hydraulics of the pipeline in the conveyance network is

presented. The efficiency of the irrigation system of Gromola is evaluated by means of SIMODIS with the support of field data for the irrigation season 1994.

The use of SIMODIS as decision support system in the study area is described in Chapter 8. The procedure is applied to simulate alternative strategies of water management and to evaluate the resulting performance by means of irrigation efficiency indicators. The impact of the reduction of available water resources is evaluated in some detail.

In Chapter 9, the limitations and the possible future evolutions of the proposed procedure for planning management as well as for real-time operations of the irrigation system are discussed.

Finally, the summary and main conclusions are presented and the main innovative issues of this study highlighted.

## 2 The model SIMODIS (Simulation and Management of On Demand Irrigation Systems).

### 2.1 Schematisation of the irrigation network.

The irrigation water conveyance network is a hierarchic system (Fig. 2.1). The main pipeline of the irrigation network conveys water from the main reservoir or water diversion to each *primary unit*. In the case of pressurised systems, the primary network can be branched or looped. Within each primary unit ( $i$ ), water is conveyed by means of a smaller pipeline to the different delivery devices in each "*secondary unit*" ( $i,j$ ). A secondary unit is a cluster of plots, or "*tertiary units*", served by a common delivery node  $ij$  of the network. A tertiary unit ( $i,j,k$ ) represents the elementary area of the system, such as a cadastral mapping unit, or a portion of it with homogeneous soil and crop. In the schematisation adopted in this study, each tertiary unit is described as a one-dimensional column for which the soil water balance is modelled.

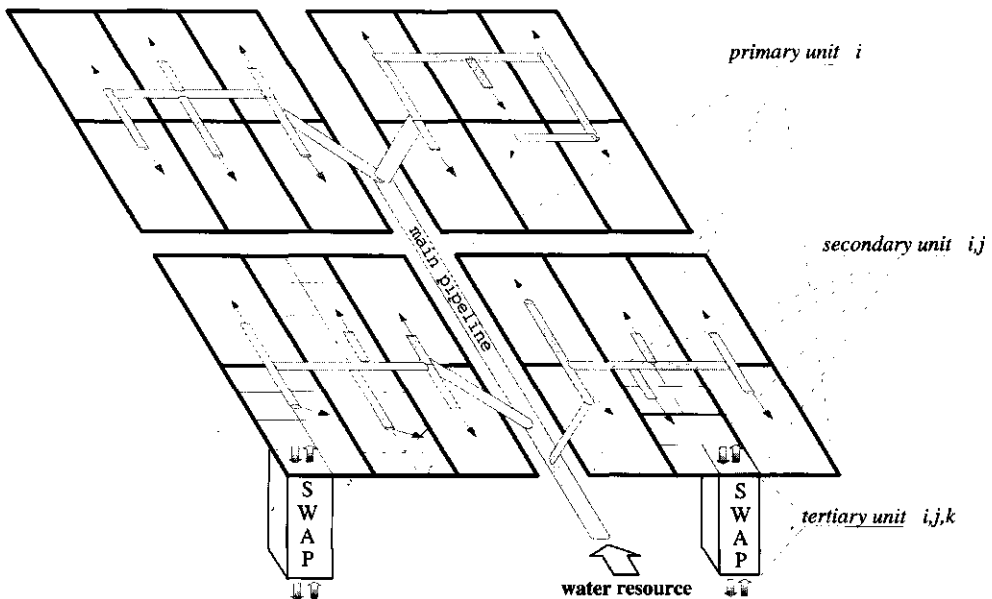


Fig. 2.1 Conceptual schematisation of the irrigation water conveyance network as a hierarchic system.

From the output of the soil water balance model i.e. the vertical distribution of soil water content  $\theta$  and pressure head  $h$ , the soil water deficit is calculated and the tertiary units where critical water stress conditions occur are identified. If one could relate the soil water deficit in each unit to the water volume at the point of delivery, the operation of the irrigation network would be easily simulated. We should first consider three subsequent constraints:

- the outlet is able to deliver the total amount of water required  $I_{ij}$  in each time step;
- the total demand of water is less or equal to the available water;
- the pipelines of the conveyance network are actually able to convey at each outlet the amount of water requested.

These three conditions determine the tertiary units that can be effectively irrigated and the corresponding amount, due account taken of the farmers' irrigation scheduling criteria.

## 2.2 Simulation of on-demand irrigation systems

To simulate the operation of on-demand irrigation systems, the link between the soil water balance in each tertiary units of the irrigation district and the conveyance and delivery network is shown in Fig. 2.2.

Box nr.1 represents the soil water balance from which the soil water deficit is calculated for each day  $d$ . Potential evapotranspiration rates in each tertiary unit  $E_{p_{i,j,k}}$  are determined from *satellite images* and ground meteorological data. Successively, the soil water balance calculations are made. The output of this elaboration in each tertiary unit are the vertical distributions of soil water content and pressure head from which the soil water deficit respect to saturation  $\delta_{i,j,k}$  in the root zone is calculated.

In Box nr.2, the tertiary units needing irrigation are identified on the basis of predefined scheduling criteria. These criteria should be defined in a such a way that they reflect the farmers' attitudes in scheduling irrigation. For these units, the flag  $f_{i,j,k}$  is set to 1. The corresponding volume of irrigation water  $I_{i,j,k}$  is determined as a function  $F$  of the simulated soil water deficit and of the irrigated area  $A_{i,j,k}$ . Assuming a fixed farm efficiency  $\eta_{i,j,k}$ , the amount of water delivered at the outlet of secondary unit  $i,j$  at a given time step is given by the sum of water demand of the corresponding tertiary units  $i,j,k$ :

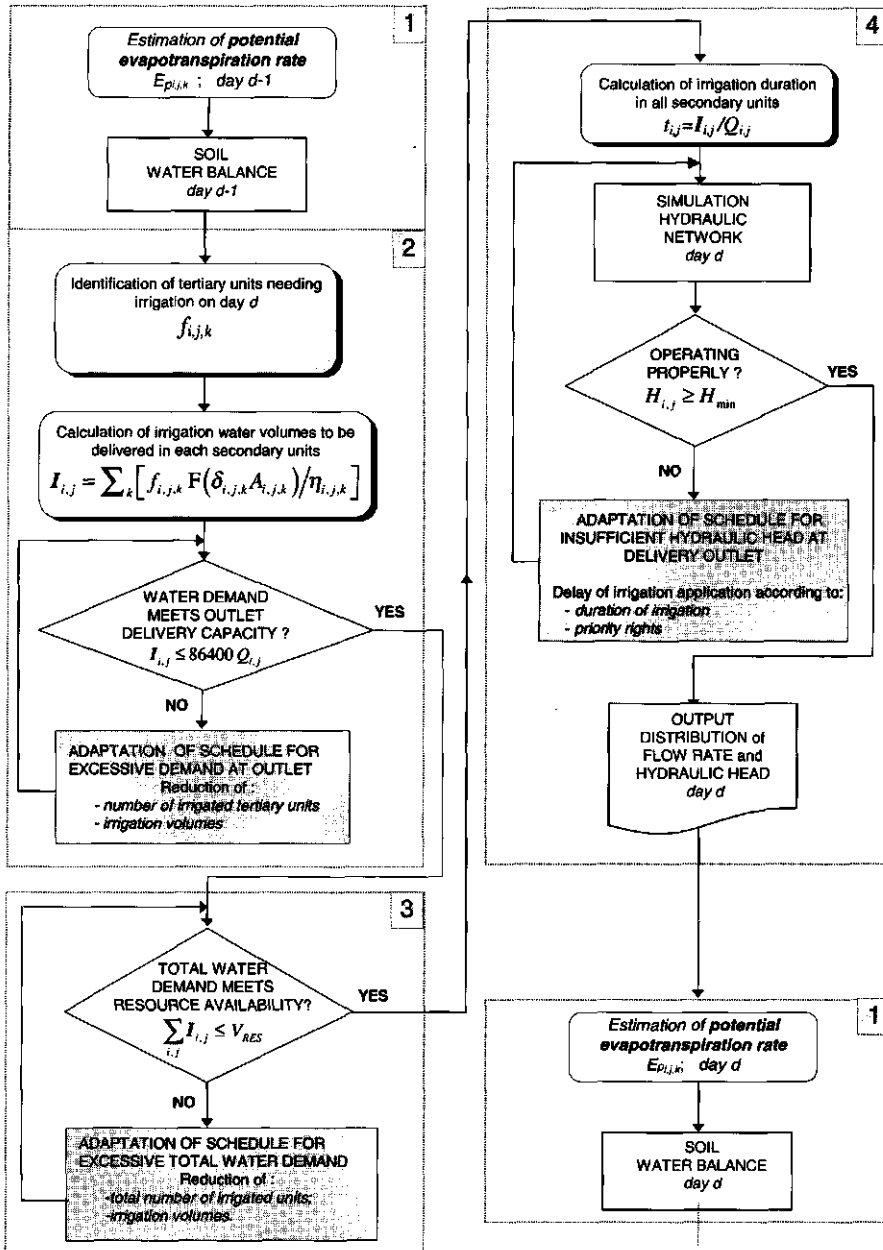


Fig. 2.2 Flow-chart of SIMODIS. Box numbers indicate:  
 1) Spatial variability of soil water deficit (tertiary units)  
 2) Spatial variability of farmers' water demand (secondary units)  
 3) Water resources availability (scheme level)  
 4) Structural capability of the irrigation water conveyance network.

$$I_{i,j} = \sum_k \left[ \frac{f_{i,j,k}}{\eta_{i,j,k}} F(\delta_{i,j,k}, A_{i,j,k}) \right] \quad (2.1)$$

The flow rate in each secondary unit,  $Q_{ij}$ , depends on the constructive characteristics of the outlet and on the value of hydraulic head  $H$ . In many cases, as it happens in networks with limited-rate demand, the outgoing flow rate  $Q_{ij}$  is practically constant for  $H > H_{min}$  over a wide range of  $H$ .

Thus, *condition 1* consists of a comparison between the irrigation volume in Eq.(2.1) with the maximum volume deliverable in one day with a fixed flow rate equal to  $Q_{ij}$ .

The availability of water resources, which represents the *condition 2* is tested in Box nr.3. The irrigation schedule has to be modified if the total irrigation water exceeds the amount of water daily available  $V_{RES}$ .

The simulation of water flow in the pipelines of the conveyance network (Box nr.4) can be run only after the first two conditions are satisfied. At this point, assuming the same starting time for all the irrigation units, the hydraulics of the network is simulated. This configuration corresponds to the peak demand for the considered day. If this step is not successful, i.e. the calculated hydraulic head in certain nodes is too low, it is necessary to modify the distribution of water demand  $\{I_{ij}\}$  given as input. For this purpose, one might consider assigning different levels of priority to each parcel, depending on the duration of irrigation,  $t_{ij}$ , or the crop type. As an alternative, it could be considered to reduce the amount of water application. The water demand distribution  $\{I_{ij}\}$  is corrected and tested again, until the simulation of the conveyance network is successfully completed and *condition 3* is met.

At this point, the water balance calculations for the following date are made assuming that the water deliveries are equal to the last adapted demand distribution.

From the description given above, we see how different models and tools are used in the simulation of the irrigation system. This translates the conceptual scheme presented in Chapter 1 into a computational management tool. The link between remote sensing, hydrological and hydraulic simulation models is provided by the procedure proposed in this study and called 'SIMODIS' (<http://www.simodis.unina.it>). Basically, SIMODIS is a data-base model which interfaces the different modules and simulation tools and enables an easy exchange of data with the users i.e. the irrigation managers. The digital format of SIMODIS data allows their direct introduction in a GIS environment for further analyses. The main attractiveness in using simulation tools lies in the possibility of tuning one or more variables and evaluating the results. To this extent, the described procedure SIMODIS takes into account engineering issues and farmers

water needs in an integrated, deterministic way. This issue is very relevant for the simulation of different scenarios for alternative water management schemes. Thus, it is possible to identify which strategy improves the *efficiency of irrigation* while matching the water demand with the limited capacity of the system in terms of either structural restrictions or water resource availability.

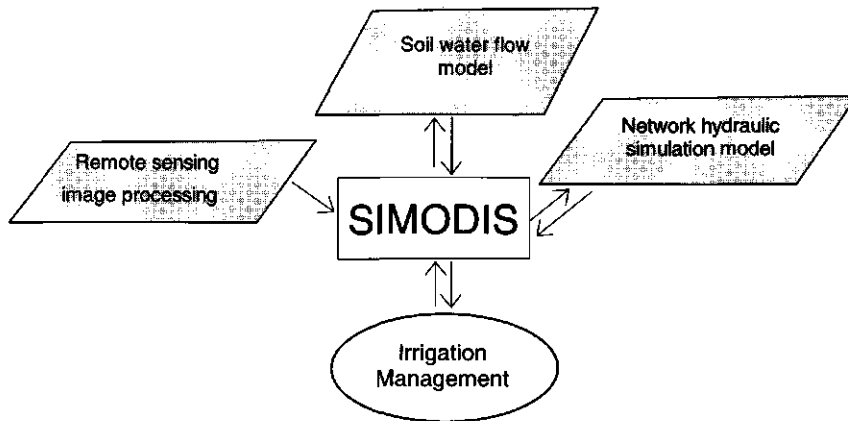


Fig. 2.3 The interface model SIMODIS provides the link between the different technical tools used and the input-output data flow.

### 2.3 Evaluation of the efficiency of irrigation with SIMODIS.

There are several ways to assess the performance of irrigation by means of *indicators* (Wolters, 1992; Solomon et al., 1999). A commonly accepted definition of irrigation *efficiency* has been given by Burt et al. (1997):

$$\varepsilon = \frac{\text{Irrigation water beneficially used}}{\text{Irrigation water applied} - \text{Soil water storage variation}} \quad (2.2)$$

From a general point of view, the optimal value of  $\varepsilon$  is 1; a lower  $\varepsilon$  indicates a possible misuse of irrigation water, while  $\varepsilon$  larger than 1 indicates an insufficient application of irrigation.

As will be described in Chapter 3, it is possible to estimate through SIMODIS on a daily basis the variables needed to calculate  $\varepsilon$  for each tertiary unit. The actual transpiration  $T$  is an estimate of the irrigation water beneficially applied, while the irrigation water volume applied  $I$  results from the final scheduling adaptation of Box nr.4 in Fig. 2.2. Both  $T$  and  $I$  can be calculated for a single day or integrated over a given time interval between two dates  $d_1$  and  $d_2$ . Thus, the irrigation efficiency  $\varepsilon$  for the generic tertiary unit  $i,j,k$  can be estimated by means of the following relationship:

$$\varepsilon_{1,i,j,k} = \frac{\int_{d_1}^{d_2} T_{i,j,k}(n) dn}{\left( \sum_{d_1}^{d_2} \frac{I_{i,j,k}(n)}{A_{i,j,k}} \right) - \Delta W_{i,j,k}} \quad (2.3)$$

In Eq.(2.3) the variable  $n$  represents the generic day of simulation and  $\Delta W_{i,j,k}$  is the variation of soil water storage in the time interval ( $d_2-d_1$ ).

The efficiency indicator at the upper hierarchic levels i.e. the secondary and primary units is defined as the average values of  $\varepsilon_{1,i,j,k}$  for the corresponding tertiary units. Since the conveyance losses can be neglected for pressurised irrigation system, the aggregated value of  $\varepsilon_1$  is also valid to evaluate the efficiency of the entire irrigation system.

To consider the influence of local hydrological conditions on the performance of irrigation, the indicator introduced in similar form by Menenti et al. (1990) has been used:

$$\varepsilon_{2,i,j,k} = \frac{\int_{d_1}^{d_2} [T_{i,j,k}(n) - T_{i,j,k}^*(n)] dn}{\left( \sum_{d_1}^{d_2} \frac{I_{i,j,k}(n)}{A_{i,j,k}} \right) - \Delta W_{i,j,k}} \quad (2.4)$$

where  $T_{i,j,k}^*$  represents the transpiration that would have occurred in absence of irrigation. This indicator assess the *effectiveness* of irrigation resulting from the application of a given irrigation volume  $I_{i,j,k}$ , compared to non-irrigated conditions. The main difference with  $\varepsilon_1$  is that  $\varepsilon_2$  takes implicitly into account the rainfall, the soil hydraulic behaviour and the interaction between unsaturated soil and groundwater flow. Therefore, the value of  $\varepsilon_2$  depends strongly on the actual hydrological and pedological conditions and it is usually lower than 1. Assuming that transpiration under irrigated conditions is equal to sum of the specific water volume applied and soil water storage variation, a value of  $\varepsilon_2 = 0.2$  means an increment of 20% of transpiration compared to non-irrigated conditions.

The efficiency indicators  $\varepsilon_1$  and  $\varepsilon_2$  will be used to compare different scenarios corresponding to alternative water management strategies. It should be noticed that low values of  $T$  and  $I$  in Eqs.(2.3) and (2.4) may produce values of indicators  $\varepsilon_1$  and  $\varepsilon_2$  close to 1. Therefore when different scenarios are compared on the basis of the values of  $\varepsilon_1$  and  $\varepsilon_2$ , it should be verified that the ratio  $T/T_p$  between actual and potential transpiration  $T_p$  is not much smaller than 1.



### 3 Spatial distribution of farmers' water demand

---

#### 3.1 Outline of calculation steps

The first calculation in SIMODIS is represented by the soil water balance from which the soil water deficit in the root zone is assessed. This is done (Fig. 2.2-Box nr.1) for each tertiary unit of the irrigation district in two steps:

- estimation of *evapotranspiration* under conditions of optimum soil water and disease-free well fertilised crops;
- application of the agrohydrological simulation model SWAP, to estimate the actual soil water balance terms and the vertical distribution of soil water content  $\theta$  and pressure head  $h$ .

Successively, the results of these calculations are used in SIMODIS (Box nr.2) to determine the spatial distribution of farmers' water demand, accordingly to pre-defined criteria for the identification of tertiary units demanding irrigation water as well as for the calculation of the corresponding water volume.

#### 3.2 Estimation of evapotranspiration.

The evapotranspiration rate  $E$  ( $\text{cm d}^{-1}$ ) from a canopy uniformly covering the soil surface may be estimated using the well-known combination equation of Penman-Monteith (Monteith, 1965; 1990; Rijtema, 1965):

$$E = \frac{8640}{\lambda} \frac{s(Q^* - G) + c_p \rho_a (e_s - e_a) / r_{a,H}}{s + \gamma(1 + r_c / r_{a,H})} \quad (3.1)$$

where:

$s$  is the slope of the saturated vapour pressure-temperature curve  $e_s(T)$  ( $\text{kPaK}^{-1}$ )

$Q^*$  is the net radiation flux density ( $\text{Wm}^{-2}$ )

$G$  is the heat flux density into the soil ( $\text{Wm}^{-2}$ )

$c_p$  is the air specific heat ( $\text{J kg}^{-1}\text{K}^{-1}$ )

$\rho_a$  is the air density ( $\text{kg m}^{-3}$ )

$(e_s - e_a)$  is the vapour pressure deficit, given by the difference between saturated and actual vapour pressure (kPa) at the given air temperature  $T_a$

$r_{a,H}$  is the *aerodynamic resistance* for heat transport ( $\text{sm}^{-1}$ ), which depends on the wind-speed and on the aerodynamic properties of the surface

$\lambda$  is the latent heat of vaporisation of water ( $\text{J kg}^{-1}$ )

$\gamma$  is the thermodynamic psychrometric constant ( $\text{kPa K}^{-1}$ ), and  $r_c$  is the *canopy resistance* ( $\text{s m}^{-1}$ ), depending on crop physiology.

The minimum set of climatic data needed for the calculation are the air temperature  $T_a$  ( $^{\circ}\text{C}$ ), the relative humidity  $RH$  (%), the wind speed  $U_z$  ( $\text{m s}^{-1}$ ), and the flux density of incoming short wave radiation  $K^{\downarrow}$  ( $\text{W m}^{-2}$ ). The remaining variables in Eq.(3.1) can be either directly measured or estimated from  $T_a$ ,  $RH$ ,  $U$  and  $K^{\downarrow}$  (Smith, 1990; Jensen et al., 1990; FAO, 1998).

In particular, when net radiation flux density is not directly measured, it can be estimated as:

$$Q^* = (1-r)K^{\downarrow} + L^* \quad (3.2)$$

with  $r$  (-) representing the *surface albedo* and  $L^*$  ( $\text{W m}^{-2}$ ) the net incoming long-wave radiation flux density. This latter term can be estimated from  $T_a$ ,  $e_a$  and  $K^{\downarrow}$  (FAO, 1998).

The soil heat flux density,  $G$ , can be related to the net radiation flux density reaching the soil surface. Choudhury et al. (1987) investigated the effects of vegetation cover on the attenuation of net radiation and found the following empirical relationship:

$$G = C_G (-\beta LAI) Q^* \quad (3.3)$$

where the parameter  $C_G \in [0.3; 0.4]$  represents the ratio  $G/Q^*$  for bare soil surfaces;  $\beta$  is an extinction coefficient that can be taken equal to 0.5, although its value varies with canopy geometry and solar zenith angle.

In most practical applications, the resistance  $r_{a,H}$  is calculated as a function of crop height  $h_c$  (m) and wind-speed  $U_z$  ( $\text{m s}^{-1}$ ):

$$r_{a,H} = \frac{\ln\left(\frac{z_U - d}{z_{0m}}\right) \ln\left(\frac{z_T - d}{z_{0h}}\right)}{k^2 U_z} = \frac{\ln\left(\frac{z_U - 0.667h_c}{0.123h_c}\right) \ln\left(\frac{z_T - 0.667h_c}{0.0123h_c}\right)}{0.168 U_z} \quad (3.4)$$

In the argument of logarithmic functions appearing in Eq.(3.4),  $z_U$  and  $z_T$  are respectively the measurement heights for wind-speed and temperature,  $d$  is the zero-plane displacement height and the variables  $z_{0m}$ ,  $z_{0h}$  represent the roughness lengths for momentum and heat respectively being estimated from  $h_c$  (Brutsaert, 1982). Consequently, the resistance  $r_{a,H}$  becomes a function of crop height and wind speed.

The canopy resistance  $r_c$  depends on incoming solar radiation, vapour pressure deficit and soil water status. Under *potential* conditions, i.e. when soil water is not limited, the canopy resistance reaches a minimum value  $r_{c,min}$  that can be estimated using the expression (Szeicz and Long, 1969; Jensen et al., 1990):

$$r_{c,\min} = \frac{r_{leaf,\min}}{LAI_{eff}} \quad (3.5)$$

In Eq.(3.5)  $r_{leaf,\min}$  is the minimum stomatal resistance of a single leaf, approximately equal to  $100 \text{ s m}^{-1}$  (Allen, 1986) and  $LAI_{eff}$  is the fraction of leaf area index  $LAI$  effectively taking part in the evapotranspiration process. It is common to take  $LAI_{eff}=LAI$  until the value of  $0.5LAI_{max}$  is reached, after which  $LAI_{eff}$  is kept constant. Kelliher et al. (1995) showed that a minimum value  $r_{c,\min}=50$  to  $70 \text{ s m}^{-1}$  applies to most crops hence the relationship (3.5) is valid for  $LAI = 4$ . For larger values of  $LAI$ , a constant  $r_{c,\min}$  is taken.

Thus, the *potential evapotranspiration rate of a canopy at full soil cover*  $E_p$  is calculated by means of Eq.(3.1) to (3.5), where, besides the climatic data, the characteristics of the canopy, i.e.  $LAI$ ,  $r$  and  $h_c$ , have to be known.

Equation (3.1) has been recently introduced in the standard FAO procedure to determine crop water requirements (FAO, 1998). In this case, the reference rate  $E_{ref}$  ( $\text{cm d}^{-1}$ ) is calculated for a standard crop with height of

#### Erratum (p. 19)

$$E_{ref} = \frac{8640}{\lambda} \left[ \frac{s(0.77K^4 + L^* - G) + \frac{\rho_a c_p U (e_s - e_a)}{208}}{s + \gamma(1 + 0.34U)} \right] =$$

$$= \frac{8640}{\lambda} \left[ \frac{s(0.77K^4 + L^* - G) + \frac{0.0104 \gamma \lambda U (e_s - e_a)}{T_a + 273.3}}{s + \gamma(1 + 0.34U)} \right] \quad (3.6)$$

In the previous equation, a water density of  $1000 \text{ kg m}^{-3}$  has been implicitly assumed, while  $\rho_a$  and  $c_p$  have been replaced by the following simplified relationships (Jensen et al., 1990):

$$\rho_a = \frac{3.486 p_a}{(T_a + 273)} \quad (3.7)$$

$$c_p = \gamma \frac{0.622 \lambda}{p_a} \quad (3.8)$$

$$c_p = \gamma \frac{0.622 \lambda}{p_a}$$

where  $p_a$  (kPa) is the atmospheric pressure. The constant 8640 in Eqs.(3.1) and (3.6) implies the use of average daily values for the required meteorological data.

When calculating the potential evapotranspiration rate  $E_p$  for other types of crops, it is possible to apply Eq.(3.1), together with equations (3.2) to (3.5) by introducing the appropriate values of parameters  $r$ ,  $LAI$ ,  $h_c$ . Alternatively the use of empirical coefficients  $K_c$  depending on crop type and phenology might be considered:

$$E_p = K_c E_{ref} \quad (3.9)$$

Experimental values of 'crop coefficients'  $K_c$  have been proposed by Doorenbos and Pruitt (1977). Due to its simplicity, the crop coefficient approach is still widely used in irrigation scheduling (FAO, 1998). In reality, the value of  $K_c$  is related to the actual development of the canopy and to the environmental conditions (Stanghellini et al., 1990). By combining Eq.(3.9) with Eq.(3.6),  $K_c$  can be analytically defined as:

$$K_c = \frac{E_p}{E_{ref}} = \frac{[s(Q^* - G) + c_p \rho_a (e_s - e_a) / r_{a,H}][s + \gamma(1 + 0.34 U)]}{\left[ s(0.77K^\downarrow + L^* - G) + \gamma \frac{0.0104 \gamma \lambda}{T_a + 273.3} U (e_s - e_a) \right] [s + \gamma(1 + r_c / r_{a,H})]} \quad (3.10)$$

By substituting Eqs.(3.2) to (3.5) in the respective terms of Eq.(3.10),  $K_c$  can be expressed as an explicit function of the canopy properties,  $LAI$ ,  $r$  and  $h_c$ , and of the meteorological data  $K^\downarrow$ ,  $T_a$ ,  $RH$ ,  $U$ . Therefore, Eq.(3.10) can be synthetically written as:

$$K_c = f(K^\downarrow, T_a, RH, U ; r, LAI, h_c) \quad (3.11)$$

The Penman-Monteith equation (3.1) is valid for a complete soil cover. For canopies not covering completely the soil surface, we need to distinguish between soil evaporation and canopy transpiration. The potential soil evaporation rate  $E_{s,p}$  can be estimated from  $E_p$  as a function of  $LAI$  (Belmans et al., 1983):

$$E_{s,p} = E_p e^{-cLAI} \quad (3.12)$$

where  $c$  is an extinction coefficient. This relationship is in agreement with the approach suggested by Ritchie (1972), which is based on the extinction of net radiation as an exponential function of  $LAI$ .

The potential transpiration rate  $T_p$  is then derived as the residual term between potential evapotranspiration and soil evaporation rates:

$$T_p = E_p - E_{s,p} \quad (3.13)$$

To summarise, the estimation of potential evapotranspiration in SIMODIS is made by means of Eqs.(3.6) and (3.11). Eqs.(3.12) and (3.13) are successively used to complete the input data set for the soil water balance model, as described in the following Section.

### 3.3 The soil water balance model.

The soil water balance model is required in SIMODIS to estimate the soil water deficit (Box nr.1 in Fig. 2.2) and to schedule irrigation (Box nr.2). The variation of soil water content  $\theta(z,t)$  ( $\text{cm}^3 \text{cm}^{-3}$ ) during a given time interval  $\Delta t$  over the soil profile between  $z$  and  $z = 0$  can be expressed by the relationship:

$$\int_0^z [\theta(z,t+\Delta t) - \theta(z,t)] dz = \Delta W = (P_n + I_n - E_s - T + v)\Delta t \quad (3.14)$$

Eq.(3.14) is the continuity equation in finite differences form for a given soil profile, where  $\Delta W$  is the change in specific soil water storage,  $P_n$  and  $I_n$  are respectively the precipitation and irrigation rates actually infiltrating through the soil surface,  $E_s$  the actual evaporation rate from the soil,  $T$  the actual transpiration rate from the crop and  $v$  is the water flux density (which can be upward or downward) through the bottom of the soil profile.

Previous models of soil water balance used for irrigation scheduling (Smith, 1992; Singh et al., 1995; FAO, 1996) introduce several simplifications in the calculation of Eq.(3.14). In this type of models, the soil profile is described as a reservoir of given capacity  $W_{max}$ . The influence of the groundwater flow on the soil water balance, represented by  $v$ , is often neglected. Simpler models assume  $E_s = E_{s,p}$  and  $T = T_p$ . In other cases, the actual evapotranspiration rate ( $E_s + T$ ) is calculated by multiplying  $E_p$  with a coefficient that is linearly related to the specific soil water storage  $W$ . Irrigation application is then scheduled when water depletion in the reservoir is larger than a prefixed threshold value. The irrigation volume per unit area is usually taken proportional to the amount of water required to refill the soil to its capacity  $W_{max}$ .

During the last decades, a much better knowledge of water flow in the soil-crop-atmosphere system has been achieved. This progress has led to the development of mathematical models for the numerical simulation of water flow. If carefully calibrated and validated, these models allow for a much better estimation of water balance terms than reservoir models and they can be used in the practical solution of problems related to the precision management of water resources.

In these models, the soil reservoir is a dynamic continuum, where the water flow in the soil-plant-atmosphere system is described (Philip, 1966). The behaviour of this system, often indicated with the acronym SPAC (Soil-Plant-

Atmosphere Continuum), is determined by the soil hydraulic properties, the groundwater flow and the surface conditions.

When unsaturated conditions prevail in a large portion of the soil profile, such as in irrigated areas and semi-arid regions, water flow is mainly in the vertical direction. The temporal variation of soil water content  $\theta(z,t)$  at a given depth can be described by means of the following differential equation (Hillel, 1998; Feddes et al., 1988; Santini, 1992):

$$\frac{\partial \theta}{\partial t} = \frac{\partial}{\partial z} \left[ k(h) \cdot \left( 1 + \frac{\partial h}{\partial z} \right) \right] - S \quad (3.15)$$

where  $k(h)$  ( $\text{cm d}^{-1}$ ) is the unsaturated hydraulic conductivity,  $h$  is the soil water pressure head,  $z$  is the vertical coordinate (positive upward) and  $S$  is the water uptake by roots per unit volume of soil per time ( $\text{cm}^3 \text{cm}^{-3} \text{d}^{-1}$ ). This equation results from the combination of the mass conservation equation and the equation of Darcy extended for water unsaturated soils (Hillel, 1998).

According to the model proposed by Feddes et al. (1978), root water uptake  $S$  can be described as a function of  $h$ :

$$S = S(h) = \alpha(h) S_{\max} = \alpha(h) \frac{T_p}{z_r} \quad (3.16)$$

with  $z_r$  (cm) being the thickness of the root zone and  $\alpha(h)$  a semi-empirical function of pressure head  $h$ . As shown in Fig. 3.1, the shape of the function  $\alpha(h)$  depends on four critical values of  $h$ , which are related to the type of crop and to the potential transpiration rates.

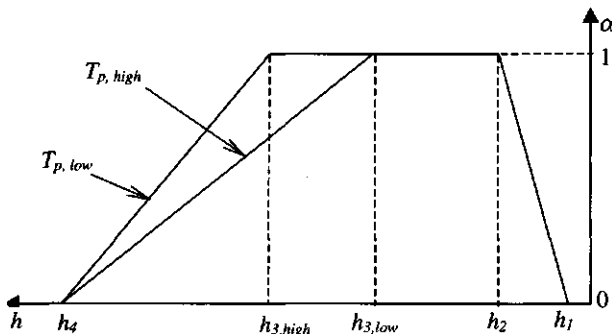


Fig. 3.1 Root water uptake function  $\alpha(h)$ ; the critical values of pressure head  $h$  are crop-dependent;  $h_3$  has two different values respectively for high and low potential transpiration rate (after Feddes et al., 1978).

Eqs.(3.15) and (3.16) are the basic relationships of the agrohydrological model SWATRE, which is widely used for the simulation of soil and crop water balance (Belmans et al., 1983; Feddes et al., 1988). Several improvements to

SWATRE and the inclusion of solute transport and crop growth models have led to the present comprehensive simulation tool named SWAP (Dam et al., 1997).

The Eqs.(3.15) and (3.16) are solved to determine the vertical distributions of pressure head  $h(z,t)$  and soil water content  $\theta(z,t)$  and all the terms of water balance for each time step. Eq.(3.15) for a soil profile of depth  $z^*$  of known hydraulic characteristics functions  $\theta(h,z)$  and  $k(h,z)$  is solved numerically. This requires the definition of the initial condition, that is the distribution  $h(z,t=0)$  or  $\theta(z,t=0)$ , and the conditions on the boundaries, at  $z=0$  and  $z=-z^*, \forall t>0$ .

### 3.4 Calculation of farmers' water demand

The analysis of the distributions  $h(z,t)$  and  $\theta(z,t)$  is a valuable guidance for irrigation scheduling and several applications at farm scale are reported in literature (Wesseling et al., 1988; Feddes et al., 1992; Elmaloglu et al., 2000). Irrigation schedules and volumes can be fixed according to the values of  $\theta$  and  $h$  in the root zone (Dam et al., 1997).

In SIMODIS, irrigation should be applied when a threshold value  $h_{crit}$  for pressure head is reached in the root zone (or at a given depth). The value of  $h_{crit}$  is taken within the interval  $[h_s; h_a]$  of the root water uptake function in Fig. 3.1, thus indicating the occurrence of water stress. In the same instant of time, the soil water deficit  $\delta$  (cm) in a given portion of the soil profile between  $z$  and  $z+\Delta z$  is given by the expression:

$$\delta = \int_z^{z+\Delta z} [\theta_s(z) - \theta(z)] dz \tag{3.17}$$

The irrigation water volume to be applied can be either a prefixed amount or it is calculated as a fraction  $i_r$  of the soil water deficit  $\delta$ . In this latter case the irrigation volume  $I_o$  ( $m^3$ ), net of water losses due to on-farm distribution equipment, is:

$$I_o = 100 i_r \delta A \tag{3.18}$$

where  $A$  is the irrigated area (ha). The value of  $i_r$  depends on the irrigation criteria adopted by individual farmers and it can be determined from field measurements of irrigation volumes applied in coincidence of simulated or measured soil water deficit  $\delta$ .

In SIMODIS, the identification of tertiary units to be irrigated and the calculation of the corresponding water volume are done in the step represented by Box nr.2 of Fig. 2.2. By introducing for each tertiary unit the corresponding value of on-farm efficiency  $\eta_{i,j,k}$  and the identification flag of irrigated units  $f_{i,j,k}$  in Eq.(3.18) we derive the distribution of *farmers' water demand* on a given day:

$$\{I_{i,j,k}\} = 100 \frac{f_{i,j,k}}{\eta_{i,j,k}} i_r \delta_{i,j,k} A_{i,j,k} \tag{3.19}$$

Eq.(3.19) is similar to Eq.(2.1) with the function  $F$  given by the product  $i_r \delta_{i,j,k} A_{i,j,k}$ .

An example of calculated profiles of  $h(z,t)$  and  $\theta(z,t)$  is given in Fig. 3.2. The simulation refers to a three-layered soil, with a ground water table at 2 m depth. In this example, the assumed threshold is  $h_{crit} = -500$  cm. At time  $t$  the average pressure head in a portion of soil profile, i.e. the root zone between  $z_1$  and  $z_2$ , has a value of  $-636$  cm, which is lower than  $h_{crit}$  (Fig. 3.2.a). When this condition occurs, irrigation should be applied. At the same instant  $t$ , the soil water deficit respect is equal to  $6.5$  cm (Fig. 3.2.b). Assuming  $i_r = 0.4$ , the irrigation volume per unit area in this case is  $2.6$  cm.

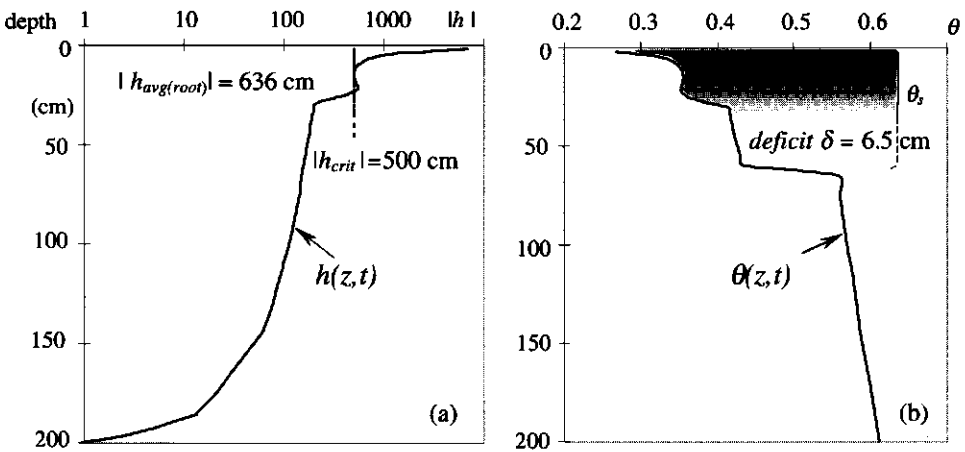


Fig. 3.2 Example of SWAP output concerning the vertical distribution of pressure head  $h$  (a) and soil water content  $\theta$  (b) in a three-layered profile with the ground water table at 2 m depth at time  $t$ . Critical values of pressure head and soil water deficit in the root zone are used to determine irrigation schedules and amounts.

### 3.5 Definition of boundary conditions.

The boundary conditions for the solution of Eqs.(3.15)-(3.16) are expressed in terms of the dependent variable  $h$  (“Dirichlet” condition) or the exchanged flux densities through the boundaries (“Neumann” conditions).

At the upper boundary and in absence of ponds the water flux density  $v^*$  through the soil surface during a time step  $\Delta t$  can be calculated as:



$$v^* = \text{MIN} \left\{ \left[ -k(h) \left( \frac{\partial h}{\partial z} + 1 \right) \right]; (E_s - P_n - I_n) \right\} \quad (3.20)$$

The first term in the minimum function of Eq.(3.20) is the Darcian soil water flux across the surface and it can be either positive i.e. directed upward, or negative, such as in the case of infiltration. Under saturated conditions Eq.(3.20) can be calculated assuming  $h = 0$  at  $z = 0$  or  $h = h_p$  if ponds are presents. In absence of infiltration, the value of  $h$  at  $z = 0$  is considered in equilibrium with the atmosphere and can be calculated from the state equation of air with known temperature and relative humidity. Details on the algorithm used in SWAP to determine the exact expression of the upper boundary condition can be found in Dam et al. (1997).

The potential soil evaporation rate and the amount of intercepted precipitation are determined by the vegetation cover at the soil surface and by the climatic variables. Among the variables describing the vegetation cover,  $K_c$  and  $LAI$  have the largest impact on the upper boundary condition. In particular, the  $LAI$  is used to estimate the soil evaporation and the canopy transpiration, as shown by Eq.(3.12) and (3.13), and the amount of precipitation and irrigation water intercepted by the canopy. In SIMODIS the semi-empirical model of interception described by Braden (1985) is applied. This model is expressed by the relationship:

$$P_n = P - aLAI \left( 1 - \frac{1}{1 + \frac{s_c \cdot P}{aLAI}} \right) \quad (3.21)$$

where  $P$  is the precipitation above the canopy ( $\text{cm d}^{-1}$ ),  $a$  ( $\text{cm d}^{-1}$ ) is an empirical parameter representing the crop saturation per unit foliage area ( $\approx 0.28$  for most crops) and  $s_c$  (-) is the fractional vegetation cover, which can be related to  $LAI$  by means of empirical relationships. A relationship similar to Eq.(3.21) is used to estimate  $I_n$  where  $P$  is substituted by  $(I/A)$ .

The boundary condition at the *bottom* of the considered one-dimensional soil column can be defined in three ways by specifying: i) a value of the pressure head at the bottom, ii) a fixed flux density through the bottom, or iii) a flux density through the bottom as a function of groundwater table depth. The first type of condition is often used when groundwater depths recordings are available. This type of condition, however, can not be used in scenario simulations, unless the water table depth is artificially fixed. The second option may be taken when it is possible to identify an impermeable layer, which determines a "zero" flux, or when the water table is deep enough to leave the soil profile unsaturated, so that the percolation flux density equals the value of hydraulic conductivity for the prevailing pressure head at the bottom (unit gradient).

In many situations, these bottom boundary conditions are not realistic: the soil profile is partially saturated in the upper portion and there is some exchange of water with the under-laying water saturated aquifer. In such cases, the flux through the bottom of the soil profile can be related to the depth of the groundwater table. This third type of condition was introduced by Belmans et al. (1983) to relate the drainage rates to the average groundwater table depth  $\phi$ . A typical form of flux-head relationship  $v(\phi)$  is given by the expression:

$$v = a \exp(b|\phi|) \quad (3.22)$$

Similar relationships have been found by Ernst and Feddes (1979) for different types of soils and areas in the Netherlands. The coefficients  $a, b$  in Eq.(3.22) have to be determined empirically for each soil-aquifer system by means of local experiments or regional groundwater flow studies (Bakel, 1986).

### 3.6 Regional application of SWAP to irrigation districts.

In the schematisation adopted in SIMODIS (Fig. 2.1) the model SWAP is applied in distributed form by considering each tertiary unit of the irrigation system as a one-dimensional independent column. The application of SWAP in this distributed form requires the knowledge of the spatial and temporal distribution of the input variables, with special regard to the boundary conditions and to the soil hydraulic characteristics  $\theta(h)$  and  $k(h)$  (Fig. 3.3)

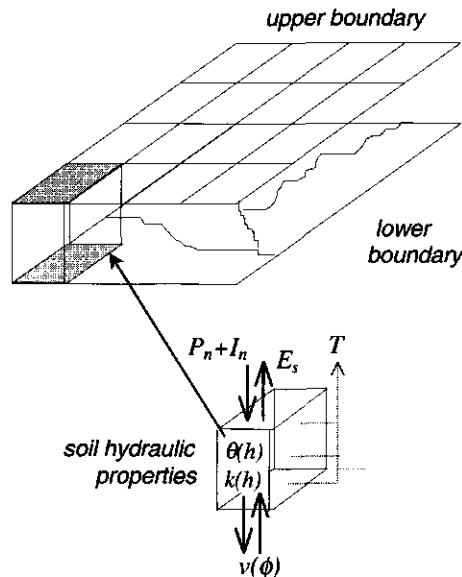


Fig. 3.3 Schematisation for the application of SWAP in SIMODIS: the spatial distributions of the upper and lower boundary conditions as well as the soil hydraulic properties are required.

As described in Section 3.5, the upper boundary condition is dominated by the status of vegetation which can be parameterised by  $LAI$  and  $K_c$ . These variables may largely differ over short distances (in the order of tens of meters) and relatively short time-lags (a few days to few weeks). Conversely, the lower boundary has a much coarser variability in space and in time which can not be easily identified.

The study of the spatial variability of soil hydraulic characteristics is *per se* a subject of study for soil scientists and different approaches have been attempted to tackle this problem (Wösten et al., 1986; Genuchten et al., 1992; Warrick, 1998).

The collection of all the input data of SWAP for each tertiary unit of an irrigation area can be very costly and time consuming. It is thus needed to set up methodologies to reduce such costs and to minimise the time required. Moreover, a compromise is needed between the accuracy of the results and the effort required for the acquisition of input data.

### 3.6.1 *Spatial distribution of the upper boundary condition.*

The flux densities of soil evaporation, transpiration and infiltration, which determine the upper boundary condition, are estimated from the meteorological data and from the status of vegetation cover by means of the relationships described in Sections 3.2 and 3.5. More precisely, for given climatic conditions, the spatial distribution of fluxes across the upper boundary is mostly related to the canopy variables, as shown by Eqs.(3.9) to (3.13) and (3.21). Thus, assuming that the meteorological data are uniform over a certain area, *the spatial distribution of the upper boundary condition is governed by the canopy variables, i.e.  $r$ ,  $LAI$ ,  $h_c$  or  $K_c$  and  $LAI$ .*

It is possible to calculate directly  $E_p$  by using Eqs.(3.1) to (3.5) with the appropriate values of  $r$ ,  $LAI$  and  $h_c$ ; alternatively, the corresponding  $K_c$  values can be calculated from Eq.(3.10). This second option is preferred in SIMODIS because of the reduced run-time required, since only the temporal series of  $K_c$ ,  $LAI$  for each plot and  $E_{ref}$  are input to the SWAP module of the procedure. If  $K_c$ -tables are used instead of Eq.(3.10), a separate estimation of  $LAI$  is needed to calculate  $E_s$  from Eq.(3.12). As mentioned in the introduction, remotely sensed images can be processed for estimating the canopy variables and the crop coefficient. The methodologies for achieving this task will be described in detail in Chapter 4. In practice, *image processing provides a raster map of  $K_c$  for each acquisition date.* Then, by crossing the boundary map of tertiary units with the  $K_c$  map, the average value of  $K_c$  of each tertiary unit can be calculated. Finally, a linear interpolation can be applied between two consecutive remote acquisitions to estimate the  $K_c$  for any intermediate date.

### 3.6.2 *Spatial distribution of the lower boundary condition.*

The condition at the lower boundary of the soil profile is expressed by the relationship  $v(\phi)$  between the flux (positive or negative) across the lower boundary and the groundwater table depth  $\phi$ . As mentioned in Section 3.5, this function can be estimated from field measurements or from groundwater flow simulation models.

Three-dimensional groundwater flow can be described by means of finite-elements techniques (Bear and Verruijt, 1987). In some models, i.e. SIMGRO (Querner et al., 1989), the groundwater flow can be coupled with the unsaturated soil water flow. In each node of the horizontal finite-element grid of SIMGRO, the flux exchange between the unsaturated soil and the saturated groundwater system is simulated by means of a simple model representing the root zone and the subsoil. Therefore, for each time step, i.e. one day, SIMGRO gives the groundwater depth  $\phi$  and the exchanged flux  $v$ . If the groundwater model has been validated and a good agreement is found between simulated and measured water table depths, the simulated values of  $\phi$  and  $v$  can be used to find out an analytical function  $v(\phi)$ . A data set comprising simulated values of  $v$  and  $\phi$  during dry and wet periods can be considered to represent the possible range of groundwater table fluctuations. The empirical relationship  $v(\phi)$  depends also on the soil properties and it can be considered as a concise description of the interactions between soil and groundwater flow. From the output of the groundwater flow model, the function  $v(\phi)$  can then be calculated in each node of the finite element grid.

An example of this elaboration is shown in Fig. 3.4. The fitting curve in Fig. 3.4.c represents the function  $v(\phi)$  in the considered node and it can be defined by means of regression techniques.

In order to reduce the amount of calculation required, the function  $v(\phi)$  can be determined by averaging the output data of adjacent nodes with similar soil characteristics. Doing so, the influence on the model output deriving from the variability of the conditions at the soil surface, i.e. land use and vegetation, can be smoothed.

### 3.6.3 *Spatial distribution of the soil hydraulic characteristics.*

The hydraulic characterisation requires the collection and the analysis of undisturbed soil samples of adequate volume (Boels et al., 1978; Wendroth et al., 1993). Due to the spatial variability of soil hydraulic properties, the field and laboratory work needed for the characterisation of large areas, i.e. an irrigation district, was developed.

Many studies try to relate the soil hydraulic characteristics to more easily measurable variables such as textural data, by means of so-called pedo-transfer-functions, shortly PTF (Genuchten et al., 1992; Romano and Santini, 1997).

An advantage of this approach is that soil texture data, i.e. obtained from soil

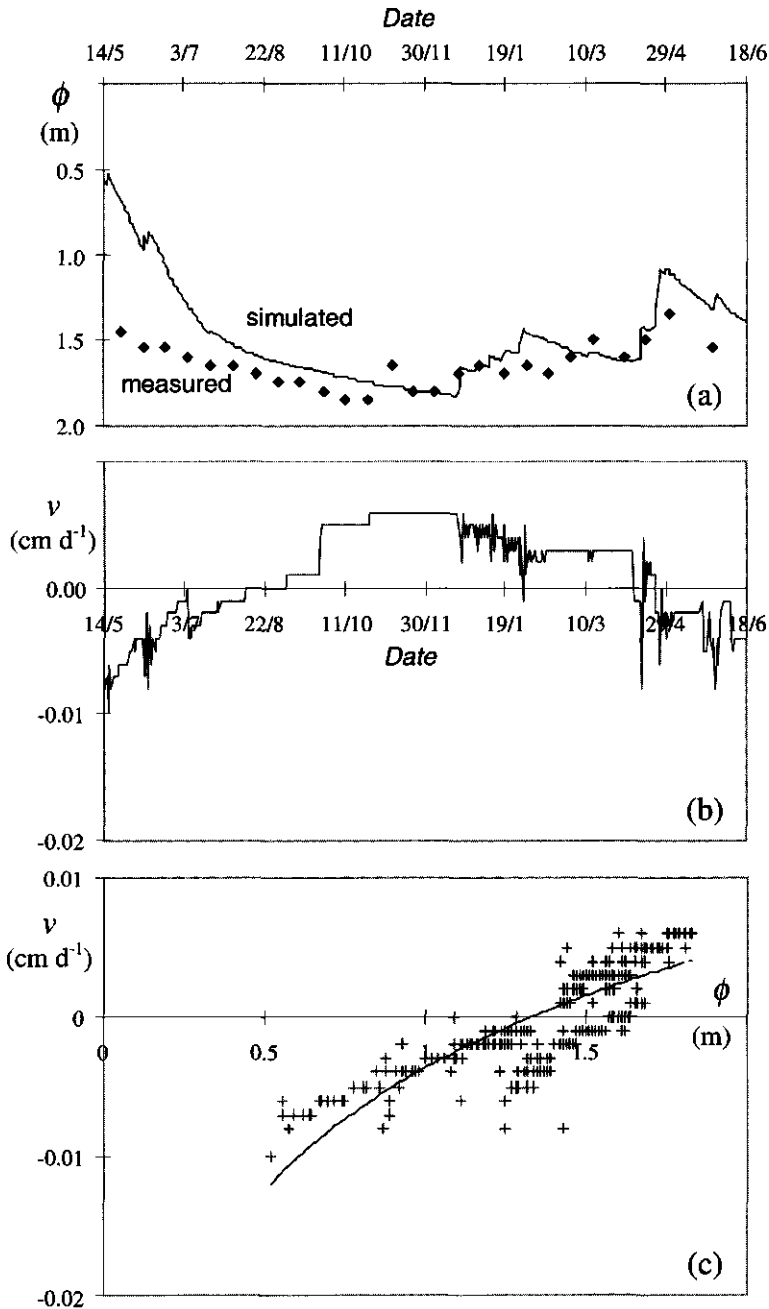


Fig. 3.4 Derivation of the relationship  $v(\phi)$  from the output of the groundwater model SIMGRO: (a) Simulated values of groundwater table depth  $\phi$ ; (b) Flux exchanged between the subsoil layer and the groundwater; (c): Combined together as  $v(\phi)$ . Positive fluxes indicate capillary rise.

surveys, are more widely available than soil hydraulic functions. Recently, efforts have been made to build comprehensive data-bases relating laboratory and field observations of soil water retention and hydraulic conductivity to other soil physical data derived from pedological surveys (Wösten, 1999).

On the basis of these concepts, D'Urso and Basile (1997) have proposed a method for mapping the soil hydraulic characteristics, which is based on the use of calibrated pedo-transfer-functions. The method consists of the following steps:

1. calibration of the pedo-transfer-function in each soil mapping unit to estimate  $\theta(h)$  and  $k(h)$  from soil textural data in selected locations within the area surveyed;
2. definition of homogeneous hydrological mapping units from the spatial distribution of so-called '*functional properties*' (Wösten et al., 1986) derived from SWAP by using the  $\theta(h)$  and  $k(h)$  curves determined in step 1.

The method is particularly applicable if a sufficiently detailed soil map i.e. at scale 1:10.000 is available.

*Calibration and application of pedo-transfer-functions to estimate  $\theta(h)$  and  $k(h)$ .* Models describing the soil water retention function  $\theta(h)$  are mainly based on the schematisation of pore-size distribution in relation to soil particle-size distribution. If we divide the particle size distribution curve in different ranges  $[M_i, R_i]$ , where  $M_i$  is the solid mass fraction and  $R_i$  the particle radius in a generic  $i^{\text{th}}$  textural class, we can relate  $M_i$  to the corresponding pore volume and soil water content  $\theta_i$  by means of the equation:

$$\theta_i = \frac{(\rho_p - \rho)}{\rho_p \sum_{j=1}^i M_j} \quad (3.23)$$

where  $\rho_p$  is the particle density and  $\rho$  the soil bulk density.

The pore radius  $\varphi_i$  in the same  $i^{\text{th}}$  class can be converted to soil water pressure head  $h_i$  by means of the known equation of capillarity:

$$|h_i| = \frac{2\sigma_w \cos \tau}{\varphi_i \rho_w g} \cong \frac{0.15}{\varphi_i} \quad (3.24)$$

where  $\sigma_w$  is the surface tension of water,  $\tau$  is the contact angle between water and surface of soil particles,  $\rho_w$  is the density of water and  $g$  the gravity acceleration. Thus, if we can determine the pore radius  $\varphi_i$  we can associate to each  $[M_i, R_i]$  a pair of values  $[\theta_i, h_i]$ .

The relationship between  $R_i$  and  $\varphi_i$  is related to the geometry of pores within the soil, which can be very complex, especially in fine-textured and structured soils. In the physical-empirical model of Arya and Paris (1981), the pore

radius  $\phi_i$  and the corresponding particle radius  $R_i$  are related by means of the expression:

$$\phi_i = R_i \sqrt{\frac{2}{3} \left( \frac{\rho_p - \rho}{\rho} \right) n_i^{(1-\psi)}} \quad (3.25)$$

where  $n_i$  is the number of spherical particles in the  $i^{\text{th}}$  range and  $\psi$  is an empirical constant (-). The variable  $n_i$  can be determined from the solid mass fraction  $M_i$  corresponding to the particle radius  $R_i$  by means of the expression:

$$n_i = \frac{3M_i}{4\pi R_i^3 \rho_p} \quad (3.26)$$

The constant  $\psi$  has been introduced in Eq. (3.25) to account for the geometrical differences between uniform packing of spherical particles and a natural soil. Arya and Paris found that  $\psi$  can be taken equal to 1.38 for a variety of soil types. By analysing retention data obtained on undisturbed samples, Basile and D'Urso (1997) found that the relationship between  $R_i$  and  $\phi_i$  can be very different from that resulting from Eq.(3.25) with  $\psi=1.38$  (Fig. 3.5).

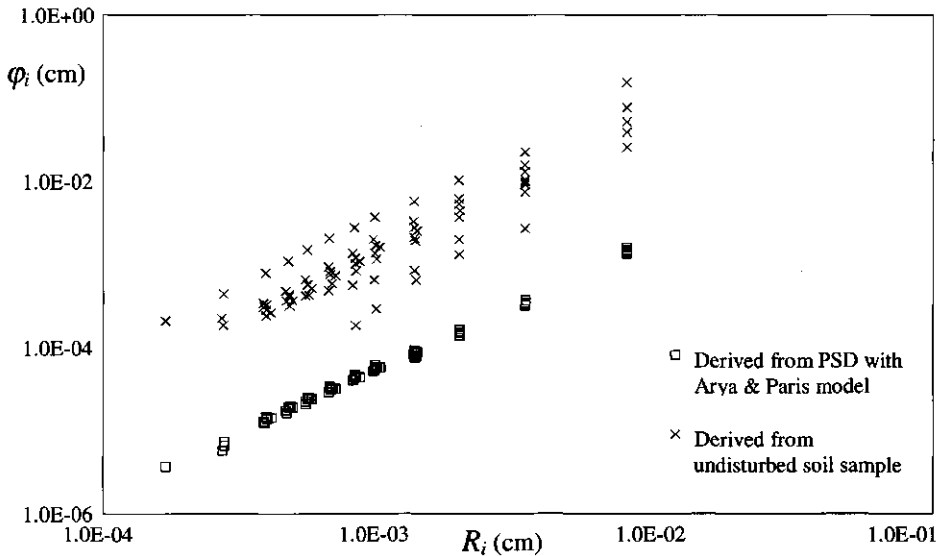


Fig. 3.5 Plot of particle radius,  $R_i$ , and pore radius values,  $\phi_i$ , of a clay-loam soil derived from laboratory investigations and from the Arya and Paris model.

The plot in Fig. 3.6 shows that the assumption made by Arya and Paris is acceptable for sandy soils, but not for the clay-loam soil considered in this example. In the case of the clay-loam soil in Fig. 3.6, the function  $\psi(h)$  is strongly

non linear with an asymptotic value around 1.1. Similar results on other fine-textured soils have confirmed that  $\psi$  cannot be considered constant as in Eq.(3.25) but is a function of the pressure head  $h$ :

$$\phi_i = R_i \sqrt[3]{\frac{2(\rho_p - \rho)}{\rho}} n_i^{[1-\psi(h)]} \tag{3.27}$$

By means of the calibration procedure described by Basile and D'Urso (1997) the  $\psi(h)$  function is derived from retention data observed on undisturbed samples of a representative profile in each mapping unit. The calibrated function  $\psi(h)$  is then introduced in Eq.(3.25) to extract a set of values of  $[R_i, \phi_i]$ , corresponding to  $[\theta_i, h_i]$ , for each location where textural information is available.

The resulting  $[\theta_i, h_i]$  were used to estimate the parameters  $\{\theta_s, \theta_r, \alpha_{VG}, n_{VG}\}$  of the function  $\theta(h)$  in the analytical form defined by van Genuchten (1980):

$$\theta = \theta_r + \frac{\theta_s - \theta_r}{\left(1 + |\alpha_{VG} h|^{n_{VG}}\right)^m} \tag{3.28}$$

where  $m = (1 - 1/n_{VG})$ .

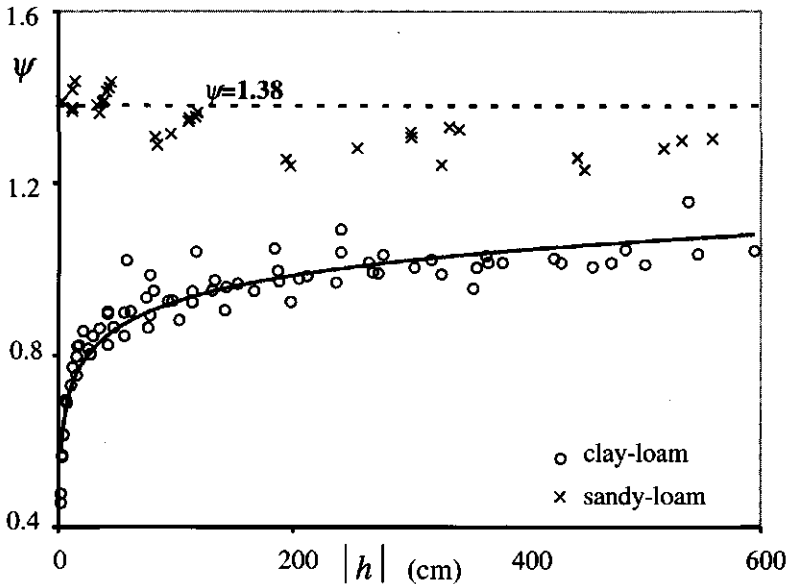


Fig. 3.6 : Relationship between the empirical parameter  $\psi$  and soil water pressure head  $h$ .

The estimation of hydraulic conductivity  $k(h)$  is more difficult than that of the retention function and larger errors should be expected (Genuchten and Leij, 1992; Mualem, 1992). If water retention data are available, the soil hydraulic conductivity can be estimated according to the theoretical approach of Mualem



(1976). This model combines an empirical S-shaped curve for the retention function with the pore-size distribution theory of Mualem to derive the analytical expression for the relative unsaturated hydraulic conductivity  $k(h)/k_s$  (Genuchten, 1980):

$$\frac{k(h)}{k_s} = Se^l [1 - (1 - Se^{1/m})^m]^2 \quad (3.29)$$

where  $k_s$  is the hydraulic conductivity at saturation,  $Se$  is given by  $[(\theta - \theta_r)/(\theta_s - \theta_r)]$  and the exponent  $l$  represents a tortuosity factor, which can be fixed at 0.5 (Nielsen and Luckner, 1992). To apply the model of van Genuchten expressed by Eq.(3.29), it is necessary to estimate  $k_s$  with available data. Compared to the retention function, fewer indirect methods have been developed for  $k_s$  and in most cases the resulting accuracy is rather limited. As with  $\theta(h)$ , there are purely empirical methods based on regression analysis with observed data (Jabro, 1992; Rawls et al., 1992) and semi-empirical models such as those proposed by Brutsaert (1968). To determine the value of  $k_s$ , Mishra and Parker (1990) suggested the following empirical relationship, which is also used in this study:

$$k_s = c (\alpha_{vG})^2 \sqrt{(\theta_s - \theta_r)^5} \quad (3.30)$$

where  $c$  is an empirical constant to be determined from reference data.

*Spatial distribution of functional properties for mapping homogeneous hydrological units.* Having estimated the hydraulic characteristic functions in selected locations, we need to extend this information to each tertiary unit of the irrigation district (Fig. 2.1). Geostatistical techniques that are intensively used in many soil surveys (Webster and Oliver, 1990; Warrick, 1998) could be applied to produce local estimations of the soil hydraulic properties, but these techniques require large data sets to determine the bi-dimensional spatial variability of the soil parameters investigated.

The methodology used in this study is based on a crossing of information between the soil map and the soil hydraulic data obtained in the previous step. This latter data set is used to calculate by means of SWAP some *functional properties* (Wösten, 1986). The functional properties represent a practical way to describe the hydrological behaviour of the whole soil profile, assuming specific water management criteria and boundary conditions (Hack-ten Broeke et al., 1996). For the purpose of the present study, the functional properties were defined as the time required to reach a specified value of pressure head  $h$  at certain soil depths. In each profile, a drying process starting from near saturation is simulated with SWAP assuming an uniform grass cover with a constant potential evapotranspiration flux and a fixed groundwater table depth at the bottom of the soil profile. From the output of simulation runs, the mean value of pressure head  $h$  within a portion of the soil profile, i.e. between 10 and 30 cm soil depth, is computed for each day. An example of this elaboration is shown in Fig. 3.7.

The spatial distribution of functional properties indicates the areas with similar hydrological behaviour. By crossing the boundaries of the soil mapping units and the areas with similar values of functional properties, a new map is derived with units characterised by similar pedological characteristics and functional properties. The boundaries of the new mapping units can be drawn by applying a discrete technique of interpolation or by means of visual interpretation.

Finally, for the main soil horizons of each new mapping unit one set of soil hydraulic parameters describing  $\theta(h)$  and  $k(h)$  is found and used for the application of SWAP in the same area.

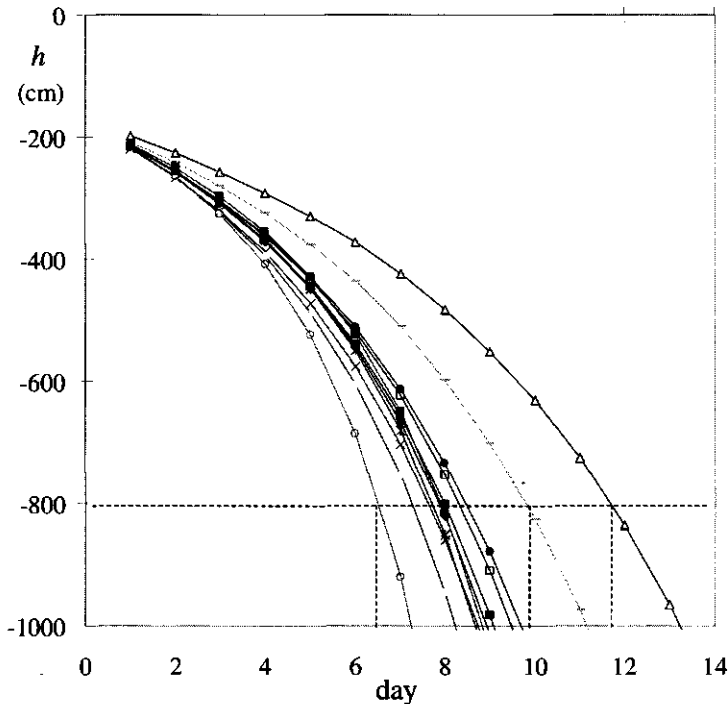


Fig. 3.7 Decrease of soil water pressure head  $h$  at the 10-30 cm soil depth for different profiles of the same soil mapping unit. The functional property has been defined as the number of days required to reach the value  $h = -800$  cm.

### 3.7 Conclusions

In this chapter the approach to estimate the spatial distribution of farmers' water demand has been presented. To achieve this task the one-dimensional soil water flow model SWAP was applied for each tertiary unit of the irrigation district, thus obtaining the spatial distribution of soil water deficit at any given

time. The simulated application of irrigation water in SIMODIS is scheduled on the basis of the soil water content  $\theta(z)$  and pressure head profiles  $h(z)$ .

The application of SWAP in distributed form requires the knowledge of the spatial distribution of the boundary conditions and of the soil hydraulic characteristics.

To determine the upper boundary condition the potential transpiration rate  $T_p$ , the soil evaporation rate  $E_{s,p}$  and the net precipitation rate  $P_n$  were required. These quantities were calculated from the agrometeorological data and the canopy variables  $LAI$  and  $K_c$  estimated by means of remote sensing techniques, as will be described in Chapter 4. In particular, a function relating the value of the crop coefficient  $K_c$  to the canopy variables  $LAI$ , albedo and height was introduced.

The lower boundary condition was defined by means of a function relating the water flux through the bottom of the soil profile to the groundwater table depth  $\phi$ . This function was estimated in an empirical way by means of a regional groundwater flow simulation model.

Finally, a two-step procedure based on the use of a calibrated pedo-transfer function was presented to map the soil hydraulic properties required to determine the farmers' water demand as described above.

## 4 Satellite remote sensing approach to determine crop coefficients

---

### 4.1 Current uses of remote sensing in support of irrigation management

The observations of the Earth surface in different regions of the electromagnetic spectrum by means of remote sensors have been used for about three decades to monitor land surface patterns. The potentiality of remote sensing techniques in irrigation and water resources management is now widely acknowledged (FAO, 1995; Schultz et al., 2000). The use of remote sensing in this field can be mainly addressed to two broad issues: the estimation of some important *water balance terms*, i.e. evapotranspiration and soil moisture, and the mapping of land *attributes*, such as *land use*, i.e. irrigated versus not irrigated areas, and *land cover*, including crops and vegetation characteristics.

One of the earliest and still widely investigated applications of remote sensing is based on the estimation of *actual evapotranspiration* by means of measurements of the radiometric surface temperature. Assuming that the radiometric surface temperature is equal to the aerodynamic temperature  $T_o$ , it is possible to derive the latent heat flux  $\lambda E$  from the surface energy balance equation (Becker et al., 1995; Kustas et al., 1996):

$$\lambda E = Q^* - G - \rho_a c_p \frac{T_o - T_a}{r_{a,H}} \quad (4.1)$$

where the last term represents the sensible heat flux. When heterogeneous surfaces are imaged with air or space-borne sensors, the difference between the aerodynamic temperature and the radiometric surface temperature can be large (Kustas, 1990). Thus, in order to obtain reliable estimates of  $\lambda E$  empirical adjustments are in general applied to determine the correct value of  $r_{a,H}$ . Heilman et al. (1976) used calibrated airborne radiometric techniques and ground-based measurements of  $Q^*$ ,  $G$ ,  $T_o$ ,  $U$  to estimate instantaneous values of  $\lambda E$  by means of Eq.(4.1) on different crops. On a similar approach, Jackson et al. (1977) found that daily values of  $\lambda E$  could be estimated from one-time-a-day measurements of surface temperature, by neglecting the soil heat flux density  $G$  and introducing two empirical parameters  $A, B$  in Eq.(4.1):

$$\lambda E = Q^* + A - B (T_o - T_a) \quad (4.2)$$

This technique has been applied for mapping  $\lambda E$  from Landsat TM images (Moran et al., 1990; Sugita et al., 1992). In the estimation of  $\lambda E$  on a regional scale relationships similar to Eq.(4.2) have been applied to low-resolution satellite data (Seguin et al., 1983; Taconet et al., 1986; Vidal et al., 1990). Thermal radiometric techniques have also been used to identify water stress conditions in cropped areas by means of "indicators" derived from radiometric measurements (Jackson et al., 1981).

The potentiality and limitations of passive and active microwave sensors for monitoring *soil water content* have been evidenced in many recent studies; a review of the current status of research in these fields can be found in Engman et al. (1995) and Petty et al. (1996). Mapping soil water content, and thus the corresponding deficit in a defined portion of the soil profile, would be a very suitable application of remote sensing in irrigation management. But due to the complexity of microwave backscattering of vegetated surfaces, the limited penetration depth in the soil and the technical characteristics of instruments available today and in the near future, there are serious limitations in the use of microwave space-borne sensors in this field.

The remote sensing techniques described above, aimed at detecting terms of soil water balance, have produced a better understanding of land surface-atmosphere processes and their parameterisation (Bastiaanssen, 1995; Feddes, 1995; Wood, 1995). Their support to the actual operation of irrigation systems however is rather limited. In terms of spatial and temporal resolution there are major limitations due to the capabilities of current satellites systems. Airborne sensors appear more suitable from a technical point of view (Moran, 1994), but the resulting costs on a routine basis are seldom justified. Another constraint to be considered is the large time-lag between data acquisition and information transfer to the final users. Information such as the occurrence of water stress in a specific location of an irrigation district should be made available to the end-user almost in real time.

For the purposes of the present study, a more suitable approach is given by mapping *land cover*. This application of remote sensing data can be considered as operational in irrigation management (FAO, 1995; Li Jiren et al., 1997). Inventories of irrigated areas and crop statistics can be performed with satisfactory accuracy in a cost-effective way by means of high resolution satellites, such as Landsat TM and SPOT. In addition, the temporal dynamics of land cover characteristics is compatible with the re-visit time of these space platforms.

Examples of performance evaluation of irrigation systems at different levels of complexity by combining remote sensing with ground ancillary data have been reported by Menenti (1990), Menenti et al. (1990, 1995). Satellite-derived maps of irrigated crops can be combined with look-up-tables of crop coefficients  $K_c$  to produce *crop water requirements maps* (Estes et al., 1978). This

method does not achieve accurate results unless detailed information about planting date and actual canopy development in each mapping unit are given. Better results can be obtained when crop classification is made on multitemporal acquisitions (Menenti et al., 1986). Nevertheless, the attribution of an unique crop coefficient  $K_c$  to each field only on the basis of crop type information is questionable. As mentioned before, the canopy structure and development rather than the crop typology determine to a great extent the crop water requirements. Algorithms for retrieving biophysical parameters of vegetation, such as LAI, biomass density and canopy roughness from remote sensing data with different spatial and temporal resolution have been tried out (Hall et al., 1995). As shown in Section 3.2, these canopy variables determine the value of crop coefficient  $K_c$ . By means of model simulations of the surface energy balance and radiation transfer, Choudhury et al. (1994) investigated the relationships between  $K_c$  and different red and infrared reflectance ratios, i.e. the *vegetation indices*. A  $K_c$ -value derived from field measurements of a soil-adjusted vegetation index (Huete, 1988) has been used by Bausch (1995) to perform irrigation scheduling of corn fields.

Starting from this baseline, *a new approach is proposed here to estimate crop water requirements by mapping the value of crop coefficients  $K_c$ , as defined in Eq.(3.9), from the spectral reflectance of vegetated surfaces measured by means of satellite images.*

#### 4.2 New methodology to estimate crop coefficients from satellite images.

In Eq.(3.10) and (3.11), the crop coefficient  $K_c$  has been expressed as an explicit function of the climatic variables  $\{K^{\downarrow}, T_a, RH, U\}$  and of the canopy parameters, LAI,  $r$  and  $h_c$ . The availability of multiple observations of canopy properties during different phenological stages allows the construction of a temporal series of  $K_c$  values for the considered crop. Since the same canopy properties in Eq.(3.11) determine also the reflectance behaviour of vegetated surfaces, it is possible to establish an implicit or explicit *correlation* between multi-spectral measurements of canopy reflectance  $\rho_{\lambda}$  ( $\lambda=1,2,\dots, n$  bands) and the corresponding  $K_c$  values (Bausch et al., 1987; Azzali et al., 1991; Choudhury et al., 1994; D'Urso et al., 1995).

Hence, two different approaches for mapping crop coefficients from satellite data can be taken:

- 1) Classification algorithms based on the definition of spectral classes corresponding to different crop coefficients  $K_c$  assigned from ground truth observations. This technique will be further referred as the '*classification approach*'. In this case, an *implicit* correlation between  $\{\rho_{\lambda}\}$  and  $K_c$  is assumed

- 2) Definition of analytical functions relating  $\{\rho_\lambda\}$  to  $r$ ,  $LAI$  and  $h_c$  needed for the calculation of  $K_c$  by means of Eq.(3.11). In this '*analytical approach*', the relationship between  $K_c$  and  $r$ ,  $LAI$  and  $h_c$  will be *explicitly* defined.

### 4.3 Classification approach

Classification algorithms are the most common techniques for interpreting satellite multispectral data in land resources monitoring. Almost every software package for image analysis includes several classification procedures with different approaches.

The classification process involves two main steps: the definition of spectral classes, which define the spectral characteristics of the *mapping units*, and the association of each image pixel to one or more mapping unit, based on the similarity between the spectral characteristics of each image pixel and the spectral classes. These two steps can be either performed in an automated way (*unsupervised classification*) or by means of *a-priori* definition of the spectral classes (*supervised classification*).

In an *unsupervised* classification, the analyst has to decide only the number of classes in the final output. The spectral characteristics of each class are automatically defined from a preliminary statistic of the spectral values of all image pixels; then, each pixel is assigned to the most similar class. Once the classification has been performed ground-truth information on a set of classified pixels is used to define the *attributes* of each class, i.e. land-use and crop type.

In a *supervised* classification, the spectral classes are defined from the extraction of the spectral characteristics or *signatures* of ground-reference objects having known attributes. Several signatures may contribute to the definition of one spectral class. A vector of mean reflectance values  $\mu$  and a variance-covariance matrix,  $|V|$  are then associated to each class. In doing so, we create, prior to the classification process itself, a *training* set of signatures which will be used for assigning each image pixel to a class. In the subsequent step, the classification is performed on the basis of a pixel-to-class proximity measurement in an  $n$ -dimensional space, where  $n$  is the number of spectral bands considered. Different proximity measurements can be applied for this purpose. When data are normally distributed parametric methods are widely used, which are based on the probability,  $p_{x,i}$  of a given pixel, identified by a vector  $x$  in the spectral space, to belong to a class  $i$ .

Although unsupervised and supervised classifications are largely used for mapping land use attributes, they are not straightforwardly applicable for the purpose of this study. In the classification of an image for the identification of areas with similar crop water requirements, the attributes of classes are not strictly linked to the corresponding land-use but are defined in a different way, i.e. as range intervals of crop coefficient values. Indeed because of differences in canopy

development, different crops may have the same  $K_c$  value or  $K_c$  may largely vary within the same land-use.

This approach, which was firstly applied by Azzali et al. (1991), is a *hybrid* classification procedure based on a combination of both supervised and unsupervised techniques and is particularly suitable for mapping crop coefficients. Firstly an unsupervised classification, i.e. by means of clustering algorithms, is applied to the mean spectral values of an image subset including the pixels of ground-truth plots with known  $K_c$  values. This step corresponds to the *class formation*. Then, the resulting spectral classes are used as training signatures for the supervised classification of the whole image.

Due to the specificity of this classification objective, the significance of the spectral signatures characterising each class and the reliability of the classification output require a careful evaluation. These aspects can be validated in an efficient way by means of appropriate statistical techniques which allow to take into account the spectral variability of both the image and the signature sets (D'Urso and Menenti, 1996). Firstly the signatures forming the training set of the classifier are analysed in terms of their spectral *separability*. Secondly, the reliability of classification output is estimated using the technique of *thresholding* (Swain, 1978) for different values of confidence levels. A global performance index is then derived by combining these two different steps of the classification process. This global index enables the operator to select the best performing procedure among alternative strategies with different spectral signatures and classification algorithms.

#### 4.3.1 Class formation and evaluation

In image processing *agglomeration* techniques, i.e. hierarchical and non-hierarchical clustering (Webster et al., 1990), are often applied to the spectral reflectance values of reference ground plots with known physical attributes for establishing homogeneous groups of objects with similar spectral behaviour. Since different clustering algorithms are available, the choice of the best set of spectral signatures is not unique. Thus we need a criterion to assess which set of signatures, among several alternatives, should be preferred for the final classification.

The theory of pattern recognition offers many different criteria to evaluate the quality of spectral signatures used to train a classifier with one of the main aspects being considered is their reciprocal *separability*.

*Separability* measurements between two spectral classes  $i, j$  may greatly reduce the occurrence of errors of commission and omission (Jensen, 1986). It is known that the probability of these errors, below indicated as  $p_{E(i,j)}$ , is related to the statistical separability between spectral classes, which may be quantified by estimating their relative *divergence*. Assuming that the spectral classes are normally distributed, the divergence can be estimated from the statistical parameters, mean vector  $\mu$  and variance-covariance matrix  $|\mathbf{V}|$  for each pair of



spectral class. Swain and King (1973) emphasised the effectiveness of the Jeffries-Matusita distance  $JM$  for divergence estimates, which is defined as:

$$JM_{ij} = \sqrt{2(1 - e^{-a^*})} \quad (4.3)$$

where the parameter  $a^*$  is a function of  $\mu_i$  and  $|\mathbf{V}_i|$  (Swain, 1978).  $JM_{ij}$  can range between 0 and  $\sqrt{2}$ , having the upper limit when  $\alpha$  approaches infinity. When more than two classes are present multiclass separability can be estimated by taking:

$$JM_m = \frac{1}{m(m-1)} \sum_{i=1}^{m-1} \sum_{j=i+1}^m JM_{ij} \quad (4.4)$$

where  $m$  is the number of classes considered. Most image processing packages include the routines for calculating  $JM_{ij}$ ; an example of algorithm can be found in Jensen (1986).

It is possible to demonstrate that the upper and lower bounds of probability  $p_{E(i,j)}$  of classification errors (omission and commission) are related to the value of the Jeffries-Matusita distance (Swain, 1978). A satisfactory degree of separability is achieved when the  $JM_m$  distance is higher than 1.25, corresponding to a probability of errors not exceeding 0.10. When  $JM_m$  values are higher than 1.275, the probability of errors will be lower than 0.05. This divergence estimate is used here to derive a normalised separability index  $JM^*$  by dividing the Jeffries-Matusita value by  $\sqrt{2}$ , which is the maximum possible value:

$$JM^* = \frac{JM_m}{\sqrt{2}} \quad (4.5)$$

Thus, a satisfactory degree of separability is achieved for  $JM^* > 0.88$ , corresponding to  $JM_m > 1.25$ . The measurement of class separability is helpful for a preliminary evaluation and refinement of spectral signatures definition in the class formation step. Its usefulness can be especially appreciated when different object agglomerations are examined for producing the training sets to be used in the classification procedure.

### 4.3.2 Pixel class membership and reliability of the classification.

As mentioned before, the attribution of each image pixel to one or more spectral classes is decided according to 'pixel-to-class' distance criteria. A common definition of pixel-to-class probabilistic distance is the so-called Mahalanobis distance  $D_{x,i}$  (Mahalanobis, 1927):

$$D_{x,i} = \left| (\mathbf{x} - \boldsymbol{\mu}_i)^T \mathbf{V}_i^{-1} (\mathbf{x} - \boldsymbol{\mu}_i) \right| \quad (4.6)$$

where  $\mathbf{x}$  is the vector of pixel reflectance values with the spectral class characteristics being given by  $\boldsymbol{\mu}_i$  and  $|\mathbf{V}_i|$ . When using a maximum likelihood decision rule, image pixels are automatically assigned to a class in such a way that

$p_{x,i}$  is highest and corresponding to the smallest  $D_{x,i}$  value. It often happens that for the same pixel there is no significant difference among the distance values for different classes. This especially occurs when some pixels are likely to belong to more than just one class or to none of the pre-defined spectral classes. When the classifier tends to allocate all pixels, the confidence level associated with the assignment of pixel  $x$  to class  $i$  is low. As a consequence, the resulting classification will be highly unreliable. In most cases, the reason for this unreliability still resides in the class formation step.

The Mahalanobis distance can be used to screen those pixels whose membership to the corresponding class is below a pre-defined threshold. In other words, this corresponds to assigning a pixel to a class only if the resulting probability  $p_{x,i}$  corresponds to a confidence level greater than a pre-defined value. A 'rejection' class may be formed by grouping together all those pixels with a distance measurement,  $D_{x,i}$ , larger than a threshold value. Increasing threshold values will extend the rejection class. This technique, known as 'thresholding', is included in most image processing software and can be applied to discard those pixels that are not correctly classified at the given confidence level.

Considering that the percentage of 'rejected' pixels at a given confidence level may be taken as a measurement of reliability, this technique can be adopted to develop a performance indicator of classification. Swain (1978) remarks that when data are normally distributed the frequency of Mahalanobis distances approaches a Chi-square distribution with a number of degrees of freedom equal to the dimensionality of data, e.g. the number of spectral bands examined.

Under this assumption, each threshold value corresponds to a confidence level which can be determined from Chi-square tables. Thus, a plot of the percentage of rejected image pixels versus confidence level may be derived by assigning different thresholding values, as shown by Meuwissen (1989). The shape of the resulting curve is a measure of the performance of the classification procedure (Fig. 4.1).

A rapidly dropping curve (such as curve "I" in Fig. 4.1) is

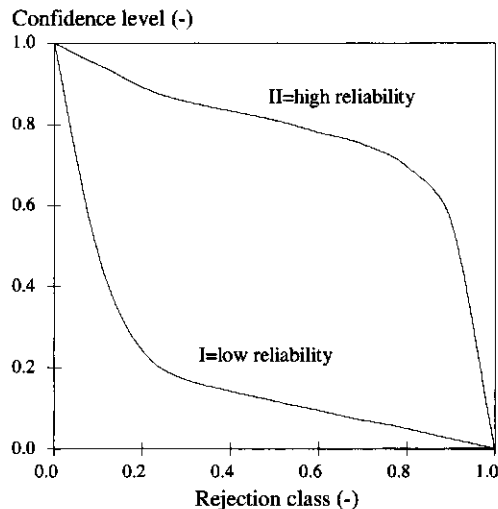


Fig. 4.1 Thresholding curves for post-classification performance. On the abscissa the fraction of "rejected" pixels are given, on the ordinate the confidence level of classification.

an indicator of scarce reliability, since most pixels are already rejected at low confidence levels. On the opposite side, an ideally perfect classification would show a straight line parallel to the horizontal axis in correspondence of 100% percentage of classified pixels.

Actually, a satisfactory degree of reliability is expected with the curve showing a marked convexity above the horizontal axis (as "II" in Fig. 4.1). Therefore, the technique of thresholding can be used to estimate the reliability of different classification results from the measurement of the area below the corresponding curve.

A 'thresholding index'  $A^*$  is given by the area below the curve:

$$A^* = \int_0^1 A(t_p) dt_p \quad (4.7)$$

where  $t_p$  indicates the threshold value of the horizontal abscissas.

Class separability and classification reliability are complementary to each other. Low separability does not directly imply that the rejection class formed during the thresholding analysis is large at low confidence value and viceversa. For this reason, the normalised performance indicators derived from Eqs.(4.5) and (4.7) that concern respectively the class formation and the classification stages, can be combined to define a Classification Performance indicator  $CP$ :

$$CP = JM^* A^* \quad (4.8)$$

This parameter can be used for a post-processing comparison and selection of the best classification among different alternative procedures. In common applications, a range of variation between 0.4 and 0.6 can be expected.

The classification approach can be usefully applied when there is no detailed ground-truth information about the canopy characteristics in the study area, i.e.  $LAI$ , fractional vegetation cover  $s_c$  and crop height  $h_c$ . In such a situation, it is rather difficult to assign a precise value of  $K_c$  to a certain pixel, but it is possible to identify a more or less broad range of values which is typical for a given class or mapping unit.

#### 4.4 Analytical approach.

The analytical approach for mapping the crop coefficient  $K_c$  is based on the direct application of Eq.(3.11). The maps of the vegetation properties required in this equation, namely the surface albedo,  $r$ , the leaf area index,  $LAI$  and the crop height,  $h_c$ , are obtained from the processing of multispectral satellite images. Using ground-based meteorological data, the  $K_c$  values for each pixel are calculated from Eq.(3.11), as shown in Fig. 4.2.

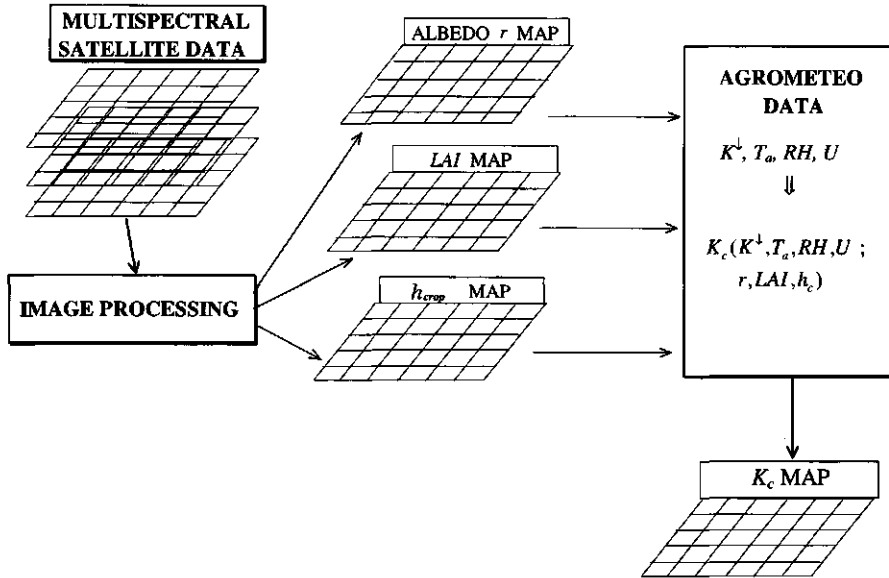


Fig. 4.2 Conceptual framework of the analytical approach for mapping crop coefficients.

The canopy reflectance results from the interaction of many different elements, such as the leaf area index, leaf angle distribution, spectral properties of leaves and soil and the relative geometry of illumination and observation. Furthermore, when sensors are carried on board aeroplanes or orbiting platforms we have to consider also the influence of atmospheric absorption and scattering at different wavelengths.

Consistent efforts have been paid in modelling the canopy reflectance behaviour either on a physical basis (Verhoef, 1984; 1998; Camillo, 1987; Pinty et al., 1990) or approaching the problem in an empirical way (Hatfield et al., 1985; Price, 1992). Due to the number of parameters required to define the canopy Bi-directional Reflectance Distribution Functions (*BRDF*), the inversion of physical models is practically an undetermined problem with the current high-resolution satellite sensors.

Simplified methods to estimate the canopy characteristics from satellite-based surface reflectance can be found by introducing some assumptions. In most cases the canopy is generally assumed to behave as a Lambertian surface, thus the canopy reflectance is constant with the angle of observation. Within the limitations of accuracy that this assumption implies, empirical models relating the canopy geometrical parameters to different types of vegetation indices can be defined and used for the purpose of this study.

#### 4.4.1 Estimation of spectrally integrated hemispherical reflectance (albedo)

The solar spectrally integrated hemispherical reflectance, here defined as the *albedo*  $r$ , is one of the driving variables in the radiation budget of a surface, as expressed by Eq.(3.2). For a given sun altitude,  $r$  can be generally expressed as follows:

$$r = \int_{300}^{2500} \frac{\left[ \int_0^{2\pi} \int_0^{\pi/2} K^\uparrow(\vartheta, \Phi, \lambda) \cos \vartheta \sin \vartheta \, d\vartheta \, d\Phi \right]}{K^\downarrow(\lambda)} d\lambda \quad (4.9)$$

with  $K^\uparrow(\vartheta, \Phi, \lambda)$  indicating the reflected solar radiance ( $\text{Wm}^{-2}\text{sr}^{-1}$ ) at wavelength  $\lambda$  (nm) and expressed as a function of viewing angles at zenith,  $\vartheta$ , and at azimuth,  $\Phi$  respectively. Kimes et al. (1987) have shown with simulated data that the error of estimation of surface reflectance in red and near-infrared wavelengths from nadir observation is strongly influenced by the canopy structure and the solar zenith angle. The effect of sun elevation on the surface reflectance has been quantified by Menenti et al. (1989). Field measurements in the range 300-2500 nm on different types of surfaces showed a variation of  $r$  during the day. Hence an empirical function was derived to relate  $r$  at a given moment of the day to that measured at a given reference condition. Thus, as pointed out by Asrar et al. (1993), in the estimation of  $r$  from satellite data we have to solve three main problems: the directional integration of spectral radiance detected by the sensor, the spectral integration to obtain the *planetary* albedo, that is at top-of-atmosphere height, and the correction of atmospheric effects in each spectral band for deriving the surface albedo  $r$  from the planetary albedo  $r_p$ .

The current sensor capabilities, such as those of Landsat Thematic Mapper used in this study, impose several simplifications. In first instance we will consider that the surface is Lambertian. In this case, we neglect any dependence of  $K^\uparrow$  on  $\vartheta$  and  $\Phi$  and  $r$  can be estimated from any direction of observation. Considering that radiance measurements are performed at different wavelengths, the spectral integration is approximated in discrete form, as expressed by the following relationship:

$$r = \pi \int_0^\infty \frac{K^\uparrow(\lambda)}{K^\downarrow(\lambda)} d\lambda \cong \pi \sum_{\lambda_i} \frac{K_{\lambda_i}^\uparrow (d^0)^2}{E_{\lambda_i}^0 \cos \vartheta^0} \quad (4.10)$$

In Eq.(4.10) the spectral reflected radiance,  $K_{\lambda_i}^\uparrow$  ( $\text{W m}^{-2}$ ), and the extraterrestrial solar irradiance,  $E_{\lambda_i}^0$  ( $\text{W m}^{-2}$ ), are integrated values over the width of each spectral band  $\lambda_i$ ;  $\vartheta^0$  and  $d^0$  are the solar zenith angle and the sun-earth distance in Astronomical Units. When using Thematic Mapper reflectance measurements  $r_{\lambda_i}$ , the *planetary* albedo, can be calculated as (Menenti, 1984):

$$r_p = \sum_{\lambda} w_{\lambda} r_{\lambda} \quad \lambda = 1, 2, \dots, 5, 7 \quad (4.11)$$

where the weighting factors  $w_i$  are given by:

$$w_{\lambda} = \frac{E_{\lambda}^0}{\sum_{\lambda} E_{\lambda}^0} \quad (4.12)$$

The extraterrestrial solar irradiance  $E_{\lambda}^0$  in each Thematic Mapper band and the corresponding values of  $w_{\lambda}$  are summarised in Tab. 4-1. The *surface* albedo  $r$  can be also determined by means of the Eq.(4.11), if reflectance corrected values for atmospheric effects,  $\rho_{\lambda}$ , are used:

$$r = \sum_{\lambda} w_{\lambda} \rho_{\lambda} \quad \lambda = 1, 2, \dots, 5, 7 \quad (4.13)$$

Tab. 4-1 Spectral characteristics of Landsat 5 Thematic Mapper bands. Band-widths and solar exo-atmospheric irradiance have been given by Epema (1990), the corresponding weighting coefficients were calculated with Eq.(4.12).

Band	Center wavelength (nm)	Band-width (nm)	$E_{\lambda}^0$ ( $W m^{-2}$ )	$w_{\lambda}$ (-)
TM-1	485	66	129.16	0.2212
TM-2	560	82	149.98	0.2569
TM-3	660	67	104.32	0.1787
TM-4	830	128	134.02	0.2295
TM-5	1650	217	47.59	0.0815
TM-7	2215	252	18.78	0.0322

#### 4.4.2 Estimation of Leaf Area Index

Several studies have shown that the estimation of LAI from remote sensing depends on many factors, such as leaf optical properties, their spatial distribution and orientation with respect to the illumination and viewing angles and the soil background effects (Curran et al., 1988; Baret et al., 1991). An accurate estimation of LAI from remote sensing can only be obtained from inversion by canopy reflectance models that take into account all these factors. As mentioned before, this approach requires simultaneous multi-directional observations which are not possible with current satellites systems. The results of the research in this field will probably lead to space-borne sensors able to image the same object with different observation angles in a short time, thus particularly suitable for LAI.

A simple and feasible approach is based on empirical relationships between  $LAI$  and nadir-viewing measurements of  $r_\lambda$  in the red and infrared bands. This approach implicitly assumes that all other factors, except  $LAI$ , influencing the spectral response of canopy are fixed. Different vegetation indices,  $VI$ , can be defined to reduce the effects of soil reflectance. Experimental observations have shown that these vegetation indices can be related to  $LAI$  (Huete, 1988; Baret et al., 1991):

$$VI = VI_\infty - (VI_\infty - VI_s) e^{-\beta LAI} \quad (4.14)$$

Eq.(4.14) describes the variation of absorption and reflection of radiation in a canopy partially covering the soil. The parameter  $VI_s$  depends on the soil reflectance and corresponds to the value of vegetation index for bare soil, while  $VI_\infty$  corresponds to full cover. The parameter  $\beta$  is an extinction coefficient, corresponding to the increase of  $VI$  for an unitary increase of  $LAI$ . Moving from this approach, Clevers (1989) and Price (1992), among others, have suggested semi-empirical models for the retrieval of  $LAI$  from vegetation indices.

The simplified model CLAIR (Clevers, 1989) is based on the *Weighted Difference Vegetation Index* ( $WDVI$ ) defined as follows:

$$WDVI = \rho_i - \rho_r \frac{\rho_{si}}{\rho_{sr}} \quad (4.15)$$

where  $\rho_r$  and  $\rho_i$  indicate the reflectance of observed canopy in the red and infrared bands respectively, while  $\rho_{sr}$  and  $\rho_{si}$  are the corresponding values for bare soil conditions. The  $LAI$  is related to  $WDVI$  of the observed surface through the expression:

$$LAI = -\frac{1}{\alpha^*} \ln \left( 1 - \frac{WDVI}{WDVI_\infty} \right) \quad (4.16)$$

In Eq.(4.16),  $\alpha^*$  is an extinction coefficient, similarly to  $\beta$ , to be determined from simultaneous measurements of  $LAI$  and  $WDVI$ ;  $WDVI_\infty$  is the asymptotical value of  $WDVI$  for  $LAI \rightarrow \infty$ . A relationship similar to Eq.(4.16) was derived by Price (1992).

This approach has been validated by means of numerical models simulating the reflectance of leaf and canopy in a wide range of conditions (Clevers et al., 1993). These models confirmed that an accurate estimate of  $LAI$  requires the knowledge of the leaf angle distribution, and, to a minor extent, of other factors, such as sun-zenith angle, chlorophyll content and mesophyll structure. For this reason the parameters of empirical functions relating vegetation indexes to  $LAI$  are site and crop dependent as demonstrated also by several investigations (Moran et al., 1991; Price, 1992; Thenkabail et al., 1994). Thus the determination of empirical parameters entering in simple  $LAI$  models based on vegetation indices, such as Eq.(4.16), should be carried out on site for each different land cover.

Furthermore, the value of vegetation indices is influenced by atmospheric absorption and diffusion of radiation. An example of this effect on the relationship between *WDVI* and *LAI* is shown in Fig. 4.3. The *WDVI* was derived for given *LAI* reference values by combining an atmospheric correction algorithm and the canopy reflectance model SAIL (Verhoef, 1984; Verhoef and Menenti, 1998).

As evidenced in the plot of Fig. 4.3, the relationship between *WDVI*, as calculated from top-of-atmosphere reflectance values, and *LAI* is largely affected by the atmospheric effects. If an accurate correction is not performed, the empirical parameters of Eq.(4.15) and (4.16) should be determined for each acquisition.

This problem can introduce large errors in the estimation of *LAI* when multitemporal analyses are performed. The plots in Fig. 4.4 show the effect of soil reflectance on the *LAI*(*WDVI*) relationship. If an unique average value of soil reflectance ratio  $\rho_s/\rho_{sr}$  is taken for each image (Fig. 4.5), an overestimation of *LAI* may be expected in case of a bright soil i.e. sand in the range of *LAI* [1; 3]. The underestimation in the higher range is not determined by the soil influence, but by the artificial effect of "saturation" resulting from the application of extinction-type function, as Eq.(4.14).

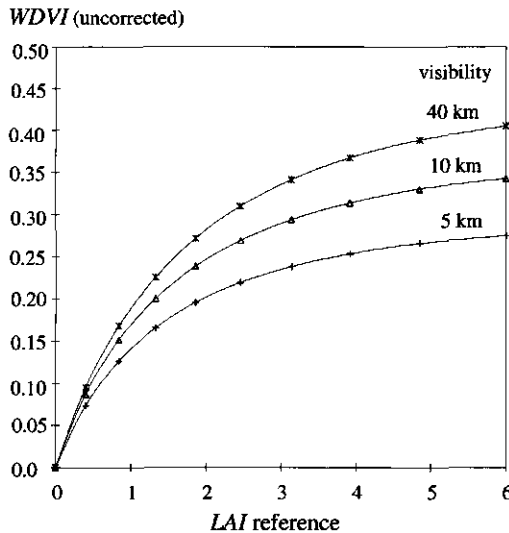


Fig. 4.3 Influence of visibility of 5, 10 and 40 km on the relationship between the leaf area index *LAI* and the Weighted Difference Vegetation Index *WDVI*. As input parameters were considered: zenith angle  $45^\circ$ , light clay soil, plagiophile leaf area distribution (mean inclination  $45^\circ$ ), leaf reflectance values in TM bands equal to 0.114; 0.186; 0.114; 0.468; 0.304; 0.164 respectively.



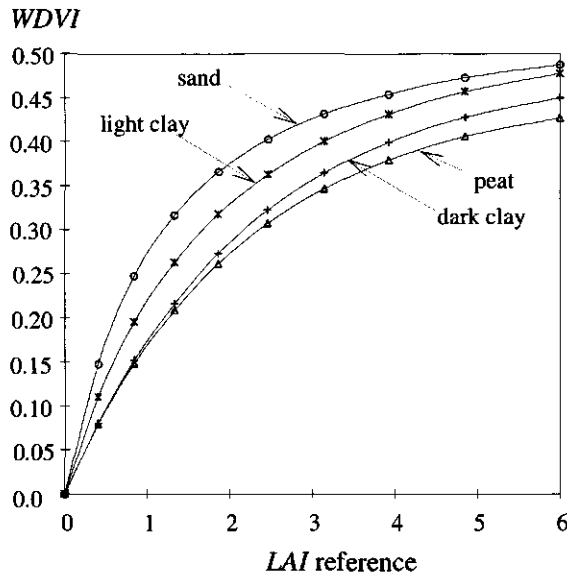


Fig. 4.4 Influence of reflectance properties of different soils on the relationship between Leaf Area Index LAI and Weighted Difference Vegetation Index calculated with a simulation model of canopy reflectance.

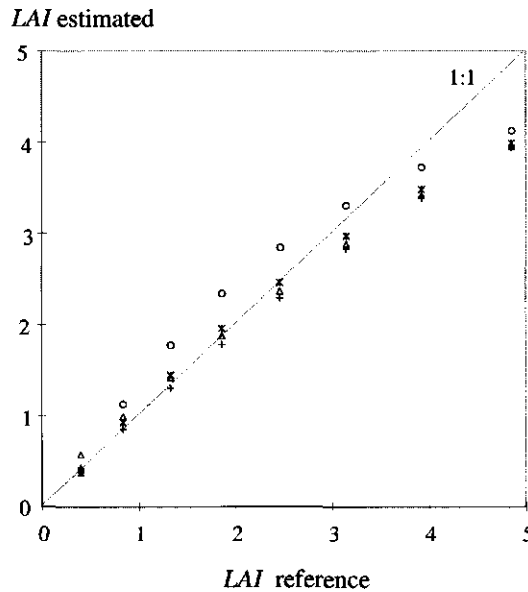


Fig. 4.5 Comparison between estimated and reference values of Leaf Area Index LAI for the soil data of Fig. 4.4 assuming  $\rho_{si}/\rho_{sr}=1.4$  in Eq.(4.16) and  $\alpha^*=0.4$  in Eq.(4.15). Simulations refer to a visibility value of 10 km and the leaf and canopy parameters of Fig. 4.3.

#### 4.4.3 Estimation of canopy aerodynamic properties

Aerodynamic properties of uniform vegetation canopies are strictly linked to crop height  $h_c$  and to Leaf Area Index  $LAI$ . In analogy with  $LAI$ , some correlation between vegetation indices and canopy roughness parameters may be found. Moran et al. (1991) tried out a purely empirical relationship linking the roughness length  $z_{0m}$  of alfalfa to the ratio of reflectance in near-infrared and red bands. A similar approach has been adopted by Bastiaanssen (1995) for estimating the surface energy balance with the EFEDA experiment data-set. Diversely, Kustas et al. (1998) estimated the crop heights from land-cover classifications of Landsat images and used the resulting values for calculating the resistance  $r_{a,H}$  from Eq.(3.4).

A more physically-based approach can be attempted by means of active sensors, such as radar and laser techniques. Attema et al. (1978) tried out a description of microwave backscattering, which has been tested either by means of X-band measurements (Bouman, 1991) and by using polarimetric radar in L and C bands during the MAC Europe campaign (Clevers et al., 1996). The results of these researches indicate that the influence of soil background and of soil and vegetation wetness are limiting factors for a reliable estimation of canopy geometrical properties. Schmullius et al. (1996) have shown that the relationship between crop height and microwave backscattering in C-band obtained with ERS-1 SAR is strictly crop-dependent, while no correlation was found with L-band backscattering data of airborne E-SAR. Future research on the use of multi-frequency polarimetric SAR instrumentation might lead to substantial improvements in this field, but at present very little contribution from microwave sensors can be expected for our purpose.

More promising results have been obtained by Menenti and Ritchie (1994), which estimated the aerodynamic roughness from the profiling of surface elevation with airborne laser altimeter data. At present this technique, however, can not be considered to be applicable on a routine basis.

Considering the difficulties related to the estimation of canopy aerodynamic properties, we suggest to perform a preliminary analysis on the sensitivity of Eq.(3.4) to the crop height  $h_c$  with the actual meteorological data of the study-area. This analysis will outline the precision required for the estimation of  $h_c$  to calculate  $K_c$ . In most cases, considering all the limitations described in the Section 4.3, the association of a mean crop height to each land-use class derived from satellite data, may result in a satisfactory compromise in areas where the absolute accuracy of  $r_{a,H}$  is of minor concern in the calculation of daily values of  $E_p$ .

## 4.5 Conclusions

In this Chapter we have shown that multispectral remote sensing techniques can be used to estimate a value of the crop coefficient  $K_c$  which takes into account the actual development and architecture of the canopy. Two different approaches have been proposed:

- application of a hybrid classification algorithm based on both unsupervised and supervised techniques (classification approach);
- definition of an analytical relationship between canopy reflectance and  $K_c$  (analytical approach).

In the first case statistical measurements of class separability and classification reliability have been defined to evaluate the classification procedure. From these statistical measurement a Classification Performance indicator has been derived to compare the output of different classifications. In the analytical approach, the canopy reflectance is used to estimate the variables  $r$ ,  $LAI$  and  $h_c$  from which the value of  $K_c$  is calculated. The difficulties related to a precise determination of the canopy variables have been described. Most limitations occur because the current satellite platforms do not allow multiple directional observations, as required for an estimate of canopy bidirectional reflectance distribution functions. Nevertheless, the accuracy that can be actually achieved with empirical methods is sufficient for the objective of this study. Indeed, a relatively large error in the estimation of  $LAI$  for scarcely developed canopies may be of minor importance when calculating  $K_c$ . The influence of  $LAI$  on  $K_c$  is related to the canopy resistance  $r_c$  in Eq.(3.5), which has a constant value for  $LAI > 4$ . For this reason, the saturation effect cited in the higher range of  $LAI$  does not affect the reliability of estimate of  $K_c$ . The same reasoning can be applied to the estimation of  $r$  and  $h_c$ , but the actual agrometeorological condition should be taken into account.

From a general point of view, *the analytical approach requires a rather detailed ground-truth* in order to calibrate the empirical relationships between the canopy properties and the reflectance values, but the resulting  $K_c$  values are mapped continuously. *The classification approach appears more feasible when only limited information about the canopy characteristics is available.*

## 5 Case-study in the Sele Plain, Italy: the Gromola irrigation district

### 5.1 Irrigation in the Sele plain.

In southern Italy a long tradition in the practice of irrigation exists. During the years 1920-1935 the reclamation of wetlands and the construction of irrigation and drainage canal networks led to a substantial evolution of agricultural practices. At the same time, state-controlled associations of farmers i.e. the 'Consorti di Bonifica e di Irrigazione' were entrusted with the management of new infrastructures. The investigation described here was carried out in the Gromola irrigation district which is located in the area of the Consortium of Irrigation of Paestum in the Sele river plain.

The Consortium of Paestum covers an extension of 16 000 ha, of which approximately 11 000 ha are irrigated. This area is delimited by the Sele river on the north, by the Tyrrhenian sea on the west and by the mountains of Cilento on the east and south. The mean annual precipitation  $P$  is 904 mm, while the mean annual reference evapotranspiration  $E_{ref}$  according to Blaney-Cridde formula is 1115 mm. The monthly distribution of  $P$  and  $E_{ref}$  is given in Fig. 5.1.

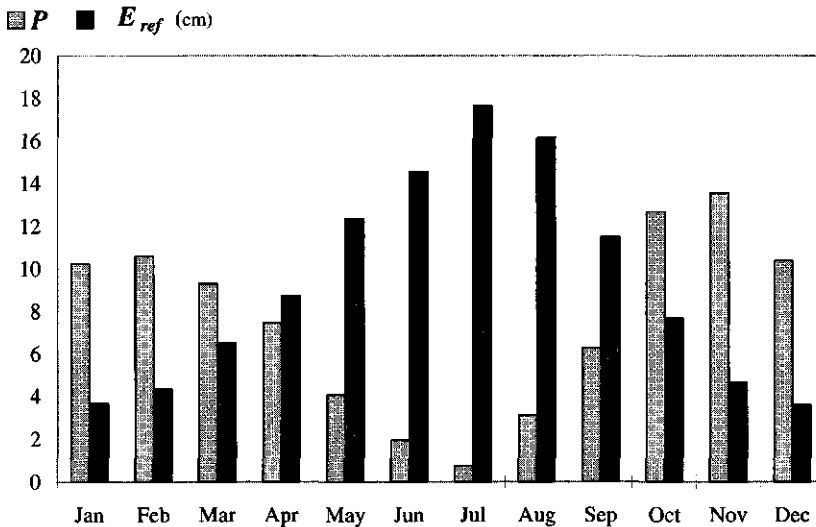


Fig. 5.1 Average monthly values of precipitation  $P$  and reference evapotranspiration  $E_{ref}$  in the Sele plain calculated by means of Blaney-Cridde formula. Data refer to the period 1979-1990 (adapted from D'Amato et al., 1992).

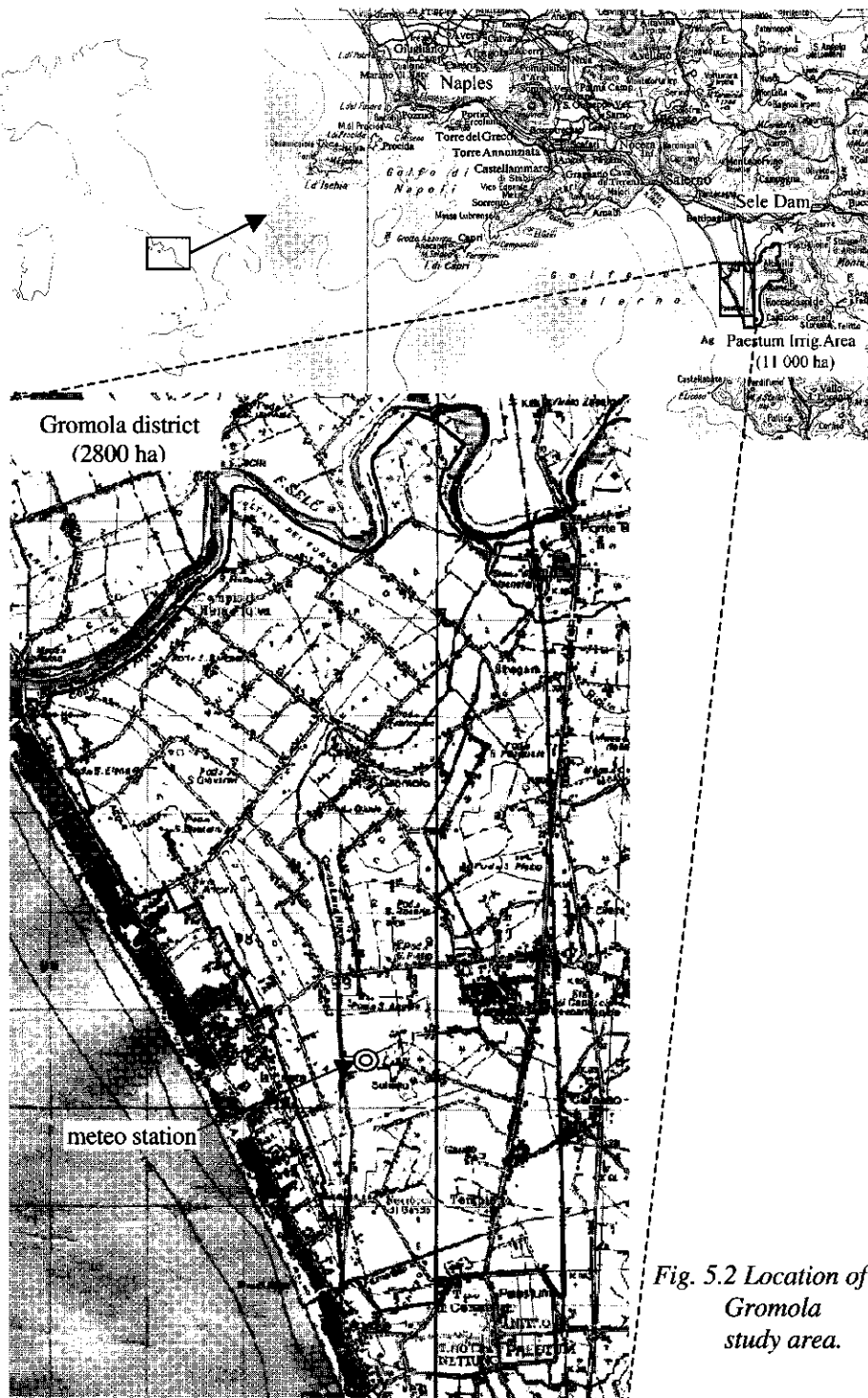


Fig. 5.2 Location of Gromola study area.

Perennial crops like artichokes are present in almost one third of the irrigated area; fruit trees, mainly peaches, apricot and pears are also present in a minor fraction (6%). Double cropping is practised in almost 60% of the irrigated area. Winter vegetables, such as crucifers and potatoes, and forages alternate with maize in approximately 25% of the total area and with summer vegetables like solanaceous crops, lettuce and cucurbits. Irrigation is intensively applied from May to September.

During the 1930's a small dam on the Sele river was built for water supply of the civil, industrial and agricultural activities and for the production of electricity. When the first irrigation project started in 1950, the Consortium obtained water rights to divert a maximum of  $4 \text{ m}^3\text{s}^{-1}$  from the reservoir. Irrigation water was distributed by means of an open canal network from which farmers pumped water for sprinkling or diverted it into farm furrows. Water distribution was manually regulated by gate-men who operated gates and weirs according to a defined rotational schedule.

The need for improving the irrigation system efficiency and for reducing water losses required the renovation of the conveyance network. In 1990 a first project has been undertaken by partially substituting the old canals with a pressurised pipeline system in two sub areas: 'Gromola' of 2800 ha and 'Seude' of 1000 ha. These works were finished in 1993 and allow for a *on-demand* irrigation schedule. Compensating storage capacities are provided by two reservoirs with a total capacity of  $85\,000 \text{ m}^3$ . Irrigation water is pumped into these reservoirs which also maintain the required *hydraulic head for the pressurised network*.

The rapid development of economical activities in the area, following the re-use of reclaimed lands, and the contemporary decrease of water resources have forced a progressive reduction of water allocation to irrigation. The actual available flow rate at the Sele dam is now  $2 \text{ m}^3\text{s}^{-1}$ . In case of water shortages an additional pumping of  $1 \text{ m}^3\text{s}^{-1}$  downstream the dam can be activated.

Although dramatic drought conditions have not been faced yet, the current equilibrium in the irrigation system may collapse if fast changes in cropping practices occur and water resources decrease further. These considerations are leading to new criteria to assess irrigation fees. Until now, irrigation fees have been fixed in relation to the extension of the irrigated area. A first attempt is nowadays being made by the Consortium administration toward water fees based on metering actual water consumption.

## 5.2 Description of the study-area in the Gromola irrigation district.

The Gromola irrigation district covers an area of approximately 2800 ha (Fig. 5.2). The irrigation water is diverted from the main canal to the pumping station that serves the two districts of Gromola and Seude. Assuming that all the

*Tab. 5-1 Technical characteristics of the Gromola irrigation water conveyance network*

---

Main pipelines length :	14 km
“ “ diameter :	500-1500 mm
Secondary network length:	62 km
“ “ diameter:	125-450 mm
Pumping station:	4x450 l/s
Compensation reservoir:	45 000 m <sup>3</sup>

---

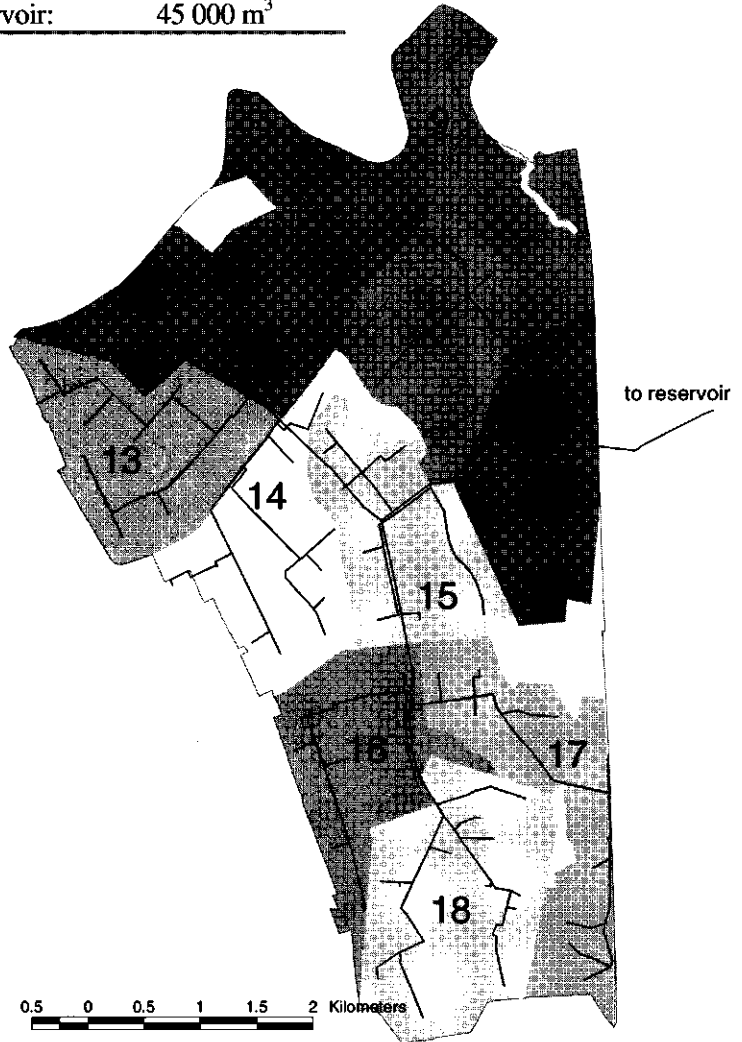


*Fig. 5.3 Irrigation conveyance network in the Gromola district. Primary units are numbered from 8 to 18.*

four pumps are operated during 24 hours a day, the maximum theoretical flow rate which can be lifted to the compensation reservoir of Gromola district is  $1.8 \text{ m}^3\text{s}^{-1}$ . In practice the total water availability never exceeds  $75\,000 \text{ m}^3\text{d}^{-1}$  (corresponding to 50% of full pumping capacity).

The conveyance and distribution network is divided in 11 primary units, serving an average area of 260 ha (Fig. 5.3). At the *secondary* level of the network, as defined in Section 2.1, there are a total of 390 units with an average area of 6.7 ha covering about 3000 tertiary units. Since the farm size ranges from 1.7 to 55 ha, in most cases a single secondary unit serves multiple farm owners. The outlet delivering water to each secondary unit is equipped with a device limiting the maximum flow rate to 10, 12.5 or  $30 \text{ dm}^3\text{s}^{-1}$  according to the extension and the numbers of tertiary units served (*limited rate demand schedule*).

In order to investigate irrigation management at farm level, 66 farmers were interviewed. The farmers were selected according to their location, extension of irrigated area, soil and crop type. The questionnaire prepared for this purpose included aspects such as the irrigation technique, the factors influencing the irrigation schedule, the application volume and the duration of each irrigation.

From the interviews analysis, it appeared that sprinkler irrigation is the most largely practised method (Fig. 5.4). Only 7% of the farmers extract groundwater for irrigation. Most farmers stated that the pressurised network has improved agricultural production, but only 25% is completely satisfied with the operation of the network. During the peak period, due to excessive water demand or insufficient hydraulic head, it appeared necessary to close the water delivery in one or more primary units.

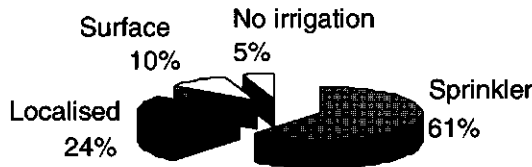


Fig. 5.4 Irrigation methods identified by interviews with the farmers in the Gromola district.

The irrigation schedule is mainly based on the farmer's perception of soil water deficit. About 9% of the farmers decide to apply irrigation according to their estimate of soil dryness, 42% when crop stress is observed and 31% when both of these conditions occur. Only 2% of the farmers irrigate at fixed intervals. The fact that irrigation is driven mainly by the farmers' perception of crop water stress and soil dryness makes the Gromola district particularly suitable for studying the application of SIMODIS, because irrigation management in SIMODIS is mainly based on the soil water balance. Duration of irrigation is fixed in 34% of the cases



and many farmers stop irrigation when either infiltration decreases (27%) or water ponds are noticed (11%). Although it was not possible to precisely identify the preferential hours for irrigation, because of excessive solar irradiation or windy conditions 46% of farmers do not irrigate between 11 to 16 h. About 25% of the interviewed regularly applies irrigation during night hours.

### **5.3 Data acquisition**

The application of SIMODIS to the case-study presented requires the acquisition of the following data:

- topographic information
- hydraulic conveyance and distribution network
- agrometeorological data
- satellite images
- crop data
- soil hydrological data
- groundwater measurements.

It should be noticed that a sub-set of the mentioned data groups (with the exclusion of topographic information and hydraulic network data) are used for validating the different modelling components of SIMODIS. All data sets have been introduced in a Geographic Information System.

#### **5.3.1 Topographic data**

The basic layer in the GIS is represented by the topographic boundaries of the tertiary units in the Gromola district. These boundaries have been digitised on a UTM grid by crossing a recent topographic map at scale 1:10.000 with the actual cadastral map. Each tertiary units is identified by a code XX-YY-ZZ, where XX and YY represent respectively the primary and secondary unit where they are located and ZZ is the progressive number within the secondary unit. The vector layer of tertiary units is associated to a data base which includes crop type, soil type and bottom boundary condition codes.

#### **5.3.2 Characteristics of water conveyance and distribution system**

The geometrical characteristics of the pipelines of the conveyance and distribution network have been taken from the construction plan of the District. The network is divided in 450 segments or *branches* and 450 nodes. The branches representing the primary and secondary level pipelines in the Gromola district have been digitised in a vector layer of the GIS (Fig. 5.3). A node corresponds to

an outlet serving a secondary unit or to a change of pipeline diameter or roughness. Each node is identified by a numeric code representing the primary and secondary unit, with its elevation above sea level and the maximum flow rate allowed in case the node is coincident with an outlet. Each segment is identified by the initial and the final node and characterised by its length, diameter and friction coefficient.

The amount of irrigation water delivered can be measured at the outlet of each secondary and primary unit. During the irrigation season of 1994, the water volumes delivered in each primary unit were collected daily. The total irrigated area in the Gromola district during 1994 was 2670 ha, with a gross water consumption of 7.3 hm<sup>3</sup> corresponding to 273 mm. The average daily consumption from May to September was 38 500 m<sup>3</sup> (with a peak value of 71 000 m<sup>3</sup> on Aug.9<sup>th</sup>). The graphs in Fig. 5.5 show the data for three primary units with maximum, average and minimum seasonal consumption respectively. Irrigation volumes were also measured in correspondence of 32 secondary units. An example of daily water volumes used by maize, vegetables and artichokes is given in Fig. 5.6.

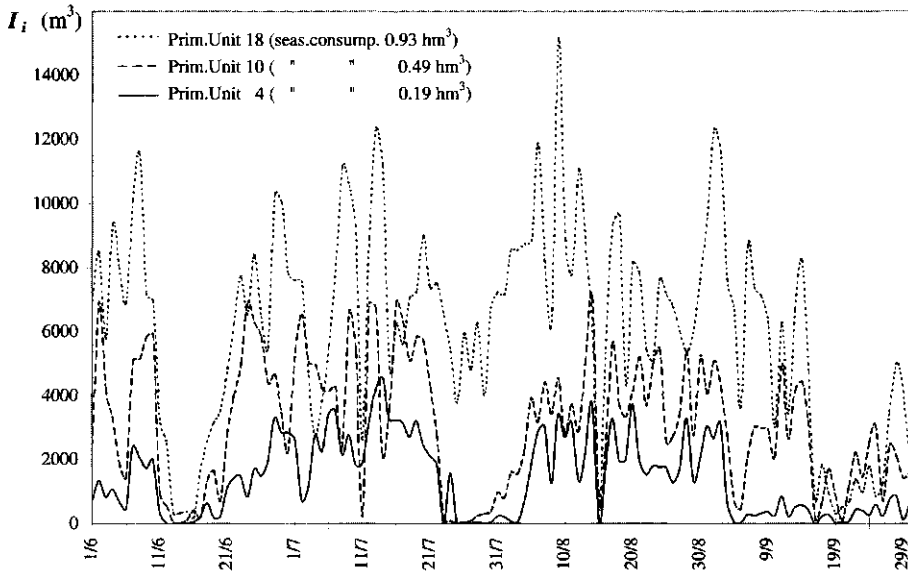


Fig. 5.5 Daily irrigation water volumes  $I_i$  measured at the outlets of three primary units in the Gromola district area during 1994.

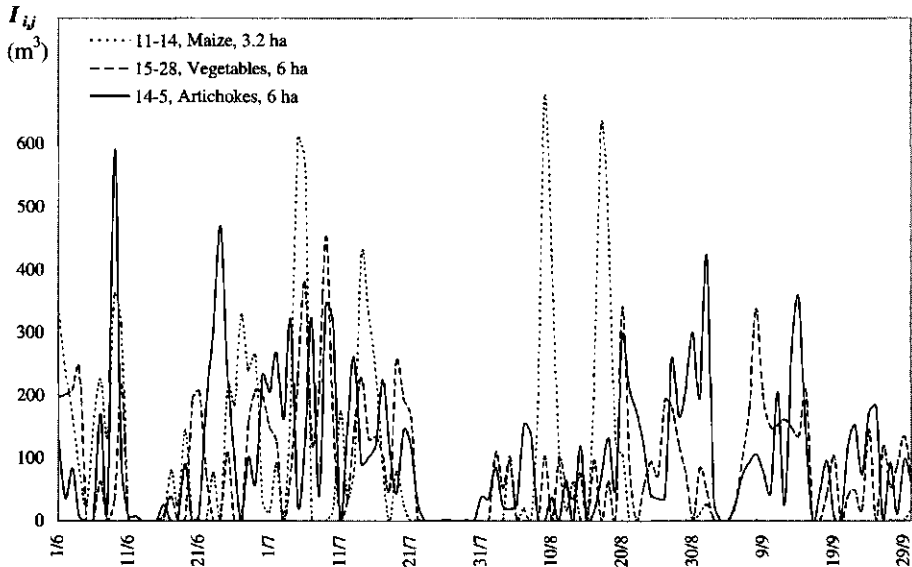


Fig. 5.6 Daily irrigation water volumes  $I_{ij}$  measured at the outlets of three secondary units with maize, vegetables and artichokes in the Gromola district during 1994.

### 5.3.3 Agrometeorological data acquisition

An electronic datalogging unit was installed in an irrigated plot in the Gromola area (Fig. 5.2) at the beginning of November 1993. Instantaneous values of precipitation,  $P$  (cm), global incoming solar radiation in the range 400-1100 nm,  $K^\downarrow$  ( $\text{W m}^{-2}$ ), air temperature  $T_a$  ( $^\circ\text{C}$ ), relative humidity  $RH$  (%), wind speed  $U$  ( $\text{m s}^{-1}$ ) and direction,  $U_\phi$  (rad), were measured at 2 m height and sampled every second. Average hourly and daily values were stored in digital form. Examples of data acquired during the first ten days of January and July 1994 are given in Fig. 5.7.

Daily reference evapotranspiration,  $E_{ref}$ , for the Gromola irrigation district was calculated by Eq.(3.6). Net radiation,  $Q^*$ , and soil heat flux,  $G$ , were determined from  $K^\downarrow$  by means of Eq.(3.2) and (3.3) with reference to the standard crop parameters, i.e.  $LAI = 2.88$ ,  $r = 0.23$  and  $h_c = 0.12$  m. In Eq.(3.6) the radiation and aerodynamic terms of evapotranspiration can be separately calculated. In the graph of Fig. 5.8, the total  $E_{ref}$  and the two aerodynamic and radiation components are plotted for the first decade of January '94. As shown in this graph, the aerodynamic term is the prevalent component of reference evapotranspiration during winter months, while during the summer the most relevant contribution is due to the radiation term. Therefore the accurate estimation of crop height needed to determine the aerodynamic resistance term is not so relevant during the irrigation season.

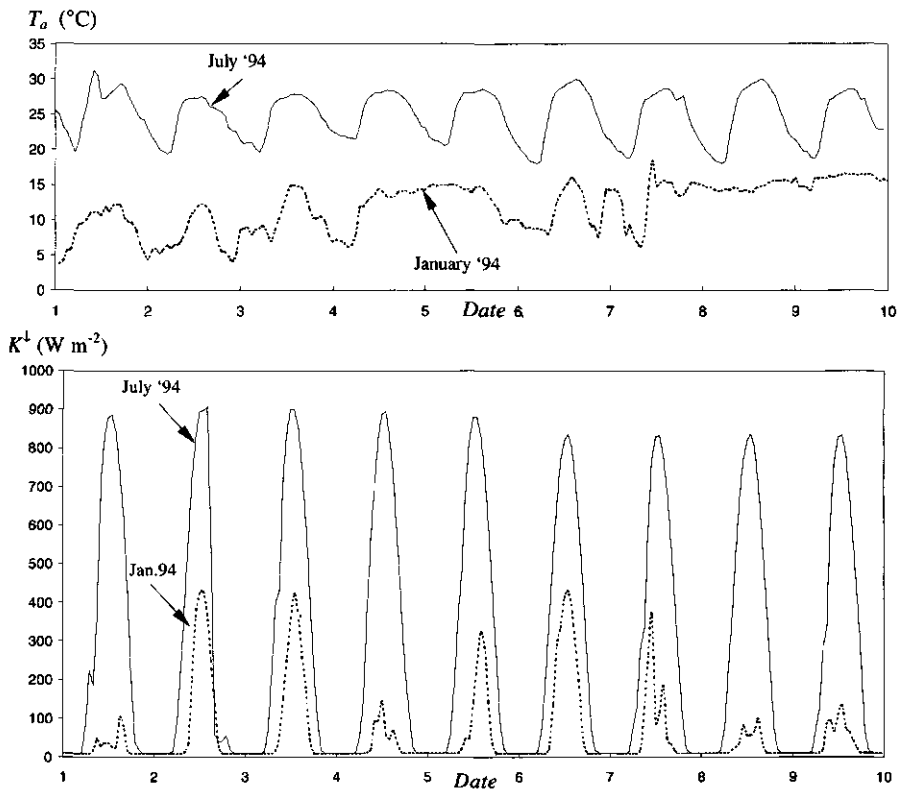


Fig. 5.7 Hourly values of air temperature  $T_a$  and incoming short-wave radiation  $K^\downarrow$  measured during the first ten days of January 1994 (dashed line) and July 1994 (continuous line).

### 5.3.4 Acquisition of Landsat TM images and geometrical rectification.

The Gromola district is located in the centre of frame 32 of orbit 189 of Landsat TM 5. During the study-period it was possible to acquire nine cloud-free mini-scenes (Tab. 5-2).

For each mini-scene a sub-set image of the Gromola area was extracted. In the preliminary processing, the images were geometrically rectified to the Universal Transversal Mercator projection system (UTM) by means of a first order transformation of the coordinates. The transformation coefficients were determined by applying a least-square regression to a set of 24 ground control points. Pixels were resampled with a nearest-neighbour technique (Jensen, 1986) on a square grid with spacing of 30 m. A final accuracy corresponding to a Root Mean Square error of 0.5 pixels ( $\pm 15$  m) was obtained for each image.

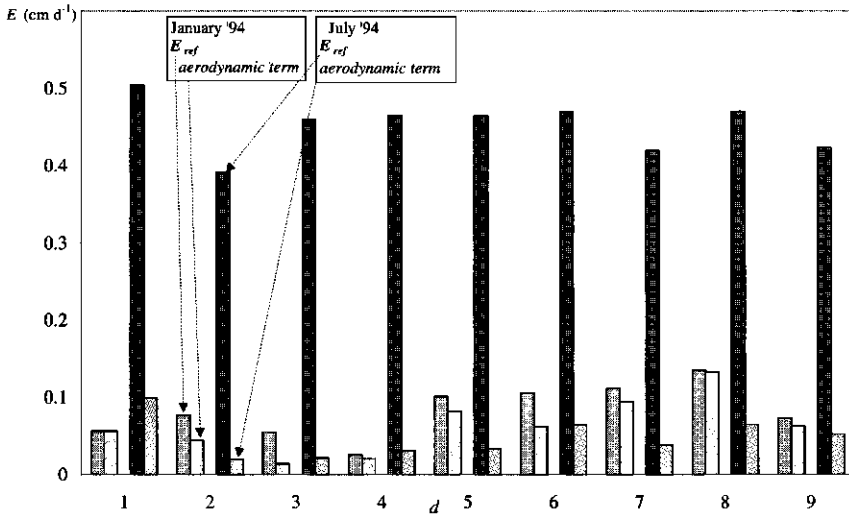


Fig. 5.8 Daily values of  $E_{ref}$  and of the corresponding aerodynamic term for the first decade of January 1994 (first pair of bars) and July 1994 (second pair of bars).

Tab. 5-2 Summary of Landsat TM 5 image acquisitions for the Gromola district.

Ref. image	Date	UTC (h)	sun elevation (°)	sun azimuth (°)	horiz. visibility (km)
1	Nov. 11 <sup>th</sup> , 1993	9.03	27.45	152.54	22
2	Jan. 30 <sup>th</sup> , 1994	9.02	24.29	145.37	18
3	May 22 <sup>nd</sup> , 1994	9.00	57.99	120.13	20
4	Jun. 23 <sup>rd</sup> , 1994	9.00	59.03	113.97	16
5	Jul. 25 <sup>th</sup> , 1994	8.59	55.61	117.60	16
6	Aug. 10 <sup>th</sup> , 1994	8.58	52.78	122.64	13
7	Sep. 9 <sup>th</sup> , 1994	8.58	45.13	135.09	15
8	Oct. 13 <sup>th</sup> , 1994	18.57	35.49	145.68	22
9	Nov. 14 <sup>th</sup> , 1994	8.56	26.04	150.92	19

### 5.3.5 Land use and cropping pattern

Detailed information concerning land use and crop development was acquired during the observation period.

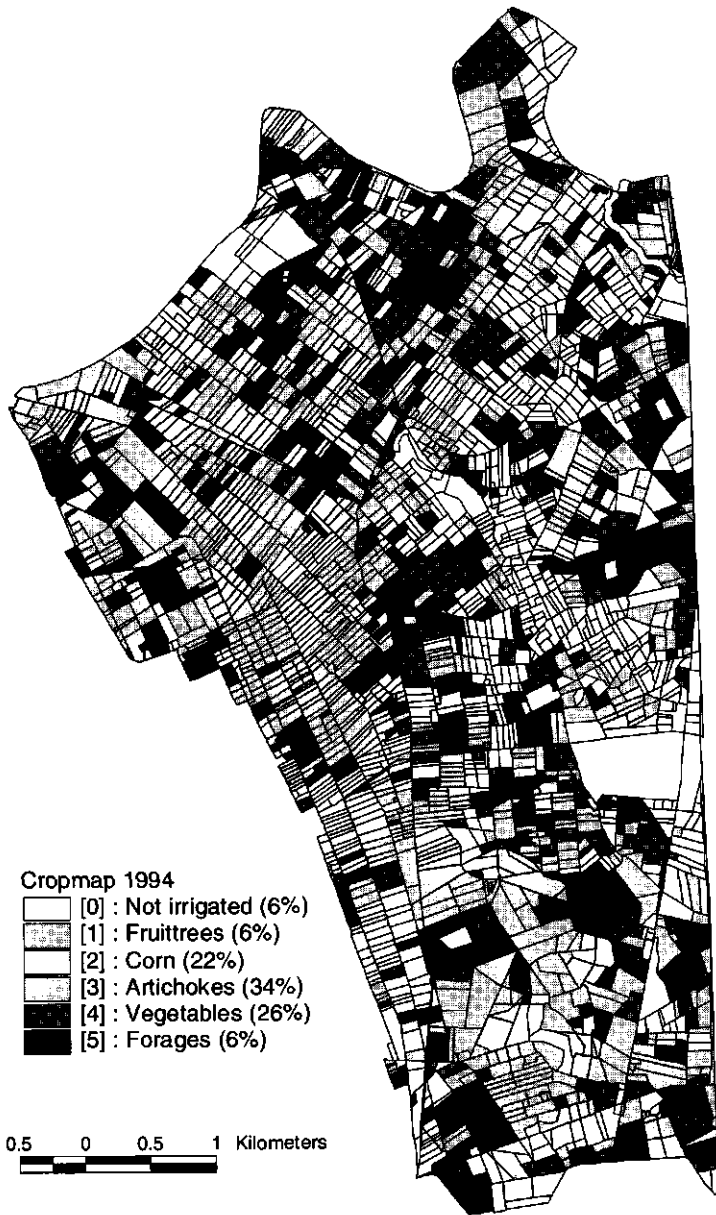


Fig. 5.9 Crops distribution in the tertiary units of the Gromola district and areal percentages for the irrigation season 1994.

Land use was monitored in three areas covering a total surface of approximately 490 ha where 39 fields plots were selected to monitor leaf area index and crop height. The selection criterion was based on crop type, starting date of cultivation, extension and shape of the plot. Since these measurements are needed to interpret the digital images of Landsat, which has a resolution of 30 x 30 m, fields with rectangular shape and size larger than 2 ha were considered.

A supervised classification of land use was made on a multitemporal image using the Landsat TM acquisitions of May, July and September. This choice allowed a better discrimination of the different spring and summer crops. The resulting crop distribution and statistics are given in Fig. 5.9. From the multitemporal classification, the total irrigated area resulted of 2650 ha approximately corresponding to 94% of the total area served. This crop distribution map was used to associate to each tertiary unit the input data concerning rooting depths and the critical soil water pressure heads characterising the root uptake of each crop type (Tab. 5-3). The values  $h_{3,H}$ ,  $h_{3,L}$  and  $h_4$  were taken from Taylor and Ashcroft (1972) with small adaptation on the basis of local observations.

Tab. 5-3 Critical pressure head values for water uptake of crops (Fig. 3.1) in the Gromola district.

Crop	$h_{3,H}$ (cm)	$h_{3,L}$ (cm)	$h_4$ (cm)
Fruit trees	-500	-800	-10000
Maize	-400	-700	-10000
Artichokes	-400	-600	-8000
Vegetables	-400	-700	-8000
Grass, forages	-400	-700	-8000

Ground-truth data included the measurement of Leaf Area Index  $LAI$  and crop height  $h_c$ . In each field,  $LAI$  was measured by means of a LICOR LAI-2000 canopy digital analyser (Welles, 1990) in coincidence of each planned LANDSAT-5 pass from November '93 to November '94. The LAI-2000 instrument consists of a wide-angle lens, an optical sensor and a compact control unit, which can be easily carried by the operator and interfaced to a personal computer. The lens incorporates a filter for radiation below 490 nm scattered by the foliage and it can be partially shaded with special caps.

The control unit enabled the measurement and storage of canopy gap fraction in 5 viewing directions, from which it was possible to estimate  $LAI$  and other information on canopy structure, i.e. fraction of sky visible from beneath the foliage and mean leaf inclination. The instrument and the algorithm used for the calculation of  $LAI$  were tested for different crops. By comparing directly

determined *LAI* values with the estimates obtained with the digital analyser an absolute accuracy of 15% was obtained (Welles and Norman, 1991).

To avoid the influence of direct sun-light, which determines an under-estimation of *LAI* with this apparatus, measurements were taken in early morning and afternoon. A lens-cap was used to hide the operator and the sun from the field of view of the sensor. A set of 24 readings was taken in different adjacent positions within each field to get an average *LAI* value. Simultaneously with each measurement, crop heights and descriptive information concerning the vegetative development were recorded. The temporal variation of *LAI* for two different land uses is presented in Fig. 5.10 and Fig. 5.11.

Assuming the fraction of sky visible from beneath the canopy in the zenith direction is the complement to 1 of the fractional vegetation cover  $s_c$ , the empirical relationship between *LAI* and  $s_c$  shown in Fig. 5.12 was found by means of non-linear regression on the data set collected in the study area.

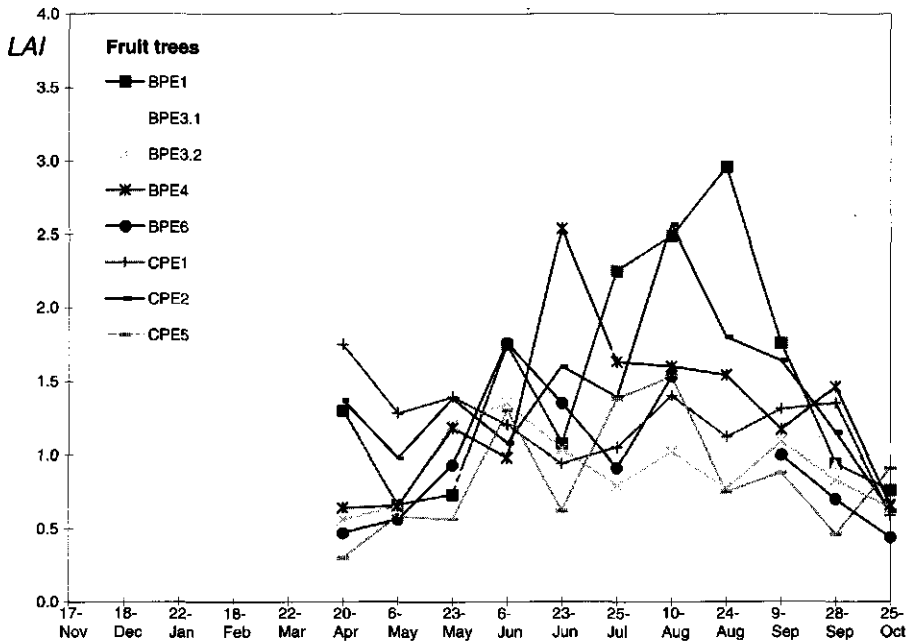


Fig. 5.10 Leaf Area Index (*LAI*) measurements for fruit trees in the Gromola district from November 1993 to November 1994.



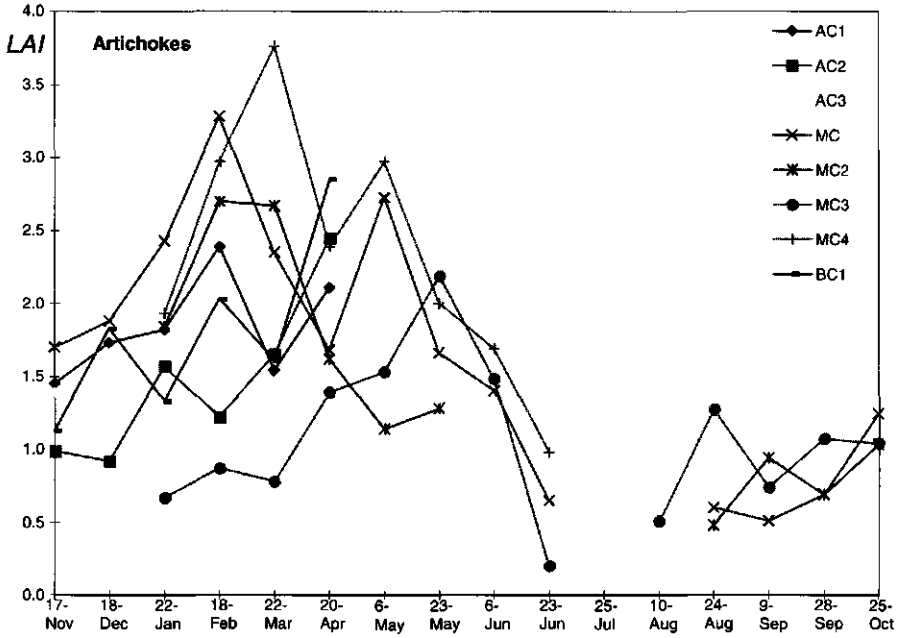


Fig. 5.11 Leaf Area Index (LAI) measurements for artichokes in the Gromola district from November 1993 to November 1994.

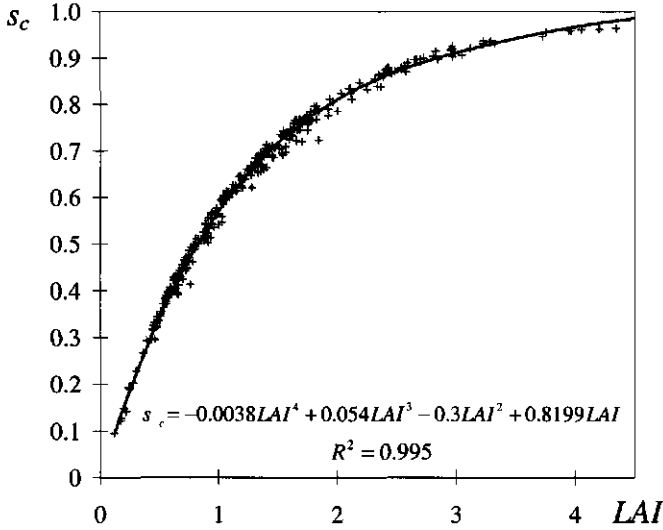


Fig. 5.12 Relationship between LAI and fractional vegetation cover  $s_c$ .

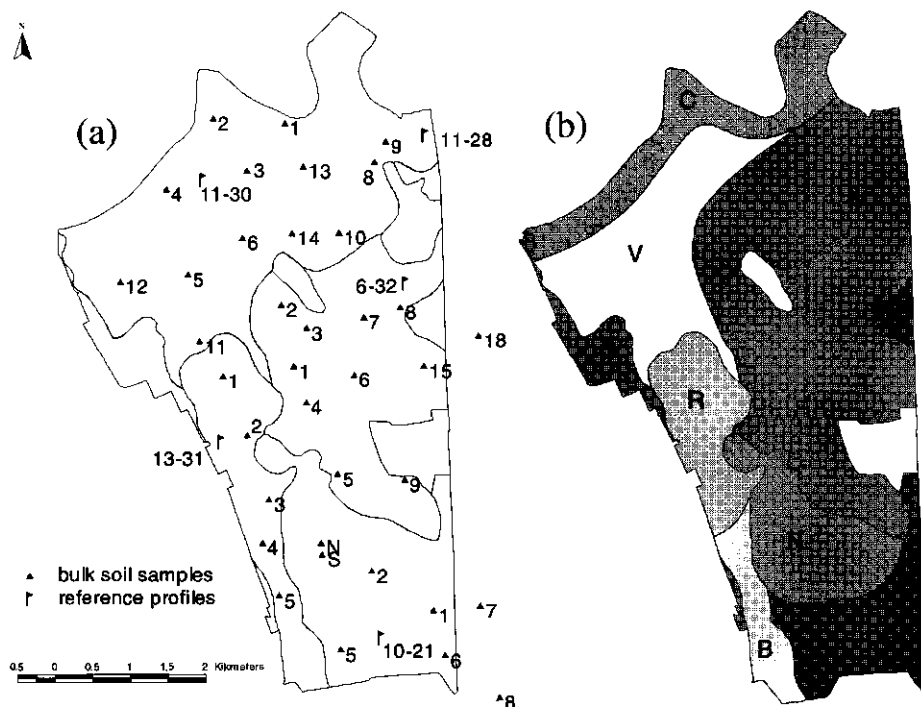


Fig. 5.13 (a) Soil map and sampling locations; data of reference profiles are given in Tab. 5-4. (b) new map units with homogeneous soil hydraulic characteristics; parameters are given in Tab. 5-5.

### 5.3.6 Soil hydrological data

The soil hydrological data group includes two categories of measurements: soil hydraulic characteristics and monitoring of soil water content.

*Soil survey and hydraulic characterisation of reference profiles.* A soil map at scale 1:10.000 has been realised by the Consortium in 1989. Within the Gromola district, 4 soil units are present and they are indicated as 6, 10, 11 and 13 in Fig. 5.13a. From the pedological study the dominant soil textures in the area resulted clay loam and silty clay. In each unit it was possible to identify a reference profile being indicated in Fig. 5.13.a with labels 6-32, 10-21, 11-30 and 13-31. In order to derive the soil hydraulic parameters, a sampling campaign of the reference profiles and 40 locations scattered over the entire Gromola district was performed.

Undisturbed soil cores with a height of 9 cm and a diameter of 8.5 cm were collected in the main horizons of the reference profiles for each mapping unit by means of a steel cylindrical sampler. The laboratory technique for determining the

soil water retention curve  $\theta(h)$  was similar to the classical evaporation method of Wind (Boels et al., 1978; Wendroth et al., 1993). Its application was described in detail by Basile and D'Urso (1997). Examples of the resulting retention curves are presented in Fig. 5.14.

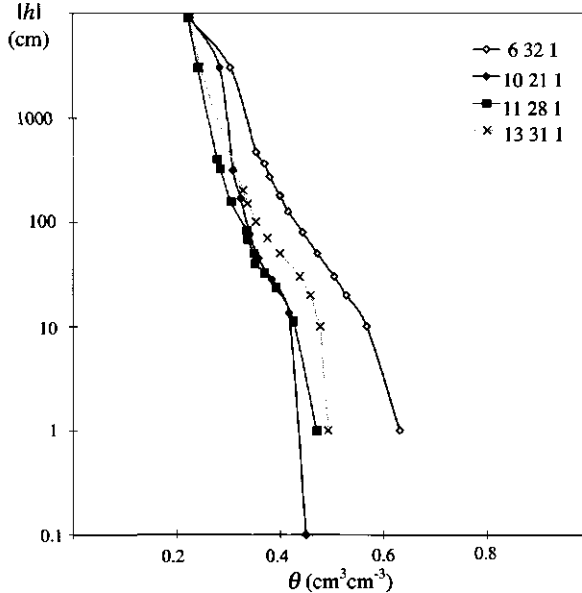


Fig. 5.14 Laboratory measurements of the soil water retention on undisturbed soil samples taken from the first horizon of the reference profiles for the four mapping units.

The analytical expression of van Genuchten for the soil water retention curve [Eq.(3.28)] was fitted to the laboratory measurements of  $[\theta, h]$  pairs. The resulting parameters are given in Tab. 5-4. Saturated hydraulic conductivity,  $k_s$ , was determined on the same sample set by using the falling-head permeameter method; data are also reported in Tab. 5-4.

Afterwards, samples were dried to determine the dry bulk density and the particle-size distribution. Bulk soil samples collected from the main soil horizons in 40 random sites were used to determine the particle-size distribution curve. Texture analysis was performed by means of the hydrometer method for the size range between 0.002 and 0.5 mm and wet sieving for 0.5+2 mm. Examples of the resulting particle size distribution curve for the mapping unit 10 are shown in Fig. 5.15.

The calibrated pedo-transfer-function approach described in Section 3.6.3 was applied to the soil horizons of each reference profile associated with a soil mapping unit. For each reference profile a different analytical expression was found to fit the  $\psi(h)$  function to be used in Eq.(3.25).

Tab. 5-4 Description of soil reference profiles and correspondent hydraulic parameters of van Genuchten (1980). The tortuosity factor  $l$  was assumed to be equal to 0.5. Abbreviations of USDA texture classes indicates: SL: sandy loam; CL: clay loam; SIC: silty clay.

Unit	Prof.	Depth (cm)	Type	USDA texture	$\theta_s$ ( $\text{cm}^3\text{cm}^{-3}$ )	$\theta_r$ ( $\text{cm}^3\text{cm}^{-3}$ )	$n_{VG}$	$\alpha_{VG}$ ( $\text{cm}^{-1}$ )	$k_s$ ( $\text{cm d}^{-1}$ )
6	32	0-30	Ap1	SL	0.644	0.000	1.132	0.194	360
6	32	30-60	Ap2	SL	0.622	0.000	1.176	0.048	480
6	32	60-120	Ckm	SL	0.617	0.000	1.205	0.005	10
10	21	0-40	Ap	SL	0.463	0.162	1.198	0.147	1080
10	21	40-70	B2	SL	0.580	0.112	1.272	0.049	211
11	28	0-70	Ap	CL	0.472	0.199	1.335	0.106	264
11	28	70-90	A1	CL	0.429	0.188	1.328	0.037	43
11	30	0-45	Ap	SIC	0.507	0.138	1.320	0.035	31
11	30	45-85	A1	SIC	0.559	0.235	1.300	0.023	8
13	31	0-30	Ap1	SIC	0.496	0.210	1.463	0.037	7
13	31	30	Ap2	CL	0.484	0.142	1.136	0.188	1920

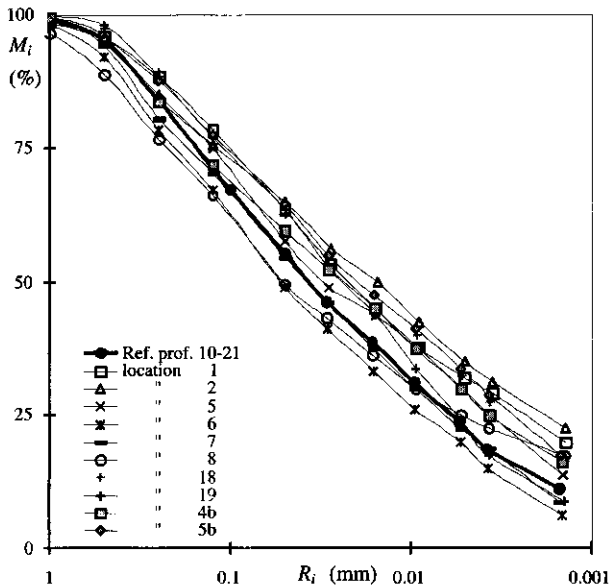


Fig. 5.15 Distribution curve of solid mass percentage  $M_i$  versus particle radius  $R_i$  for the first horizon of mapping unit 10.

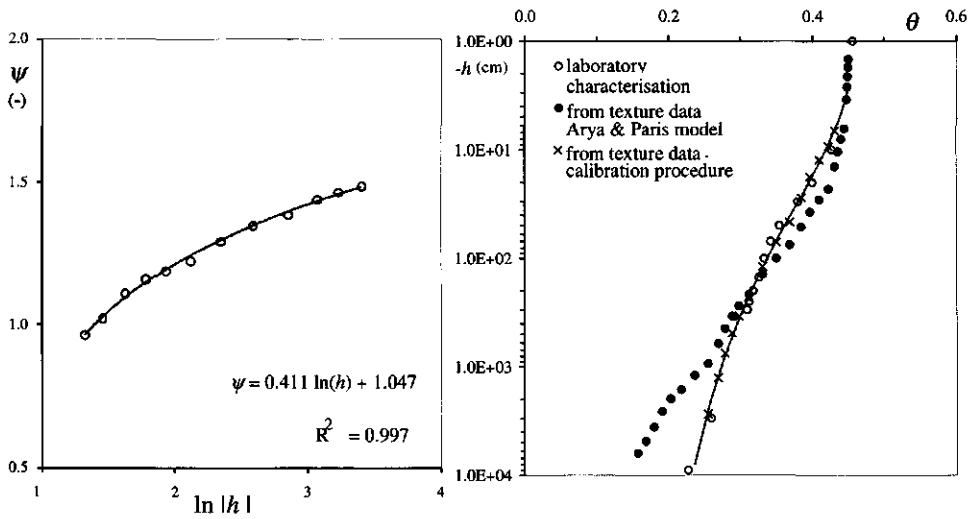


Fig. 5.16 Calibration of the pedo-transfer function  $\psi(h)$  derived from Arya and Paris model (left) and corrected soil water retention curve (right). The figure on the right also shows the comparison between corrected and uncorrected data.

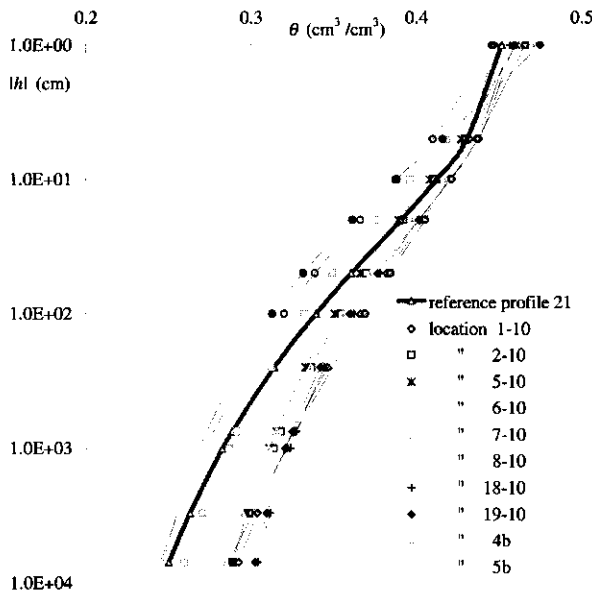


Fig. 5.17 Soil water retention curves derived by means of the calibrated pedo-transfer function on the soil textural data of Fig. 5.15.

An example of the  $\psi(h)$  function and the resulting correction on the estimate of  $\theta(h)$  curve for the top layer of unit 10 is illustrated in Fig. 5.16. Then the saturated hydraulic conductivity  $k_s$  was estimated by means of Eq.(3.30) with the empirical constant  $c$  set to 0.9.

The calibrated functions  $\psi(h)$  were subsequently used for determining the  $\theta(h)$  curve for each location where soil textural information was available (Fig. 5.13.a). As the soil water pressure head  $h_i$  in the generic  $i^{\text{th}}$  texture range can be expressed as a function of corresponding pore radius  $\varphi_i$  through the capillary equation, Eq.(3.25) can be re-written as follows:

$$\varphi_i = R_i \sqrt{\frac{4}{6} \left( \frac{\rho_p - \rho}{\rho} \right) n_i^{1-\psi[h(\varphi_i)]}} \quad (5.1)$$

The unknown pore radius  $\varphi_i$  in Eq.(5.1) can be determined by means of iterative algorithms for each pair of values  $[M_i, R_i]$  given in the particle size distribution curve. The  $\theta(h)$  curves for the first horizon on soil mapping unit no.10 and resulting from this calibration procedure are shown in Fig. 5.17. The retention data were used to fit the van Genuchten analytical expression for  $\theta(h)$  and  $k(h)$ . By comparing the values of  $\theta$  resulting from the described procedure on four samples with independent measurements in the range  $[-300 \leq h \leq -1 \text{ cm}]$ , the average error of estimate was less than 0.04.

*Derivation of functional soil hydraulic properties and delimitation of homogeneous units.* The functional properties approach described in Section 3.6.3 was applied for each location where estimates of  $\theta(h)$  and  $k(h)$  were available from the pedo-transfer function approach. To represent "summer" conditions, a drying process starting from near saturation was simulated, assuming a constant potential evapotranspiration flux density of  $0.5 \text{ cm d}^{-1}$  on the upper boundary, a fixed groundwater table depth of 2 m for the lower boundary condition and a uniform grass cover.

From the output of simulation runs, the mean value of soil water pressure head  $h$  between soil depths 10 and 30 cm was computed for each day. The number of days needed to reach a value of  $h$  less than  $-800 \text{ cm}$ , indicated as  $d_{800}$ , was considered as the *functional property* in each location. The resulting spatial distribution of  $d_{800}$  was used to identify areas with similar hydrologic behaviour. The original soil map was re-classified by considering the spatial distribution of the functional property  $d_{800}$ . The result of this elaboration is shown in Fig. 5.13.b.

The boundaries of the new map units were drawn according to a discrete technique of interpolation using external landscape features as well as roughly visual delimitation. Finally, for each new mapping unit the average  $\theta(h)$  and  $k(\theta)$  curves were identified and the corresponding van Genuchten parameters were determined (Tab. 5-5).

Tab. 5-5 Soil hydraulic parameters according to van Genuchten (1980) for the new soil mapping units of Fig. 5.13b. The tortuosity factor  $l$  was assumed equal to 0.5.

UNIT	Depth (cm)	$\theta_s$ ( $\text{cm}^3\text{cm}^{-3}$ )	$\theta_r$ ( $\text{cm}^3\text{cm}^{-3}$ )	$n_{VG}$ -	$\alpha_{VG}$ ( $\text{cm}^{-1}$ )	$k_s$ ( $\text{cm d}^{-1}$ )
B	0-30	0.038	0.456	1.10	0.167	2438
	30-70	0.157	0.579	1.27	0.028	70
C	0-45	0.163	0.482	1.38	0.062	171
	45-75	0.179	0.556	1.32	0.082	452
M	0-70	0.202	0.465	1.34	0.101	280
	70-90	0.151	0.425	1.25	0.079	193
N	0-40	0.250	0.449	1.41	0.070	67
	40-70	0.025	0.602	1.18	0.054	563
P	0-30	0.107	0.442	1.15	0.092	427
	30-60	0.051	0.588	1.20	0.037	221
	60-120	0.000	0.605	1.25	0.004	3
R	0-30	0.182	0.490	1.33	0.053	117
	30-60	0.300	0.500	1.47	0.115	184
S	0-70	0.000	0.387	1.29	0.380	10462
	0-30	0.082	0.635	1.15	0.238	499
T	30-60	0.176	0.634	1.39	0.025	71
	60-120	0.000	0.605	1.25	0.004	3
V	0-45	0.107	0.502	1.24	0.059	265
	45-85	0.127	0.549	1.20	0.074	486

### 5.3.7 Monitoring of groundwater table depth

The hydrogeology of the alluvial plain of the Sele river basin is characterised by the presence of a phreatic aquifer overlaying a complex multilayer aquifer system (Cassa per il Mezzogiorno, 1981). The phreatic aquifer originates from alluvial deposits and it reaches an average depth of 15 m below soil surface. There is practically no interaction between the phreatic aquifer and the multilayer aquifer. The mountainous region situated on the eastern border of the case-study area has a calcareous lithology. This area is considered to be the main contributor to the recharge of the multilayer deep aquifer. Groundwater fluxes originate from this recharge area in the direction of sea, causing a hydraulic gradient of 0.6% in the eastern part of the alluvial aquifer (Cassa per il Mezzogiorno, 1983). Poor quality of groundwater, due to the presence of sodium-chlorine salts in the deep multilayer aquifer limits to a great extent the extraction of groundwater for irrigation.

Groundwater table depths were measured in 18 observation wells scattered over the area (Fig. 5.18). In the Tab. 5-6 the range of variation for each observation well is given. The average observed depth was 1.9 m, with an average minimum of 1.4 and an average maximum of 2.3 m.

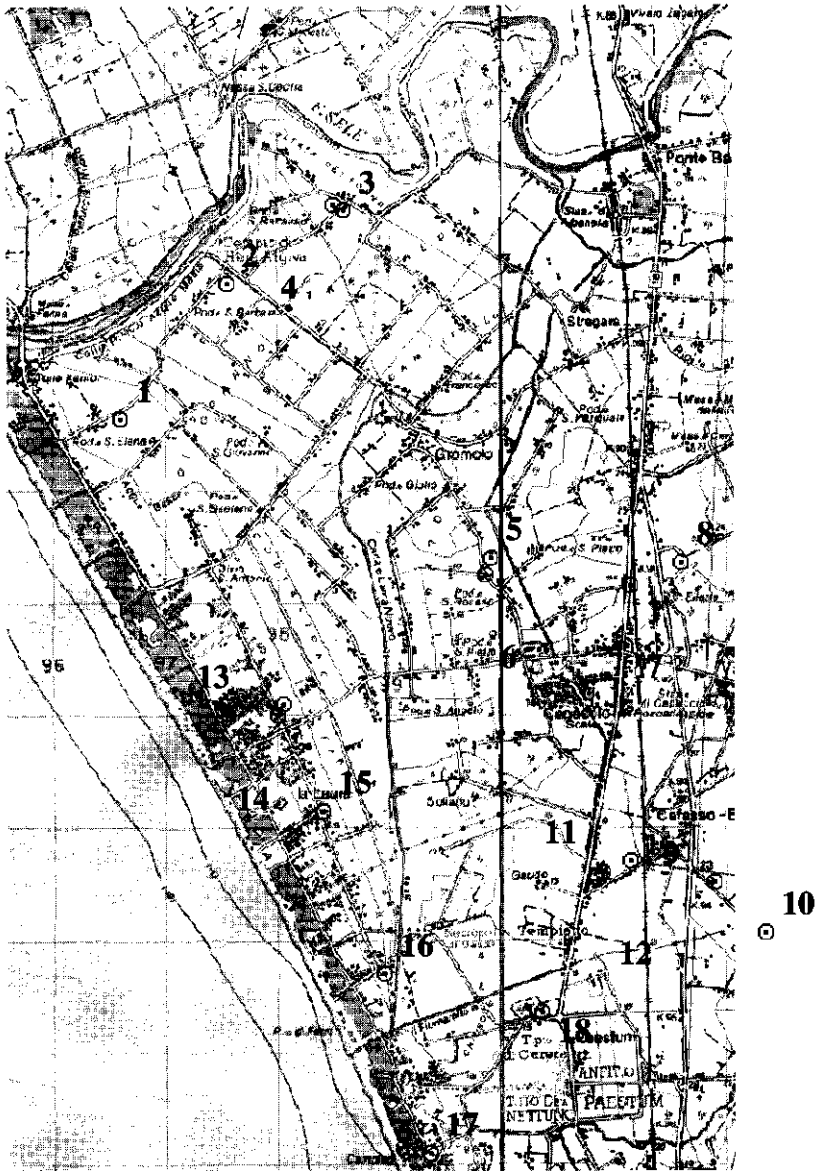


Fig. 5.18 Location of the observation well for groundwater monitoring in the study-area



Tab. 5-6 Summary of groundwater table depth measurements during 1994

Obs.well n.	m. a.s.l.	avg.	min.	max.
1	2.0	1.6	1.2	1.8
2	2.5	2.2	1.5	2.4
3	4.0	0.8	0.6	1.1
4	4.0	0.8	0.4	1.0
5	14.0	3.1	2.4	3.8
6	14.0	2.6	2.1	3.1
7	25.0	1.9	0.7	3.4
8	24.0	3.0	2.1	3.7
9	24.0	0.8	0.2	1.3
10	22.0	1.1	0.9	1.3
11	22.0	1.1	0.7	1.4
12	19.0	2.0	1.4	2.4
13	6.0	1.6	1.3	1.9
14	6.0	2.6	2.2	2.9
15	7.0	3.4	2.9	3.9
16	6.0	2.1	1.9	2.3
17	5.0	1.5	1.1	1.7
18	16.0	10.2	9.9	10.7

An example of the temporal evolution of the groundwater table depth during the irrigation season of 1994 is presented in Fig. 5.19. In this figure the plots are aggregated for each soil mapping unit. When considering the elevation of the wells, the presence of an hydraulic gradient from east to west in the inland areas and from north to south in areas nearer to the coastline can be noticed. This confirms the existence of groundwater flow from the recharge area of the aquifer located at north-east of the study-area.

### 5.3.8 Map of lower boundary condition

The function  $v(\phi)$  characterising the water fluxes through the bottom boundary of the soil profiles modelled in SWAP was determined in the study-area by means of the procedure described in Section 3.6.2. The groundwater model SIMGRO was applied to an area covering approximately 60 km<sup>2</sup> in the left portion of the Sele river lower plain including the study-area. This enlarged area was chosen for a better identification of the boundary conditions of the finite elements grid, composed by 240 triangular elements (corresponding to 140 nodes). The entire simulation area was sub-divided in 8 regions corresponding to the soil mapping units. The calibration of the groundwater model was made with the support of the groundwater table depth in the observation wells during 1994.

Case-study in the Sele Plain, Italy: the Gromola irrigation district

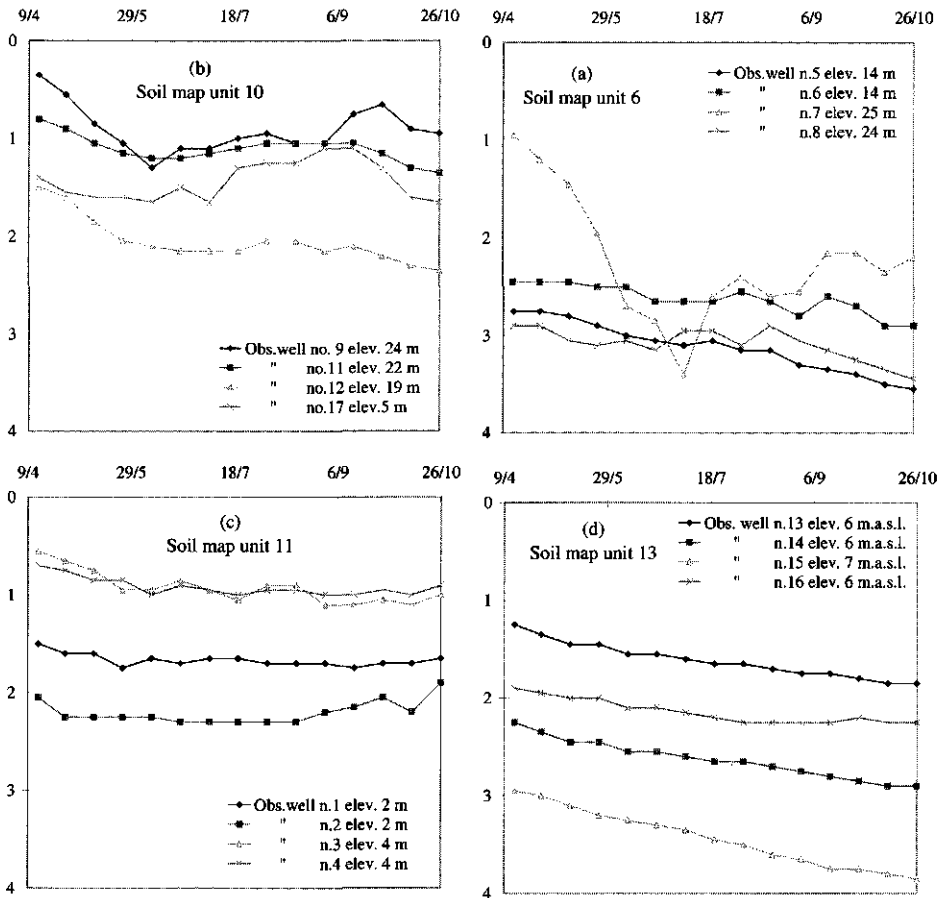


Fig. 5.19 Groundwater table depths during the irrigation season of 1994 in the Gromola district. Frame (a) refers to observation wells located within the soil mapping unit nr.6; in analogy, frame (b) for soil mapping unit 10, (c) for soil unit 11 and (d) for soil unit 13.

Numerical experiments with data from November 1993 to November 1995 were run. The output of SIMGRO was aggregated for each subregion and the resulting  $v(\phi)$  functions were plotted.

An example of the output for one region of the case-study area is given in Fig. 5.20. In spite of the coarse discretisation of the simulation grid, which partly explains the scatter of some points, it was possible to clearly identify an analytical function for interpolating the majority of plotted data, represented in the figure by the continuous line. The resulting function  $v(\phi)$  was taken as the bottom boundary condition for the application of SWAP. GIS tools have been used to establish the geographical correspondence between the grid nodes and the soil columns to which the model was applied.

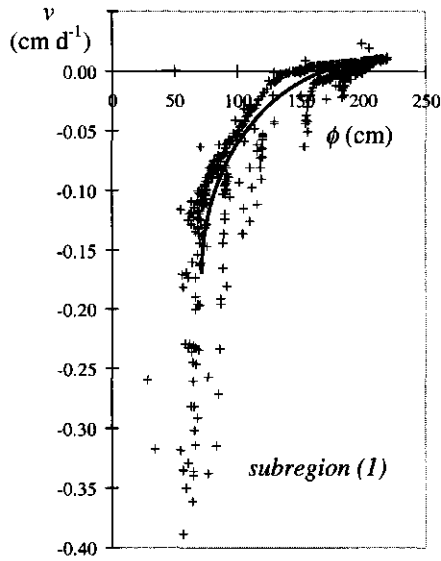
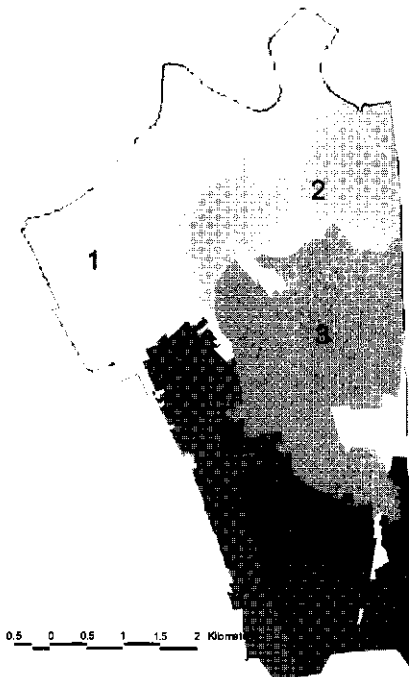


Fig. 5.20 Relationship between the average values of the water flux at the bottom of the unsaturated zone ( $v$ ) and the phreatic surface depth ( $\phi$ ) in a sub-region of the Gromola area.



- 1)  $v = -0.90 e^{(-0.028\phi)}$
- 2)  $v = -1.35 e^{(-0.008\phi)}$
- 3)  $v = -0.90 e^{(-0.025\phi)}$
- 4)  $v = -0.80 e^{(-0.040\phi)}$
- 5)  $v = -0.34 e^{(-0.006\phi)}$

Fig. 5.21 Map of bottom boundary conditions and corresponding functions  $v(\phi)$  between water flux  $v$  through the soil profile bottom and the groundwater table depth  $\phi$ .

The spatial distribution of bottom boundary condition and the corresponding  $v(\phi)$  function for the case-study area are shown in Fig. 5.21.

#### 5.4 Validation of the SWAP model.

The validation of SWAP was made with the support of soil water content  $\theta$  measurements by means of Time-Domain Reflectometry (TDR) as developed by Topp (Topp et al., 1980). The temporal variations of  $\theta$  were measured in two selected locations with TDR probes permanently installed in the soil.

In the first location, two series of four TDR probes were installed in an artichoke plot nearby the meteo-station. Three-rods coaxial probes (Zegelin et al., 1989) of 14 cm length and 3.5 cm rod-spacing were used for this purpose. The probes were positioned horizontally at depths 11, 27, 43 and 60 cm below the soil surface. The datalogging unit of the meteo-station was used to control a Tektronix 1502-B cable-tester and the multiplexing device. TDR reflectograms were automatically digitised in 251 points and stored in the data-logger memory. An example of reflectogram acquired in this installation is given in Fig. 5.22.

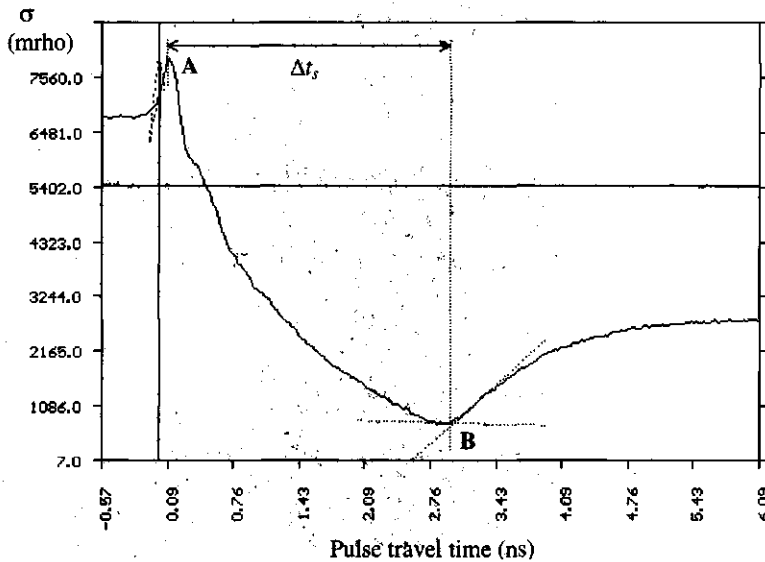


Fig. 5.22 Example of a TDR reflectogram acquired at 23 cm soil depth in the Gromola area. Soil texture is classified as clay-loamy. On the vertical axis, the voltage reflection  $\sigma$  is indicated. The pulse travel time  $\Delta t_s$  is given by the abscissas difference of points A and B, representing the beginning and the end of the soil probe.

In the second location, three TDR probes were installed at depths of 20, 40 and 60 cm respectively with vegetable crops. Acquisition of TDR reflectograms was manually done at regular intervals from July to October 1994 using a TDR unit similar to the previous installation and connected to a notebook-computer.

From the travel time of a TDR pulse,  $\Delta t_s$ , it is possible to determine an "apparent" soil permittivity  $\epsilon_a$  by means of the following relationship (Roth et al., 1992; Whalley, 1993):

$$\frac{c\Delta t_s}{2L_p} = \sqrt{\epsilon_a} = \Gamma \quad (5.2)$$

where  $c$  is the velocity of electromagnetic waves in vacuum ( $c=3\cdot 10^{10}$  m s<sup>-1</sup>),  $L_p$  is the length of the probe (cm) and  $\Gamma$  is the refraction index. The soil permittivity  $\epsilon_a$  can be empirically related to  $\theta$  by means of the so-called "universal" Topp's polynomial expression (Topp et al., 1980). Similarly, a linear relationship between  $\Gamma$  and  $\theta$  has been found (Heimovaara, 1993). By using these "universal" relationships, the absolute error in the estimate of  $\theta$  is not larger than 0.05 in most mineral soils having limited clay contents and no solutes (Jacobsen et al., 1995). For the clay-loam soil of the TDR installation at the meteo station of Gromola, the calibration of  $\Gamma$  versus  $\theta$  was made on undisturbed soil columns in the laboratory. The resulting relationship is shown Fig. 5.23.

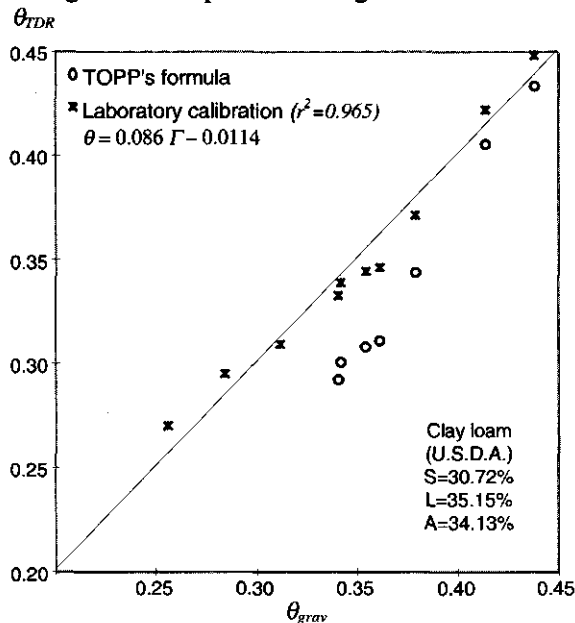


Fig. 5.23 Calibration of TDR soil water content  $\theta_{TDR}$  versus gravimetric  $\theta_{grav}$  measurements for a clay loam of the Gromola study area and comparison with the so-called 'universal' relationship of Topp (Topp et al., 1980).

By using the calibration relationship of Fig. 5.23, instantaneous soil water content profiles were automatically acquired every day at 16.00 hours from March to July 1994.

The soil water content measurements were compared with the values simulated by SWAP. The TDR installation falls within the unit R of the map of homogeneous soil hydraulic areas (Fig. 5.13.b). Simulations were made by using the corresponding parameters in Tab. 5-5. To define the upper boundary condition the  $LAI$  and the crop height  $h_c$  were measured in the same plot of the TDR installation, while the surface albedo was fixed to 0.18.

The comparison between measured and simulated soil water storage calculated over the 5–50 cm soil depth is shown in Fig. 5.24. It should be noticed that the measured values are corresponding to the TDR reading taken at 4.00 p.m., while the simulated values should be considered as daily averages. For this reason, some measurement points can be very different from the simulated ones, if rainfall events took place in the proximity of TDR acquisition i.e. outlier points on dates 9<sup>th</sup> of April and 9<sup>th</sup> of May. The average error of estimate amounted to 1.5 cm, which is comparable to the measurement error of TDR and is satisfactory for the application considered.

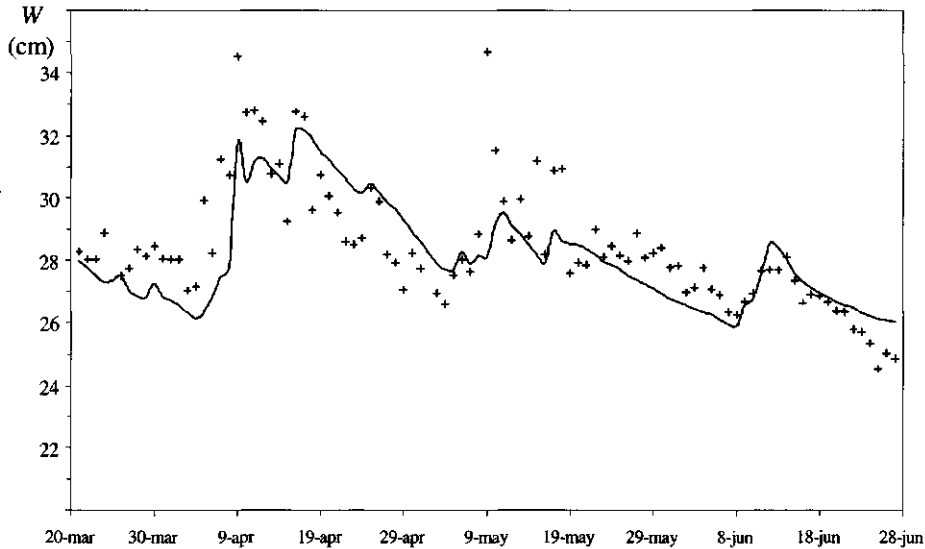


Fig. 5.24 Comparison of simulated (-) versus measured (+) soil water storage between  $z=-5$  cm and  $z=-55$  cm in proximity of the meteo station in the Gromola district in 1994.

## 5.5 Conclusions

In this Chapter the description of the case-study area in the irrigation district of Gromola was presented. The amelioration of the conveyance network, with the substitution of the old open-channels with pressurised pipelines, represents one of the main reasons for the choice of this study-area.

The acquisition of field data and the preparation of inputs for the application of SIMODIS were illustrated. The methodologies described in Sections 3.6.2 and 3.6.3 for the definition of the lower boundary condition and for the identification of the soil hydraulic input data were applied.

From the analysis of simulated and measured time-series of groundwater table depths  $\phi$  it was possible to determine the expression relating the water flux density through the bottom boundary and the groundwater table depth. The soil hydraulic retention and conductivity functions were estimated from textural data available in several locations by means of calibrated Pedo-Transfer Functions. On the basis of these estimates of the soil hydraulic properties, a functional property was calculated with SWAP to identify area with similar hydraulic behaviour. From the results of these calculation, the study-area was classified in nine mapping units to which a unique set of soil hydraulic variables was assigned.

Finally, the validation of SWAP was made by comparing the specific soil water storage as simulated by the model and measured with TDR.

## 6 Mapping crop coefficients in the Gromola irrigation district from Landsat TM images.

---

The concepts outlined in Chapter 4 to map the crop coefficient values  $K_c$  pixelwise have been applied to the Gromola irrigation area using Landsat TM images acquired on the dates reported in Tab. 5-2. Both the *classification* and the *analytical* approaches have been applied with the surface reflectance data derived from satellite images. To calculate the directional at-surface spectral reflectance the satellite images have to be corrected for the atmospheric effects.

### 6.1 Estimation of at-surface directional spectral reflectance.

#### 6.1.1 Methodological approach

Spectral radiance measured by satellite sensors  $K^{\uparrow}_{TOA,\lambda}$  was derived from quantum radiance,  $DN_{\lambda}$ , in each band  $\lambda$ , by applying the following linear calibration relationship:

$$K^{\uparrow}_{TOA,\lambda} = A_{0,\lambda} + A_{1,\lambda} \cdot DN_{\lambda} \quad (6.1)$$

where the wavelength dependent calibration parameters,  $A_{0,\lambda}$  and  $A_{1,\lambda}$ , are related to the sensor technical characteristics and operating features. The appropriate set of parameters for Landsat TM can be found in Epema (1990).

The composition and the state of the atmosphere influence in a significant way the reflectance of Earth surface detected from space. Scattering of sunlight by air molecules and aerosols mainly occurs in the visible wavelength range; conversely, absorption by water vapour affects the infrared region. A schematic description of atmospheric effects is given in Fig. 6.1. The directional spectral reflectance observed at the top of the atmosphere results from four different contributions:

$$K^{\uparrow}_{TOA,\lambda} = K^{\uparrow}_{a,\lambda} + K^{\uparrow}_{b,\lambda} + (K^{\uparrow}_{s,\lambda} + K^{\uparrow}_{d,\lambda}) \quad (6.2)$$

The first term,  $K^{\uparrow}_{a,\lambda}$ , represents the contribution of atmospheric scattering of solar radiation; the second,  $K^{\uparrow}_{b,\lambda}$ , is the "background" contribution, due to the influence of objects in the vicinity of the observed surface (adjacency effect); the third term is the sum of the contribution of direct  $K^{\uparrow}_{s,\lambda}$  and diffuse  $K^{\uparrow}_{d,\lambda}$  reflection from the observed surface (*target* reflectance). To determine these quantities the



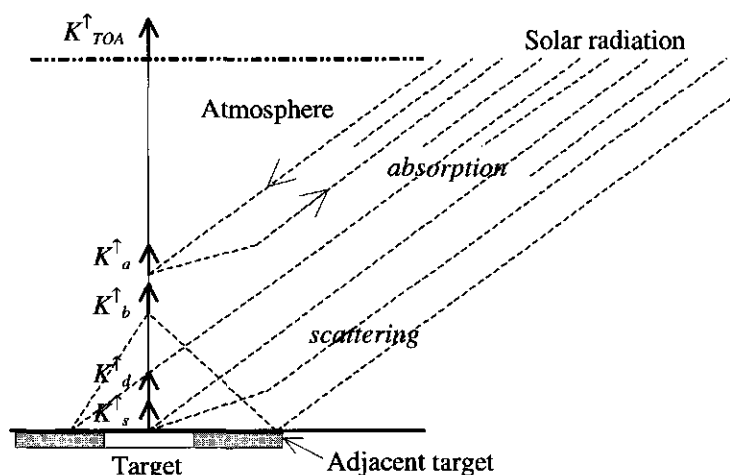


Fig. 6.1 Schematic representation of the different terms contributing to the radiance  $K_{TOA}^{\uparrow}$  ( $Wm^2$ ) observed from the top of the atmosphere. The subscript  $\lambda$  was omitted for simplicity (adapted from Verhoef, 1996).

parameters characterising the transmissivity of atmosphere e.g. the aerosol optical thickness have to be estimated.

In this study, the quantum radiance  $DN_{\lambda}$ , obtained in bands 1 to 5 and 7 of Thematic Mapper, was transformed in surface reflectance by means of the four-stream atmospheric correction model proposed by Verhoef (1985; 1996). In this model the spectral directional surface reflectance  $\rho_{\lambda}$  is estimated by the relationship:

$$\rho_{\lambda} = [G_{0,\lambda} + (G_{1,\lambda} - G_{0,\lambda})\rho_{b,\lambda}]DN_{\lambda} + [O_{0,\lambda} + (O_{1,\lambda} - O_{0,\lambda})\rho_{b,\lambda}] \quad (6.3)$$

where  $G_{0,\lambda}$ ,  $G_{1,\lambda}$ ,  $O_{0,\lambda}$ ,  $O_{1,\lambda}$ , are the *correction coefficients* for each spectral band and  $\rho_{b,\lambda}$  is the spectral *background reflectance*, which is given as input. To calculate the set of correction coefficients an estimation of aerosol optical thickness is required. The prior knowledge of the surface reflectance of well identified targets i.e. "dark" objects is applied for this purpose.

The value of background reflectance  $\rho_{b,\lambda}$  is fixed according to the average reflectance of a portion of image surrounding the target. For large and homogeneous targets  $\rho_{b,\lambda}$  can be taken equal to the target reflectance  $\rho_{\lambda}$  and Eq.(6.3) reduces to:

$$\rho_{\lambda} = \frac{G_{0,\lambda} \cdot DN_{\lambda} + O_{0,\lambda}}{1 + (G_{0,\lambda} - G_{1,\lambda})DN_{\lambda} + (O_{0,\lambda} - O_{1,\lambda})} \quad (6.4)$$

The assessment of the accuracy of the correction algorithm should be performed by means of reliable ground-truth measurements made on large and homogeneous targets. Since this task can not be easily achieved, the correction procedure might be evaluated by comparison of the spectra of "stable" objects such as coniferous forest, sand, glass houses, urban areas retrieved from TM images at different dates after atmospheric correction.

### **6.1.2 Application to the case-study area**

*Reference target.* In the case-study of the Gromola irrigation district, the estimation of correction coefficients  $\{G_{0,\lambda}, G_{1,\lambda}, O_{0,\lambda}, O_{1,\lambda}\}$  was carried out by assigning a known spectral reflectance to a portion of the Tyrrhenian sea included in the Landsat miniscenes. The sea surface was assumed as a "reference" target with known reflectance. The sea surface spectral reflectance in the visible wavelength range can not be assumed equal to zero. The variability of the water depth as well as the concentration of suspended and dissolved materials determines a range of variability between 0.01 and 0.04 of reflectance in bands 1, 2 and 3 of Thematic Mapper (Spitzer et al., 1987).

Hence two different approaches were compared. Firstly, the surface reflectance of sea water was assumed equal to 0.01 in the TM band 1 and 0 in all other bands of TM; the results of this first atmospheric correction will be further referred to as AC-1. Successively, a sea surface reflectance of 0.02 in bands 1 to 3 was considered. Horizontal visibility information (Tab. 5-2) from an aeronautical meteo-station nearby was also used to adjust the input data for a better estimation of the aerosol optical thickness; this correction will be referred as AC-2.

*Background reflectance.* In both correction procedures AC-1 and AC-2, the effect of the background reflectance was evaluated. As a first approximation, background and target reflectance were assumed to be equal and Eq.(6.4) was applied (AC-1-A; AC-2-A). These latter images were then used to calculate the "average" spectral reflectance over different portions of the image corresponding to a percentage of the sea surface included that varied from 20% to 50%. For each of these sub-images, the average spectral reflectance of all pixels was calculated from Eq.(6.4). The resulting values were alternatively considered as background reflectance and then Eq.(6.3) was applied to estimate the surface reflectance of each pixel (AC-1B, AC-2B and following).

*Analysis of results.* In Fig. 6.2, two examples of the spectra resulting from this elaboration on the image of July 25<sup>th</sup> are shown. The graph in Fig. 6.2.a refers to a fully vegetated area with a vegetation index of 0.9 (according to the reflectance values obtained with AC-1-A), while Fig. 6.2.(b) refers to a bright bare soil. Both targets are located at a minimum distance of 200 pixels from the coast line.

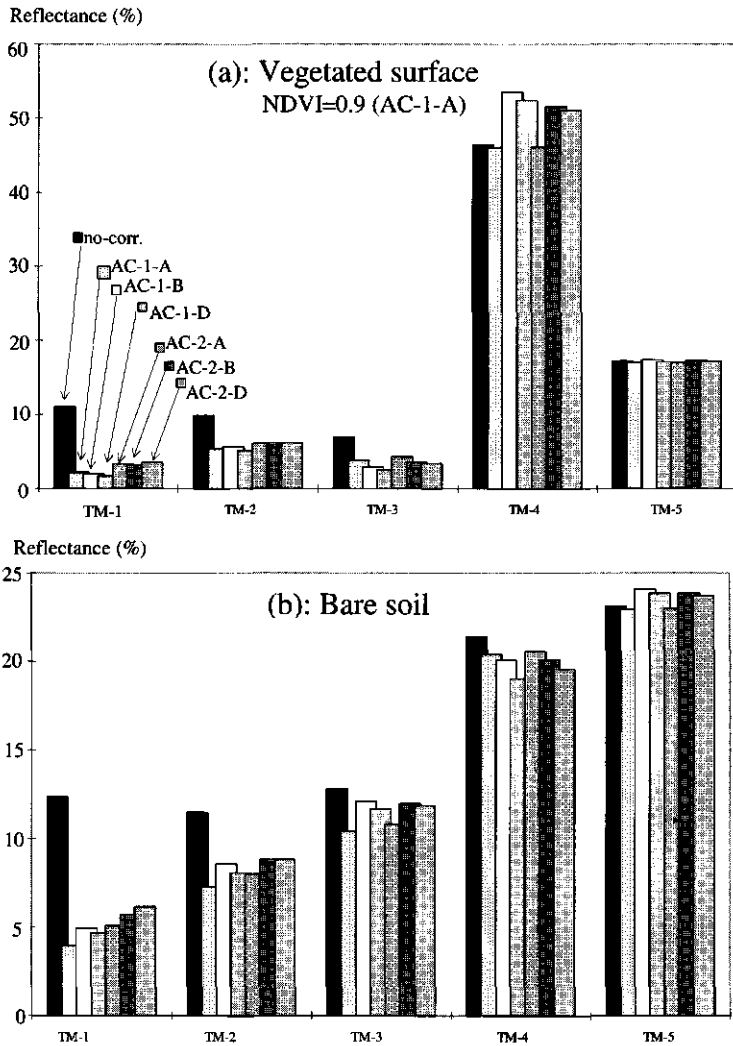


Fig. 6.2 Spectral reflectance in bands 1 to 5 of Thematic Mapper resulting from the application of different correction procedures performed on the image of July 25<sup>th</sup>, 1994, of the Gromola study area for a vegetated surface (a) and bare soil (b). Black-coloured bars result from neglecting the atmospheric effects. AC-1 refers to zero reflectance for the sea surface except in band TM1, while AC 2 considers a value of 0.02 for bands TM1 to TM3. AC-X-A assumes background reflectance equal to target reflectance, while AC-x-B to AC-x-D consider a background reflectance calculated on a circle area of 7.5 km radius differently positioned within the image.

From the comparison of Fig. 6.2.a and Fig. 6.2.b it is possible to notice that when considering bare soil surfaces, the influence of atmospheric scattering and absorption is negligible in bands 5 and, to a minor extent, also in band 4. As expected, the visible range, i.e. bands 1 to 3, is significantly influenced by the type of atmospheric correction applied. The overall effect of atmospheric correction is in general an increase of image contrast when bands 1 to 4 are used for the image visualisation. From the comparison of different correction procedures in Fig. 6.2, we see that when background reflectance is taken equal to that of the target, as in the case of corrections AC1-A and AC2-A, the reflectance in band 4 is significantly underestimated for vegetated surfaces and overestimated for bare soils. Another conclusion is that the different position of the window selected for the preliminary calculation of background reflectance, in AC1-B to D and AC2-B to D, does not affect the results in a significant way. In this case, the assumption of different values of sea water reflectance also does not affect the results in a significant way.

The influence of sea reflectance on the estimation of background reflectance is more relevant when considering areas close to the coast line. In Fig. 6.3, the multitemporal spectrum of a spot of the coastal eucalyptus forest is shown for the correction procedures AC-1-B and AC-2-B. The reflectance of this target can be considered rather constant during the summer. The graphs show that the underestimation of sea reflectance may produce unrealistic spectra, as in the case of the image acquired in June, for those pixels which are situated near the coast-line.

Finally, the correction procedure AC-2-B, which uses also information on the visibility, was judged to be the most reliable one, as confirmed by the minor variations of spectra shown in Fig. 6.3, compared to that resulting from the other procedures. The correction coefficients and background reflectance used for the nine images are given in Appendix I.

## **6.2 Application of the classification approach for mapping crop coefficients.**

In the classification approach, an implicit correlation between  $\{\rho_\lambda\}$  and  $K_c$  is assumed. As explained in Section 4.3, the classification algorithms are based on the definition of spectral classes corresponding to different crop coefficients  $K_c$  assigned from ground truth observations.

### **6.2.1 Signature extraction and spectral classes**

The sites of Leaf Area Index measurement, described in 5.3.5, were used to extract the spectral signatures to be used for the classification of the images. A mean vector of spectral reflectance for each ground-truth plot was extracted from the atmospherically corrected images no.4 to 7 (Tab. 5-2). Totally 77 spectral

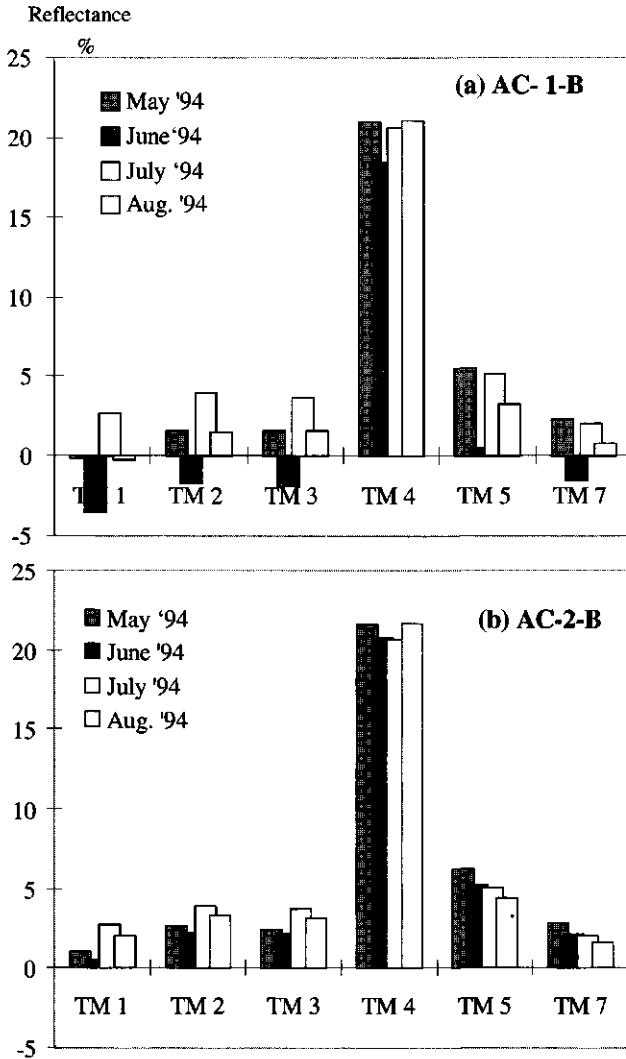


Fig. 6.3 Directional surface reflectance in the TM bands for a portion of the coastal eucalyptus forest in the Gromola study-area. The spectra in (a) result from the application of the AC-1-B procedure, in (b) from AC-2-B. The difference between the two corrections concerns the assumed value for sea surface reflectance.

samples were defined and a  $K_c$ -value was assigned to each one of them according to the procedure described by Doorenbos and Pruitt (1977).

To apply the classification approach described in Section 4.3, the following six different sets of spectral signatures were defined:

Mapping crop coefficients in the Gromola irrigation district from Landsat TM images.

- 1) NO\_clus: each spectral sample was considered as a single spectral signature;
- 2) Kc6: the signatures were formed by grouping in 6 classes the spectral samples on the basis of their  $K_c$ -values. The predefined intervals of  $K_c$  for each class are given in Tab. 6-1;
- 3) BT4w6: a non-hierarchical (dynamic) clustering technique was applied to the reflectance values of the samples in bands 3, 4 and 5 in order to define six spectral classes. The clustering criterion was based on maximising the Euclidean distance between the groups centroids, identified by the mean vector of each class (Webster and Oliver, 1990; Genstat 5 Committee, 1987);
- 4) BT5r7: similarly to BT4w6, 7 spectral classes were defined in bands 2, 3, 4, 5 and 7;
- 5) NH4m6: non-hierarchical clustering based on maximising the total Mahalanobis distance between groups, which also consider the variation within the groups. This clustering was applied to data in bands 3,4 and 5;
- 6) MD4c6: similarly to NH4m6, but the clustering criterion was based on minimising the determinant of the sum-of-squares and product (SSP) matrix within groups. This technique is also known as Wilks's criterion (Webster and Oliver; 1990).

*Tab. 6-1 Crop coefficient  $K_c$ , variance of  $K_c$  between classes and separability index,  $JM^*$ , for the different sets of signatures*

SET	NO_clus	Kc6	BT4w6	BT5r7	NH4m6	MD4c6
$K_c(1)$	-	<0.4	0.412	0.412	0.533	0.467
$K_c(2)$	-	0.4-0.6	0.592	0.551	0.799	0.559
$K_c(3)$	-	0.6-0.8	0.813	0.777	0.801	0.818
$K_c(4)$	-	0.8-0.9	0.836	0.822	0.802	0.900
$K_c(5)$	-	0.9-1.0	0.924	0.839	0.805	0.956
$K_c(6)$	-	>1.0	1.004	0.939	0.858	0.981
$K_c(7)$	-	-	-	1.004	-	-
var( $K_c$ )	-	-	0.049	0.040	0.014	0.047
$JM^*$	0.956	0.600	0.838	0.859	0.645	0.766

Except the set Kc6, the value of  $K_c$  was not considered as a variable in the clustering, but it was successively calculated by averaging the values of the samples allocated to each class. Class separability was then estimated by means of

the Jeffrey-Matusita normalised distance  $JM^*$ , expressed by Eq. (4.5). In Tab. 6-1 the resulting  $JM^*$  indexes and  $K_c$  values for each set are summarised.

The analysis of Tab. 6-1 shows that the various clustering criteria lead to different  $K_c$  -values in each respective class. As expected, the highest separability applies to the non-clustered set NO\_clus, where  $JM^*=0.956$ . The set BT4w6 gave the largest differentiation of  $K_c$  -values among the 5 clustered sets, i.e. Kc6 through MD4c6 and it had the second-best separability. For all sets, the  $JM^*$  values below the threshold of 0.88 imply a probability of classification errors greater than 0.10; in particular, a very unsatisfactory separability resulted for the sets Kc6 and NH4m6. Thus, from this first step of the analysis, the best set of signatures were BT4w6, BT5r7 and MD4c6.

### 6.2.2 Performance assessment of classifier

In the second stage of the procedure, the above-mentioned spectral sets were used as training sets to carry out the supervised classification of the images of the Gromola study area. A maximum-likelihood procedure based on Mahalanobis distance [Eq.(4.6)] as agglomeration criterion was applied. For each training set a different classification output was obtained. In order to perform the *thresholding* analysis described in 4.3, the minimum values of Mahalanobis distance of each pixel, that is the value corresponding to the class assigned to each pixel, were stored in a separate file. From this information, the percentage of rejected pixels for different confidence level values was calculated for each classified image.

The resulting thresholding curves for the image of June 23<sup>rd</sup>, are shown in Fig. 6.4 . The classification indicator,  $A^*$ , calculated by means of Eq.(4.7) for the images of June and July are given in Tab. 6-2. The lowest reliability corresponds to the non-clustered set NO\_clus; the highest one results for the spectral set Kc6. The set BT4w6 produces the best classification reliability among the clustered training sets. Similar results were found in the processing of images acquired on different dates. The set with 7 spectral classes, BT5r7, in spite of the good separability index,  $JM^*$  (Tab. 6-1), is the second worst performing set for the reliability analysis after NO\_clus.

The classification performance indicator,  $CP^*$ , defined by Eq.(4.8), was finally calculated for all the classifications made on the images of June 23<sup>rd</sup> and July 25<sup>th</sup>. The results are summarised in Tab. 6-2, from which it is possible to conclude that the best results were obtained with the classification BT4w6 for both images. This results is of particular interest if we consider that the spectral set BT4w6 is also showing the best differentiation of  $K_c$  -values among the classes, as reported in Tab. 6-1. This means that the use of classification performance indicators, such as the separability and thresholding indexes, is a valuable tool to improve both the significance and the reliability of classification procedures.

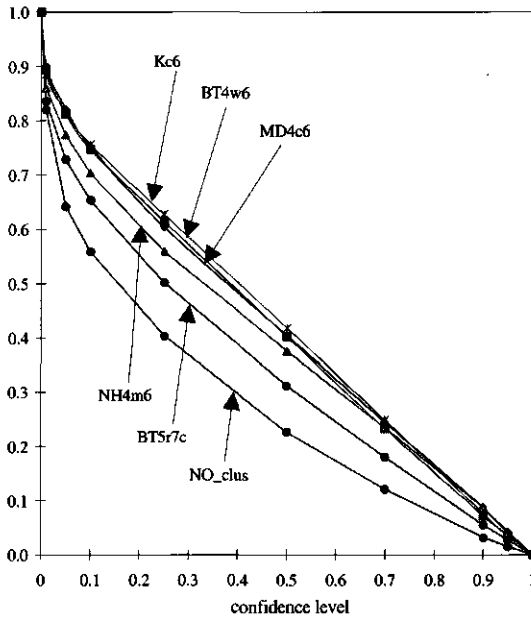


Fig. 6.4 Thresholding curves for alternative classification procedures applied to the image of June '94. X axis: confidence level associated to the fraction of rejected pixels (Y axis).

Tab. 6-2 Performance indicators for different classification outputs of the June and July '94 images.

SET	June 23 <sup>rd</sup> , 1994		July 25 <sup>th</sup> , 1994	
	A*	CP*	A*	CP*
NO_clus	0.271	0.259	-	-
Kc6	0.413	0.248	0.476	0.286
BT4w6	0.392	0.329	0.415	0.348
BT5r7	0.325	0.280	-	-
NH4m6	0.368	0.237	0.411	0.265
MD4c6	0.403	0.308	0.411	0.315



### 6.3 Application of the analytical approach for mapping crop coefficients

The analytical approach is based on the application of Eq.(3.11). In this case, to calculate the value of  $K_c$  in each tertiary unit estimates of  $r$ ,  $LAI$  and  $h_c$  from Landsat TM data were used in conjunction with ground-based meteorological data. The approach consists of the following steps:

- definition of an analytical relationship between  $K_c$  and  $r$ ,  $LAI$ ,  $h_c$  for each satellite image; the parameters of such relationship depend on the average meteorological conditions during the period of satellite pass
- estimation of  $r$ ,  $LAI$  and  $h_c$  from surface reflectance data
- derivation of  $K_c$  map by applying the relationship found in step 1 to the corresponding satellite image.

#### 6.3.1 Sensitivity of crop coefficient values to meteorological variables and canopy properties.

*Meteorological variables.* According to Eq.(3.11), the value of  $K_c$  is not only dependent on the canopy variables, but also on the meteorological data. Canopy variables, except albedo  $r$  which depends also on the soil surface moisture, change slowly over time. Significant changes of canopy variables may be observed over a period of 1 to 2 weeks, while meteorological data vary from hour to hour.

To apply the explicit relationship between  $K_c$  and the canopy variables  $r$ ,  $LAI$ ,  $h_c$ , we need to evaluate the dependence of  $K_c$  on meteorological conditions around the date of the satellite acquisition. Assuming constant values for the canopy variables for a period of say 10 days, we can calculate the relative change of  $K_c$  respect to the average value  $K_{c,10}$  calculated over 10 days:

$$\Delta K_c = \frac{(K_c - \overline{K_{c,10}})}{K_{c,10}} \quad (6.5)$$

Fig. 6.5 to Fig. 6.7 show the results of the calculation of Eq.(6.5) for twenty days of July '94. The value of  $K_c$  in Eq.(6.5) was calculated by means of Eq.(3.10) assuming different range of values of canopy variables  $LAI$ ,  $h_c$  and  $r$ . During the period considered the meteorological variables were varying within the 25% of the average value, with exception of the wind-speed having a variation exceeding 100%. As shown in Fig. 6.5, the resulting variation of  $K_c$  is less than 10% with exception of one day for  $LAI = 4$ . In a similar way, the plots in Fig. 6.6 and Fig. 6.7 confirm a range of variability of  $K_c$  within 10% in most cases.

If we neglect these variations, we can assume that for given meteorological conditions during a period of 1 to 2 weeks the average value of  $K_c$  depends on the canopy variables  $r$ ,  $LAI$ ,  $h_c$  only (see also Fig. 4.2):

$$K_c(K^\downarrow, T_a, RH, U; r, LAI, h_c) = K_c(r, LAI, h_c) \quad (6.6)$$

The function  $K_c(r, LAI, h_c)$ , calculated over a period of 10 days, has a general characteristic shape in the domain  $(r, LAI, h_c)$ , and its exact position depends on the meteorological variables.

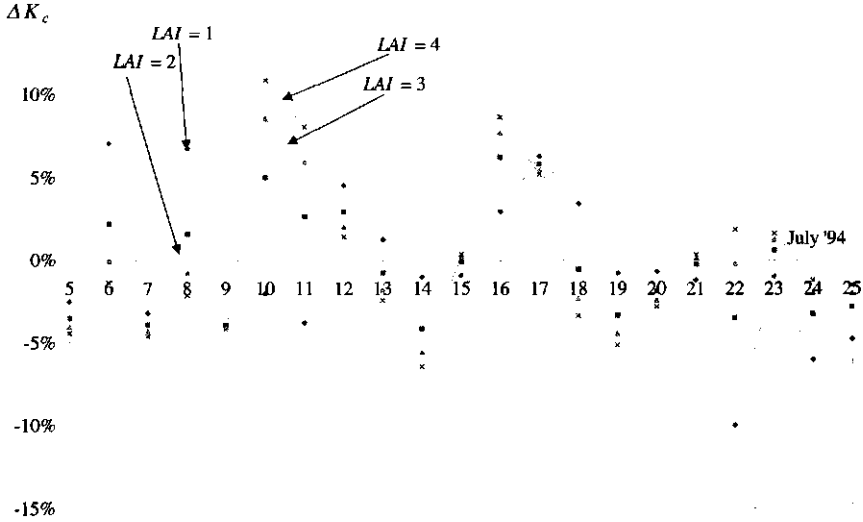


Fig. 6.5 Variation of the crop coefficient  $K_c$  respect to the moving average calculated over 10 days [Eq.(6.5)] in the LAI range [1;4] assuming fixed canopy height  $h_c = 0.4$  m and albedo  $r = 0.18$ .

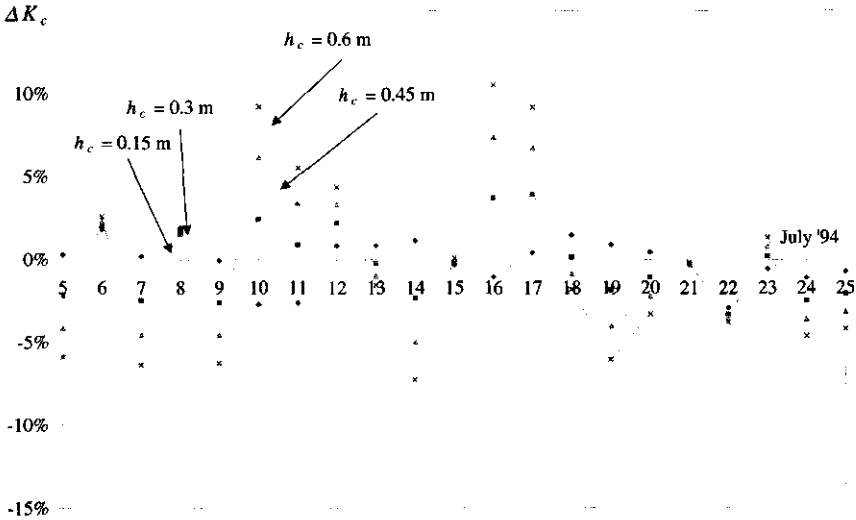


Fig. 6.6 Variation of the crop coefficient  $K_c$  respect to the moving average calculated over 10 days [Eq.(6.5)] in the  $h_c$  range [0.15;0.6] assuming fixed LAI= 2 and albedo  $r = 0.18$ .

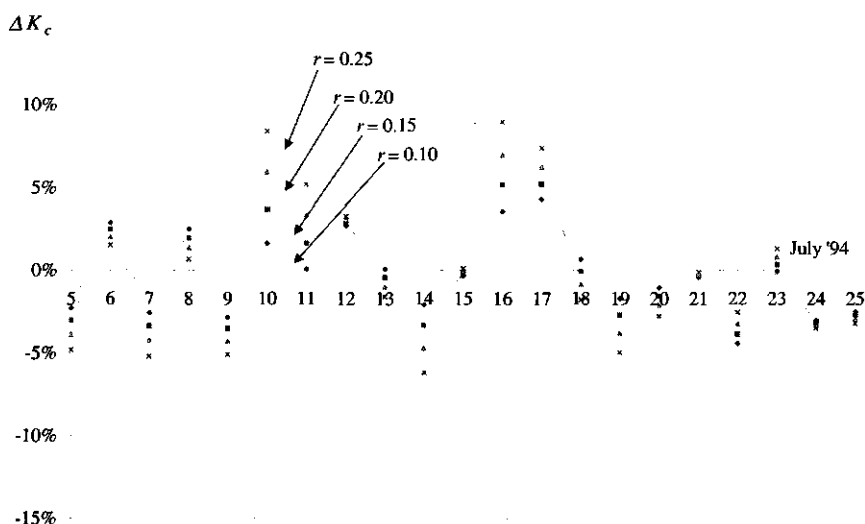


Fig. 6.7 Variation of the crop coefficient  $K_c$  value respect to the moving average calculated over 10 days [Eq.(6.5)] in the  $r$  range [0.10;0.25] assuming fixed  $LAI=2$  and crop height  $h_c = 0.40$  m.

We consider now the sensitivity of  $K_c$  to  $r$ ,  $LAI$  and  $h_c$ .

**Albedo.** The plots in Fig. 6.8 show the projection of  $K_c(r, LAI, h_c)$  in the plane  $K_c - LAI$  for the image of November 11<sup>th</sup> 1993 (Fig. 6.8.a) and of June 23<sup>rd</sup> 1994 (Fig. 6.8.b). In both cases, the value of  $h_c$  was set to 0.40 m and  $r$  was varying from 0.10 to 0.25. The sharper increase of  $K_c$  in November, if compared with that in June, is determined by the influence of the aerodynamic term in Eq.(3.10). The relative importance of albedo  $r$  increases with higher solar radiation. So, the increase of  $K_c$ , that corresponds to a decrease in  $r$ , is more pronounced in summer conditions than in autumn.

**Leaf Area Index.** The previous considerations are confirmed by considering the slope of the lines in Fig. 6.9, where  $K_c$  versus  $r$  is plotted for different  $LAI$  values and  $h_c = 0.40$  m. The plots refer to the same dates of Fig. 6.8. The relationship between  $K_c$  and  $r$  can be very well approximated by a linear function; the value of  $LAI$  determines the position of the plot-lines in the  $K_c - r$  plane. These plots show that the sensitivity of  $K_c$  to  $LAI$  is higher than to other variables.

**Crop height.** The influence of crop height  $h_c$  on the value of  $K_c$  is considered in Fig. 6.10, which shows that the sensitivity of  $K_c$  to  $h_c$  is larger during autumn (Fig. 6.10.a) than during summer (Fig. 6.10.b). This behaviour can be explained with the increasing importance of the aerodynamic term in the estimation of potential evapotranspiration during the periods with less solar radiation.

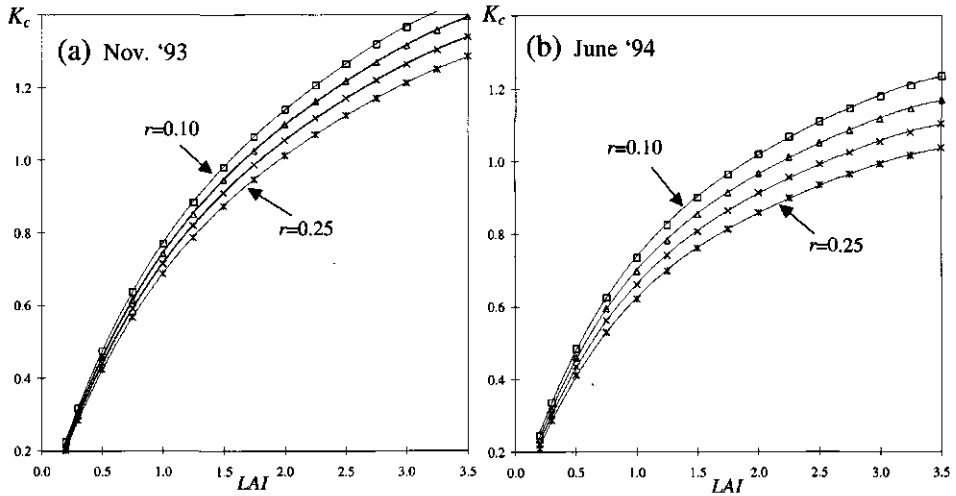


Fig. 6.8 Relationship between the crop coefficient  $K_c$  and the Leaf Area Index, LAI, for a surface albedo  $r$  ranging from 0.10 to 0.25; crop height  $h_c$  is assumed to be equal to 0.4 m.  $K_c$  is calculated as the average value for the decades of images acquisition date at (a) November '93 and (b) June '94.

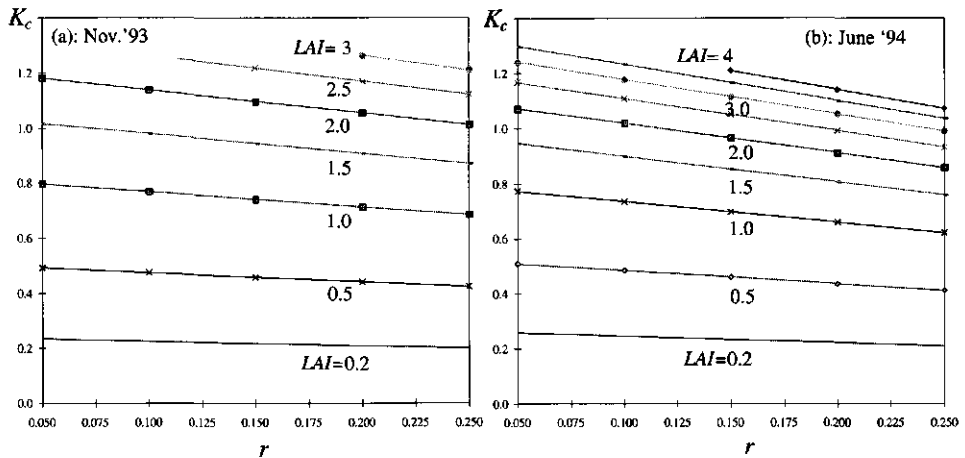


Fig. 6.9 Relationship between the crop coefficient  $K_c$  and the hemispherical spectrally integrated reflectance albedo  $r$  for different values of LAI and crop height  $h_c = 0.4$  m, in (a) November '93 and in (b) June '94.

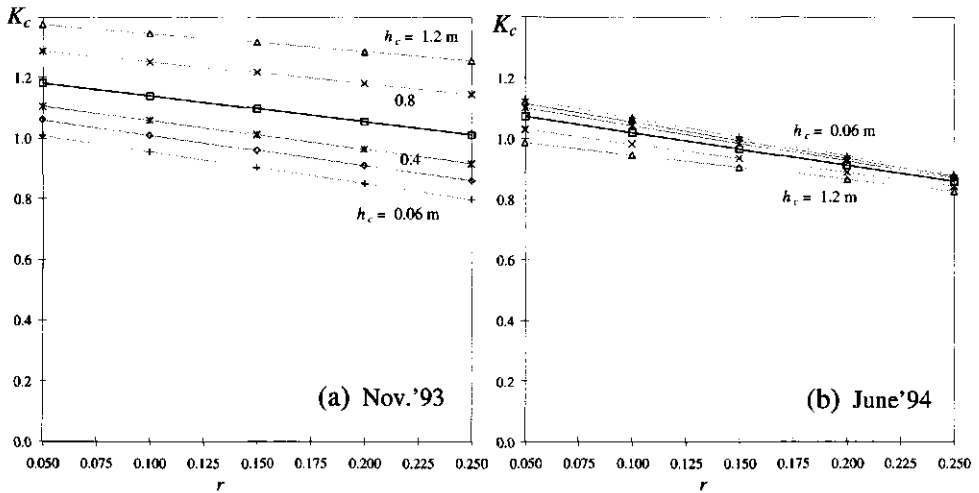


Fig. 6.10 Relationship between the crop coefficient  $K_c$  and the albedo  $r$  for a crop height  $h_c$  ranging from 0.06 and 1.2 m, assuming  $LAI=2.0$  in (a) November '93 and in (b) June '94.

Under summer conditions,  $K_c$  hardly depends on  $h_c$ . For low solar radiation, as in the case of Fig. 6.10.a,  $K_c$  increases with  $h_c$ , while the increase is small at high solar radiation (Fig. 6.10.b). This apparent contradiction is explained again by the increase of the ratio  $r_c/r_{a,H}$  with  $h_c$  in (3.11). In the case of Fig. 6.10.a, the reduction of the radiation term, which is already small, is compensated by the increase of the aerodynamic term.

Thus it is possible to conclude that in this case-study the value of  $K_c$  is mainly dependent on  $LAI$  and, to a lesser extent, on the surface albedo,  $r$ . For the climatic conditions of the case-study considered here, an average constant value  $h_c=0.4$  m was assumed. As shown in Fig. 6.10, this assumption determines an error of  $K_c$  not larger than 0.2, occurring only during autumn and winter, which are periods of less importance in the context of irrigation studies, and of 0.1 during summer. From this sensitivity analysis the following conclusions can be drawn.

- Assuming constant  $r$ ,  $LAI$  and  $h_c$  over a period of 1-2 weeks, the value of  $K_c$  exhibits a variation of  $\pm 10\%$  due to the variability of meteorological data during the same period
- For the climatic conditions of the Gromola district,  $K_c$  is mainly dependent on the value of  $r$  and  $LAI$
- During the irrigation season, i.e. the high solar radiation period, for the calculation of  $K_c$  the crop height  $h_c$  can be taken as a constant.

Finally a value of  $h_c = 0.40$  m was considered in the application of the analytical approach to the Gromola district.

### **6.3.2 Estimation of hemispherical surface reflectance and LAI from directional surface reflectance.**

The estimation of the hemispherical and spectrally integrated *surface albedo*  $r$  was done by means of Eq.(4.13) and the weighting coefficients are presented in Tab. 4-1. The lowest average  $r$  was found in the image of Nov.'93 ( $r_{avg}=11.2$ ,  $std.dev=2.4$ ), whilst the highest was in June 23<sup>rd</sup> '94 ( $r_{avg}=14.3$ ,  $std.dev=3.1$ ). The resulting values of  $r$  for specific surfaces were found in good agreement with data reported from literature (Dubayah, 1992; Russell et al., 1997).

In the calculation of  $K_c$  by means of Eq.(3.11),  $r$  is linearly interpolated between two consecutive satellite passes. As a consequence, the variation of  $r$  with changing surface soil moisture is not considered. This assumption may appear rather questionable however, especially for surfaces with partial ground cover. The influence of soil moisture on the spectral properties in such conditions was analysed by e.g. Kustas et al. (1994) from data obtained during the MONSOON'90 experiment. In this case,  $r$  was measured by means of low-altitude spectral data on different dates. By comparing observations before and after several rainfall events at eight sites, the maximum observed variation of  $r$  was 0.03. The effect of variation of this order of magnitude on  $K_c$  is negligible. As shown already in Fig. 6.5, a variation of  $r$  of  $\pm 0.05$  determines an error of estimate of  $K_c$  between 0.01 and 0.05 for LAI values of 1.0 and 2.5 respectively.

The *Leaf Area Index* was derived from directional surface reflectance by applying the model CLAIR, i.e. by means of Eq.(4.15) and (4.16). The analytical procedure for producing LAI maps from satellite-based images of spectral surface reflectance can be summarised in the following steps:

- identification of the soil-line slope for the estimation of bare soil reflectance ratio in bands 3 and 4 needed in Eq.(4.15)
- calculation of the Weighted Difference Vegetation Index  $WDVI$  for all pixels
- estimation of the empirical parameters  $WDVI_{\infty}$  and  $\alpha^*$  using ground measurements
- calculation of LAI for all pixels.

For each image, different bare soil surfaces were identified and their corresponding reflectance values in bands 3 and 4 were plotted. Examples for the images of November 11<sup>th</sup>, 1993, and June 23<sup>rd</sup>, 1994, are given in Fig. 6.11.a and Fig. 6.11.b.

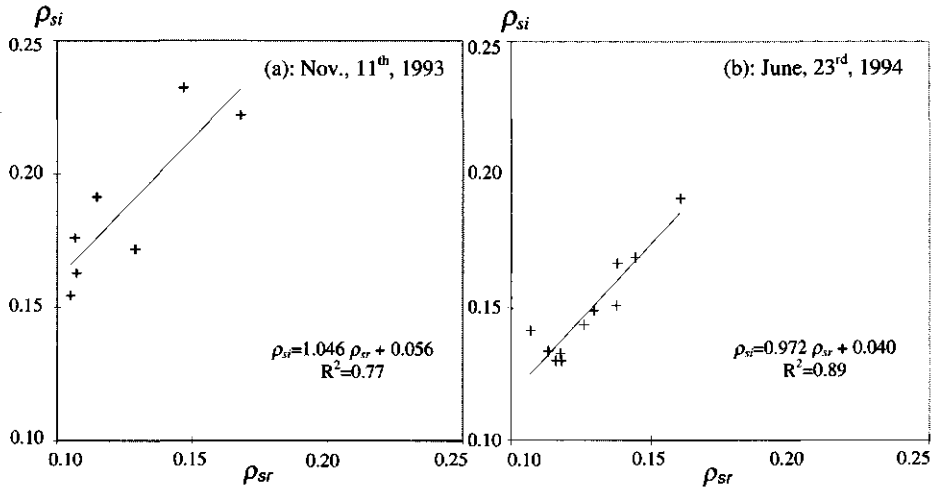


Fig. 6.11 Scatter-plot of bare-soil surfaces reflectance in bands 3 ( $\rho_{sr}$ ) and 4 ( $\rho_{si}$ ) for the Gromola study area on (a) November '93 and on (b) June '94.

Linear regression techniques were applied to determine the slope of the so-called *soil line*  $\rho_{si}/\rho_{sr}$ . The range of soil line slope was found between 0.97 (June) and 1.26 (September).

Similarly to the determination of the soil-line slope, fully vegetated areas were identified in each image for the calculation of  $WDVI_{\infty}$ , representing the value of  $WDVI$  for  $LAI \rightarrow \infty$ . The resulting  $WDVI_{\infty}$  were varying from 0.45 to 0.54. The average value of 0.51 was used to process the  $WDVI$  images for all dates by using Eq.(4.15).

The following step is the estimation of the empirical parameter  $\alpha^*$ , required for the estimation of  $LAI$  from Eq.(4.16). This parameter is dependent on the shape and orientation of the foliage and it may largely vary for different crops and development stages. The value of  $\alpha^*$  was estimated by using field measurements of  $LAI$  concurrent with the obtained images. This data set was randomly divided in two groups: the first one containing 92 elements was used for the calibration of  $\alpha^*$ , while the second one with 36 data was used for the validation. The value of  $\alpha^*$  was determined for each field measurement by inversion of Eq.(4.16) with  $WDVI_{\infty} = 0.51$ . The frequency distribution of the resulting  $\alpha^*$  for all data is shown in Fig. 6.12. In 60% of the cases  $\alpha^*$  was in the range [0.34; 0.54] with an average value of 0.50.

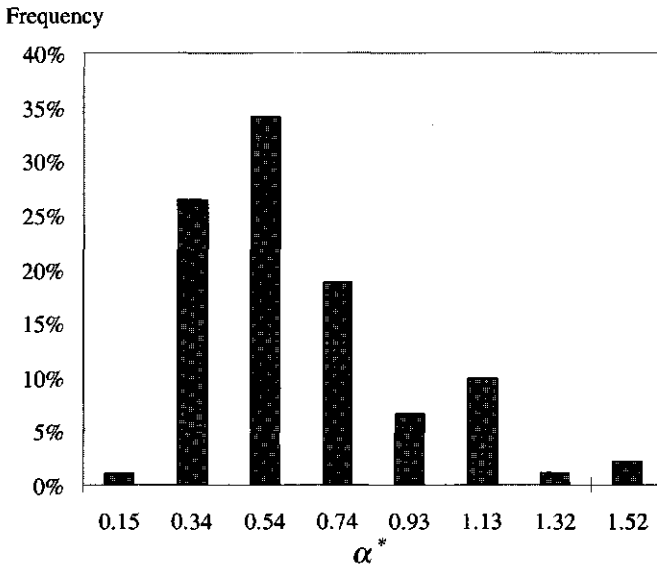


Fig. 6.12 Frequency distribution of the empirical parameter  $\alpha^*$  resulting from the inversion of Eq.(4.16) applied to the entire data set of the ground reference plots.

The calibration of Eq.(4.16) was performed by means of regression analyses techniques applied to observed and estimated *LAI* values. Data points corresponding to possible field measurement errors were progressively discarded from the regression analysis. The final value of  $\alpha^*$  was found by maximising the number of points used in the regression and the resulting correlation coefficients. On the base of 72 data with  $R^2=0.74$ , the final value of  $\alpha^*$  was found to be equal to 0.42. By substituting the appropriate values of the empirical parameters  $\alpha^*$  and  $WDVI_\infty$  in Eq.(4.16), we obtained the empirical relationship between *LAI* and *WDVI* for the Gromola irrigation district:

$$LAI = -\frac{1}{0.42} \ln \left( 1 - \frac{WDVI}{0.51} \right) \quad (6.7)$$

Eq.(6.7) was used to estimate the *LAI* for each image acquired in the case-study. An example of output is given in Colour Plate 1 (June 23<sup>rd</sup>, 1994).

A comparison between measured *LAI* and estimates made by means of Eq.(6.7) is given in Fig. 6.13. The error of estimate evidenced by the scatter of points in the plot of Fig. 6.13 is mainly determined by the assumption of a constant  $\alpha^*$  in Eq.(6.7), in contrast with the distribution resulting from the reference data set shown in Fig. 6.12.



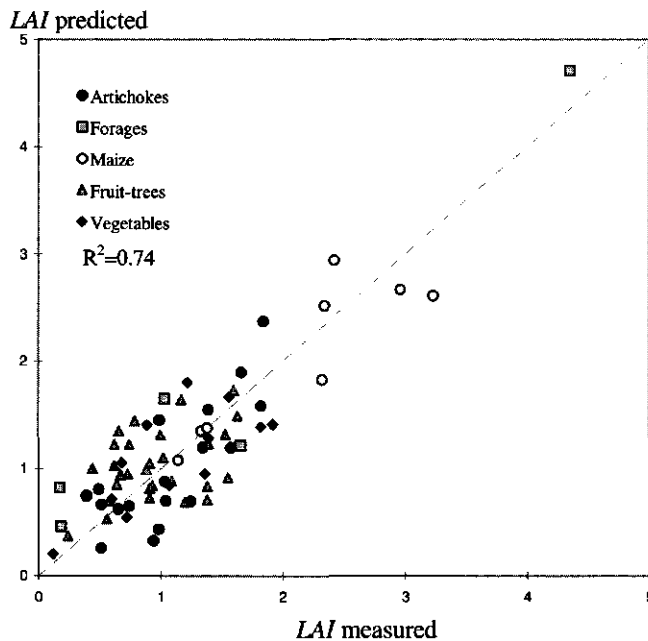


Fig. 6.13 Estimates of LAI of various crops by means of Eq.(6.7) from the calibration data set.

The empirical relationship (6.7) has been verified by using the 36 independent data points (validation data set). In this case, a satisfactory correlation between measured and predicted LAI was found ( $R^2 = 0.616$ ). The mean of absolute errors of estimate was 0.31 (Fig. 6.14). This error of estimate corresponds to a variation of  $K_c$  equal to 0.06 for  $r = 0.15$  and  $LAI = 2$ . A larger error i.e. in the order of 0.1-0.15 of  $K_c$  is found for  $LAI < 1$ . The accuracy of estimation of LAI is satisfactory for the application presented here, but it could be insufficient for more detailed studies.

From the analysis of the data presented here, we may conclude that the estimation of LAI from nadir-viewing satellite based reflectance is satisfactory for irrigation applications in the range [1; 4]. In the lower range of LAI, i.e. for  $LAI < 1$ , the reported error of 0.31 may be too large in many vegetation studies. For  $LAI > 4$ , the  $WDVI$ -LAI relationship has a saturation effect which hamper a good estimation of the actual value of LAI. Nevertheless, the consequences of these drawbacks on the estimation of  $K_c$  are rather limited and the methodology can be usefully applied. Indeed,  $K_c$  reaches its maximum value when LAI values are larger than 4-5. Furthermore, the crop coefficient has minor practical relevance, in terms of water budget, during the early stage of crop development, i.e. for  $LAI < 1$ .

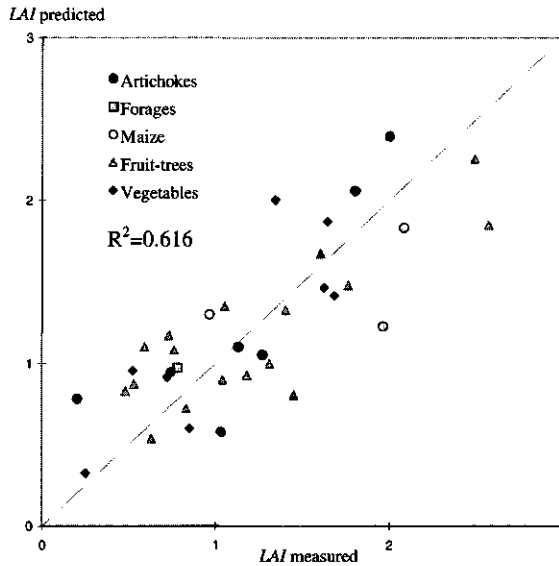


Fig. 6.14 Scatterplot of measured versus predicted LAI values using Eq.(6.7) with an independent data set.

### 6.3.3 Derivation of the crop coefficient map

To reduce the run-time in SIMODIS, the calculation of  $K_c$  was separately made for each satellite pass for all tertiary units. The resulting  $K_c$  maps are input to SIMODIS, which interpolates the value of  $K_c$  between two consecutive satellite passes. To evaluate the error deriving from this simplification, we can analyse the plots in Fig. 6.15. Assuming a crop with different LAI and  $r$  values on three dates, the calculation of  $E_p$  has been made in three different ways:

- direct calculation of Eqs.(3.1) to (3.5), with the values of LAI and  $r$  interpolated between two consecutive satellite passes. This calculation refers to the plot indicated as "direct calc" in the legend of Fig. 6.15
- calculation of  $E_p$  by means of Eq.(3.9), with  $K_c$  values determined by means of Eq.(3.10) on the date of satellite acquisition and successively interpolated between two consecutive satellite passes
- the same, but with  $K_c$  values calculated on the day of satellite pass as the average value over 10 days.

It can be concluded that interpolation of  $K_c$  produces the same results of the direct calculation of  $E_p$  with interpolated  $r$  and LAI values. In doing so, the relationship  $K_c(r, LAI)$  can be explicitly derived for each satellite image.

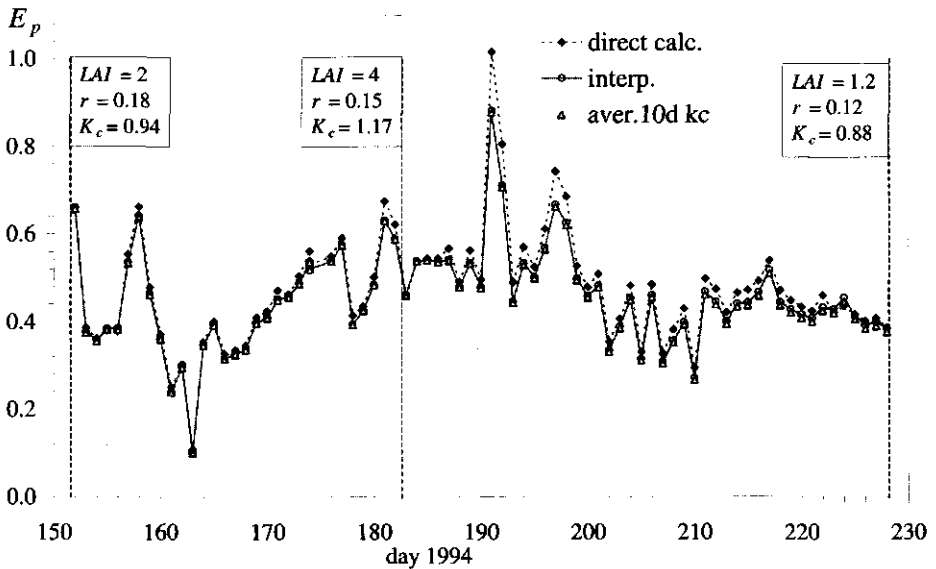


Fig. 6.15 Comparison of potential evapotranspiration  $E_p$  calculated with three different interpolation techniques between two satellite passes (indicated with flags): “direct calc” refers to interpolation of  $r$  and  $LAI$ ; “interp” refers to interpolation of  $K_c$  while “aver10 d kc” is obtained by interpolating  $K_c$  averaged over a period of 10 days around the date of satellite acquisition.

In practice, after the preliminary elaboration described in Sections 6.3.1 and 6.3.2, the procedure to derive the  $K_c$  map from at-surface spectral data is the following:

- Derivation of the albedo  $r$  map by using Eq.(4.13) with the appropriate weighting coefficients, such as those given in Tab. 4-1 for Landsat TM 5
- Derivation of the  $LAI$  map by means of Eq.(6.7)
- Derivation of the  $K_c$  map by applying Eq.(3.10) pixelwise with the values of  $r$  and  $LAI$  resulting from the previous step and crop height  $h_c=0.4$  m. The calculation is made for a period of 10 days around the date of satellite acquisition and then averaging out  $K_c$ .

An example of the resulting  $K_c$  map in raster format is shown in Colour Plate 2.a. The same map in vector format is shown in Colour Plate 2.b. The latter is derived by averaging the value of  $K_c$  for the pixels belonging to each tertiary unit of the Gromola irrigation district.

### 6.4 Conclusions

The classification and the analytical approach for mapping crop coefficients in the Gromola irrigation were applied by using data from Landsat TM images. In the classification approach a thematic map with 6 classes was derived by means of classification performance indicators. In the analytical approach a map of continuous  $K_c$ -values expressed as a function of satellite-based estimates of  $r$  and  $LAI$  was built.

A comparison of the two different maps for the image of June 23<sup>rd</sup>, 1994, is given by the histogram in Fig. 6.16. Assuming a reference evapotranspiration of  $4.5 \text{ mm d}^{-1}$ , the sum of differences between the analytical and the classification approach leads to a difference of  $2634 \text{ m}^3 \text{ d}^{-1}$  of the total potential evapotranspiration, corresponding to 3% of the average value for the Gromola irrigation area for the considered period.

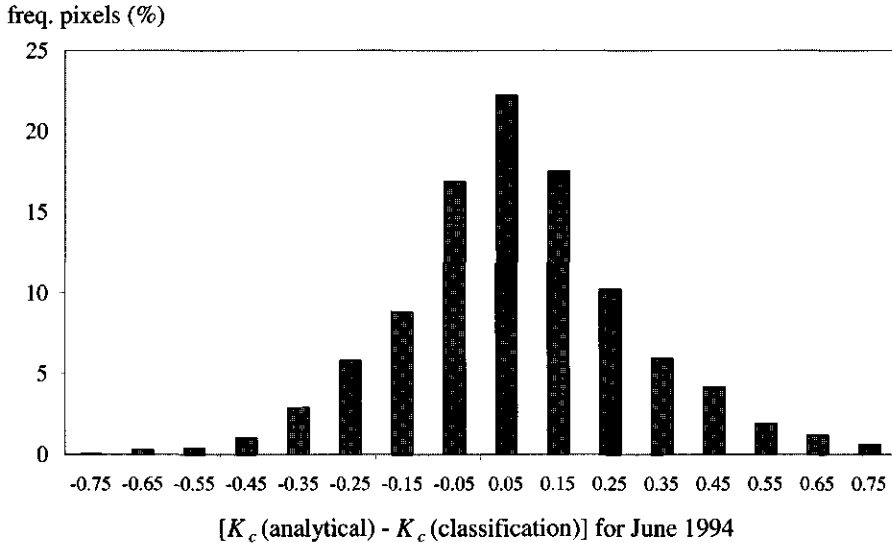


Fig. 6.16 Histogram of differences between the crop coefficient values obtained with the analytical and the classification approach in the Gromola irrigation district.

Due to the unavailability of reliable reference measurements of the crop coefficient for different crop types and acquisition dates, it is not possible to assess and compare the absolute accuracy of the two methods. An indirect evaluation of the two methods can be performed using the values of the canopy parameters  $LAI$ ,  $r$  and  $h_c$ . For this reason, the analytical approach appears more appropriate when field observation of canopy parameters are available, as in the present case-study. Furthermore, once the empirical relationships such as Eq.(6.7) have been defined

for a specific site, they can be used for processing images acquired on different dates.

*The classification approach might be preferred when field measurement of canopy properties are not available.* In such situations, reference values of crop coefficients  $K_c$  might be assigned by using tables similar to those proposed by Doorembos et al. (1977) to the image pixels in the training set selected for the image classification.

## 7 Application of SIMODIS in the Gromola irrigation district.

---

### 7.1 Data organisation.

The input data required to run SIMODIS are divided in six main groups:

- Meteorological data
- Tertiary units topology
- Geometrical and hydraulic characteristics of the conveyance network pipelines
- Soil hydrology data
- Crop data
- Irrigation scheduling and management options.

All the raster and vector layers have been organised in a Geographical Information System (GIS) in order to facilitate the flow of input and output in SIMODIS.

The meteorological data set includes the daily values of rainfall and reference evapotranspiration. In the case of the Gromola study area one meteorological station was considered representative for the entire district.

The main layer of the GIS contains the attributes and the topographic boundaries of all tertiary units (see Section 5.3.1). In the database associated to this layer each unit is identified by a code corresponding to its position within the conveyance network; the irrigated area  $A_{i,j,k}$ , the soil and crop type are also indicated.

The network data are stored in a separate file including a branch table and a node table. The *branch* table contains the initial and final nodes of each pipeline, indicated with  $i,j$  and  $i,j+1$  respectively, the corresponding length  $L_{i,j}$ , diameter  $D_{i,j}$  and hydraulic friction coefficient  $\omega_{i,j}$ . In the *node* table the elevation above mean sea level and, for water delivering nodes, the outlet discharge  $Q_{i,j}$  are specified.

The soil type, the bottom boundary condition and the crop type of each tertiary unit are specified by numeric codes in the GIS. The soil code is linked to Tab. 5-5, where the van Genuchten' soil hydraulic parameters are given for each

mapping unit (Fig. 5.13.b). In a similar way, the bottom boundary condition code is associated to a specific relationship between the flux at the bottom of the unsaturated zone of the soil profile and the groundwater depth (Fig. 5.21).

The crop code, as resulting from the map in Fig. 5.9, is linked to two tables indicating the rooting depths and the critical values of soil water pressure head for the different crop types, i.e. Tab. 5-3. The  $LAI$  and  $K_c$  for the different satellite acquisitions are stored in a separate file. As mentioned in Section 6.3.3, the average values of  $LAI$  and  $K_c$  in each tertiary unit are derived by crossing the vector layer of units borders with the raster maps of canopy variables obtained by means of the procedures described in Chapter 3. The fractional vegetation cover  $s_c$ , needed in SIMODIS to estimate the canopy water interception according to Eq.(3.21), is calculated from  $LAI$  by using the relationship shown in Fig. 5.12.

The last group of data includes the scheduling and management options. The scheduling options data are used in SIMODIS to start the irrigation and to determine the corresponding volume per unit area as explained in Section 3.4. The management options are the total amount of water resources daily available  $V_{RES}$  and the minimum hydraulic head  $H_{min}$  required at the network outlets.

Examples of input files can be found at URL: <http://www.simodis.unina.it>.

The different steps of SIMODIS have been introduced in Chapter 2 and summarised in Fig. 2.2. The main outline of the procedure to simulate the operation of the irrigation water conveyance network and the data-flow is given in Fig. 7.1.

## **7.2 Estimation of potential evapotranspiration in the Gromola irrigation district.**

By using the maps of  $K_c$  derived from the analytical approach in Chapter 6, we can estimate the potential evapotranspiration  $E_p$  for the all the tertiary units of Gromola district. A linear interpolation between two consecutive satellite passes is applied to determine the  $K_c$  values of each tertiary unit on a daily basis. These data are then used to define the upper boundary condition of SWAP from which the spatial distribution of soil water deficit is calculated.

We can also use the  $K_c$  and  $LAI$  maps to calculate the water balance of the entire Gromola district during the irrigation season '94. The results of this calculation are shown in Fig. 7.2, where the water balance terms are given per unit irrigated area. In the evaluation of crop water requirements we can consider  $E_{s,p}$  and  $T_p$  separately by means of Eqs. (3.12) and (3.13).

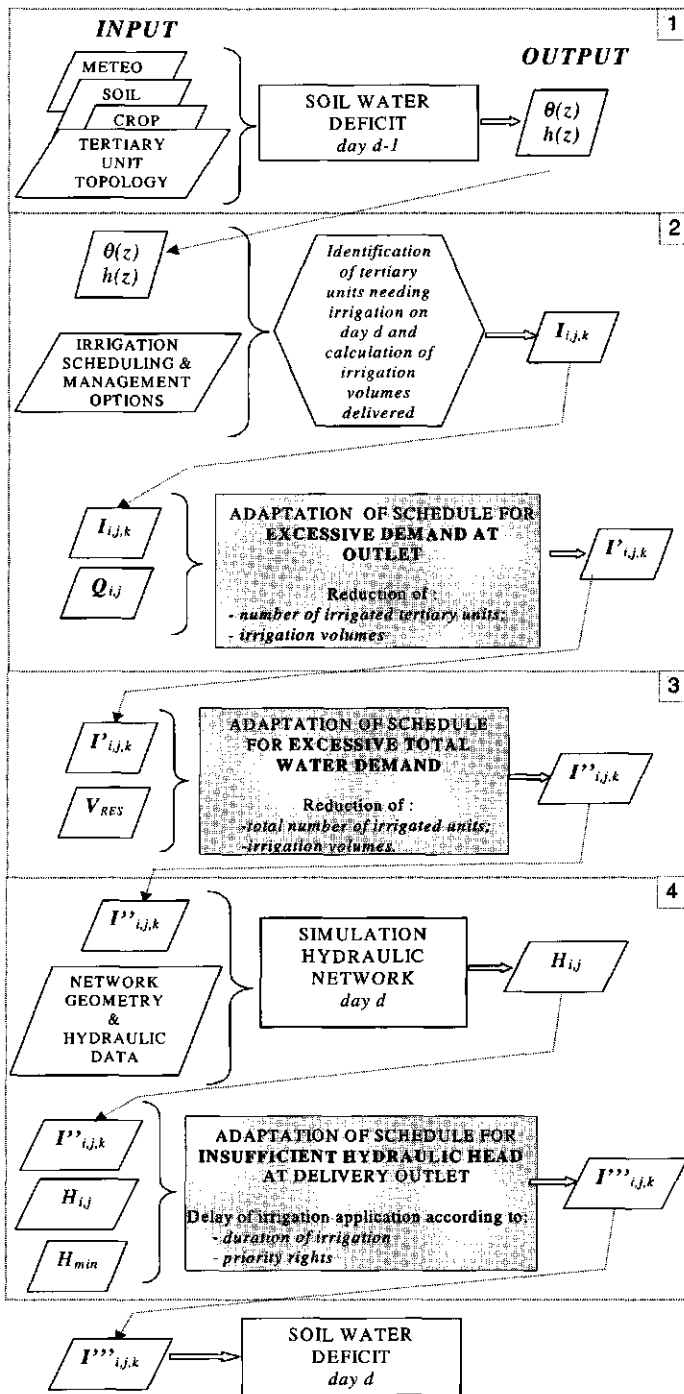


Fig. 7.1 Outline of SIMODIS to compute the operation plan of the irrigation system.



The calculation of  $(E_{s,p} + T_p - P)$  for the entire irrigation district from June to September 1994 resulted of  $6\,927\,864\text{ m}^3$ , while the total water consumption  $I$  measured in the study area (see Section 5.3.2) was  $4\,770\,430\text{ m}^3$ .

If we consider only  $T_p$  ( $4\,176\,469\text{ m}^3$ ) in the calculation of crop water requirements, the total water consumption results in an excess of  $2\,619\,761\text{ m}^3$ . This value rises to  $3\,944\,761\text{ m}^3$  if we add the initial soil water storage  $W_0$  ( $1\,325\,000\text{ m}^3$ ) which average value per unit area can be estimated in about 5 cm.

These data show that without irrigation the water deficit is large; on the other hand the difference between  $T_p$  and  $(P+I)$  reveals also that irrigation water in the Gromola district is applied *ad abundantiam*, thus leaving large margins for a more rational usage of water resources.

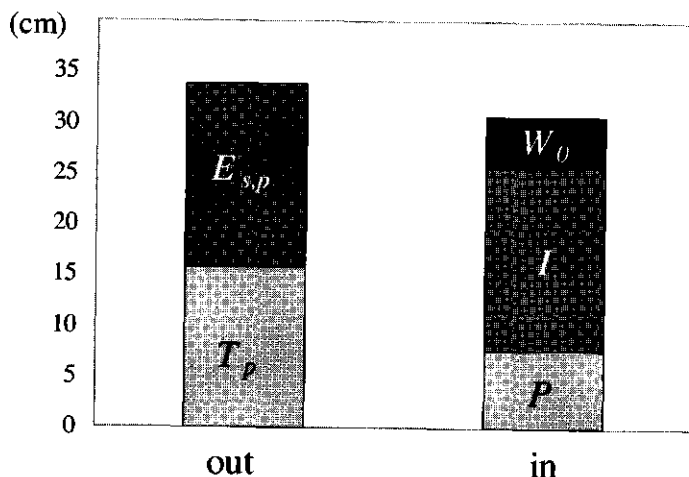


Fig. 7.2 Cumulative water balance of Gromola irrigation district for the period 1<sup>st</sup> June-30<sup>th</sup> September '94. The vertical axis gives the respective values per unit irrigated area.

### 7.3 Spatial distribution of soil water deficit

The estimation of the *spatial distribution of soil water deficit* on daily basis represents the first step of SIMODIS (Box nr.1 in Fig. 7.1). This is the result of the combined application of the remote sensing techniques to map crop coefficients, as described in Chapter 6, and of the *soil water balance model* SWAP (see Chapter 3).

The input data required include soil, crop and agrometeorological variables. Specific software has been developed to extract the data of each tertiary unit from the GIS and to prepare the input file in the correct format for SWAP. The output of SWAP, i.e.  $T$ ,  $E_s$ , and the vertical profiles of  $\theta$  and  $h$  for the considered day  $d$  and for each tertiary unit are stored in a table. Once this table has been imported in the GIS, the results of water balance calculations can be viewed in the form of

maps. An example of such output is given in the Colour Plate 3, where the spatial distribution of  $T$  for day 192 of the year 1994 is represented. On this day, the total volume of water transpired was 51 042 m<sup>3</sup> with an average value of 0.26 cm. The soil water deficit  $\delta$  is then calculated from the profile of  $\theta$  in each tertiary unit. The spatial distribution of  $\delta$  between 10 and 50 cm depths is shown in Colour Plate 3.b.

#### 7.4 Spatial distribution of farmers' water demand and first adaptation of schedule.

The *spatial and temporal distribution of farmers' water demand* is estimated from the soil water deficit distribution according to the irrigation scheduling options, given in the input, due account taken of the farm distribution efficiency and of the actual delivery capacity of the outlet in each secondary unit (Box nr.2).

*Scheduling options.* As described in 3.4, the profiles of soil water content  $\theta(z)$  and pressure head  $h(z)$  simulated by SWAP on day  $d$  are used in SIMODIS to identify the tertiary units needing irrigation and to determine the corresponding water volumes.

Different options are available to schedule irrigation and to determine the water volume to be applied in tertiary units. The day of irrigation is set according to one of the following criteria:

- i. The average value of the soil water pressure head in a defined portion of the soil profile, i.e. the root zone, is below the critical value  $h_3$  for the given crop (Fig. 3.1; Tab. 5-3):

$$\left\{ h_{avg} = \frac{\int_{z_1}^{z_1+\Delta z} [h(z)] dz}{\Delta z} \right\} \leq h_3$$

- ii. A given threshold value of the ratio between actual and potential transpiration (stress factor  $S_f$ ) is reached:

$$\frac{T}{T_p} \leq S_f .$$

When in a tertiary unit either one of these criteria is met, irrigation application starts. The corresponding amount of water can be either a fixed quantity per unit area or can be determined as a fraction  $i_r$ , [0; 1] of the soil water deficit  $\delta_{i,j,k}$  calculated from Eq.(3.17). Considering the irrigation distribution efficiency  $\eta_{i,j,k}$  at farm level, e.g. on the basis of the equipment or method used, the water volume  $I_{i,j,k}$  (m<sup>3</sup>) to be delivered at the generic tertiary unit of area  $A_{i,j,k}$  (ha) on day  $d$  is thus calculated from Eq.(3.19):

$$I_{i,j,k} = i_r \frac{\delta_{i,j,k} A_{i,j,k}}{\eta_{i,j,k}} f_{i,j,k} 100 \quad (7.1)$$

where  $f_{i,j,k}$  is a control flag which is initially set to 1 for the tertiary units irrigated on the day considered.

Finally, the water volume  $I_{i,j}$  at the outlet of the secondary unit  $i,j$  on day  $d$  is given by the sum of volumes corresponding to the tertiary units of lower hierarchic level:

$$I_{i,j} = \sum_k I_{i,j,k} \quad (7.2)$$

An example of farmers' water demand distribution  $\{I_{i,j,k}\}$  for the day 192 of 1994 is shown in the Colour Plate 4. Tertiary units needing irrigation are shown in colours and the corresponding water demand was calculated from the soil water deficits of Colour Plate 3.b assuming  $i_r = 0.5$ . The total number of tertiary unit demanding water was 236 belonging to 142 different secondary units. The average amount of farmers' water demand per unit irrigated area was 3.78 cm. The sum of irrigation volumes resulted of 74 334 m<sup>3</sup>, with an average value of 495 m<sup>3</sup> per tertiary unit.

*Adaptation of schedule to match the delivery capacity of the outlets.* In a limited-demand schedule, as in the Gromola district, the flow rate at each outlet has a fixed value  $Q_{i,j}$  (m<sup>3</sup>s<sup>-1</sup>) depending on the hydraulic characteristics of the delivery device. Therefore, we need to verify that the outlet is able to deliver the total amount of water required  $I_{i,j}$  on day  $d$  as resulting from Eq.(7.2). This condition is expressed by the relationship:

$$I_{i,j} \leq Q_{i,j} 86400 \quad (7.3)$$

The values  $Q_{i,j}$  for each delivery outlet are stored in the network database of SIMODIS. At the end of the calculations of water volumes for all the tertiary units needing irrigation, Eq.(7.3) is evaluated. If the water demand  $I_{i,j}$  at outlet  $i,j$  exceeds the volume of water that is possible to deliver in 24 hours, one should reduce either the water demand  $I_{i,j}$  or the number of the tertiary units served by the outlet considered. The first alternative is the only one possible when there is just one tertiary unit demanding water and the corresponding volume exceeds the outlet delivery capacity. When there are multiple tertiary units demanding water contemporarily, the second alternative, that is the reduction of units served, is more likely to happen in reality, provided that a certain degree of flexibility among the farmers exists.

Thus, in SIMODIS the irrigation schedule is adapted as follows:

- i. When there is only one tertiary unit to be irrigated at the generic node  $i,j$  and the corresponding demand exceeds the outlet capacity [Eq.(7.3)], the irrigation volume is reduced to the outlet capacity, i.e.:

$$I_{i,j,k} = I_{i,j} = Q_{i,j} 86400$$

The volume reduction is made by setting  $i_r$  as:

$$i_{r,new} = \frac{I_{i,j} n_{i,j,k}}{100 \delta_{i,j,k} A_{i,j,k}} = 864 \frac{Q_{i,j} n_{i,j,k}}{\delta_{i,j,k} A_{i,j,k}} \quad (7.4)$$

- ii. When there are multiple tertiary units to be irrigated at node  $i,j$  and the sum of the corresponding water demand does not meet the condition in Eq.(7.3), the flag  $f_{i,j,k}$  is progressively forced to 0 starting from the tertiary units with lower values of  $I_{i,j,k}$  until the condition in Eq.(7.3) is satisfied or the situation (i) applies. The tertiary units for which  $f_{i,j,k}$  has been set to 0 on day  $d$  have a priority for irrigation on day  $d+1$ .

Both adaptation criteria aims to simulate what could happen in the reality. While the adaptation (i) is related to an individual farmer, the adaptation (ii) implies that multiple farmers sharing a common outlet agree on a priority criteria based on the amount of water demand.

The result of this scheduling adaptation is a new distribution of farmers' water demand  $\{I'_{i,j,k}\}$  (Box nr.2 in Fig. 2.2). The new set of flags  $\{f'_{i,j,k}\}$  corresponding to the water demand distribution  $\{I'_{i,j,k}\}$  identifies the tertiary units to be irrigated on the considered day  $d$ .

For example, on day 192 the reduction of irrigation volumes (adaptation .i) was applied in 19 cases, which are shown with green colour in Plate 4. In other 29 tertiary units shown in red colour the flag  $f_{i,j,k}$  was forced to 0 (adaptation .ii). The total reduction of volume was 12375 m<sup>3</sup>, corresponding to approximately 13% of the total water volume for day 192.

## 7.5 Adaptation of irrigation schedule for excessive total water demand.

While the previous adaptation of the irrigation schedule depends on the self-organisation of the farmers within each secondary unit, the successive levels of adaptation are under the control of the management board of the irrigation district. The management board controls the water resource i.e. the dam diversion gate, and regulates the water flow in the conveyance system.

Having estimated the farmers water demand  $\{I'_{i,j,k}\}$ , the amount of available water resources should match the total water volume needed:

$$\sum_{i,j,k} I'_{i,j,k} \leq V_{RES} \quad \forall d \quad (7.5)$$

This condition is represented by Box nr.3 in Fig. 2.2. The volume of available water resources  $V_{RES}$  can be constant or variable in time. When the condition in Eq.(7.5) is not satisfied, it is necessary to partially or totally reduce the farmers' water demand distribution, by closing the outlets in one or more units at primary or secondary level. This operation is usually made by the technicians of

the irrigation district. From a technical point of view, the control of primary units is easier than that of secondary units, because of the reduced number of actions required in the first case. In alternative, the outlets of secondary units could be remotely controlled, but this possibility is very expensive in terms of hardware and cabling.

In both cases i.e. closing the outlets at primary or secondary level the adaptation of irrigation schedule should be made on the basis of objective criteria in order to reduce possible water stress conditions affecting the crop production. In SIMODIS it is possible to rank the primary (and secondary) units according to the total water volume to be delivered at the corresponding outlets on the considered day. In this case the procedure firstly identifies the units with lesser volumes of water demand and afterwards progressively closes their outlets, starting from those with smaller demand until Eq.(7.5) is positively verified. In this case the flag  $f'_{i,j,k}$  is set to 0 for all the tertiary units belonging to the primary (or secondary) units forced to close. Similarly to the first condition, the results of this second adaptation of schedule, with flags  $\{f''_{i,j,k}\}$  results in a new water distribution  $\{I''_{i,j,k}\}$ .

In the Gromola district, the maximum volume of water available  $V_{RES}$  was assumed to be constant and equal to 71 000 m<sup>3</sup> per day, corresponding to the maximum value observed during the irrigation season 1994. On day 191, the total water volume computed by SIMODIS was 91 625 m<sup>3</sup>. The corresponding water volumes for each primary unit are plotted in Fig. 7.3.

To reduce the total water demand below 71 000 m<sup>3</sup> the primary units 12, 13, 14 and 17 corresponding to those with lower volumes and plotted as blank columns, were closed. This type of operation can be easily done by the management board, which holds the control of water flow in the conveyance network.

In Fig. 7.3 the volumes on day 192 are also shown. In this case, the total volume demanded is 81 523 m<sup>3</sup>, thus requiring the closure of the primary units 11 and 16. The global reduction of water volume was 10 870 m<sup>3</sup>. The tertiary units that are not irrigated are indicated in yellow in the Colour Plate 4. Among these units, 3 were already closed after the scheduling adaptation (ii) described in Section 7.4 and 8 were subjected to a reduction of irrigation volume in force of scheduling adaptation (i).

Scenarios with different values of  $V_{RES}$  were simulated and the results will be shown in Chapter 8.

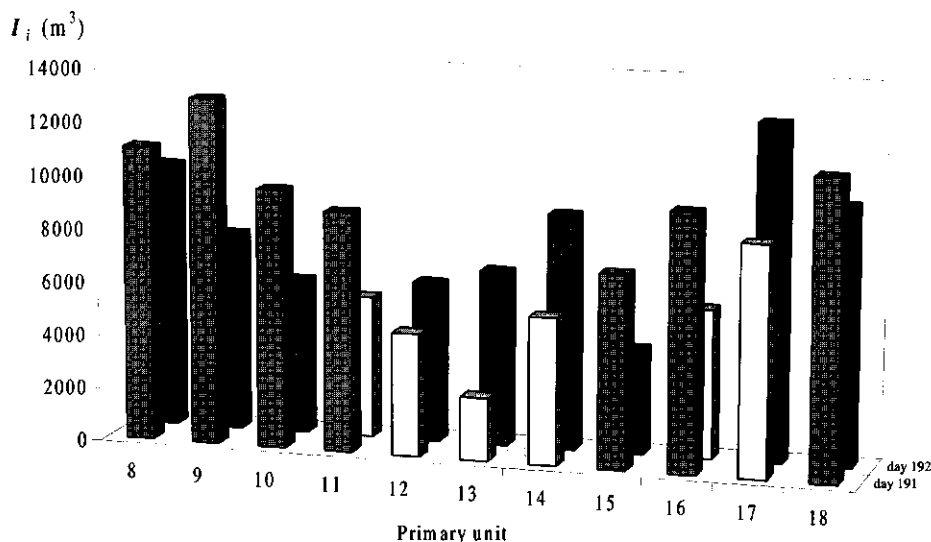


Fig. 7.3 Example of irrigation schedule adaptation following a demand in excess to water resource availability, with  $I_i$  representing the water volume demand of each primary unit. The primary units with blank columns should be closed on the day considered to satisfy Eq.(7.5). Columns in front are for day 191, in the back for day 192.

## 7.6 Adaptation of schedule for insufficient hydraulic head at delivery outlet

### 7.6.1 Distribution of flow rates

The last condition to be verified (Box nr.4 in Fig. 2.2) is the structural capability of the conveyance network to deliver the water distribution resulting from the previous schedule adaptations. The demand water distribution  $\{I''_{i,j,k}\}$  can be applied if the hydraulic head at each open outlet of the network is greater or equal to a threshold value  $H_{min}$  required to correctly operate the irrigation equipment at the farm:

$$H_{i,j} \geq H_{min} \quad \forall i, j \quad (7.6)$$

In the hydraulic design of the irrigation water conveyance network of Gromola a minimum value hydraulic head  $H_{min} = 30$  m was considered satisfactory for most farms in the district.

The distribution of the hydraulic head  $H_{ij}$  is calculated by simulating the water flow in the pipelines. The flow rates in the pipelines of the conveyance network, and thus the spatial distribution of  $H_{ij}$ , are depending on the number of outlets contemporarily opened. In the reality the starting time of each outlet is variable and thus there are infinite different configurations of water flow rates in the network that can accomplish the given water demand distribution  $\{I''_{ij,k}\}$ . Each flow rates configuration is corresponding to a different distribution of hydraulic head  $H_{ij}$ . The temporal variability of the starting time depends on the behaviour of individual farmers and it can not be easily reproduced.

In SIMODIS we consider that all the outlets of a given water demand distribution  $\{I''_{ij,k}\}$  on a given day  $d$  are operated simultaneously at time  $t_0 = 0$ . The irrigation duration  $t_{ij}$  i.e. the time interval required to deliver the water demand  $I_{ij}$  at the generic outlet is related to the flow rate characteristic of the delivery device. Indicating with  $t_{min}$  the lowest duration of irrigation, all the outlets demanding water are simultaneously operating during the time interval  $[0; t_{min}]$ . In this time interval the water flow rate at the head of the conveyance network is the highest. This flow rate configuration corresponds also to the lowest distribution of  $H_{ij}$ .

If a flow rate limiter is installed at the outlet, such as in the case of a limited-rate demand network, the outlet discharge  $Q_{ij}$  is constant and it does not dependent on  $H_{ij}$ . The duration of irrigation is thus given by:

$$t_{i,j} = \frac{\sum(I''_{i,j,k})}{Q_{i,j}} \quad (7.7)$$

By means of Eq.(7.7) the farmers' water demand  $\{I''_{ij,k}\}$  is transformed in a distribution of irrigation duration  $t_{ij}$ . Considering Eq.(7.3),  $t_{ij}$  is always greater than 0 and smaller or equal to 86 400 s.

### 7.6.2 Hydraulic simulation model of the conveyance system

The hydraulic simulation model adopted in SIMODIS is based on the following assumptions:

- The hydraulic head at the beginning of the conveyance system i.e. the compensation reservoir of Gromola district is fixed i.e. 71 m above sea level
- The outlet discharge  $Q_{ij}$  is fixed and not dependent on the hydraulic head  $H_{ij}$  at the node
- The water flow in each pipeline of the conveyance network is considered at steady-state, i.e. no transient phenomena are simulated
- The water delivering outlets i.e. those serving the secondary units with duration  $t_{ij} > 0$  [Eq.(7.7)] are operated simultaneously.

As mentioned in the previous Section the latter hypothesis corresponds to the heaviest working condition for the conveyance network i.e. the distribution of lowest hydraulic head  $H_{i,j}$  for the given water distribution  $\{P''_{i,j,k}\}$ . Thus the condition in Eq.(7.6) would be met also by considering any other configuration of flow rates in the conveyance system.

To simulate the water flow, the conveyance network of pipelines is schematised in  $n$  nodes and  $l$  branches. Each node corresponds to an outlet serving a secondary unit or to a change of pipeline diameter or roughness. A branch is a pipeline connecting two adjacent nodes with constant diameter  $D_{i,j}$ , roughness  $\omega_{i,j}$  (m) and flow rate  $q_{i,j}$ . The roughness  $\omega_{i,j}$  is a characteristic of the pipeline walls material and is commonly found in technical handbooks. The corresponding values for the pipelines in the Gromola district were introduced in the database described in 7.1.

In each node corresponding to an outlet with discharge  $Q_{i,j}$  it is possible to write the continuity equation of water flow:

$$q_{i,j-1} - q_{i,j} = Q_{i,j} \quad (7.8)$$

Considering a pipeline of length  $L_{i,j}$  connecting the nodes  $i,j$  and  $i,j+1$ , the hydraulic head loss  $\Delta H$  between the two extremities of the pipeline is calculated by means of the known equation:

$$\Delta H_{i,j} = H_{i,j+1} - H_{i,j} = B_{i,j} \frac{q_{i,j} |q_{i,j}|}{(D_{i,j})^5} L_{i,j} \quad (7.9)$$

where the loss factor  $B_{i,j}$  ( $s^2 m^{-1}$ ) is a function of the friction coefficient  $\Lambda$ , which depends on the Reynolds number  $Re$  (-) and on the pipeline roughness:

$$B_{i,j} = \frac{8\Lambda}{g\pi^2} = 0.0826\Lambda(Re, \omega) \quad (7.10)$$

The Reynolds number is calculated from flow velocity, pipeline diameter and water kinematic viscosity which was fixed at  $1.2 \cdot 10^{-6} m^2 s^{-1}$ .

In a looped network with  $m$  rings, the following relationship holds (Arredi, 1981):

$$l = m + n - 1 \quad (7.11)$$

The flow rates  $q_{i,j}$  in the branches of the rings of a looped network are unknown, because the water can follow any direction along the ring. Therefore, to determine the distribution of hydraulic head  $H_{i,j}$  we need to determine  $q_{i,j}$ .

In the network there are  $n-1$  independent relationships such as Eq.(7.8). Then, the equilibrium principle imposes that the sum of the head losses along the  $m$  branches of each ring must be zero:

$$\sum (\Delta H_{i,j})_m = 0 \quad (7.12)$$



which can be written, by substituting Eq.(7.9), as:

$$\sum (\Delta H_{i,j})_m = \sum \left( B_{i,j} \frac{q_{i,j} |q_{i,j}|}{D_{i,j}^5} L_{i,j} \right)_m = 0 \quad (7.13)$$

Considering the relationship in Eq.(7.11), the system of  $(m+n-1)$  equations (7.8) and (7.13) can be solved to determine the flow rates in  $l$  branches of the network. Due to the non-linearity of Eq.(7.13), different iterative techniques can be applied to solve the equations system and finally calculate the distribution of  $H_{i,j}$  from the resulting flow rates  $q_{i,j}$  (Arredi, 1981).

If the constraints specified by Eq.(7.6) are met, the water distribution  $\{I''_{i,j,k}\}$  is the final one and the corresponding irrigation volumes are included in the input for the simulation of soil water balance of the following day  $d+1$ .

### 7.6.3 Irrigation schedule adaptation for insufficient hydraulic head at outlet

If the constraint specified by Eq.(7.6) is not met i.e.  $H_{i,j} < H_{min}$  in correspondence of one or more outlets delivering irrigation water, a third and last adaptation of schedule is required. This occurrence is generally due to an excessive head loss along one or more pipelines, as a consequence of a large flow rate or a too small pipeline diameter [Eq.(7.9)].

In SIMODIS, the reduction of the flow rate is made in two steps:

- the number of outlets operating simultaneously is progressively reduced
- the secondary units served by those outlets with lower hydraulic head are considered as not operating (flag  $f_{i,j,k}$  is set to 0 for the considered day).

In the first step, the hydraulic verification of the network on day  $d$  is repeated by considering that the outlets corresponding to units with smaller irrigation duration  $t_{i,j}$  do not operate simultaneously with those having a duration greater than a given threshold, say 8 hours. Indeed, the probability  $p_{i,j}$  that an outlet with duration  $t_{i,j}$  is open at a given instant  $t$  during day  $d$  is given by:

$$p_{i,j} = \frac{t_{i,j}}{86400} \quad (7.14)$$

Smaller probability values indicate that the corresponding outlets can be operated at different starting times, while those operating for a time longer than a prefixed threshold of, say, 8 hours, have a larger probability to be simultaneously operated. For example, the histogram in Fig. 7.4 shows the series of values of  $t_{i,j}$  obtained in the Gromola district on day 192. The number of outlets with duration smaller than the threshold value of 8 hours are 50 over a total 142.

By removing the assumption that all the outlets are simultaneously operating, the calculation of the hydraulic head distribution  $H_{ij}$  in the network is repeated by excluding the outlets with duration smaller than 8 hours. The progressive reduction of the number of outlets is continued until the condition in Eq.(7.6) is positively satisfied. In such case, the schedule adaptation is not needed because the outlets excluded by the simulation are considered open at different times during the same day  $d$ .

If the condition in Eq.(7.6) is not satisfied when all outlets with duration  $t_{ij}$  smaller than 8 hours have been excluded from the calculation, the water distribution  $\{I''_{ij,k}\}$  is considered inadequate for the hydraulic network. Therefore, the water demand distribution must be adapted by setting the irrigation flag  $f_{ij,k}$  at 0 for the nodes where Eq.(7.6) fails:

$$f''_{ij,k} = 0 \quad \forall i, j \quad \text{where} \quad H_{i,j} \leq H_{min}$$

Similarly to the previous adaptations of schedule, a priority for irrigation on day  $d+1$  is assigned to the tertiary units served by the closed outlet. The new set of irrigation flags determine the last adapted water distribution  $\{I'''_{ij,k}\}$  which will be considered for the simulation of soil water balance on day  $d$ .

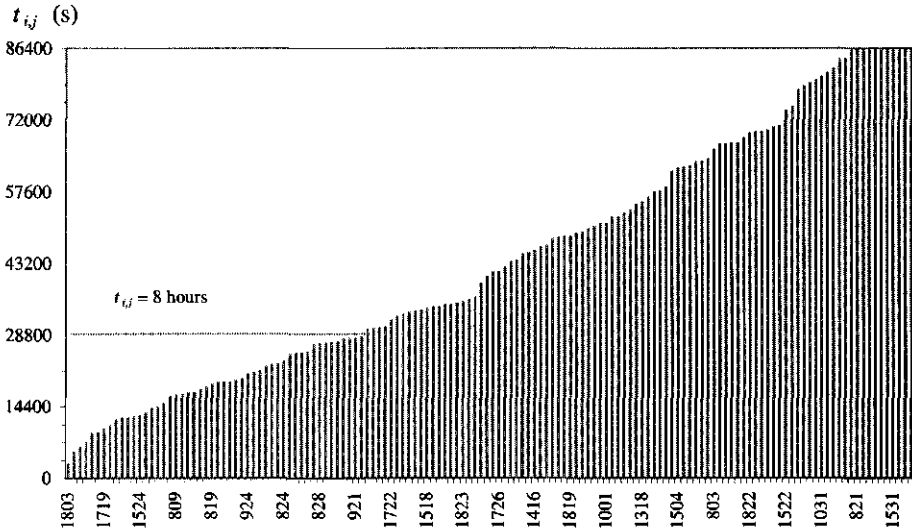


Fig. 7.4 Ordered irrigation duration times on day 192 in the Gromola district. Samples of secondary units codes are given on the horizontal axis.

## 7.7 Irrigation scheduling parameters in the Gromola district.

The actual criteria adopted by farmers to schedule irrigation are determined by many factors, which can be time dependent and subjective. The stochastic component in farmers irrigation habits and preferences is neither negligible nor easily identifiable. Since the irrigation scheduling parameters in SIMODIS are purely deterministic, it is impossible to exactly reproduce the actual operation of irrigation at the level of the single tertiary or secondary unit. The discrepancies between the actual and the simulated irrigation schedule are smoothed out by aggregating the output of SIMODIS at primary unit level.

Starting from these considerations, the measurements of irrigation water volumes acquired during 1994 have been used to evaluate the irrigation scheduling parameters of SIMODIS, as defined in Section 7.4, for the farmers of Gromola irrigation district. In particular the value of  $i_r$  in Eq.(7.1) was identified. From the analysis of several gauge measurements at secondary and primary unit levels, the following scheduling parameters were found:

- starting of irrigation when the average soil water pressure head  $h$  in the root zone was less than the critical value  $h_3$ ;
- farmers' water demand determined as 50% ( $i_r = 0.5$ ) of the soil water deficit calculated between  $z = -10$  and  $z = -50$  cm.

The value of  $V_{RES}$  in Eq.(7.5) was fixed to 71 000 m<sup>3</sup>, corresponding to the peak value of cumulative water consumption measured during the irrigation season '94, as mentioned in Section 5.3.2. The critical pressure head at the delivery outlet  $H_{min}$  was set at the nominal design value of 30 m. We have noticed that the chosen value of  $i_r$  corresponds to an average water application per unit area of approximately 4 cm during the months of July and August.

The plot in Fig. 7.5 shows the comparison between the measured and simulated daily values of total irrigation volumes  $I$  from June to September 1994. The cumulative value of  $I$  simulated by SIMODIS resulted of 4 340 467 m<sup>3</sup>, while the measured volume was 4 770 430 m<sup>3</sup>. From Fig. 7.5 we see that *the temporal evolution of  $I$  is correctly reproduced.*

When we consider such comparison for distinct primary units and for smaller time intervals, i.e. the peak period between day 170 and 203, the average deviation between the simulated and measured irrigation volumes was -17%. An example plot for the primary unit 17, having an extension of 249 ha, is given in Fig. 7.6. The cumulative irrigation volume simulated from day 170 to 203 was 184 102 m<sup>3</sup> compared to a gauge value of 190 100 m<sup>3</sup>, corresponding to a -3% difference. Similarly to the plot in Fig. 7.5, the temporal variation of simulated volumes was in agreement with the measurements.

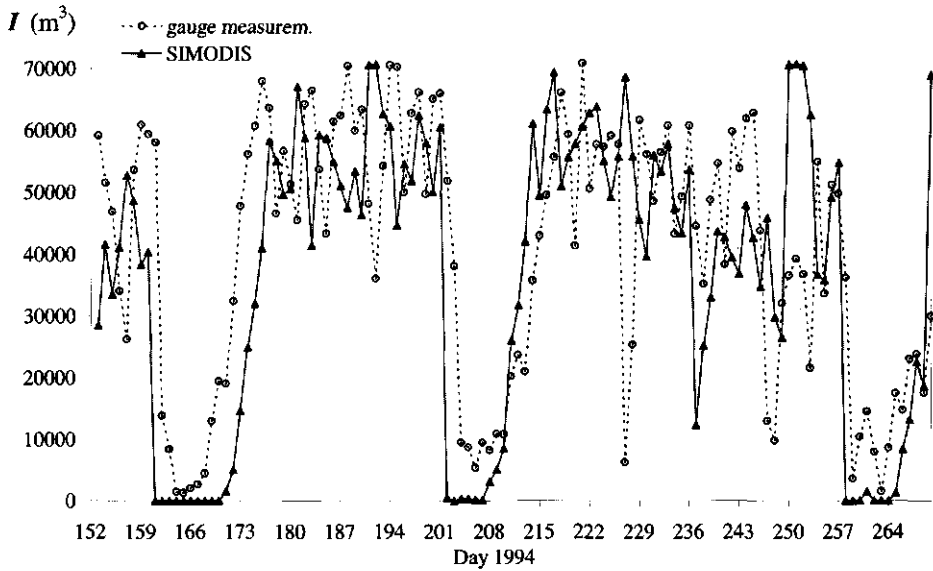


Fig. 7.5 Comparison between gauge simulated and measured irrigation volumes  $I$  from June to September 1994 in the Gromola district. Irrigation volumes were determined assuming a soil water deficit irrigation fraction  $i_r=0.5$ .

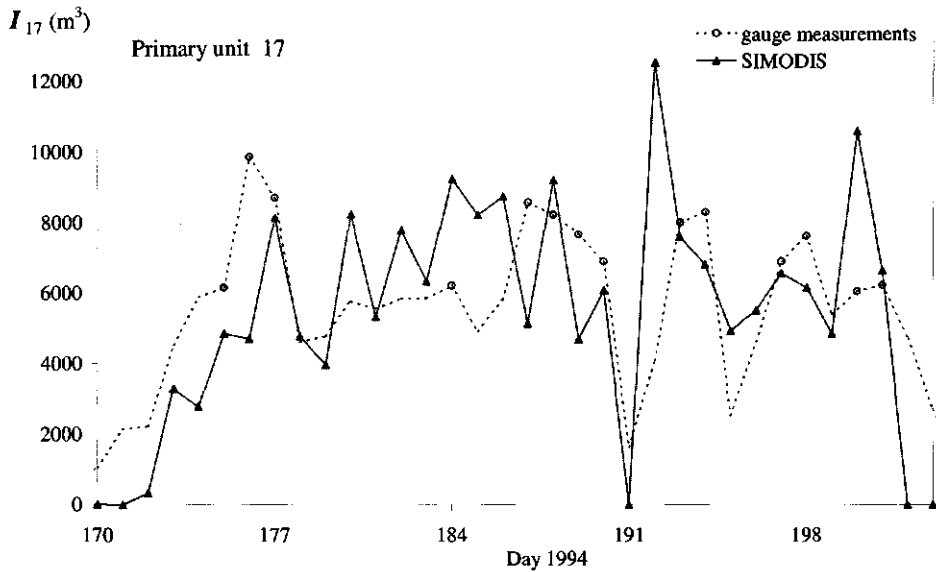


Fig. 7.6 Comparison between simulated and measured irrigation volumes  $I_{17}$  from June to September 1994 for the primary unit 17 (249 ha). The cumulative difference is -3%.

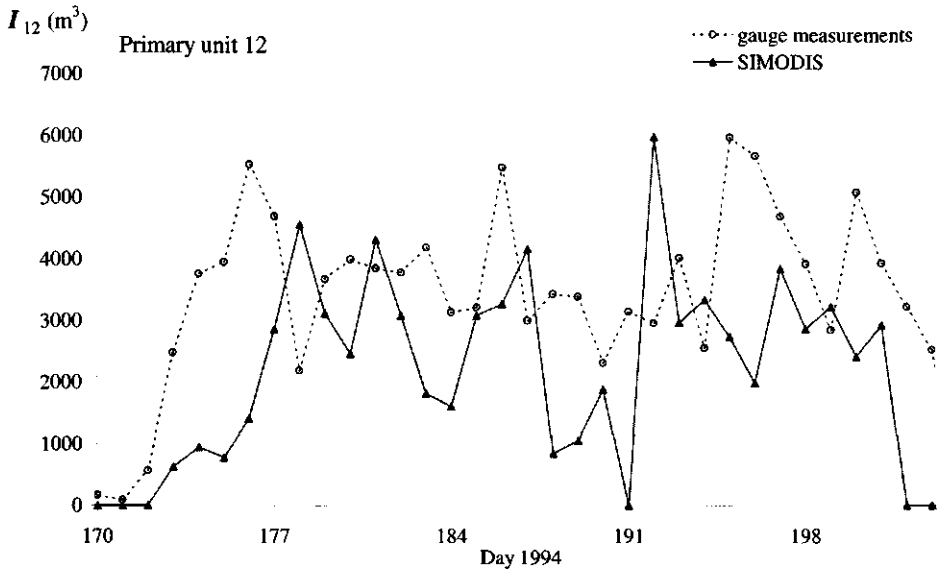


Fig. 7.7 Comparison between simulated and measured irrigation volumes  $I_{12}$  from June to September 1994 for the primary unit 12 (213 ha). The cumulative difference is -37%.

In the case of unit 12 (Fig. 7.7) the difference between simulated and measured values rises to -37%. This can be explained by the circumstance that 55% of the irrigated area of primary unit 12 is cropped with artichokes, which is not productive during the period considered and the  $LAI$  values are low. This determines simulated irrigation volumes lower than measured. In reality, irrigation is applied to sustain the crop in the quiescence state. In this case, the amount of water applied is very much dependent on the habits of individual farmers and it is likely that misuses of irrigation water occur. When we consider a different period i.e. from day 209 to 240 when the crop cycle restarts, the difference between simulated and measured volumes for primary unit 12 reduces to -5%.

A much larger variability of differences between simulated and measured volumes was found at the secondary unit level. Gauge measurements were available in approximately 32 secondary units, with an average served area of 6.5 ha. An example plot for the secondary unit 10-7 is shown in Fig. 7.8. In this case, the secondary unit irrigates different fields with alfa-alfa and maize. The cumulative irrigation volume simulated in SIMODIS in the period shown in Fig. 7.8 is  $7915 \text{ m}^3$ , which is approximately 50% higher than the measured volume, corresponding to  $5128 \text{ m}^3$ . When considering a secondary unit with a single crop type, such as unit 18-3 in Fig. 7.9, the difference is only 1% for a simulated cumulative irrigation volume of  $6130 \text{ m}^3$ .

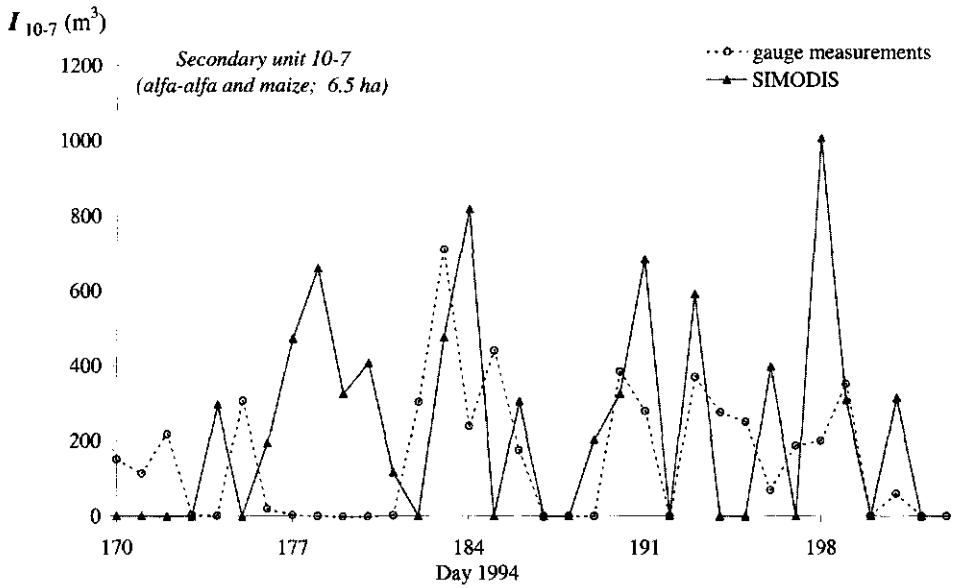


Fig. 7.8 Comparison between simulated and measured irrigation volumes  $I_{10,7}$  in the secondary unit 10-7 with two different crops. The cumulative difference is 54%.

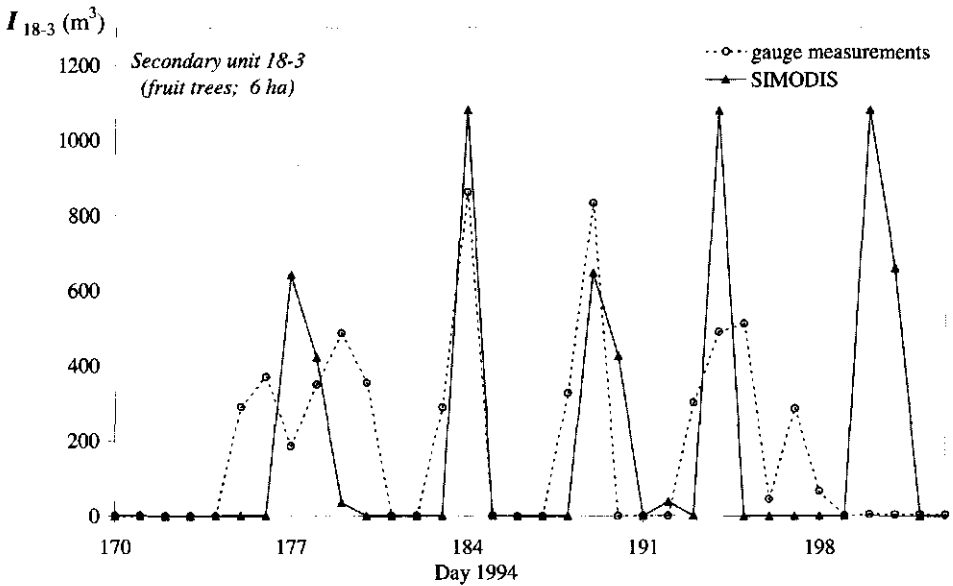


Fig. 7.9 Comparison between measured and simulated irrigation volumes  $I_{18,3}$  in the secondary unit 18-3. The cumulative difference is 1%.

## 7.8 Evaluation of irrigation efficiency.

The irrigation water in the Gromola district during 1994 was applied in such a way that the actual transpiration was kept at its potential value  $T_p$ , as shown also in Fig. 7.2. By analysing the results of SIMODIS for the simulation run described in the previous Section, the average value of the transpiration ratio  $T/T_p$  from June to September '94 was lower than 0.9 in only 24 tertiary units (less than 1%).

The irrigation efficiency indicators  $\varepsilon_1$  and  $\varepsilon_2$  evaluated by means of Eqs.(2.3)-(2.4) and successively averaged out for the entire district, were respectively 0.956 and 0.189. The values for the single primary units are shown in Fig. 7.10. The value of  $\varepsilon_1$  is higher in the units having lower  $\varepsilon_2$ , i.e. units 12 and 13. These units are located closer to the Sele river and to the shoreline (Fig. 5.3); they are characterised by a shallower groundwater table and very low ground elevation as shown by the plots in Fig. 5.19 for the mapping unit of Fig. 5.13.a. Furthermore, the average value of  $K_c$  in these units is smaller than elsewhere. These characteristics determine reduced irrigation volumes, i.e. high  $\varepsilon_1$  value, and less difference between irrigated and non-irrigated conditions, i.e. low  $\varepsilon_2$  values.

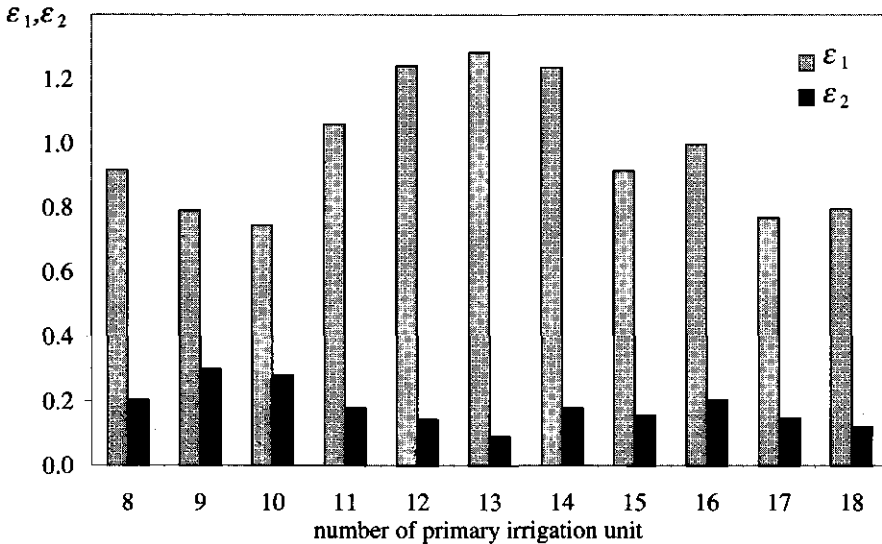


Fig. 7.10 Average values (June to September '94) of irrigation performance indicators  $\varepsilon_1$  and  $\varepsilon_2$  for each primary unit in the Gromola district.

The temporal variation of  $\varepsilon_2$  is shown in Fig. 7.11. The monthly values of the indicator followed the same tendency of the seasonal values of Fig. 7.10. At this time interval the minimum values were found for the primary unit 13 and the maximum for units 9 and 10. The highest effectiveness of irrigation was in July for all units, with the exception of primary unit 14. The difference between July

and other months is particularly pronounced in units 8 and 10, which can be explained by the larger presence of maize and vegetables compared to other crop types. The map of  $\epsilon_2$  is shown in the Colour Plate 5. The value of  $\epsilon_2$  depends on bottom boundary condition, soil hydraulic properties and crop type. As a consequence, the beneficial effect of irrigation is mainly related to the location of the farm within the district.

This local effect is confirmed when we analyse the average values of  $\epsilon_2$  in relation to the soil properties and the bottom boundary condition. From the graph in Fig. 7.12 we notice large differences in the values of  $\epsilon_2$  of a given crop type for different associations of soil hydraulic properties and bottom boundary conditions. The combinations S-1 and V-1 with lower values of  $\epsilon_2$  are those corresponding to the primary units 12 and 13 (Fig. 7.10). In these areas the bottom boundary condition is very influenced by the proximity of the river and of the shore-line. Due to the shallow groundwater table and to the soil water retention characteristics of the soils types S and V (Tab. 5-5), the application of irrigation determines on average an increase of transpiration of 10% respect to non-irrigated conditions. Within the soil unit S the combination with two bottom conditions i.e. 1 and 4 produces different  $\epsilon_2$  values. Hence, here the effect of the bottom boundary condition is dominant.

Diversely in the case of the associations M-2 and R-4 the influence of soil type i.e. a limited soil water storage determines higher values of  $\epsilon_2$ .

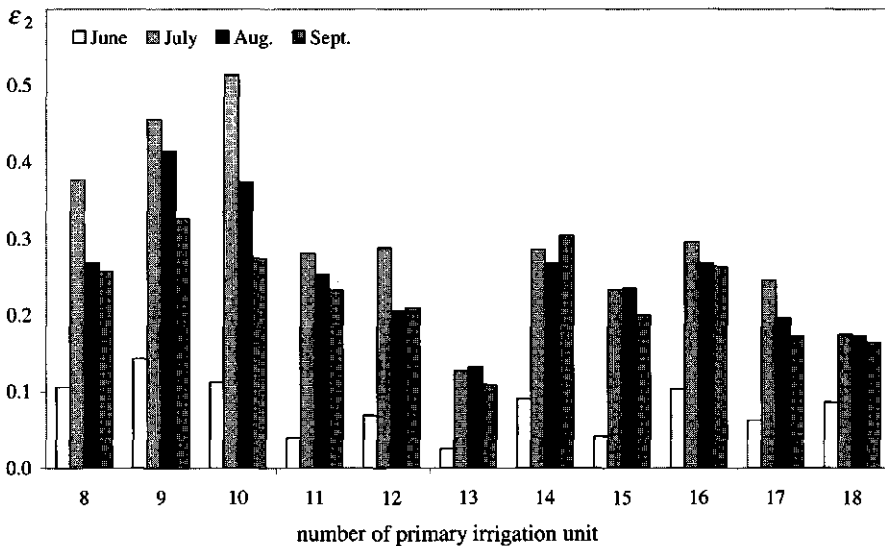


Fig. 7.11 Average monthly values of irrigation performance indicator  $\epsilon_2$  for each primary unit in the Gromola district.



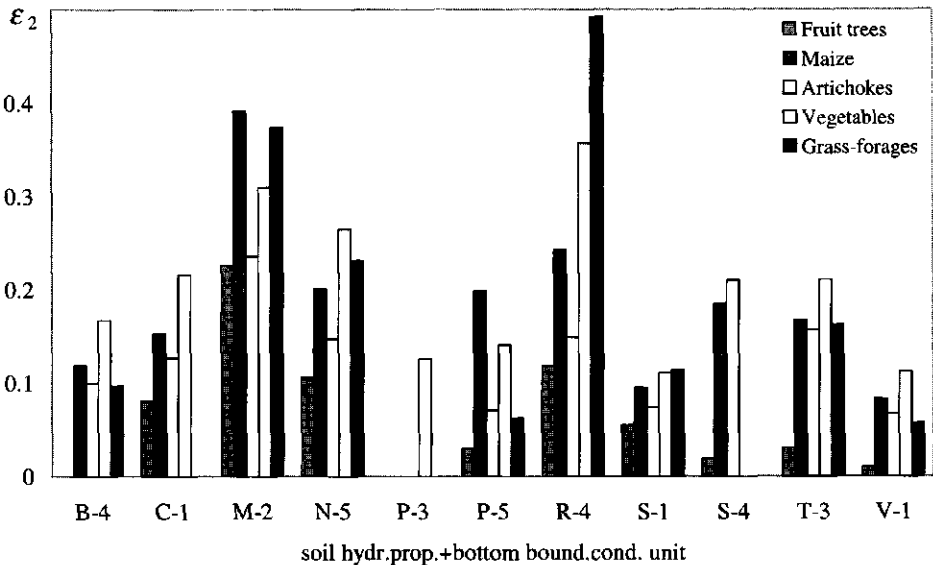


Fig. 7.12 Average values of  $\epsilon_2$  for each association of soil hydrological property unit (Tab. 5-5) and bottom boundary condition unit (Fig. 5.21).

### 7.9 Influence of the uncertainty of $LAI$ and $K_c$ values on SIMODIS.

As evidenced in Section 6.3.2, the estimation of  $LAI$  from satellite reflectance data can be affected by an error as large as 0.30. This error of estimate determines an uncertainty of  $K_c$  around 0.15. The influence of errors in the estimation of  $LAI$  and  $K_c$  on the results of SIMODIS has been evaluated by repeating the simulations with modified  $LAI$  and  $K_c$  values by introducing a random error respectively lower than 30% and 15%. Thus, four different input data sets with randomly modified  $LAI$  and  $K_c$  values were generated for each satellite acquisition (see Tab. 5-2). In Fig. 7.13 the frequency histogram of the differences between the original  $LAI$  and the modified ones is presented for the acquisition of July '94. Similar plots were obtained for the other acquisition dates. The histogram of the average deviation of  $LAI$  values for the image of July '94 is shown in Fig. 7.14.

An example of the effects of such random alterations of the input data on the results of SIMODIS is shown in Fig. 7.15. The plot shows the temporal evolution of transpiration  $T$  for the four different simulations compared to the results of the simulation with unmodified input data. The average error of  $T$  for the tertiary units of Gromola district was 12.4% in July and 13.7% in August. Such difference of results was only 3% when considering the average values of primary units and 0.2% for the district average.

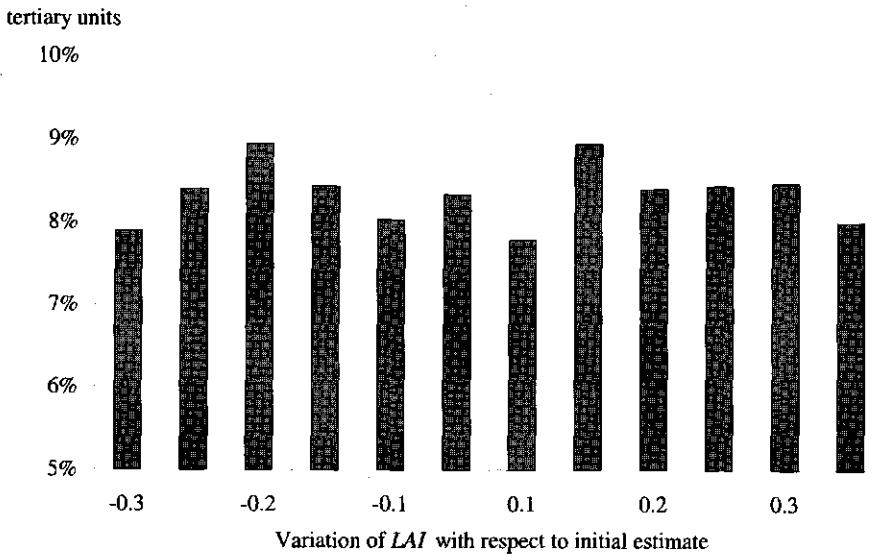


Fig. 7.13 Histogram of the relative error randomly introduced to modify the initial estimate of LAI from satellite data

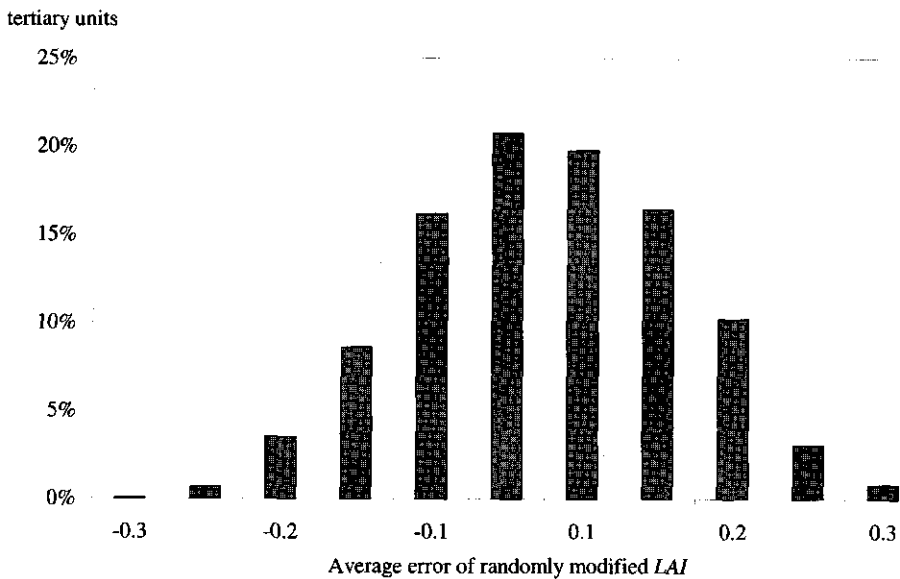


Fig. 7.14 Average deviation of original versus modified LAI values.

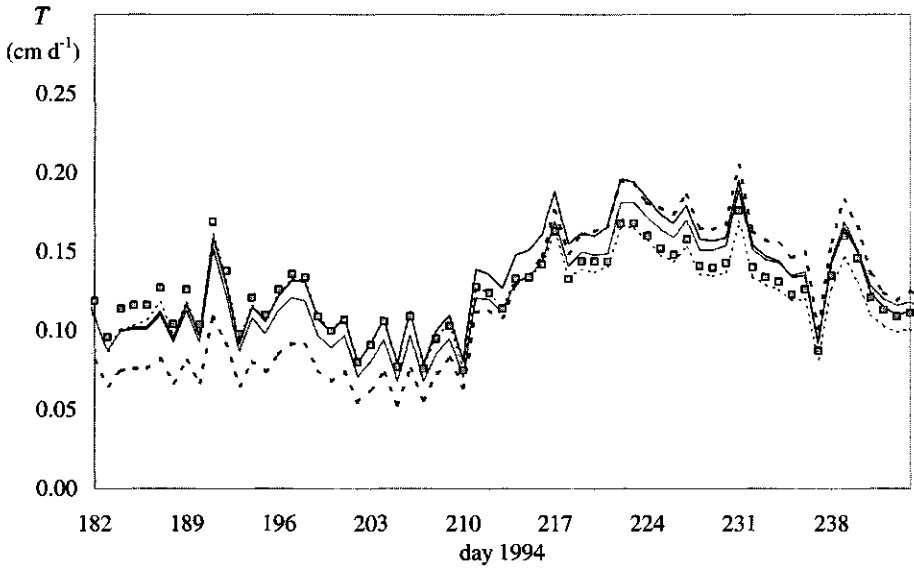


Fig. 7.15 Variation of transpiration  $T$  in a tertiary unit for different sets of LAI and  $K_c$  values, being randomly modified. Square dots represent the results of simulation with unmodified input data. The maximum absolute error introduced for LAI and  $K_c$  was respectively 30% and 15%.

Tab. 7-1 Average absolute errors of SIMODIS output for absolute errors of estimate of LAI and  $K_c$  respectively lower than 30% and 15%. Data are calculated for different levels of aggregation and temporal intervals.

$T$	Season 94	June	July	August
District	0.2%	0.2%	0.2%	0.2%
primary	1.5%	3.1%	2.5%	2.1%
secondary	9.2%	24.7%	17.2%	15.7%
tertiary	8.5%	13.4%	12.4%	13.7%
$I$	Season 94	June	July	August
District	0.5%	0.6%	0.6%	0.8%
primary	1.5%	3.1%	2.5%	2.1%
secondary	9.2%	24.7%	17.2%	15.7%
tertiary	14.4%	29.4%	23.4%	21.2%
$\epsilon_1, \epsilon_2$	Season 94	June	July	August
District	0.9%	2.2%	0.3%	0.9%
primary	1.3%	3.9%	1.4%	1.4%
secondary	6.1%	17.0%	9.1%	8.5%
tertiary	11.2%	33.9%	20.6%	17.4%

In Tab. 7-1 the average absolute errors for the output variables  $T$ ,  $I$  and the indicators  $\varepsilon_1$ ,  $\varepsilon_2$  are presented for different levels of aggregation, i.e. from tertiary unit to district, and for different time intervals. From the table we see that the effects of error of estimate of  $LAI$  and  $K_c$  are smoothed when the simulation results are averaged out from the tertiary unit to upper hierarchic levels. The largest errors are those corresponding to the irrigation volume  $I$  and the efficiency  $\varepsilon_1$  at tertiary unit level. Diversely, the errors at primary unit level are always within 4%.

We can conclude the results of SIMODIS are particularly *accurate at the level of primary unit*, but *a better estimation of  $LAI$  and  $K_c$  is needed to improve the accuracy at lower hierarchic levels* i.e. secondary and tertiary units.

## 7.10 Conclusions

In this Chapter we have described the main elaboration steps of SIMODIS which are related to the following issues:

- Spatial distribution of soil water deficit
- Spatial distribution of farmers' water demand
- Adaptation of irrigation schedule due to: i) excessive water demand at secondary unit level, ii) at district level, iii) insufficient hydraulic head at delivery outlets.

The parameters adopted in SIMODIS for scheduling irrigation i.e. the application day and the corresponding volume in relation to soil water deficit were identified by comparing the irrigation water volumes measured in the Gromola district during 1994 to the values simulated with SIMODIS. From this analysis it resulted that the irrigation volumes were corresponding to 50% of the soil water deficit respect to saturation in the soil profile between 10 and 50 cm depth. Irrigation was applied when the soil water pressure was lower than the critical value for water stress of the corresponding crop type.

The behaviour and the habits of farmers in irrigation practice determined a noticeable deviation between measured and simulated daily values of irrigation volumes at tertiary and secondary unit level. This difference, which can be considered as a stochastic factor, was very much reduced when comparing the aggregated values for a time interval of, say, one month or for primary units.

From the output of SIMODIS it was possible to estimate the irrigation efficiency through the performance indicators introduced in Section 2.3. The seasonal irrigation efficiency determined by means of indicator  $\varepsilon_1$  for the different primary units was ranging from 0.77 to 1.23, with an average value close to 1. The irrigation indicator  $\varepsilon_2$  which takes into account of the difference in transpiration between irrigated and non irrigated condition resulted in the range [0.09; 0.30] with average value of 0.19.

It was noticed that the higher  $\varepsilon_1$  values were corresponding to units with lower  $\varepsilon_2$ . This apparent contradiction was explained by considering the actual hydrological conditions of the different primary units. For the units located near to the river Sele the shallow water table resulted in lower irrigation applications (thus giving high  $\varepsilon_1$  values) but less difference between irrigated and non-irrigated conditions in terms of actual transpiration (low  $\varepsilon_2$  values). As a consequence the benefit deriving from irrigation was not only a function of the crop type but also of the local soil and hydrological conditions.

The differences among the monthly values of  $\varepsilon_1$  and  $\varepsilon_2$  at the level of primary units were rather large as shown by the histogram in Fig. 7.11.

Finally, the influence of error of estimation in  $LAI$  and  $K_c$  values on the output of SIMODIS was evaluated. Considering that the remote sensing techniques described in Chapter 6 report an average error in  $LAI$  of 0.3 and in  $K_c$  of 0.15 we considered a random variation of such variables for each tertiary unit and for each satellite image processed for the irrigation season 1994. The average error of monthly transpiration was ranging from a value of 0.2 % for the aggregation at district level to 13.7% for tertiary unit level. Similar order of magnitude was observed for the values of irrigation volumes estimated with SIMODIS.

## 8 Supporting decisions in water management of the Gromola irrigation district with SIMODIS.

---

### 8.1 Reference Scenario

Simulation scenarios can help irrigation managers to analyse the impact of a certain decision on the operation and on the performance of the irrigation system. In this Chapter, the use of SIMODIS for the *evaluation and comparison of alternative scenarios of water management* for the Gromola irrigation district is described. In this analysis, the simulation described in Section 7.7 is considered as the *Reference Scenario corresponding to the following irrigation criteria*:

- $V_{RES} = 71\,000\text{ m}^3$
- Limited flow rate  $Q_{ij}$  at outlets
- $H_{min} = 30\text{ m}$
- Farmers' water demand determined as 50% ( $i_r = 0.5$ ) of the soil water deficit calculated between  $z = -10$  and  $z = -50\text{ cm}$
- Starting of irrigation when the average soil water pressure head  $h_{crit}$  in the root zone was less than the critical value  $h_3$ .

The key-variables  $V_{RES}$ ,  $Q_{ij}$ ,  $H_{min}$ ,  $i_r$  and  $h_{crit}$  represent the characterising parameters of water management strategies. The actual modification of  $V_{RES}$  and  $Q_{ij}$  requires actions only by the irrigation system management, but they have a clear impact on the irrigation at farm level. Vice versa, the key-variables  $H_{min}$ ,  $i_r$  and  $h_{crit}$  characterise the on-farm irrigation and as such they are very subjective. The adoption of irrigation management strategies based on the modification of these variables, corresponding to the last three criteria mentioned above, requires a very good communication level between management board and individual farmers. For example, it is possible to vary the threshold  $H_{min}$  or to reduce the irrigation volume through  $i_r$  by restricting the irrigation time at farm level.

In some cases, the limitation of the specific irrigation volume  $I/A$  may result as the simplest solution since it just implies the control of a fixed duration of irrigation. This action can be easily implemented i.e. by means of timers controlling the outlets. The adoption of irrigation strategies based on the modification of the starting criteria, i.e. the value of  $h_{crit}$ , are very difficult to implement because they require a common perception of soil water status which can not be achieved without proper measurement devices in each irrigated tertiary unit.

On the basis of these considerations, the water management scenarios summarised in Tab. 8-1 were designed and simulated. In all the simulations the input data about canopy development, i.e.  $LAI$  and  $K_c$ , and the criterion for the starting of irrigation were the same as for the Reference Scenario.

In Tab. 8-1 the column  $V_{TOT}$  indicates the cumulative water consumption of Gromola district from June to September 1994 resulting from the scenarios simulations. We notice that the second highest value of  $V_{TOT}$  is corresponding to the Reference Scenario.

The scenario simulations can be divided in two groups: simulations with no reduction of the daily available water resources  $V_{RES}$ , i.e. scenarios 2, 3 and 4, and with reduction of  $V_{RES}$ , i.e. Scenarios 5 and 6.

The performance of the irrigation system in each scenario was then evaluated by means of indicators of irrigation efficiency  $\epsilon_1$  and  $\epsilon_2$  given in Eqs.(2.3) and (2.4). The average values of  $\epsilon_1$  and  $\epsilon_2$  for the Reference Scenario during the irrigation season 1994 resulted respectively of 0.965 and 0.189 for the entire district, while the average transpiration ratio  $T/T_p$  was 0.98.

Tab. 8-1 Summary of simulated scenarios. Variations with respect to the Reference Scenario (1) are indicated in italic

Scenario	$V_{RES}$ ( $m^3$ )	$Q_{ij}$ ( $m^3s^{-1}$ )	$H_{min}$ (m)	$i_r$ (-)	$I/A$ (cm)	$V_{TOT}$ ( $m^3$ )
1 (Ref.)	71 000	fixed	30	0.5	var.	4 340 467
2	<i>unlimited</i>	<i>unlimited</i>	2	0.5	var.	4 393 940
3	71 000	fixed	40	0.5	var.	4 310 799
4.1	71 000	fixed	30	<i>0.4</i>	var.	4 088 517
4.2	71 000	fixed	30	<i>0.25</i>	var.	3 384 982
4.3	71 000	fixed	30	<i>var.</i>	2	3 295 271
5	<i>55 000</i>	fixed	30	<i>var.</i>	2	3 351 332
6.1	<i>45 000</i>	fixed	30	<i>var.</i>	2	3 761 447
6.2	<i>40 000</i>	fixed	30	<i>var.</i>	2	3 499 278
6.3	<i>35 000</i>	fixed	30	<i>var.</i>	2	2 797 710

## 8.2 Unlimited on-demand irrigation schedule: Scenario 2

In the simulation of Scenario 2 the constraints on the network operation deriving from the first three criteria ( $V_{RES}$ ,  $Q_{ij}$ ,  $H_{min}$ ) were eliminated. The simulation was made assuming unlimited flow rates at the outlets and a minimum

delivery hydraulic head  $H_{min} = 2$  m. The latter hypothesis implies the minimum possible limitations to the hydraulic head losses in the network, but it obliges the farmers to lift mechanically the irrigation water to get the minimum hydraulic head required to operate irrigation equipment. In addition, the daily available volume of water resources  $V_{RES}$  was also unlimited. The distribution of farmers' water demand was determined assuming  $i_r = 0.5$  as in the Reference Scenario.

The total daily water demand exceeded the previous threshold of  $V_{RES} = 71\,000\text{ m}^3$  on 8 days, with a maximum of  $96\,000\text{ m}^3$  on day 250. The cumulative value of irrigation volume for the months from June to September, equals  $4\,393\,940\text{ m}^3$  which was slightly larger than that of the Reference Scenario ( $4\,340\,467\text{ m}^3$ ).

The seasonal efficiency indicators  $\varepsilon_1 = 0.977$  and  $\varepsilon_2 = 0.194$  were only 2% higher than the corresponding values of the Reference Scenario. The small increase of efficiency is explained by the fact that the irrigation scheduling adaptations described in Sections 7.4 and 7.5 were not needed. Only on day 151 it was necessary to close some outlets to reduce the hydraulic head losses in the network, as a consequence of the schedule adaptation described in 7.6.3.

We may conclude from these data that the *removal of operational constraints does not produce a substantial increase of irrigation performance*; diversely, the global consumptive use of water resources for irrigation is larger than the reference run and the energy cost of irrigation at farm level is higher.

### 8.3 Higher hydraulic head at the outlet: Scenario 3

Considering that a higher hydraulic head at the outlet is an advantage for the farmers, Scenario 3 aims to evaluate the increase of the threshold  $H_{min}$  in relation to the operation of the irrigation system. Contrary to this advantage, the increase of  $H_{min}$  may determine the closure of some delivery outlets, as described in Section 7.6.3.

Two simulations were made: in the first case, the threshold value  $H_{min}$  was raised to 40 m compared to 30 m in the Reference Scenario. In the second simulation,  $H_{min}$  was set to 50 m. We should consider that the hydrostatic value is 71 m. Hence in the first simulation the maximum allowable head loss is 31 m and in the second only 21 m.

With  $H_{min} = 40$  m, the closure of some outlets due to an insufficient hydraulic head was required only on days 200, 251 and 253. Thus the performance of the irrigation system was not degraded and the indicators  $\varepsilon_1$  and  $\varepsilon_2$  resulted practically equal to the Reference Scenario.

Diversely, in the second simulation run, the hydraulic threshold  $H_{min} = 50$  m determined frequent closures of outlets even on days with limited water demand and the adaptation of irrigation schedule described in 7.6.3 was not feasible because of the excessive number of outlets being closed.



From the results of Scenario 3, we may conclude that with the actual irrigation criteria practised in the Gromola district it is possible to *increase the minimum hydraulic head* at the outlets to the value of 40 m. In this case, a minimum of adaptations of irrigation scheduling would be required on few days with peak demand.

#### 8.4 Reduction of irrigation water application: Scenario 4

A significant increase in the performance of the irrigation system can be achieved by reducing the water volumes of each irrigation application. As a consequence, the number of irrigation applications in each field is generally higher and the time lag between two successive applications shorter.

In the first simulation of Scenario 4, indicated with 4.1 in Tab. 8-1, the irrigation fraction  $i_r$  was set to 0.4. This implies a reduction of irrigation water volumes applied of 20%. In this case, the irrigation performance indicators improved substantially with respect to the Reference Scenario, i.e.  $\varepsilon_1 = 1.063$  and  $\varepsilon_2 = 0.210$ , while the relative transpiration ratio was the same i.e.  $T/T_p = 0.982$ . It is interesting to notice that the total irrigation consumption from June to September was 17% lower.

We tried to further reduce the irrigation volumes by setting  $i_r = 0.25$  in Scenario 4.2. The overall performance of the system was further improved, with significantly higher values of the indicators, i.e.  $\varepsilon_1 = 1.136$ ;  $\varepsilon_2 = 0.235$  and an average relative transpiration ratio of 0.982. In analogy to Scenario 4.1 the total irrigation volume from June to September was 31% less than the corresponding one in the Reference Scenario. Furthermore, the maximum daily volume of water demand was 67 000 m<sup>3</sup>. Thus, no schedule adaptation for excessive total water demand was required. Also the threshold value  $H_{min} = 30$  m for the hydraulic head at the outlet was always met.

In order to evaluate the possibilities for further improvements of the irrigation efficiency, a *fixed specific irrigation volume*  $I/A = 2$  cm per application was considered in the simulation of Scenario 4.3. This corresponds approximately to  $i_r = 0.25$ , that is 50% of the irrigation volumes applied in the Reference Scenario.

The practical implementation of this scenario is rather easy in limited rate irrigation systems. Indeed, having a fixed flow rate at the outlet, it is possible to apply a given volume by fixing the duration of irrigation  $t_{ij}$ . The resulting values of irrigation indicators point to the *best performance* among the scenarios considered, with  $\varepsilon_1 = 1.219$ ;  $\varepsilon_2 = 0.244$ . Furthermore, the maximum daily value of the total farmers' water demand resulted of 64 000 m<sup>3</sup>. The total water volume consumed from June to September of 3 295 271 m<sup>3</sup>, corresponding to a 24% reduction with respect to the Reference Scenario.

The results of Scenarios 4.1 to 4.3 suggest that in the Gromola district is possible to *increase the performance of the irrigation system with a contemporary reduction of the total water consumption without bringing crop water stress conditions.*

By allowing a reduction of 20% of the actual irrigation volumes applied, it is possible to save approximately 17% of the seasonal volume of water needed. A further improvement can be achieved by fixing the specific irrigation volume  $I/A$  at 2 cm. In this latter case  $V_{RES}$  is 10% lower and the total seasonal water consumption is reduced by 24%.

### 8.5 Reduction of water resources daily available: Scenarios 5 and 6

In the following simulations the value of  $V_{RES}$  was progressively reduced to evaluate the behaviour of the irrigation system under scarcity conditions. In this research of the minimum value of  $V_{RES}$  and of the total seasonal water consumption the occurrence of crop water stress conditions was evaluated.

In the simulations of Scenarios 5 and 6 the specific water volume  $I/A$  applied in each irrigation was fixed to 2 cm, similarly to Scenario 4.3.

In Scenario 5 the value of  $V_{RES}$  was set to 55 000 m<sup>3</sup>. The plot in Fig. 8.1 shows the total daily water demand from June to September, as resulting from SIMODIS and from the gauge measurements.

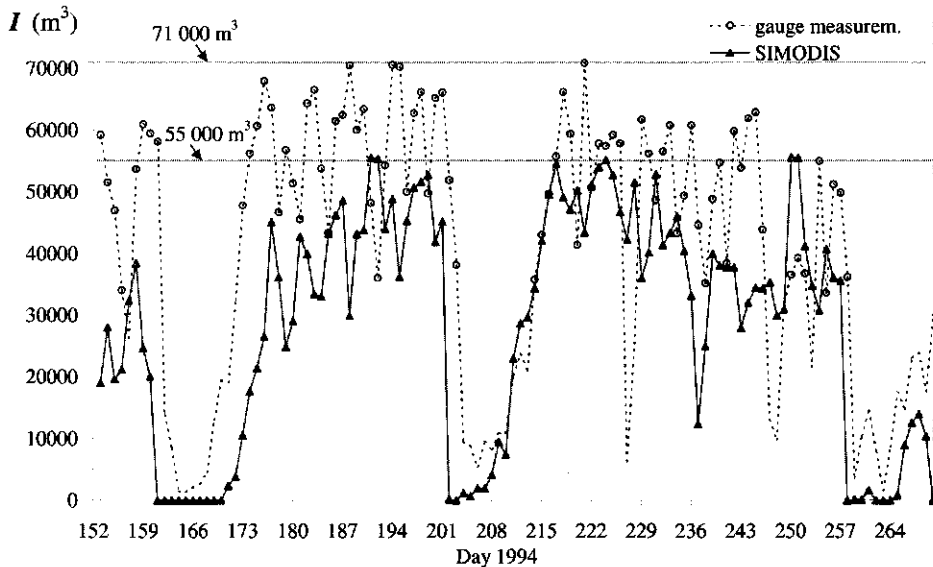


Fig. 8.1 Daily irrigation water volumes  $I$  measured and simulated in the Scenario 5 assuming  $V_{RES}=55\,000\text{ m}^3$ .

The total seasonal water consumption was  $3\,351\,332\text{ m}^3$ . The global performance of the irrigation system was comparable to that of Scenarios 4.2 and 4.3, with indicators value  $\varepsilon_1=1.169$  and  $\varepsilon_2=0.236$ . The average relative transpiration ratio was equal to Reference Scenario ( $T/T_p = 0.984$ ).

The irrigation schedule adaptation due to excessive water demand with respect to  $V_{RES}$  (see Section 7.5) was needed in 7 non consecutive days instead of 4 in the Reference Scenario. During these days one or more primary units were forcedly closed.

From the comparison between Scenarios 4 and 5 we may conclude that the *limitation of daily water availability to  $55\,000\text{ m}^3$  instead of  $71\,000$  does not imply less seasonal water consumption*. In addition the water distribution in one or more primary units is more frequently suspended than in the Reference Scenario as a consequence of excessive water demand with respect to the available water resource  $V_{RES}$ .

Considering that with the reduction of  $V_{RES}$  to  $55\,000\text{ m}^3$  there was no reduction of the average relative transpiration ratio  $T/T_p$ , we tried to further reduce the daily volume of available water  $V_{RES}$ . In Scenarios 6.1, 6.2 and 6.3 the value of  $V_{RES}$  was set respectively to  $45\,000$ ,  $40\,000$  and  $35\,000\text{ m}^3$ . Diversely from Scenario 5, in this case the closure of primary units for a water demand exceeding  $V_{RES}$  was needed for some consecutive days.

To evaluate the occurrence of water stress conditions we can analyse the plots in Fig. 8.2 and Fig. 8.3 showing the temporal evolution of  $T$  in two different tertiary units for Scenarios 6.1, 6.2 and 6.3. We see that in scenario 6.1 the transpiration is practically at its potential value. In this case, the reduction of  $V_{RES}$  and the consequent closure of primary units can be considered not limiting the transpiration. Diversely in Scenario 6.2 with  $V_{RES}=40\,000\text{ m}^3$  sensible reductions of transpiration were found during short periods of time although the average seasonal value of  $T/T_p$  for the entire district results higher than 0.95. Thus we may consider this value of  $T/T_p$  as a threshold to avoid short periods crop water stress even conditions which could be critical for crop production. From the graphs in Fig. 8.2 and Fig. 8.3 we see that an average season value  $T/T_p$  between 0.93 and 0.95 should be already considered unacceptable because it might include short periods of intense crop water stress, i.e. during the ten days centred on day 242. Similar situations can be found for the scenario 6.3, corresponding to  $V_{RES}=35\,000\text{ m}^3$ .

The histogram in Fig. 8.4 shows the distribution of seasonal average values of  $T/T_p$  for scenarios 5, 6.1 and 6.2. From the graph we see that there are more than 400 tertiary units with a value of  $T/T_p$  between 0.9 and 0.95 in the scenario 6.2 ( $V_{RES}=40\,000\text{ m}^3$ ). This means that approximately 15% of the fields in the Gromola area are subjected to crop water stress conditions similar to those shown

in Fig. 8.2 and Fig. 8.3. This percentage is around 10% for scenario 6.1 with  $V_{RES} = 45\,000\text{ m}^3$ .

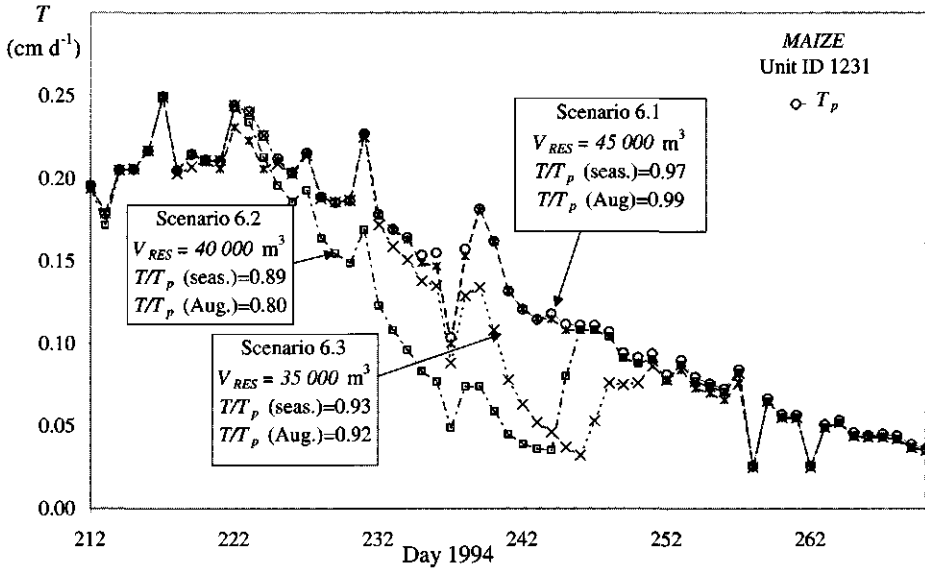


Fig. 8.2 Daily transpiration  $T$  during July and August '94 for a field with maize for Scenarios 6.1, 6.2 and 6.3 with decreasing availability of the maximum daily volume of water resources  $V_{RES}$ .

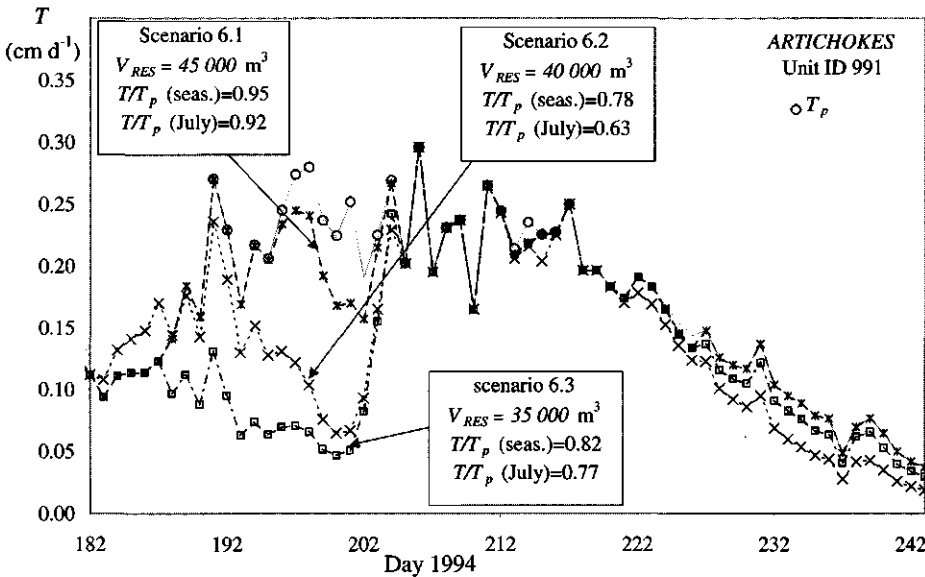


Fig. 8.3 As Fig. 8.2 but for an artichokes field.

In Scenario 6.3 the irrigation system becomes even more restricted with respect to meeting farmers' water demand. By applying the irrigation schedule adaptation described in Section 7.5, some primary units were closed for a period of 7-10 days consecutively, thus determining the occurrence of critical crop water stresses. With the purpose of increasing the elasticity of the irrigation system under conditions of severe scarcity of water, a simulation was made assuming the closure of single secondary units instead of primary units. This technical solution can be very expensive to adopt, because it requires the centralised control and operation of all the outlets.

The plot in Fig. 8.5 shows the percentage of secondary units closed in two cases: closing of primary units (solid line); closing of single secondary units (dashed line). It should be evaluated on the basis of economical considerations whether or not the reduced number of closed secondary units justifies the costs involved in the implementation of a control system for all the secondary units.

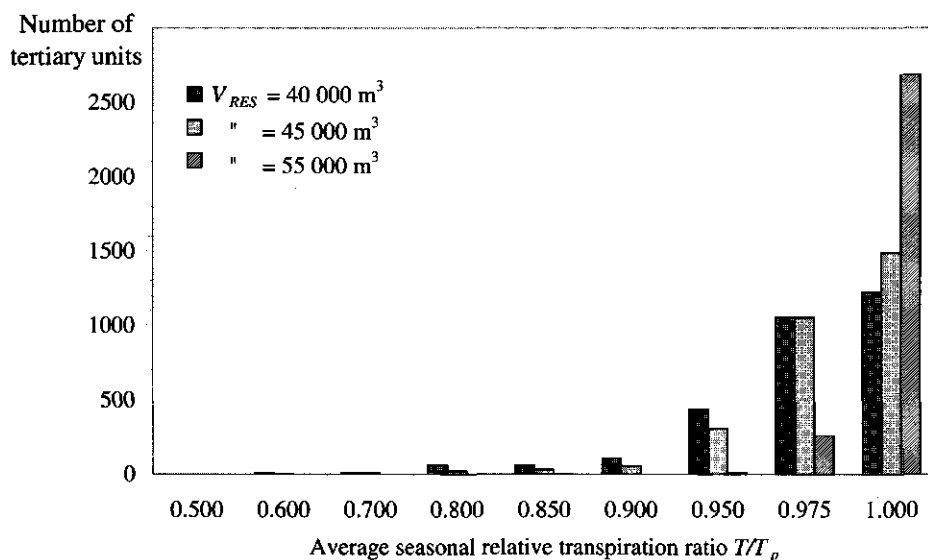


Fig. 8.4 Distribution of the seasonal average value of relative transpiration ratio  $T/T_p$  in Scenarios 5, 6.1 and 6.2 of Tab. 8-1.

## 8.6 Conclusions

The Scenario simulations presented above represent an example of the possible applications of SIMODIS to support irrigation management. From these scenarios we can derive some general indications to improve the efficiency of the irrigation system in Gromola.

A comparison of Scenarios 1 to 5 on the basis of the corresponding irrigation efficiency indicators  $\varepsilon_1$  and  $\varepsilon_2$  is shown in Fig. 8.6 and Fig. 8.7.

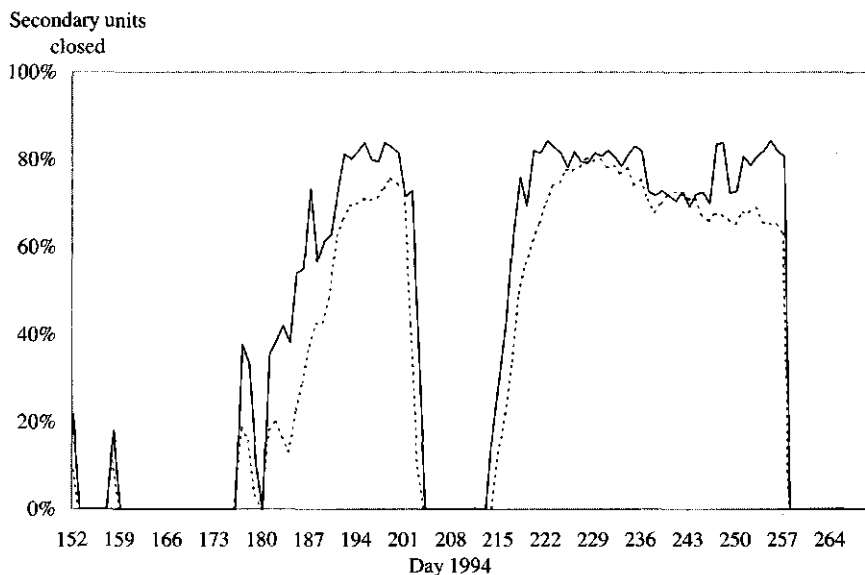


Fig. 8.5 Percentage of secondary units closed after the irrigation schedule adaptation described in 7.5 in Scenario 6.3. The solid line refers to the closing of primary units, while the dashed line refers to the closing of single secondary units.

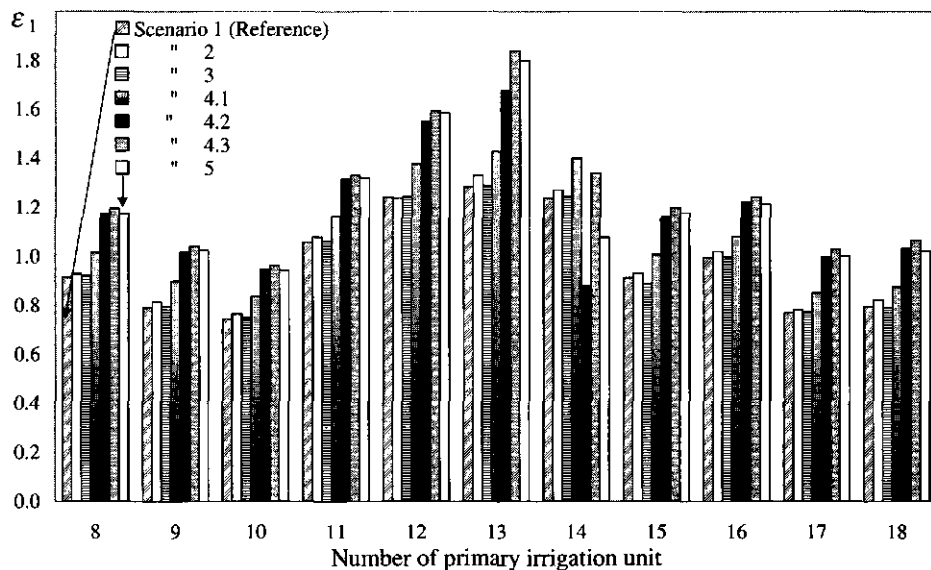


Fig. 8.6 Irrigation performance indicator  $\epsilon_1$  for the Scenarios 1 to 5 calculated for the entire district and for the irrigation season '94.

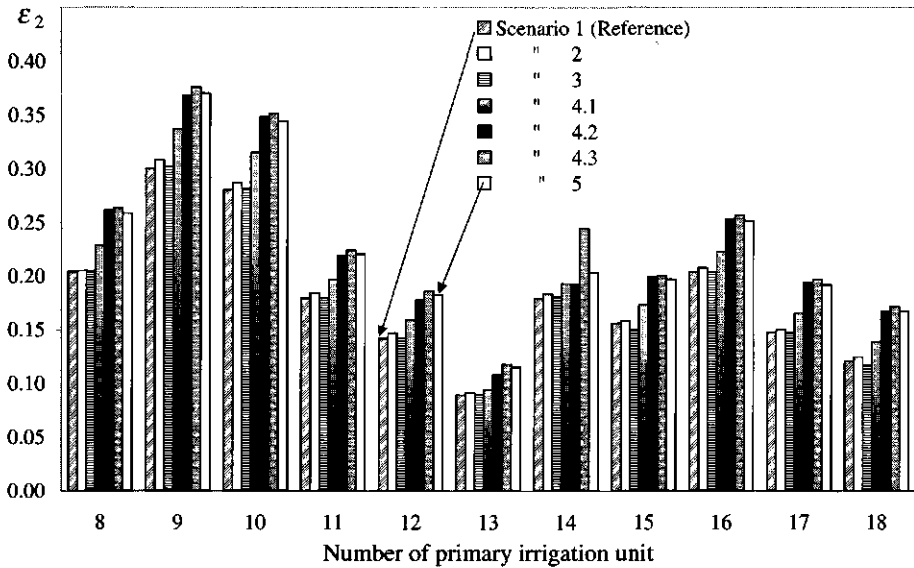


Fig. 8.7 Irrigation performance indicator  $\epsilon_2$  for the Scenarios 1 to 5 calculated for the entire district and for the irrigation season '94.

The relative differences among the primary units are similar to those of Reference Scenario in all cases. We also notice that the maximum difference in the values of performance indicators is approximately 0.2 for  $\epsilon_1$  and 0.06 for  $\epsilon_2$ , corresponding approximately to 20% of the values for the Reference Scenario. These differences are of one order of magnitude larger than the values obtained for an error in the estimation of  $LAI$  and  $K_c$  reported in Tab. 7-1.

Both indicators  $\epsilon_1$  and  $\epsilon_2$  evidence that the *most efficient scenario* is corresponding to 4.3, where the specific water volume  $I/A$  applied in each irrigation was fixed to 2 cm. Good performance was also found in Scenarios 4.2 and 5. The seasonal water consumption in Scenarios 4.2 to 5 was lower than in the Reference Scenario by a volume of approximately one million of cubic meters corresponding to 25% of measured water consumed during the irrigation season 1994.

It is important to highlights from the results of Scenario 2 that the *removal of operational constraints*, such as the flow-limiter on the outlets of the limited-rate demand schedule, *does not determine an increase of efficiency of the system*. Diversely the *limitation of water flow rate at the delivery outlets represents a practical and effective mean to reduce the misuse of irrigation water*.

From Scenario 3 we may conclude that the hydraulic network in the Gromola district is able to guarantee a minimum hydraulic head at the delivery outlet of 40 m. This information is of particular usefulness to farmers in the acquisition of farm irrigation equipment.

Another important consideration which is resulting from Scenario 4 is that the actual *performance of the irrigation system can be enhanced in a significant way by reducing the amount of water* of each application. As shown by the comparison between the Reference Scenario ( $i_r=0.5$ ) and the Scenario 4.1 ( $i_r=0.4$ ), a reduction of only 20% of the applied irrigation gift determine a tangible improvement of the overall efficiency in all primary units. Even better results are obtained with a reduction of 50% of the actual irrigation applications, as shown by Scenario 4.2 ( $i_r=0.25$ ).

*Small and frequent irrigation is the best solution to reduce the daily water demand and to improve the irrigation performance.*

As shown by Scenarios 5 and 6, the daily available water volume  $V_{RES}$  can be reduced to 45 000 m<sup>3</sup> without compromising the irrigation performance but this results in a larger seasonal volume of water consumed with respect to Scenario with  $V_{RES}=71\ 000\ m^3$ .



## 9 Outlook to the future

---

As it is now, SIMODIS can be used for a post-evaluation of the performance of the irrigation system, i.e. on a monthly or seasonal basis. This type of analysis is very rich of useful information to improve management of irrigation systems, as shown by the simulation of scenarios. For this task, SIMODIS can be considered already as a fully operational tool. Nevertheless, *the greatest attractiveness in using tools like SIMODIS is in real-time management.* In this case, it would be advisable to interface SIMODIS with a network of monitoring instruments, such as water meters, timers to monitor the duration of each water gift, agrometeorological stations for weather data and multispectral sensors to monitor vegetation development. *The combination of SIMODIS with a real-time acquisition of input data constitutes a genuine irrigation-expert system.*

At present such realisation may appear far fetched, or simply too expensive. But one should consider that the installation of monitoring devices in irrigation networks is a technological sector under full expansion. For example, during the year 2001 all the outlets of the Gromola district will be operated by means of an individual electronic card. This card can store the total allocation of irrigation water, starting time and duration and it can be programmed to set the maximum withdrawal of water or to restrict irrigation to certain hours or days. Similar devices with remote control through a mobile telephone are commercially available already.

Analogous considerations apply to real-time remote sensing of vegetation. New spaceborn platforms will become operational more and more frequently and constellations of small satellites operated by private companies will be booming during the next years. Multispectral high resolution data will become more widely available at lower costs. Thanks to the development of the Web, the time lag between satellite acquisition and availability of data to the final user will sharply decrease.

It is difficult to establish the “*cost-benefit*” effectiveness of such techniques within the context of actual irrigation systems. The implementation of SIMODIS as a real-time irrigation system could be considered feasible in areas with high value crops and a high price of irrigation water. Presently, however, irrigation water is not yet fully considered as an economic good subject to the rules of economic market, even in areas with serious water scarcity. Nevertheless, in the

future we may expect a turn round of this tendency which will increase the attractiveness of tools like SIMODIS in the management of water resources in irrigated areas.

## Summary and conclusions

---

Improving the efficiency and effectiveness of irrigation systems represents a primary goal in the management of water resources. This task can be achieved if the main *physical processes* governing the irrigation system are understood well and can be monitored. Tools such as agrohydrological simulation models and remote sensing techniques can be used for this purpose. In this thesis these methodologies have been combined in the procedure SIMODIS (Simulation and Management of On-Demand Irrigation Systems). Once implemented in a given irrigation district, SIMODIS simulates the operation of an on-demand irrigation system and it can support the decision making in the management of the system by simulating alternative water management scenarios.

The general lay-out of SIMODIS was described in Chapter 2. In the schematisation adopted in SIMODIS, the water conveyance network of pipelines constitutes the horizontal connection among the different irrigated fields (tertiary units), where the one-dimensional soil water flow model SWAP is applied. The output of SWAP provides the estimated spatial distribution of soil water deficit from which the farmers' water demand is calculated. The starting time of irrigation and the application volume are related to the soil water deficit according to predefined farmers' criteria. Successively, SIMODIS verifies that the spatial distribution of the farmers' water demand is compatible with the available water resources and the capability of the conveyance system. For this purpose a steady-state hydraulic model is used to simulate the water flow in the pipelines network. Irrigation scheduling is adapted in three subsequent steps to adjust the farmers' water demand to the mentioned operational constraints. From the output of SIMODIS indicators of irrigation efficiency are calculated.

The estimation of the spatial distribution of farmers' water demand was presented in Chapter 3. The soil water flow model SWAP was applied to calculate the vertical profiles of soil water pressure head and volumetric moisture content on a daily basis. Then irrigation was scheduled on the basis of the soil water pressure head in the root zone and the application volume was taken proportional to the corresponding soil water deficit. The result of this elaboration for all the tertiary units of the irrigation district was the spatial distribution of farmers' water demand.

This application of SWAP in distributed form requires the *boundary conditions* and the *soil hydraulic properties* to be defined for each elementary area i.e. for each tertiary unit. In SIMODIS the upper and lower boundary conditions were defined in terms of incoming and outgoing water flux densities. At the upper

---

boundary these fluxes were represented by the potential transpiration rate  $T_p$ , the soil evaporation rate  $E_{s,p}$  and the net precipitation rate  $P_n$ . These quantities were estimated from agrometeorological data and canopy variables i.e. the *crop coefficient*  $K_c$  and the Leaf Area Index  $LAI$ . An analytical expression was derived from the equation of potential evapotranspiration to calculate  $K_c$  from the values of  $LAI$ , surface albedo  $r$  and crop height  $h_c$ . The water flux density through the lower boundary  $v$  was defined as a function of the groundwater table depth  $\phi$ . The empirical function  $v(\phi)$  was determined by means of the regional groundwater flow simulation model SIMGRO. The spatial distribution of the soil hydraulic properties i.e. the soil water retention curve and the unsaturated hydraulic conductivity was established by using a calibrated pedo-transfer function. A correction to the Arya-Paris model for estimating the soil water retention curve from the soil particle size distribution in fine-textured soils was proposed.

The development of remote sensing techniques to estimate the spatial distribution of the crop coefficient  $K_c$  was presented in Chapter 4. The advantages of remote sensing in this case were the possibility of monitoring the spatial variability of crops over large areas and the estimation of a  $K_c$  value related to the actual development of the canopy. Two different approaches were proposed:

- application of a hybrid classification algorithm based on both unsupervised and supervised techniques (*classification approach*);
- definition of an analytical relationship relating the spectral reflectance of vegetation canopies to their  $K_c$  (*analytical approach*).

In the classification approach the definition of spectral classes was not known *a priori* because the  $K_c$  value was not strictly dependent on the crop type. Different clustering algorithms were applied to derive the spectral classes corresponding to different  $K_c$  values. To evaluate classifications obtained with different sets of spectral classes two statistical measurements of class separability and classification reliability were derived. These two measurements were combined to define a Classification Performance indicator which was used to select the best  $K_c$  classification.

The analytical approach was based on the direct calculation of  $K_c$  from the canopy variables  $r$ ,  $LAI$  and  $h_c$ . Satellite-based canopy spectral reflectance was used to estimate  $r$ ,  $LAI$  and  $h_c$ . In particular, it was proposed to estimate  $LAI$  by means of a semi-empirical model based on the Weighted Difference Vegetation Index  $WDVI$ . In this case concurrent field data were required to calibrate the  $LAI$ - $WDVI$  relationship.

The study area in the irrigation district of Gromola was described in Chapter 5. The field data collected for preparing the inputs for SIMODIS and for processing satellite images were described.

To identify the spatial distribution of the *lower boundary condition* and of the *soil hydraulic variables*, soil and groundwater information were elaborated by

means of the methodologies described in Chapter 3. Measurements of groundwater depth were used to calibrate the regional groundwater model SIMGRO. From the simulation results it was possible to determine in different areas of the irrigation district the relationship between water flux density  $v$  through the bottom boundary and the groundwater table depth  $\phi$ . The resulting functions  $v(\phi)$  defined the lower boundary condition as required by SIMODIS. The calibrated pedo-transfer approach of Chapter 3 was applied to estimate the soil hydraulic retention and conductivity functions in several locations where textural data were available. Areas with a homogeneous soil hydrological behaviour were identified from the analysis of simulation results of a drying cycle made with SWAP. From this elaboration it was then possible to build the map of soil hydraulic characteristics needed as input in SIMODIS.

Finally, the local validation of SWAP was done by comparing the specific soil water storage simulated by SWAP and that obtained from TDR measurements in the field.

In Chapter 6 the application of the remote sensing techniques to map the *crop coefficients*  $K_c$  from Landsat Thematic Mapper data of the Gromola irrigation district during the irrigation season 1994 was described.

The importance of the radiometric accuracy of satellite based estimates of at-surface directional spectral reflectance was highlighted. The influence of sea reflectance on the radiometric correction of the images was evaluated. The corrected spectral reflectance was then used to apply the classification and analytical approaches outlined in Chapter 4.

In the classification approach different sets of spectral classes were defined by clustering the reflectance values of ground reference fields. Successively a supervised classification was performed for each set of spectral classes. The results of different procedures were compared by means of the Classification Performance indicator derived in Chapter 4. The best results were obtained with a supervised classification based on spectral classes derived with non-hierarchical clustering of the at-surface reflectance values in bands 3, 4 and 5 of Thematic Mapper.

In the analytical approach a sensitivity analysis of the relationship between  $K_c$  and the canopy variables  $r$ ,  $LAI$  and  $h_c$  was carried out. It was shown that for the meteorological conditions existing in the Gromola during the irrigation season the influence of  $LAI$  on the value of  $K_c$  is much larger than that of  $r$  and  $h_c$ . By using the semi-empirical approach described in Chapter 4 it was possible to estimate  $LAI$  with an average absolute error of 0.31 in the  $LAI$  range of 1 to 4. This error corresponds to a variation of 0.15 in  $K_c$  value.

In Chapter 7 the application of SIMODIS to the Gromola irrigation district was described. The farmers' parameters adopted in SIMODIS for scheduling irrigation i.e. the threshold adopted to trigger water application and the

corresponding volume in relation to soil water deficit were assessed on the basis of measured irrigation water volumes collected during the irrigation season 1994. From these data it was possible to assess that farmers in Gromola apply an irrigation volume corresponding to 50% of the soil water deficit in the soil layer between 10 and 50 cm depth. Application of irrigation water was triggered by soil water pressure in the root zone reaching the estimated crop-specific stress value. The data collected indicated that the amount of water available daily was 71 000 m<sup>3</sup>. The minimum allowed hydraulic head  $H_{min}$  at the delivery outlets was set to the design value of 30 m.

By using these parameters a good agreement was found between measured and simulated monthly irrigation volumes at district and primary unit level. The temporal variation of water demand at district level was also satisfactorily reproduced. Diversely, significant differences were observed between measured and simulated irrigation volumes at tertiary and secondary unit level and for time intervals shorter than one month. These differences were explained by the larger influence of diversity in farmers' irrigation habits when evaluating the results of SIMODIS over small areas and for short time intervals.

The irrigation efficiency in Gromola was evaluated by means of indicators calculated from the actual transpiration rate and the corresponding irrigation volumes computed by SIMODIS. Local hydrological conditions affect significantly the efficiency of irrigation. For each crop type the value of the irrigation efficiency indicators was mainly determined by the combination of soil hydraulic properties and bottom boundary condition.

The influence of estimation errors of  $LAI$  and  $K_c$  as resulting from the remote sensing techniques applied in Chapter 6 on the output of SIMODIS was evaluated. When considering the output for the entire district, an error in  $LAI$  with a random error not greater than 30% (and 15% for  $K_c$ ) determined an average error for the monthly value of transpiration of 0.2 %. At primary and secondary unit levels, having an average area of 260 and 6.7 ha, the errors of SIMODIS output were around 3% and 20% respectively. From this analysis it was concluded that the results of SIMODIS are particularly reliable at the scale of primary unit while to obtain reliable results at secondary unit level i.e. with errors less than 20% a better estimation of  $LAI$  and  $K_c$  is required.

The Scenarios simulations as presented in Chapter 8 provide an example of the usage of SIMODIS in supporting irrigation management decisions. The simulation described in Chapter 7 was considered as the reference (scenario 1). Different scenarios were compared by considering the values of the irrigation efficiency indicators.

The effects of alternative strategies of water management were quantified and general indications to improve the efficiency of the irrigation system in Gromola were derived. The scenarios were identified in terms of following variables: the water volume daily available  $V_{RES}$ , the flow rate  $Q_{ij}$  and the

minimum hydraulic head  $H_{min}$  allowed at the outlets, and the soil water deficit fraction  $i$ , from which the specific irrigation volume was calculated.

In scenario 2 the limitations on  $V_{RES}$ ,  $Q_{i,j}$  and  $H_{min}$  were removed. The elimination of these operational constraints did not lead to a substantial increase of the system's irrigation efficiency. Diversely, the total water demand was larger than the reference scenario either at daily and seasonal temporal scale. Thus it was concluded that the adoption of a limited-rate demand schedule is an *effective mean to reduce possible mis-uses of irrigation water*. Furthermore a low hydraulic head at the delivery outlets is not economically convenient for farmers.

The results of scenario 3 showed that it was possible to raise the minimum hydraulic head  $H_{min}$  at the delivery outlets to 40 m instead of the 30 m of the reference scenario. In this case adaptations of irrigation schedule were more frequently required than in the reference scenario, but no decrease in irrigation efficiency was noticed. In the real world, this information may be particularly useful to farmers in acquiring farm irrigation equipment.

Scenario 4 made it clear that the reduction of the irrigation water volumes applied improved the irrigation efficiency significantly. The specific irrigation volumes applied could be reduced as much as 50%, while the average irrigation efficiency was raised by more than 20%.

Finally scenarios 5 and 6 showed that the amount of water daily available could be reduced to 45 000 m<sup>3</sup> from the actual 71 000 m<sup>3</sup> without compromising crop productivity and irrigation performance.

The case-study in the Gromola irrigation district demonstrated that SIMODIS is able to describe the behaviour of an on-demand irrigation system. The quantitative information provided by SIMODIS is a useful support to irrigation technicians, which then can take their decisions more objectively. The synergy between the use of SIMODIS and the feedback from the field practical experience can thus greatly enhance the management of water resources in irrigated areas.

From a general point of view the development of SIMODIS demonstrated that agrohydrological simulation models and remote sensing can be effectively combined to describe the operation of an irrigation system. These techniques have reached a sufficient degree of reliability to be transferred to practical applications. The application of simulation models of soil water flow like SWAP in distributed form led to several innovations, e.g. the definition of lower boundary conditions and the construction of maps of soil hydraulic properties.

---

Crop coefficients can be estimated by means of remote sensing techniques independently of SIMODIS. This is of general usefulness in the definition of the upper boundary condition of distributed hydrological simulation models. Furthermore it can be applied to estimate with satisfactory accuracy the crop water requirements at regional scale.

In the future new types of satellite sensors will probably allow for a more precise determination of the required canopy variables, thus providing novel opportunities in the integration between agrohydrological simulation models and remote sensing techniques.



## Samenvatting en conclusies

---

De verbetering van de efficiëntie en effectiviteit van irrigatiesystemen vormt de hoofddoelstelling bij het beheer van waterbronnen. Dit kan worden bereikt door de belangrijkste fysische processen die aan het irrigatiesysteem ten grondslag liggen goed te begrijpen en te monitoren. Agrohydrologische simulatiemodellen en remote sensing technieken zijn middelen die hiertoe kunnen worden ingezet. In dit proefschrift zijn beide methoden samengebracht in de SIMODIS procedure. Dit staat voor "simulatie en beheer van "on-demand" (vraag-afhankelijke) irrigatiesystemen". Eenmaal geïmplementeerd in een irrigatiedistrict wordt door SIMODIS de werking van een "on-demand" irrigatiesysteem gesimuleerd en kan het de besluitvorming in het beheer van het systeem ondersteunen door simulatie van verschillende scenario's voor waterbeheer.

De opzet van SIMODIS werd in Hoofdstuk 2 beschreven. In de voor SIMODIS gekozen schematisering vormt het watervoerende leidingstelsel de horizontale verbinding tussen de verschillende geïrrigeerde veldeenheden (tertiaire units), op welke het eendimensionale grondwaterstromingsmodel SWAP werd toegepast. De output van SWAP levert een schatting op van de ruimtelijke spreiding van het watertekort in de bodem, aan de hand waarvan de waterbehoefte van de boeren berekend wordt. Het tijdstip van aanvang van irrigatie en de toegediende hoeveelheid water worden gerelateerd aan het watertekort in de bodem met behulp van vooraf geformuleerde "boerencriteria". Vervolgens wordt door SIMODIS gecontroleerd of de ruimtelijke spreiding van de waterbehoefte in overeenstemming is met de beschikbare hoeveelheid water en de capaciteit van het leidingstelsel. Hiertoe wordt voor de simulatie van de stroming van water in het leidingstelsel een "steady-state" hydraulisch model gebruikt. Het maken van een irrigatieschema wordt in drie stappen gedaan om de waterbehoefte voor irrigatie en de genoemde operationele beperkingen op elkaar af te stemmen. Vanuit het resultaat van SIMODIS worden indicatoren voor de efficiëntie van irrigatie berekend.

De schatting van de ruimtelijke spreiding van de irrigatie waterbehoefte werd behandeld in Hoofdstuk 3. Het grondwaterstromingsmodel SWAP werd gebruikt om dagelijkse berekeningen te maken van het profiel van de verticale drukhoogte van het bodemvocht en het volumetrische vochtgehalte. Vervolgens werd de irrigatie geschematiseerd op basis van de drukhoogte van het bodemvocht in de wortelzone en werd het toe te dienen watervolume gekozen evenredig aan

---

het overeenkomstige tekort in bodemvocht. Het resultaat van deze bewerking op alle tertiaire eenheden van het irrigatiegebied leverde de ruimtelijke spreiding op van de waterbehoefte van de boeren.

Deze toepassing van SWAP in gespreide vorm vereist een definitie van enkele grensvoorwaarden en van de hydraulische bodemeigenschappen voor elk gebied afzonderlijk, dat wil zeggen voor elke tertiaire unit. In SIMODIS werden de voorwaarden van de bovengrens en ondergrens van het systeem gedefinieerd in termen van inkomende en uitgaande waterstromen. Voor de bovengrens werden deze stromen weergegeven door het potentiële transpiratiegehalte ( $T_p$ ), het bodemevaporatie gehalte ( $E_{s,p}$ ), en het netto neerslaggehalte ( $P_n$ ). Deze hoeveelheden werden door schatting bepaald uit agrometeorologische gegevens en variabelen die de bodembedekking door het gewas beschrijven, in dit geval de gewascoëfficiënt ( $K_c$ ) en de LAI ("Leaf Area Index"). Een analytische vergelijking werd afgeleid uit de formule voor potentiële evapotranspiratie ter berekening van  $K_c$  uit de waarden van LAI, de oppervlakte albedo ( $r$ ) en de gewashoogte ( $h_c$ ). De waterfluxdichtheid door de ondergrens ( $v$ ) werd gedefinieerd als functie van de diepte van de grondwaterspiegel ( $\phi$ ). Deze empirische functie  $v(\phi)$  werd bepaald met behulp van het simulatiemodel SIMGRO voor regionale grondwaterstroming. De ruimtelijke spreiding van de hydraulische bodemeigenschappen, te weten de retentiecurve van het bodemvocht en het onverzadigde hydraulische geleidingsvermogen, werd bepaald door middel van een "gecalibreerde pedo-transfer" functie. Een correctie werd voorgesteld op het Arya-Paris model ter schatting van de retentiecurve van het bodemvocht met behulp van de korrelgrootte verdeling in fijnkorrelige bodems.

De ontwikkeling van remote sensing technieken voor het bepalen van de ruimtelijke spreiding van de gewascoëfficiënt  $K_c$  werd behandeld in Hoofdstuk 4. De voordelen van remote sensing bestonden in dit geval uit de mogelijkheid van het monitoren van de ruimtelijke variatie van het gewas over grotere gebieden, en de schatting van een  $K_c$  waarde in relatie tot de actuele ontwikkeling van het gewas. Twee verschillende benaderingswijzen werden voorgesteld:

Toepassing van een hybride classificatie algoritme, gebaseerd op zowel gecontroleerde ("supervised") als ongecontroleerde ("unsupervised") technieken (*de classificatie benadering*);

Definitie van een analytische relatie die een verband legt tussen de spectrale reflectie van de vegetatie en de  $K_c$  waarde daarvan (*de analytische benadering*).

In de classificatie benadering was de bepaling van de spectrale eenheden niet a-priori vastgelegd, aangezien de  $K_c$  waarde niet alleen afhankelijk was van het gewastype. Verscheidene groepsvormende algoritmen werden toegepast ter verkrijging van spectrale klassen die overeen komen met verschillende  $K_c$  waarden. Ter evaluatie van de classificatie werden twee statistische bewerkingen

afgeleid voor de toetsing van het onderscheidingsvermogen van de klassen en van de betrouwbaarheid van de classificatie. Deze werden gecombineerd in een "classificatie indicator" om de kwaliteit van de classificatie te beoordelen. Deze indicator werd vervolgens gebruikt om de beste  $K_c$  classificatie te selecteren.

De analytische benadering was gebaseerd op de rechtstreekse berekening van  $K_c$  uit de (gewas) bedekkingsvariabelen  $r$ ,  $LAI$  en  $h_c$ . De uit satellietbeelden verkregen spectrale reflectie van de gewasbedekking werd aangewend ter schatting van  $r$ ,  $LAI$  en  $h_c$ . In het bijzonder werd voorgesteld om tot een schatting te komen van  $LAI$  door middel van een semi-empirisch model, gebaseerd op de *Weighted Difference Vegetation Index (WDVI)*. In dit geval waren veldgegevens vereist voor verdere calibratie van de relatie  $LAI$ - $WDVI$ .

Het studiegebied in het irrigatiedistrict Gromola werd beschreven in Hoofdstuk 5. De veldgegevens die werden verzameld als input voor SIMODIS voor het bewerken van satellietbeelden werden beschreven.

Ter bepaling van de ruimtelijke spreiding van de waarden van de ondergrens en van de hydraulische bodemeigenschappen, werden bodem- en grondwatergegevens bewerkt door middel van de in Hoofdstuk 3 beschreven methodieken. Meetgegevens van de grondwaterdiepte werden gebruikt om het regionaal grondwatermodel SIMGRO te calibreren. Met de verkregen resultaten was het mogelijk om op verschillende plaatsen in het irrigatiegebied de relatie te bepalen tussen de waterfluxdichtheid door de ondergrens ( $v$ ) en de diepte van de grondwaterspiegel ( $\phi$ ). De daaruit resulterende functies  $v(\phi)$  bepaalden de waarden van de ondergrens zoals voor SIMODIS vereist. De "gecalibreerde pedo-transfer" benadering uit Hoofdstuk 3 werd toegepast voor een schatting van de hydraulische retentie- en geleidingsfuncties op verschillende plaatsen waarvan gegevens over de bodemtextuur beschikbaar waren. Gebieden met een homogeen hydrologisch gedrag werden geïdentificeerd aan de hand van de resultaten van een verdrogingcyclus gesimuleerd met SWAP. Hierdoor was het mogelijk de hydraulische bodemeigenschappen in kaart te brengen, welke gebruikt werd als invoer voor SIMODIS.

Tenslotte werd een validatie van de resultaten uitgevoerd door vergelijking van bodemvochtgehalten resulterend uit SWAP met de resultaten verkregen uit TDR metingen in het veld.

In Hoofdstuk 6 werd de toepassing beschreven van remote sensing technieken om de gewascoëfficiënten  $K_c$  in kaart te brengen met behulp van de gegevens van Landsat Thematic Mapper van het Gromola irrigatiedistrict in het irrigatie seizoen 1994.

Het belang van radiometrische nauwkeurigheid bij schattingen van directionele spectrale reflectie aan de oppervlakte, ontleend aan satellietwaarnemingen, werd benadrukt. De invloed van reflectie van de zee (het studiegebied ligt aan zee) op de radiometrische correctie van de beelden werd

---

geëvalueerd. De gecorrigeerde spectrale reflectie werd vervolgens gebruikt voor de toepassing van de classificatie en de analytische benadering die in Hoofdstuk 4 uiteen werden gezet.

In de classificatie benadering werden verschillende spectrale klassen gedefinieerd door een samenvoeging (clustering) van reflectiewaarden van referentievelden. Vervolgens werd een gecontroleerde classificatie gedaan voor elke spectrale klasse. De resultaten van de verschillende procedures werden vergeleken met behulp van de indicator voor kwaliteit van de classificatie, die in Hoofdstuk 4 werd afgeleid. De beste resultaten werden verkregen met een gecontroleerde classificatie, gebaseerd op spectrale eenheden, verkregen uit een niet-hiërarchische clustering van de reflectiewaarden van de oppervlakte in de banden 3, 4 en 5 van Landsat Thematic Mapper.

Bij de analytische benadering werd een gevoeligheidsanalyse uitgevoerd voor de  $K_c$  en de bedekkingsvariabelen  $r$ ,  $LAI$  en  $h_c$ . Aangetoond werd dat bij de meteorologische omstandigheden in Gromola gedurende het irrigatieseizoen de invloed van  $LAI$  op de waarde van  $K_c$  veel groter is dan die van  $r$  en  $h_c$ . Bij gebruik van de semi-empirische benadering zoals beschreven in Hoofdstuk 4, bleek een schatting van  $LAI$  mogelijk met een gemiddelde absolute fout die een waarde van 0,31 in het  $LAI$ -traject van 1 tot 4 heeft. Deze fout komt overeen met een variatie van 0,15 in de waarde van  $K_c$ .

In Hoofdstuk 7 werd de toepassing beschreven van SIMODIS op het Gromola irrigatiedistrict. De parameter die het gedrag van boeren beschrijft bij het schematiseren van irrigatie (het moment waarop de irrigatiegift aanvangt en de daarmee samenhangende volume van de gift) in SIMODIS werd bepaald op grond van irrigatiegiften, zoals die over het irrigatieseizoen 1994 zijn gemeten. Het was mogelijk uit deze gegevens af te leiden dat de boeren in Gromola een hoeveelheid irrigatiewater toedienen die overeenkomt met 50% van het tekort in bodemvocht in de bodemzone van 10 tot 50 cm diepte. Het toedienen van irrigatiewater werd gestart wanneer de bodemwaterdruk in de wortelzone de (gewas- en groeistadium afhankelijke) kritieke waarde bereikte. De verzamelde gegevens toonden aan dat er dagelijks 71 000 m<sup>3</sup> water beschikbaar was. De minimale waterdruk  $H_{min}$  op de "delivery outlets" (de punten waar boeren het water aftappen van het hoofdstelsel) werd gesteld op de ontwerpwaarde van 30 m.

Bij het gebruik van deze parameters werd een goede overeenkomst gevonden tussen de gemeten en de gesimuleerde maandelijkse irrigatiewater hoeveelheden op het niveau van zowel het hele irrigatiedistrict als de primaire eenheden. De temporele variatie in de waterbehoefte op districtsniveau werd eveneens in voldoende mate weergegeven. Wel werden significante verschillen geconstateerd tussen de gemeten en de gesimuleerde irrigatiehoeveelheden op het niveau van secundaire en tertiaire eenheden, dit gold ook bij tijdseenheden korter dan één maand. Deze verschillen konden worden verklaard uit de grotere invloed

van verschillen in individuele gewoonten van boeren bij de toepassing van SIMODIS in kleinere gebieden en bij kortere tijdseenheden.

De efficiëntie van irrigatie in Gromola werd geëvalueerd door middel van indicatoren, berekend uit de actuele verdampingswaarde en bijbehorende irrigatiehoeveelheden, bepaald met SIMODIS. Lokale hydrologische omstandigheden hebben een grote invloed op de efficiëntie van irrigatie. Voor elk gewastype werden de waarden van indicatoren voor de efficiëntie van irrigatie in hoofdzaak bepaald door de combinatie van de hydraulische bodemeigenschappen en de waarde van de ondergrensconditie.

De invloed van de schattingsfouten van  $LAI$  en  $K_c$  (resultierend uit de toepassing van remote sensing technieken uit Hoofdstuk 6) op de output van SIMODIS werd geëvalueerd. Over het gehele district genomen trad als gevolg van een gemiddelde fout met een waarde van 30% in  $LAI$ , en van 15% in  $K_c$ , een gemiddelde fout op van 0.2% in de maandelijkse transpiratiewaarde. Op het niveau van primaire en secundaire eenheden bedroegen deze fouten respectievelijk 3% en 20%. Uit deze analyse werd geconcludeerd dat de resultaten van SIMODIS vooral betrouwbaar zijn op het niveau van het hele irrigatiedistrict en de primaire eenheden, terwijl voor het verkrijgen van betrouwbare resultaten op het niveau van secundaire eenheden (dat wil zeggen met fouten lager dan 20%) een betere schatting van  $LAI$  en  $K_c$  vereist is.

De simulatie van scenario's zoals die worden behandeld in Hoofdstuk 8 geven een voorbeeld van het gebruik van SIMODIS ter ondersteuning van besluitvorming in irrigatiemanagement. De simulatie zoals beschreven in Hoofdstuk 7 werd als referentie beschouwd (scenario 1). Verschillende scenario's werden onderling vergeleken door de waarden van indicatoren van de efficiëntie van irrigatie te bekijken.

De effecten van alternatieve strategieën in waterbeheer werden gekwantificeerd, waaruit algemene aanbevelingen ter verbetering van het irrigatiesysteem in Gromola werden afgeleid. De scenario's werden omschreven in termen van de volgende variabelen: de dagelijks beschikbare waterhoeveelheid ( $V_{RES}$ ) de stroomsterkte ( $Q_{i,j}$ ), de minimale waterdruk aan de "delivery outlets" ( $H_{min}$ ), en de fractie van het grondwatertekort ( $i_r$ ), van waaruit de specifieke irrigatiegift was berekend.

In scenario 2 werden de beperkingen vanuit  $V_{RES}$ ,  $Q_{i,j}$  en  $H_{min}$  opgeheven. Het elimineren van deze operationele beperkingen leidde niet tot een substantiële toename in de efficiëntie van het irrigatiesysteem. Toch was het totaal van de waterbehoefte zowel dagelijks als over het hele seizoen groter dan in het referentiescenario. Daaruit werd geconcludeerd dat de ingebruikneming van een beperkt vraagafhankelijk schema ("limited rate demand schedule") zoals in werkelijkheid en ook in scenario 1 het geval is, een effectief middel is tot vermindering van een mogelijk overmatig gebruik van irrigatiewater. Daarnaast is

---

een lage waterdruk bij de "delivery outlets" in economisch opzicht niet geschikt voor de landbouw.

Uit de resultaten van scenario 3 bleek dat het mogelijk was de minimale waterdruk ( $H_{min}$ ) bij de "delivery outlets" te verhogen naar 40 m in plaats van de 30 m als in het referentiescenario. In dit geval waren vaker aanpassingen in het irrigatieschema nodig dan in het referentiescenario, maar een afname in efficiëntie van de irrigatie viel niet waar te nemen. In de praktijk kan deze wetenschap nuttig zijn voor boeren bij de aanschaf van irrigatieapparatuur.

Uit scenario 4 bleek duidelijk dat reductie van de hoeveelheid irrigatiewater de efficiëntie ervan significant verbeterde. De specifieke irrigatiegiften voor verschillende eenheden konden tot 50% worden verminderd, terwijl de gemiddelde efficiëntie met meer dan 20% werd verhoogd.

Tenslotte bleek uit de scenario's 5 en 6 dat de dagelijks benodigde waterhoeveelheid kon worden teruggebracht tot 45 000 m<sup>3</sup>, in plaats van de huidige 71 000 m<sup>3</sup>, zonder aantasting van de gewasproductiviteit en de irrigatie efficiëntie.

De bestudering van de casus Gromola toont aan dat SIMODIS in staat is het gedrag te beschrijven van een "on-demand" irrigatiesysteem. De kwantitatieve informatie die door SIMODIS wordt geleverd is een nuttige ondersteuning voor irrigatiemanagers, die zo tot objectievere besluiten kunnen komen. De synergie tussen het gebruik van SIMODIS en de feedback vanuit de praktijk kan op deze manier het waterbeheer in irrigatiegebieden sterk verbeteren.

In het algemeen bleek tijdens de ontwikkeling van SIMODIS dat agrohydrologische simulatiemodellen en remote sensing op een effectieve manier kunnen worden verenigd om de werking van een irrigatiesysteem te beschrijven. Deze technieken hebben voldoende mate van betrouwbaarheid bereikt om in de praktijk te kunnen worden ingezet.

De toepassing van simulatiemodellen voor grondwaterstromingen zoals SWAP in gespreide vorm leidde tot verschillende innovaties, zoals bijvoorbeeld de definitie van de waarden van de ondergrens en tot de samenstelling van kaarten van bodemklassen met vergelijkbare hydraulische eigenschappen.

Gewascoëfficiënten kunnen worden geschat met behulp van remote sensing technieken, onafhankelijk van SIMODIS. Dit is in algemene zin van nut bij de vaststelling van de bovenste grenswaarden van gespreide hydrologische simulatiemodellen. Ook kan toepassing plaatsvinden voor een redelijk nauwkeurige schatting van de waterbehoefte van gewassen op regionale schaal.

In de toekomst zullen nieuwe satelliet sensoren het waarschijnlijk mogelijk maken de bedekkingsvariabelen nauwkeuriger te bepalen, waardoor nieuwe mogelijkheden ontstaan voor de integratie van agrohydrologische simulatiemodellen en remote sensing technieken.

## Riassunto e conclusioni

---

Il miglioramento dell'efficienza dei sistemi irrigui rappresenta un obiettivo di primaria importanza nella gestione razionale delle risorse idriche in agricoltura. Questo obiettivo richiede un'attenta conoscenza dei processi fisici che intervengono nel funzionamento di un sistema irriguo e la possibilità di un loro monitoraggio. A tal fine possono risultare di notevole ausilio strumenti quali i *modelli di simulazione idrologica* e le tecniche di *telerilevamento da satellite*. Queste metodologie sono state utilizzate in questo studio per lo sviluppo e la messa a punto della procedura SIMODIS, ideata per simulare il funzionamento di un sistema irriguo funzionante alla domanda (*Simulation and Management of On-Demand Irrigation Systems*). La procedura proposta consente di valutare diversi scenari di gestione della risorsa idrica e può pertanto essere impiegata per il supporto alle decisioni nella gestione di un comprensorio irriguo.

La struttura generale di SIMODIS è descritta nel Capitolo 2. Nella schematizzazione adottata in SIMODIS la rete di distribuzione irrigua, costituita da condotte in pressione, costituisce l'elemento di collegamento tra le singole parcelle irrigate (unità terziarie) ove il movimento verticale dell'acqua nel suolo è simulato con il modello uni-dimensionale SWAP. L'applicazione di SWAP in ciascuna parcella consente di ricavare la distribuzione spaziale del deficit di acqua nel suolo, da cui viene stimata la domanda irrigua. Il momento d'intervento irriguo ed il corrispondente volume impiegato vengono determinati in base al profilo del contenuto d'acqua nel suolo risultante dal modello SWAP, secondo criteri conformi alle modalità operative degli agricoltori. Successivamente, SIMODIS verifica che la domanda irrigua complessiva del comprensorio sia compatibile con le risorse idriche disponibili e con le capacità di trasporto idraulico della rete di distribuzione. Con riferimento a questo secondo tipo di vincolo, la verifica idraulica della rete viene effettuata ipotizzando condizioni di moto stazionario nelle condotte. In presenza di risorse idriche non disponibili in quantità sufficiente o di malfunzionamenti della rete di distribuzione, come ad esempio un carico idraulico insufficiente alla consegna, è necessario procedere alla correzione della domanda irrigua in modo che i vincoli citati siano rispettati. L'analisi dei risultati di SIMODIS consente di giungere ad una valutazione dell'efficienza irrigua del comprensorio in esame.

Nel capitolo 3 è riportata la descrizione dei criteri e dei metodi adottati in SIMODIS per la stima della distribuzione spaziale della domanda irrigua. Il modello di trasporto dell'acqua nel suolo SWAP è stato impiegato per il calcolo dei profili verticali del contenuto d'acqua e del potenziale idrico del suolo con

cadenza giornaliera. Il criterio d'intervento irriguo è legato al valore medio del potenziale nel suolo occupato dall'apparato radicale, mentre il volume d'acqua da somministrare viene fissato proporzionalmente al deficit idrico nel suolo. Attraverso l'applicazione del modello di simulazione SWAP in tutte le unità terziarie del comprensorio, viene costruita la distribuzione spaziale giornaliera della domanda irrigua.

La soluzione delle equazioni presenti nel modello di simulazione del trasporto dell'acqua nel suolo richiede però la conoscenza dei parametri relativi alle condizioni iniziali e al contorno, nonché delle caratteristiche idrauliche dei suoli. Questi dati di ingresso devono essere individuati in corrispondenza di ciascuna unità ove il modello viene applicato. In SIMODIS le condizioni al contorno inferiore e superiore del dominio interessato dalla simulazione sono state definite in termini di flussi idrici scambiati con l'esterno.

Al contorno superiore i flussi sono rappresentati dall'evapotraspirazione  $E$  e dalla precipitazione netta  $P_n$ . Queste quantità vengono calcolate con l'ausilio di dati agrometeorologici e colturali, quali il coefficiente colturale  $K_c$  e l'indice di area fogliare  $LAI$ . In questo capitolo viene derivata un'espressione analitica per il calcolo di  $K_c$ , basata sulla formula dell'evapotraspirazione potenziale e sulla conoscenza dei parametri vegetazioni caratteristici della coltura in esame, costituiti dall'albedo  $r$ , dal  $LAI$  e dall'altezza media del manto vegetale  $h_c$ .

Il flusso idrico  $v$  scambiato attraverso il contorno inferiore viene definito in funzione della profondità della falda superficiale  $\phi$ . Per l'individuazione della relazione  $v(\phi)$  è stato impiegato il modello di deflusso sotterraneo SIMGRO, opportunamente calibrato per l'area in esame.

L'individuazione dei parametri distribuiti relativi alle caratteristiche idrauliche dei suoli è stata effettuata ricorrendo ad una funzione "pedo-transfer" adattata alla tipologia di suoli considerati. In particolare, è stata introdotta una modifica al metodo di Arya-Paris per la stima della curva di ritenzione partendo da dati di più agevole determinazione quale la tessitura.

Nel Capitolo 4 viene presentata una metodologia basata sull'impiego del telerilevamento per l'individuazione della distribuzione spaziale del coefficiente colturale  $K_c$ . I principali vantaggi derivanti dall'adozione di tecniche di telerilevamento consiste nella possibilità di monitorare la variabilità spaziale delle colture su vaste aree e di giungere ad una stima di  $K_c$  che tiene conto dell'effettivo sviluppo della coltura. Sono stati proposti due approcci differenti:

- *il metodo di classificazione*, in cui viene considerata l'applicazione di un algoritmo di classificazione ibrida, basato sia su tecniche automatiche (*unsupervised*) che assistite (*supervised*);
- *il metodo analitico*, basato sulla definizione di una relazione matematica fra la riflettanza spettrale della vegetazione ed il corrispondente valore di  $K_c$ .

Nel metodo di classificazione, le classi spettrali non sono note a priori, poiché il valore del coefficiente colturale non è legato soltanto alla tipologia



colturale, ma dipende anche dall'effettivo sviluppo del manto vegetale. Per questo motivo, è necessario ricercare, attraverso tecniche numeriche di classificazione (*clustering*) la similitudine—in termini di comportamento spettrale—tra superfici vegetate con valore noto di  $K_c$ . Questi dati di riferimento consentono di definire le firme spettrali da utilizzare nella successiva classificazione assistita delle immagini. Poiché la definizione degli insiemi di firme spettrali non è unica, è necessario confrontare i risultati delle classificazioni ottenute da differenti insiemi di firme spettrali utilizzando misure statistiche di separabilità delle classi e di affidabilità della procedura di classificazione. Queste misure sono state combinate in un *indice di valutazione della classificazione*, da utilizzarsi per l'individuazione dell'insieme di firme spettrali più idoneo.

Il metodo analitico è basato sul calcolo diretto di  $K_c$  dai dati meteorologici e dai parametri vegetazionali  $r$ ,  $LAI$  ed  $h_c$ . Questi ultimi vengono stimati dalla riflettanza spettrale delle colture derivate dalle immagini satellitari. In particolare, l'indice di area fogliare  $LAI$  viene derivato da un modello semi-empirico basato sul legame esistente tra l'indice di vegetazione  $WDVI$  (Weighted Difference Vegetation Index) e  $LAI$ . È da notare che l'impiego di questo modello richiede una preliminare calibrazione con dati di pieno campo.

L'area di studio scelta per lo sviluppo e la validazione delle metodologie proposte è il comprensorio irriguo "Gromola" ricadente nel Consorzio di Bonifica ed Irrigazione di Paestum (Salerno) ed avente un'estensione di circa 3000 ha. La descrizione dell'area e le diverse fasi di acquisizione dei dati necessari per SIMODIS sono riportate nel Capitolo 5.

I parametri distribuiti relativi alla condizione al contorno inferiore del dominio di applicazione del modello SWAP ed alle caratteristiche idrauliche dei suoli sono stati determinati applicando le metodologie descritte nel Capitolo 3. Le osservazioni del livello della falda superficiale sono state utilizzate per la calibrazione del modello di deflusso sotterraneo SIMGRO. Attraverso l'interpretazione dei risultati delle simulazioni, è stato possibile suddividere l'area di studio in zone omogenee caratterizzate da una specifica relazione fra il flusso attraverso la frontiera inferiore del suolo  $v$  e la profondità del livello freatico  $\phi$ . Le relazioni  $v(\phi)$  sono state quindi utilizzate per la definizione della condizione al contorno inferiore di SWAP.

Le curve caratteristiche di ritenzione e conducibilità idraulica dei suoli presenti sono state individuate applicando alcune funzioni "pedo-transfer", opportunamente calibrate, ai dati di tessitura raccolti in diversi profili ubicati all'interno del comprensorio di Gromola. Le caratteristiche idrauliche così determinate sono state utilizzate per simulare un processo di evaporazione in ciascun sito. I risultati di quest'elaborazione hanno portato alla definizione di zone omogenee dal punto di vista del comportamento idraulico dei suoli. È stato così possibile realizzare, partendo dalla cartografia pedologica esistente, una mappa

---

delle caratteristiche idrauliche dei suoli da utilizzare per la definizione dei dati di input in SIMODIS.

Infine, viene illustrata la validazione di SWAP eseguita attraverso il confronto dei valori simulati e misurati in campo, mediante tecnica TDR, relativi all'immagazzinamento d'acqua nel suolo.

Nel Capitolo 6 viene descritta in dettaglio l'applicazione delle tecniche di telerivamento da satellite per il monitoraggio del coefficiente colturale  $K_c$ . Nel caso di studio in esame, sono state elaborate diverse immagini acquisite nel corso della stagione irrigua 1994 dal sensore Thematic Mapper del satellite Landsat 5. Nella prima parte di questo capitolo, viene evidenziata l'importanza dell'accuratezza radiometrica nella stima della riflettanza superficiale con sensori satellitari e viene descritta la tecnica impiegata per la correzione atmosferica delle immagini Landsat per l'area di studio. In particolare, è stata valutata l'influenza della riflettanza della superficie marina, adiacente all'area di studio, sul valore di riflettanza superficiale delle colture, corretta da effetti atmosferici. I risultanti valori di riflettanza superficiale sono stati utilizzati per l'applicazione dei metodi di rilevamento del  $K_c$  descritti al capitolo 4.

Nell'applicazione del metodo di classificazione, i valori di riflettanza superficiale di alcune aree campione – di cui era noto il  $K_c$  – sono stati utilizzati per la definizione di diversi insiemi spettrali. A tal scopo sono state adottate tecniche di agglomerazione basate su differenti misure di similitudine. Successivamente, i diversi insiemi spettrali così ottenuti sono stati inseriti in un algoritmo di classificazione assistita. Le varie classificazioni ottenute sono state quindi confrontate con l'ausilio dell'indice di valutazione descritto nel Capitolo 4. I migliori risultati sono stati ottenuti impiegando nella classificazione assistita un insieme di firme spettrali derivato da tecniche di agglomerazione non gerarchica della riflettanza superficiale nelle bande 3,4 e 5 del Landsat TM.

Nella sezione dedicata all'applicazione del metodo analitico, viene preliminarmente descritta un'analisi di sensitività della relazione funzionale fra il valore del  $K_c$  ed i dati agrometeorologici e colturali ( $r$ ,  $LAI$  e  $h_c$ ). E' stato così possibile evidenziare che, considerate le condizioni climatiche del comprensorio di Gromola durante la stagione irrigua, il parametro colturale che maggiormente influenza il valore del  $K_c$  è l'indice di area fogliare  $LAI$ . Utilizzando l'approccio semi-empirico descritto al capitolo 4, in cui il  $LAI$  viene stimato dall'indice di vegetazione  $WDVI$ , e con l'ausilio di misure di pieno campo in coincidenza delle acquisizioni satellitari, è stato possibile determinare il  $LAI$  con un errore medio assoluto pari a 0.31 nell'intervallo di  $LAI$  da 1 a 4. Questo errore corrisponde ad una variazione di  $K_c$  pari a circa 0.15.

L'implementazione di SIMODIS nel comprensorio irriguo di Gromola viene descritta nel Capitolo 7. I volumi irrigui misurati durante la stagione irrigua 1994 a diversi livelli (comparto, comizio, settore) sono stati analizzati per

l'individuazione dei criteri adottati per la programmazione irrigua, ovvero il valore del potenziale idrico nel suolo usato come soglia d'intervento ed il rapporto fra volume irriguo applicato e deficit idrico. E' stato così possibile verificare che il volume mediamente applicato per unità di superficie irrigata corrisponde ad una frazione  $i_r$  pari al 50% del deficit idrico nel suolo. Analogamente, il criterio d'intervento più rispondente alle effettive modalità d'applicazione è risultato il raggiungimento di un valore critico del potenziale idrico nel suolo, dipendente dalla coltura. Le misure effettuate hanno evidenziato un consumo massimo giornaliero  $V_{RES}$  pari a 71 000 m<sup>3</sup>. L'ulteriore parametro da considerare per il funzionamento della rete di distribuzione consortile è il carico idraulico minimo all'idrante  $H_{min}$ , risultante pari a 30 m.

Le simulazioni effettuate con SIMODIS impiegando i valori indicati dei parametri  $i_r$ ,  $V_{RES}$  e  $H_{min}$  riproducono in maniera soddisfacente l'evoluzione temporale dei consumi idrici a scala di comprensorio e di unità primaria (avente un'estensione media di circa 260 ha). Differenze rilevanti sono state osservate, invece, nel confronto fra i dati riferiti a singoli settori (unità secondarie, superficie media di 6.7 ha). Queste differenze, che si riflettono soprattutto nella diversa distribuzione temporale dei consumi, sono ovviamente determinate dalla discrepanza fra i criteri di intervento adottati in SIMODIS e la gestione irrigua dei singoli agricoltori, improntata su criteri ed abitudini altamente soggettive.

L'efficienza irrigua del comprensorio è stata valutata ricorrendo agli indicatori definiti nel Capitolo 2, in funzione della traspirazione effettiva delle colture e dei corrispondenti volumi irrigui simulati in SIMODIS. E' stato evidenziato come le condizioni idrologiche e pedologiche influenzino l'efficienza irrigua in maniera significativa. Infatti, per ciascuna tipologia colturale, l'associazione fra le caratteristiche idrauliche dei suoli e la condizione al contorno inferiore è risultata determinante nel calcolo del valore degli indicatori di efficienza.

E' stato infine valutato l'effetto di un errore di stima del  $LAI$  e del  $K_c$  sui risultati di SIMODIS, con particolare riferimento alla traspirazione effettiva, ai volumi irrigui ed agli indicatori di efficienza. Le simulazioni di SIMODIS sono quindi state ripetute variando in maniera casuale  $LAI$  e  $K_c$  entro il limite massimo del 30% e 15% rispettivamente. Le variazioni dei risultati di SIMODIS -rispetto alle simulazioni con i dati non alterati- sono risultate inferiori al 3% considerando i dati aggregati a livello di unità primaria. Le differenze sono invece dell'ordine del 20% in media per le unità secondarie. Da quest'analisi si può affermare che la procedura SIMODIS consente di ottenere risultati particolarmente affidabili a livello di unità primarie, mentre per ottenere risultati a scala di unità secondarie con precisione migliore del 20% è necessario innanzitutto ridurre l'errore di stima del  $LAI$  e del  $K_c$ .

Le simulazioni di scenari presentate nel Capitolo 8 rappresentano un esempio d'impiego di SIMODIS nel supporto alle decisioni nella gestione irrigua.

Assumendo la simulazione descritta nel precedente capitolo come uno scenario di riferimento, ossia prossimo alla situazione attuale, è stata eseguita una valutazione comparativa di diverse strategie di gestione irrigua, anche ricorrendo agli indici di efficienza descritti precedentemente. E' stato così possibile ottenere alcune indicazioni per orientare la gestione irrigua del sistema verso un miglioramento dell'efficienza complessiva del sistema.

I diversi scenari simulati si differenziano innanzitutto in base alle seguenti variabili: il volume di risorse idriche disponibili giornalmente ( $V_{RES}$ ), la presenza di limitazioni, presso i gruppi di consegna aziendali, della portata massima ( $Q_{i,j}$ ) e del carico idraulico minimo  $H_{min}$ , e il rapporto  $i_r$  fra il deficit idrico nel suolo ed il volume specifico d'irrigazione.

Nello scenario 2, si è ipotizzata l'assenza di eventuali vincoli sull'esercizio alla domanda derivanti da limitazioni di portata, carico idraulico e volume giornaliero disponibile. I risultati di questo scenario hanno dimostrato che la rimozione delle limitazioni descritte, pur garantendo una maggiore elasticità di funzionamento per le aziende, non produce un sensibile incremento di efficienza irrigua. Il valore cumulato della domanda irrigua è risultato maggiore dello scenario di riferimento sia considerando il valore giornaliero che quello stagionale. Inoltre, valori troppo bassi del carico idraulico alla consegna rappresentano uno svantaggio per l'economia aziendale, ove la garanzia di un valore minimo consente di ridurre le spese energetiche per l'irrigazione. Si può quindi dedurre che l'installazione di dispositivi che limitano la portata in un impianto irriguo alla domanda consente di ridurre possibili sprechi d'acqua ed è uno strumento efficace per migliorare l'efficienza del sistema.

I risultati dello scenario 3 rivelano che è possibile incrementare il carico idraulico alla consegna da 30 a 40 m, senza compromettere l'efficienza irrigua del compresorio. In questo caso, le correzioni da apportare alla distribuzione irrigua per il rispetto di questo vincolo sono lievemente più frequenti rispetto allo scenario di riferimento, ma non determinano situazioni di particolare difficoltà da parte degli agricoltori.

Lo scenario 4 ha dimostrato che, nella realtà esaminata, la riduzione dei volumi irrigui applicati determina un incremento sostanziale dell'efficienza irrigua. In questo caso, infatti, dalla simulazione effettuata con volumi irrigui ridotti di circa il 50% rispetto ai valori attuali è risultata un'efficienza irrigua più elevata di oltre il 20%.

Le simulazioni degli scenari 5 e 6 si riferiscono a situazioni di grave carenza delle risorse idriche. E' stato così possibile valutare in 45 000 m<sup>3</sup> la disponibilità minima giornaliera per evitare l'insorgenza di condizioni di stress idrico tale da compromettere l'efficienza irrigua del compresorio.

Il caso di studio nel compresorio irriguo di Gromola ha consentito di dimostrare che la procedura SIMODIS può essere impiegata per simulare il funzionamento di un sistema irriguo alla domanda. Le informazioni ed i dati

forniti da SIMODIS costituiscono un valido aiuto per i tecnici preposti alla gestione di un comprensorio irriguo, permettendo così di valutare in maniera obiettiva il funzionamento del sistema in esame. Dalle possibili sinergie fra l'uso di procedure come SIMODIS e le esperienze maturate sul campo è possibile individuare con maggior sicurezza i criteri per uno sfruttamento più razionale delle risorse idriche nei comprensori irrigui.

Dal punto di vista tecnico-scientifico, questo studio ha dimostrato che i modelli di simulazione idrologica ed il telerilevamento da satellite possono essere impiegati congiuntamente per descrivere i processi che regolano il funzionamento di un sistema irriguo. Queste tecnologie hanno oggi raggiunto un livello di affidabilità tale da poter essere prontamente trasferite ad ambiti applicativi.

Nell'ambito dell'applicazione di modelli di simulazione del trasporto dell'acqua nel suolo, come ad esempio SWAP, in forma distribuita su vaste aree, le ricerche condotte in questo studio hanno consentito di sviluppare alcune metodologie per la definizione delle caratteristiche idrauliche dei suoli e delle condizioni al contorno.

La stima dei coefficienti colturali  $K_c$  attraverso l'analisi di immagini multispettrali telerilevate da satellite è una metodologia che può essere utilmente applicata per eseguire valutazioni più precise sui fabbisogni irrigui a scala di comprensorio o di regione.

In futuro è possibile prevedere che la disponibilità di nuovi tipi di sensori consentirà stime più precise dei parametri vegetazionali che intervengono nei processi idrologici, in modo da ampliare ancor più l'integrazione fra i modelli di simulazione idrologica e le tecniche di osservazione della Terra.

## References

- Abdellaoui R., 1986. Irrigation system design capacity for on demand operation. Ph.D. dissertation, Utah State University
- Ait Kadi M., Abdellaoui R., Oulhaj A., Essafi B., 1990. Design of large scale collective sprinkler irrigation projects for on demand operation: a holistic approach. 14<sup>th</sup> Intern. Congress on Irrigation and Drainage, Rio de Janeiro
- Allen R.G., 1986. A Penman for all seasons. *J. Irrig. and Drain. Engin.*, 112 (4): 348-368
- Arya L.M., Paris J.F., 1981. A physico-empirical model to predict the soil moisture characteristic from particle-size distribution and bulk density data. *Soil Sci. Soc. Am. J.*, 45: 1023-1030
- Arredi F., 1981. *Costruzioni idrauliche*. Vol.II, Unione Tipografica Editrice Torinese, Italia
- Asrar G., Myneni R.B., 1993. Atmospheric effects in the remote sensing of surface albedo and radiation absorption by vegetation canopies. *Remote Sensing Reviews*, 7: 197-222
- Attema E.P.W., Ulaby F.T., 1978. Vegetation modelled as a water cloud. *Radio Sci.*, 13: 357-364
- Azzali S., Menenti M., Meuwissen I.J.M., Visser T.M.N., 1991. Application of remote sensing techniques to map crop coefficients in an Argentinian irrigation scheme. In G.Tsakiris (Ed.): *Advances in Water Resources Technology*, ECOWARM/Balkema, Rotterdam: 637-644
- Bakel v. P.J.T., 1986. A systematic approach to improve the planning, design and operation of regional surface water management systems: a case study. Report 13, Institute for Land and Water Management Inst. (ICW), Wageningen, the Netherlands, 118 pp.
- Baars E., van Logchem B.P., 1993. A client-oriented and quantifiable approach to irrigation design, a case-study in Mendoza, Argentina. DLO Winand Staring Centre, Report 75.1, 119 pp.
- Baret F., Guyot G., 1991. Potential and limits of vegetation indices from LAI and APAR assessment. *Remote Sens. Environm.*, 35: 161-173
- Basile A., D'Urso G., 1997. Experimental corrections of simplified methods for predicting water retention curves in clay-loamy soils from particle-size determination. *Soil Technology*, 10: 261-272
- Bastiaanssen W.G.M., 1995. Regionalization of surface flux densities and moisture indicators in composite terrain. PhD Thesis, Wageningen Agricultural University, 273 pp.
- Battikhi A.M., Abu-Hammad A.H., 1994. Comparison between the efficiencies of surface and pressurized irrigation systems in Jordan. *Irrigation and Drainage Systems*, 8: 109-121

- Bausch W.C., Neale C.M.U., 1987. Crop coefficients derived from reflected canopy radiation: a concept. *Transactions American Soc. Agric. Engin.*, 30, 3, 703-709
- Bausch W.C., 1995. Remote sensing of crop coefficients for improving the irrigation scheduling of corn. *Agric. Water Manag.*, 27: 55-68
- Bear J., Verruijt A., 1987. Modeling groundwater flow and pollution. D. Reidel Publishing Co., Dordrecht, 414 pp.
- Becker F., Zhao-Liang Li, 1995. Surface temperature and emissivity at various scales: definition, measurement and related problems. *Remote Sensing Reviews*, 12: 225-253
- Belmans C., Wesseling J.G., Feddes R.A., 1983. Simulation of the water balance of a cropped soil: SWATRE. *J. Hydrology*, 63 (3/4): 271-286
- Bogardi J.J., 1994. Introduction of system analysis: terminology, concepts, objective functions and constraints. In Bogardi J.J. and Nachtbel H.P., (Ed.): *Multicriteria decision analysis in water resources management*. UNESCO, Paris, 23-32
- Boels D., v. Gils J.B., Veerman G.J., Wit K.E., 1978. Theory and systems of automatic determination of soil moisture characteristics and unsaturated hydraulic conductivities. *Soil Sci.*, 126: 191-199
- Bouman B.A.M., 1991. Linking X-band microwave backscattering and optical reflectance with crop growth models. PhD Thesis, Wageningen Agricultural University, 167 pp.
- Braden H., 1985. Ein energiehaushalts- und verdunstungsmodell for wasser und stoffhaushaltsuntersuchungen landwirtschaftlich genutzer einzugsgebiete. *Mittlung Deutsche Bodenkundliche Gesellschaft*, 42, 294-299
- Brutsaert W., 1968. Some methods of calculating unsaturated permeability. *Trans. of ASAE*, 10:400-404
- Brutsaert W. H., 1982. *Evaporation into the atmosphere*. D.Reidel Publishing Co., Dordrecht, 299 pp.
- Burt C.M., Clemmens A.J., Strelkoff T.S., Solomon K.H., Bliesner R.D., Hardy L.A., Howell T.A., Eisenhauer D.E., 1997. Irrigation performance measures: efficiency and uniformity. *J. Irrig. Drainage Engin.*, ASCE, 123 (6): 423-442
- Burton M.A., 1994. A simulation of water allocation policies in times of water shortage. *Irrigation and Drainage Systems*, 8: 61-81
- Camillo P., 1987. A canopy reflectance model based on an analytical solution to the multiple scattering equation. *Remote Sens. Environm.*, 23: 453-477
- Cassa per il Mezzogiorno, 1981. *Relazione Progetto Speciale per l'utilizzazione degli schemi idrici intersettoriali del Lazio meridionale, Tronto, Abruzzo, Molise e Campania*. Cassa per il Mezzogiorno, Ripartizione Progetti Idrici, Divisione 4; Arlab, Roma; 89-110
- Cassa per il Mezzogiorno, 1983. *Idrogeologia dell'Italia Centro-Meridionale*. Quaderno nr.4/2, Roma

- Choudhury B.J., Idso S.B., Reginato R.J., 1987. Analysis of an empirical model for soil heat flux under a growing wheat crop for estimating evaporation by an infrared-temperature based energy balance equation. *Agric. Forest Meteor.*, 39: 283-287
- Choudhury B.J., Ahmed N.U., Idso S.B., Reginato R.J., Daughtry C.S.T., 1994. Relations between evaporation coefficients and vegetation indices studied by model simulations. *Remote Sens. Environ.*, 50: 1-17
- Clement R., 1966. Calcul de débits dans le réseaux d'irrigation fonctionnant à la demande. *La Houille Blanche*, 5, 553-575
- Clevers J.G.P.W., 1989. The application of a weighted infrared-red vegetation index for estimating leaf area index by correcting for soil moisture. *Remote Sens. Environm.*, 29: 25-37
- Clevers J.G.P.W., van Leeuwen H.J.C., 1996. Combined use of optical and microwave remote sensing data for monitoring crop growth. *Remote Sens. Environm.*, 56: 42-51
- Clevers J.G.P.W., Verhoef W, 1993. LAI estimation by means of the WdVI: a sensitivity analysis with a combined PROSPECT-SAIL model. *Remote Sensing Reviews*, Harwood Academic Publish., U.S.A.; 7: 43-64
- Curran P.J., Wardley N.W., 1988. Radiometric leaf area index. *Int. J. Rem. Sensing*, 9 (2): 259-274
- Dam v. J.C., J. Huygen, J.G. Wesseling, R.A. Feddes, P. Kabat, P.E.V. van Walsum, P. Groenendijk and C. A. van Diepen, 1997. Theory of SWAP version 2.0. Simulation of water flow, solute transport and plant growth in the Soil-Water-Atmosphere-Plant environment. Report 71, Department Water Resources, Wageningen Agricultural University (published also as Technical Document 45, DLO Winand Staring Centre, Wageningen).
- D'Amato A., Giordano I., Concilio L., 1992. Stima dell'evapotraspirazione potenziale con diversi metodi e considerazioni sull'andamento di alcuni fattori climatici nella Piana del Sele. *Irrigazione e Drenaggio*, 39 (1): 25-32
- Doorenbos J., Pruitt W.O., 1977. Guidelines for predicting crop water requirements. *FAO Irrigation and Drainage Paper nr.24*, Rome, pp.144
- Dubayah R., 1992. Estimating net solar radiation using Landsat Thematic Mapper and digital elevation data. *Water Resour. Res.*, 28 (9): 2469-2484
- D'Urso G., Basile A., 1997. Physico-empirical approach for mapping soil hydraulic behaviour. *Hydrology and Earth System Sciences*, Europ. Geophysical Society; 4: 915-923
- D'Urso G., Menenti M., 1995. Mapping crop coefficients in irrigated areas from Landsat TM images; *Proceed. European Symposium on Satellite Remote Sensing II*, Europto, Paris, sett.'95; SPIE, Intern. Soc. Optical Engineering, Bellingham (U.S.A.); Vol.2585: 41-47
- D'Urso G., Menenti M., 1996. Performance indicators for the statistical evaluation of digital image classifications. *ISPRS J.Photogr. & Rem.Sens.*, 51 (2): 78-90



- Elmaloglu S., Malamos N., 2000. Simulation of soil moisture content of a prairie field with SWAP93. *Agric. Water Manag.*, 43: 139-149
- Engman E.T., Chauhan N., 1995. Status of microwave soil moisture measurements with remote sensing. *Remote Sens. Environm.*, 51: 189-198
- Epema G.F., 1990. Determination of planetary reflectance for Landsat-5 Thematic Mapper tapes processed by Earthnet (Italy). *Europ. Space Agency Journal*, 14: 101-108
- Ernst L.F., Feddes R.A., 1979. Invloed van grondwateronttrekking voor beregening en drinkwater op de grondwaterstand. Nota 1116 Inst. Land Water Management Res. (ICW), Wageningen, 10 pp.
- Estes J.E., Jensen J.R., Tinney L.R., 1978. Remote sensing of agricultural water demand information: a California study. *Water Resour. Res.* 14 (2): 170-176
- FAO, 1994. Irrigation water delivery models. *Proceed. FAO Expert Consultation Rome, October 1993; Food and Agriculture Organiss., Water Report nr.2; 312 pp.*
- FAO, 1995. Use of remote sensing techniques in irrigation and drainage. *Proceed. Expert Consultation FAO-Cemagref, Montpellier, Nov. 1993; Food and Agriculture Organiss., Water Report nr.4; 201 pp.*
- FAO, 1996. Irrigation scheduling: from theory to practice. *Proceedings of the ICID/FAO Workshop on Irrigation scheduling. Rome, Sept. 1995; Food and Agriculture Organiss., Water Report nr.8; 384 pp.*
- FAO, 1998. Crop evapotranspiration. Guidelines for computing crop water requirements. *Irrigation and drainage Paper nr.56, Food and Agriculture Organiss., Rome*
- Feddes R.A., Bastiaanssen W.G.M., 1992. Forecasting soil-water-plant-atmosphere interactions in arid regions. In H.J.W. Verplancke et al. (Eds.): *Water savings techniques for plant growth. Kluwer Academic Pub., The Netherlands.57-78*
- Feddes R.A., 1995. Remote sensing-inverse modelling approach to determine large scale effective soil hydraulic properties in soil-vegetation-atmosphere systems. In R.A.Feddes (Ed.): *Space and time scale variability and interdependencies in hydrological processes. Cambridge Univ. Press, U.K.; 33-42*
- Feddes R.A., Kowalik P.J., Zaradny H., 1978. Simulation of field water use and crop yield. *Simulation Monograph, PUDOC (Centre for Agricultural Publishing and Documentation), Wageningen, 189 pp.*
- Feddes R.A., Kabat P., van Bakel P.J.T., Bronswijk J.J.B., Halbertsma J., 1988. Modelling soil water dynamics in the unsaturated zone. *State of the art. J.Hydrology*, 100: 69-111
- Garcia L.A., Manguerra H.B., Gates T.K., 1995. Irrigation-drainage design and management model: development. *J. Irrig. Drainage Engin., ASCE*, 121 (1): 71-94

- Genuchten van M.Th., 1980. A closed-form equation for predicting the hydraulic conductivity of unsaturated soils. *Soil Sci. Soc. Am. J.*, 44: 892-898
- Genuchten v. M. Th., Leij F.J., 1992. On estimating the hydraulic properties of unsaturated soils. In: van Genuchten M. Th., Leij F.J., Lund L.J. Editors: *Proc. Intern. Workshop on Indirect methods for estimating the hydraulic properties of unsaturated soils*, Riverside, Ca.,: 1-14
- Genstat 5 Committee, 1987. *Genstat 5 Rel.3. Reference Manual*, Clarendon Press (Oxford), 796 pp.
- Hack-ten Broeke M.J.D., Hegmans J.H.B.M., 1996. Use of soil physical characteristics from laboratory measurements or standard series for modelling unsaturated flow. *Agric. Water Manag.*, 29: 201-213
- Hall F.G., Townshend J.R. Engman E.T., 1995. Status of remote sensing algorithms for estimation of land surface state parameters. *Remote Sens. Environm.*, 51: 138-156
- Hannan T.C., Coals V.A., 1995. Real-time water allocation for irrigation. *Water and Environm. Manag.*, 9 (1): 19-26
- Hatfield J.L., Kanemasu E.T., Asrar G., Jackson R.D., Pinter P.J., Reginato R.J., Idso S.B., 1985. Leaf Area estimates from spectral measurements over various planting dates of wheat. *Int. J. Rem. Sens.*, 6 (1): 167-175
- Heilman J.L., Kanemasu E.T., Rosenberg N.J., Blad B.L., 1976. Thermal scanner measurements of canopy temperatures to estimate evapotranspiration. *Rem. Sens. Environm.*, 5: 137-145
- Heimovaara T.J., 1993. Design of triple-wire time domain reflectometry probe in practice and theory. *Soil Sci. Soc. Am. J.*, 57: 1410-1417
- Hillel D., 1998. *Environmental soil physics*. Academic Press, London, UK, 771 pp.
- Hongyuan Y., Zhaoyi L., Shaoqiang Z., 1994. A study on the optimal allocation model of limited irrigation water. *ICID Bulletin*, 43 (2): 93-103
- Huete A.R., 1988. A soil adjusted vegetation index (SAVI). *Remote Sens. Environm.*, 25: 295-309
- Ilich N., 1993. Water resources management model (WRMM) of Alberta environment: model properties and capabilities. 15<sup>th</sup> Intern. Congress on Irrigation and Drainage, The Hague, Netherlands; Transaction of 2<sup>nd</sup> Workshop on Crop-Water Models, 15 pp.
- Indelicato S., Pappalardo A., 1981. Amelioration et modernisation des systemes collectifs d'irrigation existants en Italie. 11<sup>th</sup> Congress on Irrigation and Drainage, Grenoble, Vol.II-Part I: 235-244
- Itier B., Brunet Y., 1996. Recent developments and present trends in evaporation research: a partial survey. In Camp. C.R. et al. (Ed.): *Evapotranspiration and irrigation scheduling*. Proceedings of the Intern. Conf., S.Antonio (U.S.A.) Nov.1996; Am. Soc. Agric. Engineers; 1-20

- Jabro J.D., 1992. Estimation of saturated hydraulic conductivity of soil from particle size distribution and bulk density data. *Trans. of ASAE*, 35(2):557-560
- Jacucci G. et al., 1994. The HYDRA project: a decision support for irrigation water management. *Proceed. Intern. Conference on Land and Water Resources in the Mediterranean Region; CIHEAM-IAM-B, Vol.VI: 1-19*
- Jackson R.D., Reginato R.J., Idso S.B., 1977. Wheat canopy temperature: a practical tools for evaluating water requirements. *Water Resour. Res.*, 13: 651-656
- Jackson R.D., Idso D.B., Reginato R.J., Pinter Jr.J.R., 1981. Canopy temperature as a crop water stress indicator. *Water Resour. Res.*, 17: 1133-1138
- Jacobsen O.H. and Schjønning P., 1995. Comparison of TDR calibration functions for soil water determination. In A.Correll (Ed.); *Proceed. Symposium on TDR applications in Soil Science, Foulum (D) 1994; Danish Institute of Plant and Soil Sci.,SP Report nr.11 Vol.3: 25-33*
- Jensen M.E.,Burman R.D.,Allen R.G. *Evapotranspiration and irrigation water requirements. ASCE Manual no.701, 1990*
- Jensen J.R., 1986. *Introductory digital image processing. A remote sensing perspective. Prentice-Hall, Englewood Cliff, N.J., U.S.A.*
- Joshi M.B., Murthy J.S.R., Shah M.M., 1995. CROSOWAT: a decision tools for irrigation schedule. *Agric. Water Manag.*, 27: 203-223
- Kelliher F.M., Leuning R., Raupach M.R., Schulze E.D., 1995. Maximum conductances for evaporation from global vegetation types. *Agricultural Forest Meteorology*, 73: 1-16
- Kimes D.S., Sellers P.J., Diner D.J., 1987. Extraction of spectral hemispherical reflectance (albedo) of surfaces from nadir and directional data. *Int. J. Rem. Sens.*, 8 (12): 1727-1746
- Kularathna M.D.U.P., 1992. *Application of Dynamic Programming for the analysis of complex water resources systems. PhD Thesis, Wageningen Agricultural University, 163 pp.*
- Kustas W.P., 1990. Estimates of evapotranspiration with a one- and two-layer model of heat transfer over partial canopy cover. *J. Appl. Met.*, 29: 704-715
- Kustas W.P., Pinker R.T., Schmugge T.J., Humes K.S., 1994. Daytime net radiation estimated for a semiarid rangeland basin from remotely sensed data. *Agric. Forest Meteor.*, 71: 337-357
- Kustas W.P., Norman J.M., 1996. Use of remote sensing for evapotranspiration monitoring over land-surfaces. *Hydrological Sciences Journal*, 41 (4): 495-516
- Kustas W.P., Zhan X., Schmugge T.J., 1998. Combining optical and microwave remote sensing for mapping energy fluxes in a semiarid watershed. *Remote Sens. Environm.* 64: 116-131
- Lamaddalena N., Sagardoy J.A., 2000. Performance analysis of on-demand pressurized irrigation systems. *F.A.O. Irrigation and Drainage Paper no.59, Rome, pp.132*

- Li Jiren, C.Zhedan, X. Fuchuan, L. Jian, W. Wen, C.Lei, 1997. Application of remote sensing and GIS techniques for irrigable land investigations. In Baumgartner M.F. et al. (Eds.): Remote sensing and Geographic Information Systems for design and operation of water resources systems. IAHS Publ. No.242, Wallingford, U.K.: 17-21
- Mahalanobis P.C., 1927. Analysis of race mixture in Bengal. *J. Asiatic Soc. Bengal*, 23: 301-333
- Mankarious W.E., 1991. Application of pipeline systems in irrigation - case study: El-Hammami pilot project. In R.Wooldridge (Ed.): Techniques for environmentally sound water resources; 321-331
- Menenti M., 1984. Physical aspects and determination of evaporation in desert applying remote sensing techniques. ICW Report nr.10 (Special issue)
- Menenti M. (Ed.), 1990. Remote sensing in evaluation and management of irrigation, INCYTH-CRA, Mendoza, Argentina. 338 pp.
- Menenti M., Azzali S., Leguizamon S., Collado D.A., 1986. Multitemporal analysis of Landsat MSS and TM data to map crops in the Po valley (Italy) and in Mendoza (Argentina). *Proceed. 7<sup>th</sup> Intern. Symp. on Remote Sensing for Resource Development and Environmental Manag., Enschede (NL), Aug.1986; 1:293-299*
- Menenti M., Bastiaanssen W.G.M., van Eick D., 1989. Determination of surface hemispherical reflectance with Thematic Mapper data. *Remote Sens. Environm.*, 28: 327-337
- Menenti M., Azzali S., Visser T.N.M., 1990. Practical applications of satellite data to irrigation water management. *Proc. Intern. Symposium on Remote Sensing and Water Resources, IAH, Enschede, Nederland: 405-418*
- Menenti M., Chambouleyron J., Morabito J., Fornero L., Stefanini L., 1992. Appraisal and optimization of agricultural water use in large irrigation schemes. I. Theory. *Water Res. Manag.*, 6: 185-199
- Menenti M., Chambouleyron J., Morabito J., Fornero L., Stefanini L., 1992. Appraisal and optimization of agricultural water use in large irrigation schemes. II. Applications. *Water Res. Manag.*, 6: 201-221
- Menenti M., Ritchie J.C., 1994. Estimation of aerodynamic roughness of Walnut Gulch watershed with laser altimeter measurements. *Water Resources Research*, 30 (5): 1329-1337
- Menenti M., Azzali S., D'Urso G., 1995. Management of irrigation schemes in arid countries. In: Use of remote sensing techniques in irrigation and drainage, *FAO Water Reports nr.4, Rome,; 81-98*
- Merriam J.L., Davis G.G., 1986. Demand irrigation schedule pilot project: Sri Lanka. *J. Irrig. Drainage Engin., ASCE*, 112 (3): 185-202
- Merriam J.L., 1987. Symposium introduction. In D.Z. Zimelman (Ed.): Planning, operation, rehabilitation and automation of irrigation water delivery systems. *Proceedings Symposium of the Am. Soc. Civil Engineers; 68-71*

- Meuwissen I.J.M., 1989. Mapping of vegetation and evapotranspiration in the Rio Tunuyan irrigation scheme, Mendoza, Argentina, using satellite image. ICW Note 1965, The Winand Staring Centre, Wageningen, 42 pp.
- Mishra S., Parker J.C., 1990. On the relation between saturated conductivity and capillary retention characteristics. *Groundwater*, 28, 5:775-777
- Monteith J.L., 1965. Evaporation and the environment. In: *The state and movement of water in living organisms*, 19<sup>th</sup> Symp. Soc. Exp. Biol.: 205-234
- Monteith J.L., Unsworth M.H., 1990. *Principles of Environmental Physics.*, E.Arnold Ed., London, pp.290
- Moran M.S., Jackson R.D., Raymond L.H., Gay L.W., Slater P.N., 1990. Mapping surface energy balance components by combining Landsat TM and ground-based meteorological data. *Rem. Sens. Environm.*, 30: 77-87
- Moran M.S., Jackson R.D., 1991. Assessing the spatial distribution of evapotranspiration using remotely sensed inputs. *J.Environm.Qual.*,20,725-737
- Moran M.S., 1994. Irrigation management in Arizona using satellites and airplanes. *Irrigation Science*, 15 (1): 35-44
- Morales J.C., Marino A.M., Holzapfel A., 1992. Planning simulation model of irrigation district. *J. Irrig. Drainage Engin.*, ASCE, 118 (1): 74-87
- Mualem Y., 1976. A new model for predicting the hydraulic conductivity of unsaturated porous media. *Water Resour. Res.*, 12:513-522
- Mualem Y., 1992. Modelling the hydraulic conductivity of unsaturated porous media. In: van Genuchten M. Th., Leij F.J., Lund L.J. Editors: *Proc. Intern. Workshop on Indirect methods for estimating the hydraulic properties of unsaturated soils*, Riverside, Ca.: 15-36
- Murty V.V.N., Azar A.H., Sarwar A., Sudsaisin K., 1992. Simulation of tertiary unit efficiencies in large irrigation schemes. *Agric. Water Manag.*, 21:13-22
- Nielsen D.R., Luckner L., 1992. Theoretical aspects to estimate reasonable initial parameters and range limits in identification procedures for soil hydraulic properties. In: van Genuchten M. Th., Leij F.J., Lund L.J. Editors: *Proc. Intern. Workshop on Indirect methods for estimating the hydraulic properties of unsaturated soils*, Riverside, Ca.: 147-160
- Petty G.W., Krajewski W.F., Ritchie J.C., 1996. Satellite estimation of precipitation over land. In Rango A. (Ed.): *Special issue: remote sensing applications to hydrology. Hydrological Science Journ.* 41 (4): 433-451
- Philip J.R., 1966. Plant water relations: some physical aspects. *Ann. Rev. Plant Physiol.*, 17: 245-268
- Pinty B., Verstraete M.M., Dickinson R.E., 1990. A physical model of the bidirectional reflectance of vegetation canopies. 2. Inversion and validation. *Journal of Geophysical Research*, 95: 767-775
- Plusquellec H., Burt C., Wolter H.W., 1994. *Modern water control in irrigation: concepts, issues and applications.* World Bank Technical Paper no.246, Washington D.C. (U.S.A.); 116 pp.

- Postel S., 1993. Water and agriculture. In Gleick P.H. (Ed.): Water in crisis. Oxford University press, U.K., 56-66
- Price J.C., 1992. Estimating Leaf Area Index from remotely sensed data. Proc. IGARSS '92 (Houston), vol.1, 1500-1502
- Querner E.P. and van Bakel P.J.T., 1989. Description of the regional groundwater flow model SIMGRO. Report 7, DLO The Winand Staring Centre, Wageningen, 61 pp.
- Rangeley W.R., 1986. Scientific advances most needed for progress in irrigation. Phil. Trans. R. Soc., London, A 316, 355-368
- Rawls W.L., Ahuja L.R., Brakensiek D.L., 1992. Estimating soil hydraulic properties from soil data. In: van Genuchten M. Th., Leij F.J., Lund L.J. Editors: Proc. Intern. Workshop on Indirect methods for estimating the hydraulic properties of unsaturated soils, Riverside, Ca.,: 329-340
- Reploge J.A., Merriam J.L., 1980. Scheduling and management of irrigation water delivery systems. Proceedings of the 2<sup>nd</sup> Nat. Irrigation Symposium, Am. Soc. Agric. Engineers, 112-127
- Rey J., Hemakumara H.M., 1994. Decision support systems (DSS) for water distribution management. Theory and practice. IIMI Working Paper no.31, 44 pp.
- Rijtema P.E., 1965. An analysis of actual evapotranspiration. Agric. Res. Rep. 659, Pudoc, Wageningen, 107 pp.
- Ritchie J.T., 1972. A model for predicting evaporation from a row crop with incomplete cover. Water Resour. Res., 8 (5): 1204-1213
- Romano N., Santini A., 1997. Effectiveness of using pedo-transfer functions to quantify the spatial variability of soil water retention characteristics. J.Hydrol., 202: 137-157
- Roth C.H., Malick M.A., Plagger R., 1992. Empirical evaluation of the relationship between soil dielectric constant and volumetric water content as the basis for calibrating soil moisture measurements by TDR. J. Soil. Sci, 43: 1-13.
- Russell M.J., Nunez M., Chladil M.A., Valiente J.A., Lopez-Baeza E., 1997. Conversion of Nadir, narrow-band reflectance in red and near-infrared channels to hemispherical surface albedo. Remote Sens. Environm., 61: 16-23
- San-Payo M.M., Teixeira J.L., 1996. Use of GIS and a water balance model to estimate irrigation water requirements. In Ragab R. et al. (Ed.): "Crop-water environment models". Selected papers from the Work.Group on "Sustainable Crops and water use"; Intern. Congress on Irrigation and Drainage, Cairo: 199-208
- Santini A., 1992. Modelling water dynamics in the soil-plant-atmosphere system for irrigation problems. Excerpta nr.6, Milano (Italy)
- Schmullius C., Nithack J., 1996. Temporal multiparameter airborne DLR E-SAR images for crop monitoring: summary of CLEOPATRA campaign 1992. In

- G.Cecchi, G.D'Urso, T.Engman and P.Gudmandsen (Ed.): Remote sensing of vegetation and sea. Proc. SPIE, 2959: 37-48
- Schul J.J., 1982. Sprinkler irrigation "on demand"?. Quart. J. Intern. Agriculture, 21 (Special Issue): 4-17
- Schultz G.A., Engman E.T. (Eds.), 2000. Remote Sensing in Hydrology and Water Management. Springer-Verlag Inc., New York, U.S.A., 473 pp.
- Seguin B., Itier B., 1983. Using midday surface temperature to estimate daily evaporation from satellite thermal IR data. Int. J. Rem. Sens., 4: 371-383
- Sharda V.N., Singh S.R., 1993. A finite element model for simulation of soil moisture balance during plant growth. 15<sup>th</sup> Intern. Congress on Irrigation and Drainage, The Hague, Netherlands; Transaction of 2<sup>nd</sup> Workshop on Crop-Water Models, 24 pp.
- Singh B., Boivin J., Kirkpatrick G., Hum B., 1995. Automatic Irrigation Scheduling System (AISSUM): Principles and applications. J. Irrig. Drainage Engin., ASCE, 121 (1): 43-56
- Smith M., 1990. Expert consultation on revision of FAO methodologies for crop water requirements. FAO Report, Land and Water Development Div., Rome, 54 pp.
- Smith. M., 1992. CROPWAT A computer program for irrigation planning and management. FAO-Irrigation and Drainage Paper No. 46, Rome, 126 pp.
- Solomon K.H., Davidoff B., 1999. Relating unit and sub-unit irrigation performance. Transact. ASAE, 42(1): 115-122
- Spitzer D., Dirks R.W.J., 1987. Bottom influence on the reflectance of the sea. Int. J. Rem. Sens., 8 (3): 279-290
- Stanghellini C., Bosma A.H., Gabriels P.C.J., Werkhoven C., 1990. The water consumption of agricultural crops: how crop coefficients are affected by crop geometry and microclimate. Acta Horticulturae, 278: 509-515
- Sugita M., Brutsaert W., 1992. Landsat surface temperature and radio sounding to obtain regional surface fluxes. Water Resour. Res., 28 (6): 1675-1679
- Swain P.H., 1978. Fundamentals of pattern recognition in remote sensing. In: Remote sensing: the quantitative approach, Swain P.H. and Davis S.M. (Ed.) Mc Graw-Hill, N.Y., 136-186
- Swain P.H., King R.C., 1973. Two effective feature selection criteria for multispectral remote sensing. Proc. 1<sup>st</sup> Int. Joint Conf. Pattern Recognition, IEEE Cat. no. 73, CHO 82 1-9c, Piscataway, NJ, 536-540
- Szeicz G., Long I.F., 1969. Surface resistance of crop canopies. Water Resour. Res., 5(3): 622-633
- Taylor S.A., Ashcroft G.M., 1972. Physical Edaphology. Freeman and Co., San Francisco, CA. (U.S.A.), pp. 434-435
- Taconet O., Bernard R., Vidal-Madjar D., 1986. Evapotranspiration over an agricultural region using a surface flux/temperature model based on NOAA-AVHRR data. J. Climate Appl. Meteor., 25: 284-307

- Teoh Boon Pin, 1997. Water delivery scheduling in the Muda irrigation scheme. Information Techniques for Irrig. Systems Newsletter, Intern. Irrig. Management Institute, Sri Lanka, 3 (1): 4-7
- Texeira J.L., Farrajota M.P., Pereira L.S., 1993. PROREG, a design model for simulating the demand in irrigation projects. 15<sup>th</sup> Intern. Congress on Irrigation and Drainage, The Hague, Netherlands; Transaction of 2<sup>nd</sup> Workshop on Crop-Water Models, 15 pp.
- Texeira J.L., Fernando R.M., M.P., Pereira L.S., 1993. RELREG, a model for real time irrigation scheduling. 15<sup>th</sup> Intern. Congress on Irrigation and Drainage, The Hague, Netherlands; Transaction of 2<sup>nd</sup> Workshop on Crop-Water Models, 15 pp.
- Thiessen E.M., Loucks D.P., 1994. Computer assisted negotiation of multiobjective resources conflicts. In Bogardi J.J. and Nachtbel H.P. (Ed.): Multicriteria decision analysis in water resources management. UNESCO, Paris, 235-259
- Thenkabail P.S., Ward A.D., Lyon J.C. "Landsat-5 Thematic Mapper models of soybean and corn crop characteristics". Int. J. Remote Sensing, vol.15 (1): 49-61, 1994
- Topp G.G., Davis J.L., Annan A.P., 1980. Electromagnetic determination of soil water content measurements in coaxial transmission lines. Water Resour. Res., 16: 574-582.
- Tuijl, van, W., 1993. Improving water use in agriculture. Experiences in the Middle East and North Africa. World Bank Technical Paper no. 201, Washington D.C., U.S.A., 54 pp.
- Verhoef W., 1984. Light scattering by leaf layers with the application to canopy reflectance modeling: the SAIL model. Remote Sens. Environm., 17: 165-178
- Verhoef W., 1985. A scene radiation model based on four-stream radiative transfer theory. Proceedings 3rd Colloquium on Spectral Signatures of Objects in Remote Sensing, France, E.S.A. Publ. SP 247: 143-150
- Verhoef W., 1996. Four-stream atmospheric correction model. National Aerospace Laboratory (NLR), The Netherlands, Report TP960802-U, pp.37, Amsterdam
- Verhoef W., 1998. Theory of radiative transfer models applied in optical remote sensing of vegetation canopies. PhD Thesis, Wageningen Agricultural University, 310 pp.
- Verhoef W., Menenti M., 1998. Spatial and Spectral Scales of Spaceborne Imaging Spectro-radiometers (SASSIS). Final Report NLR-CR-98213 Natioanla Aerospace Laboratory NLR, 289 pp.
- Vidal A., Perrier A., 1990. Irrigation monitoring by following the water balance from NOAA-AVHRR thermal infrared data. IEEE Transactions on Geosci. And Rem. Sens., 28 (5): 949-954
- Younos T., Shanholta V.O., Desai C., 1993. Modeling soil water balance in a GIS environment: SWBM. 15<sup>th</sup> Intern. Congress on Irrigation and Drainage, The



- Hague, Netherlands; Transaction of 2<sup>nd</sup> Workshop on Crop-Water Models, 14 pp.
- Warrick A.W., 1998. Spatial variability. In Hillel D. (Ed.): Environmental soil physics, Academic Press NY, 655-675
- Webster R., Oliver M.A., 1990. Statistical methods in soil and land resource survey. Oxford University Press, 316 pp
- Welles J.M., 1990. Some indirect methods for estimating canopy structure" Remote Sensing Reviews, 5 (1): 31-43, Harwood Academic Publish., U.S.A
- Welles J.M., Norman J.M., 1991. Instrument for indirect measurement of canopy architecture. Agronomy J., 83: 818-825
- Wendroth O., Ehlers W., Hopmans J.W., Kage H., Halbertsma J., Wösten J.H.M., 1993. Revaluation of the evaporation method for determining hydraulic functions in unsaturated soils. Soil Sci. Soc. Am. J., 57:1436-1443
- Wesseling J.G., van den Broek B.J., 1988. Prediction of irrigation scheduling with the numerical model SWATRE. Agric. Water Manag., 14: 299-306
- Whalley W.R., 1993. Considerations on the use of time-domain reflectometry (TDR) for measuring soil water content. Journal of Soil Science, 44: 1-9
- Wösten J.H.M., 1999. The Hypress database of hydraulic properties of European soils. In J.Feyen and K.Wiyo (Eds.): Modelling of transport processes in soils, Wageningen Pers, Wageningen, 675-681
- Wösten J.H.M., Bannik M.H., De Gruijter J.J., Bouma J., 1986. A procedure to identify different groups of hydraulic-conductivity and moisture-retention curves for soil horizons. J.Hydrol., 86: 133-145
- Wood E.F., 1995. Heterogeneity and scaling land-atmospheric water and energy fluxes in climate systems. In R.A.Feddes (Ed.): Space and time scale variability and interdependencies in hydrological processes. Cambridge Univ. Press, U.K.; 3-16
- Wolters W., 1992. Influences on the efficiency of irrigation water use. Publication nr.51 Intern. Inst. Land Reclamation and Improv. (ILRI), Wageningen, 150 pp.
- Zegelin S.J., White I., 1989. Improved field probes for soil water content and electrical domain reflectometry. Water Resour. Res., 25: 2367-2376.

**Appendix I** *Correction coefficients and background reflectance for the Landsat images*

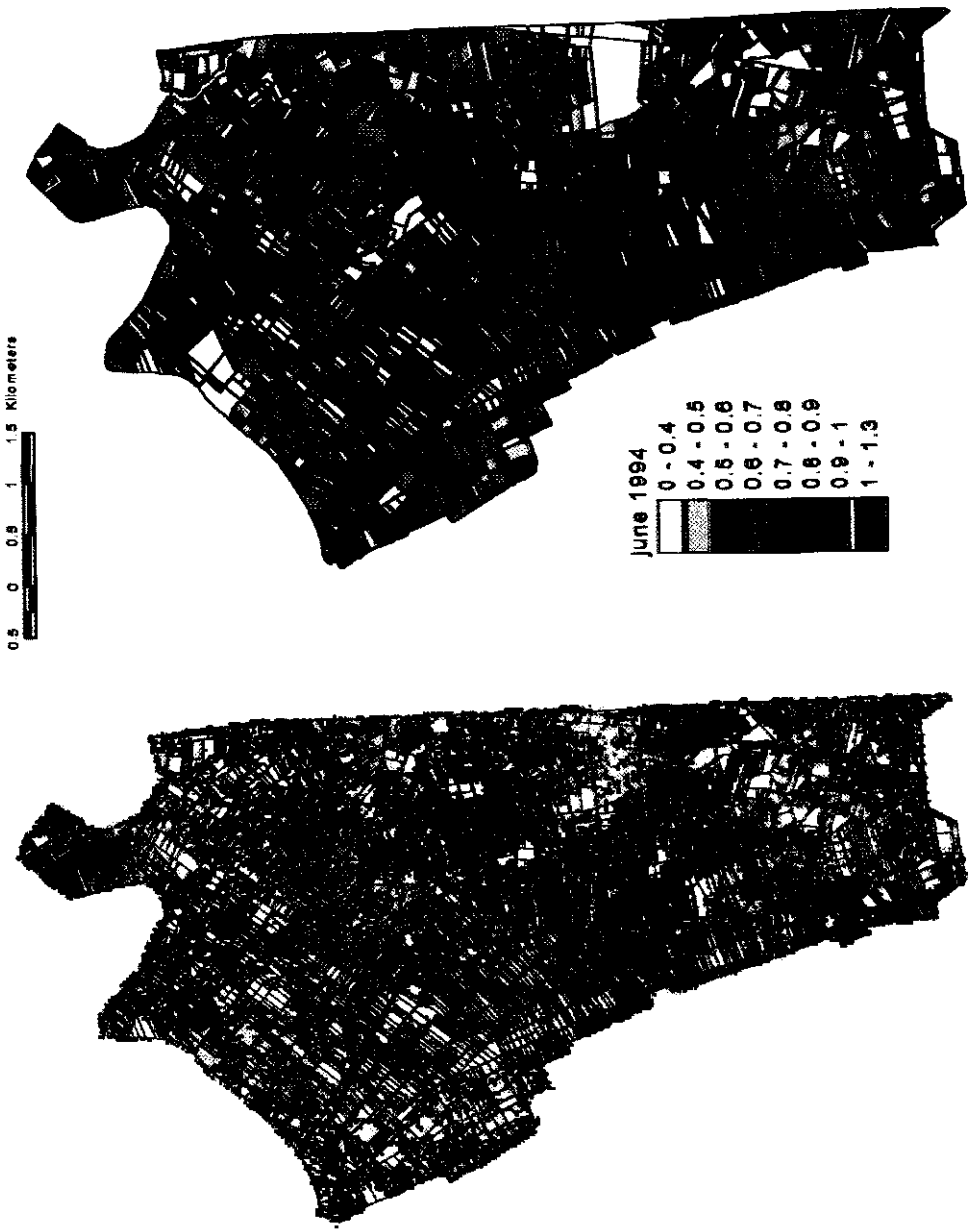
	$G_0$	$G_1$	$O_0$	$O_1$		$G_0$	$G_1$	$O_0$	
<b>NOV'93</b>					<b>JUL'94</b>				
TM-1	0.5015	0.4183	-19.03	-57.07		0.289	0.2398	-16.39	
TM-2	0.9282	0.8284	-10.7	-41.31		0.5313	0.4721	-9.13	
TM-3	0.7204	0.6731	-5.92	-30.32		0.4237	0.3945	-5.02	
TM-4	0.7852	0.7579	-3.68	-22.02		0.4676	0.4502	-2.91	
TM-5	0.4258	0.4221	-1.81	-10.62		0.2521	0.2497	-1.16	
TM-7	0.6636	0.6596	-2.28	-8.82		0.3919	0.3893	-1.39	
<b>JAN'94</b>					<b>AUG'94</b>				
TM-1	0.5986	0.4968	-22.33	-66.42		0.3291	0.2708	-19.51	
TM-2	1.0969	0.9749	-12.55	-47.9		0.6054	0.5332	-11.15	
TM-3	0.8349	0.7776	-6.93	-34.86		0.4816	0.4444	-6.35	
TM-4	0.8948	0.862	-4.27	-24.9		0.529	0.5051	-3.81	
TM-5	0.4754	0.4711	-2.05	-11.33		0.2797	0.2754	-1.55	
TM-7	0.7382	0.7336	-2.55	-9.25		0.431	0.4259	-1.72	
<b>MAY'94</b>					<b>SEP'94</b>				
TM-1	0.2525	0.2114	-13.58	-47.79		0.3107	0.2597	-14.71	
TM-2	0.4691	0.4203	-7.52	-33.99		0.5764	0.5155	-8.15	
TM-3	0.3786	0.3551	-4.08	-24.41		0.4607	0.4313	-4.45	
TM-4	0.4236	0.4102	-2.35	-16.96		0.5119	0.495	-2.64	
TM-5	0.2348	0.2333	-0.98	-7.22		0.2817	0.2795	-1.18	
TM-7	0.368	0.3664	-1.23	-5.65		0.4403	0.438	-1.48	
<b>JUN'94</b>					<b>OCT'94</b>				
TM-1	0.3002	0.2473	-18.67	-73.45		0.3904	0.3257	-16.64	
TM-2	0.5419	0.4788	-10.25	-53.36		0.7256	0.6475	-9.34	
TM-3	0.4259	0.3949	-5.56	-39.05		0.5744	0.5364	-5.19	
TM-4	0.4628	0.4445	-3.13	-27.33		0.6344	0.6119	-3.19	
TM-5	0.2437	0.2413	-1.15	-11.35		0.3466	0.3433	-1.52	
TM-7	0.3774	0.3749	-1.34	-8.5		0.5402	0.5365	-1.89	
					<b>NOV'94</b>				
						0.5157	0.4313	-18.71	
						0.9568	0.8559	-10.53	
						0.7415	0.6943	-5.81	
						0.8089	0.7821	-3.64	
						0.4415	0.438	-1.82	
						0.6894	0.6858	-2.32	

## **COLOUR PLATES**

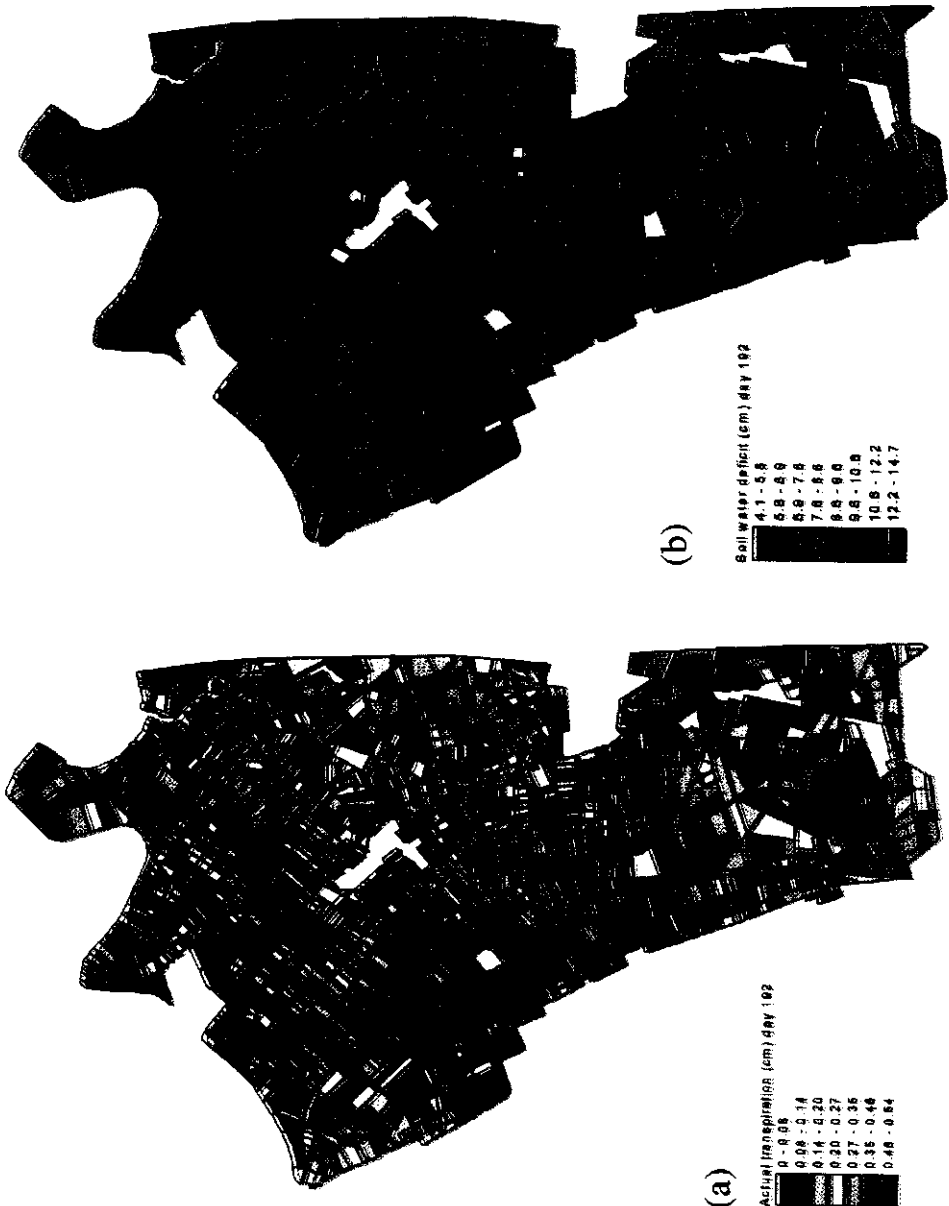
COLOR PLATE 1: *Raster map of Leaf Area Index derived from Landsat TM image of Gromola on June 23<sup>rd</sup> 1994*



COLOR PLATE 2: Raster and vector map of crop coefficient  $K_c$  derived from Landsat TM image of Gromola on June 23<sup>rd</sup> 1994





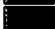
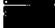
COLOR PLATE 3: *Maps of actual transpiration and soil water deficit between 10 and 50 cm depth on day 192 of 1994*



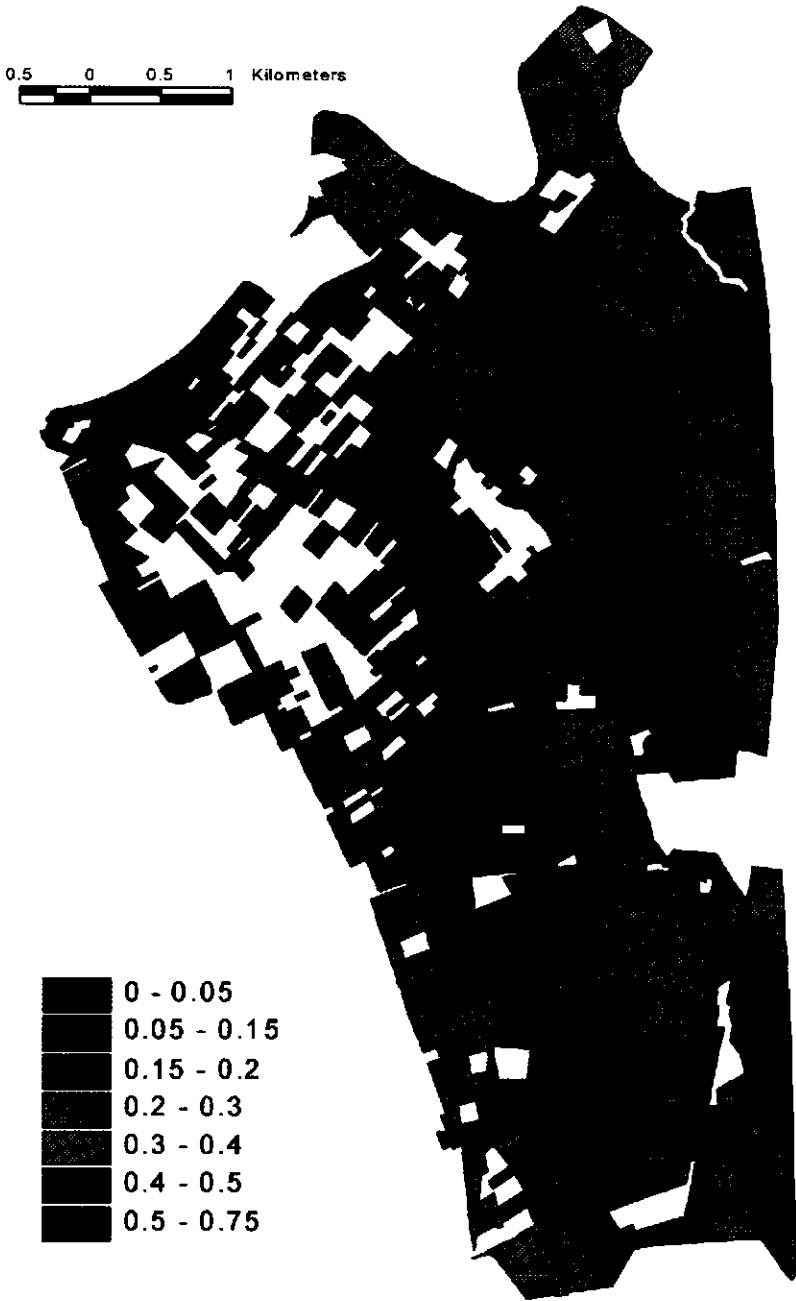
COLOR PLATE 4: *Map of farmers' water demand and irrigation scheduling adaptations on day 192 of 1994*



**Day 192 1994**

-  Irrigated
-  Not irrigated for excessive water demand (sched. adpt. Section 7.5)
-  Not irrigated (sched. adpt. ii Section 7.4)
-  Irrigated with reduction (sched. adpt. i Section 7.4)

COLOR PLATE 5: Irrigation performance indicator  $\epsilon_2$  calculated for the months from June to September 1994 for the Reference Scenario.





## **Curriculum vitae**

Guido D'Urso was born in Salerno (Italy) on August 29<sup>th</sup>, 1961. In 1985 he received *cum laude* the degree of Civil Hydraulic Engineer from the University of Naples, Italy. During 1986 he worked as Junior Scientist at the Departments of Hydraulics of the University of Naples with the one year fellowship 'Prof. Giuseppe Pistilli' sponsored by the 'Fondazione Politecnica Mezzogiorno d'Italia'. From 1988 to 1998 he was Research Assistant at the Agriculture Faculty of the University of Molise, Campobasso, Italy, where he also taught Irrigation and Agricultural Hydraulics. During 1992 and 1997 he carried out part of the research activities for this PhD thesis at the DLO-Staring Centrum of Wageningen, The Netherlands, with fellowships sponsored by the Italian National Research Council.

On November 1998 he joined the Department of Agricultural Engineering and Agronomy of the University of Naples Federico II as Associate Professor of Irrigation and Drainage.



UNIVERSITY OF NAPLES "FEDERICO II" (ITALY)  
*DEPARTMENT OF AGRICULTURAL ENGINEERING AND AGRONOMY*  
*Section Land and Water Management*

CIP-DATA KONINKLIJKE BIBLIOTEEK, DEN HAAG

D'Urso, G.

Simulation and management of on-demand irrigation systems:

A combined agrohydrological and remote sensing approach / G.D'Urso

Doctoral Thesis Wageningen University – with ref. – summary in Dutch  
and in Italian,

ISBN 90-5808-399-3